DOCTORAL THESIS

Improving Occupant Safety on Board High-Speed Planing Craft

Fatemeh Roshan

TALLINNA TEHNIKAÜLIKOOL
TALLINN UNIVERSITY OF TECHNOLOGY
TALLINN 2026

TALLINN UNIVERSITY OF TECHNOLOGY
DOCTORAL THESIS
84/2026

Improving Occupant Safety on Board High-Speed Planing Craft

FATEMEH ROSHAN

TAL TECH PRESS

TALLINN UNIVERSITY OF TECHNOLOGY
School of Engineering
Kuressaare College
This dissertation was accepted for the defence of the degree of Doctor of Philosophy (Ph.D.): 29/10/2026

Supervisor:
Associate Professor Mihkel Kõrgesaar
Naval Architecture and Hydrodynamics Research Group
Kuressaare College
Tallinn, Estonia

Co-supervisors:
Professor Pentti Kujala
Estonian maritime academy
Tallinn University of Technology
Tallinn, Estonia

Professor Karl Garme
Department of Engineering Mechanics, SCI
KTH Royal Institute of Technology
Stockholm, Sweden

Opponents:
Ph.D., Alessandro Iafrati
Istituto di Ingegneria del Mare
Consiglio Nazionale delle Ricerche
Rome, Italy

Ph.D., Claudio Lugni
Full Professor at Department of Industrial Engineering
University of Naples "Federico II"
Naples, Italy

Defence of the thesis: 18/12/2026, Tallinn

Declaration:
Hereby I declare that this doctoral thesis, my original investigation and achievement, submitted for the doctoral degree at Tallinn University of Technology has not been submitted for doctoral or equivalent academic degree.

Fatemeh Roshan

---
signature

European Union
European Regional
Development Fund

Investing
in your future

Copyright: Fatemeh Roshan, 2026
ISSN 2585-6898 (paperback)
ISBN 978-9916-80-607-4 (paperback)
ISSN 2585-6901 (PDF)
ISBN 978-9916-80-608-1 (PDF)
https://doi.org/10.23658/taltech.84/2026

Citation: Roshan, F. (2026). *Improving Occupant Safety on Board High-Speed Planing Craft* [TalTech Press]. https://doi.org/10.23658/taltech.84/2026

TALLINNA TEHNIKAÜLIKOOL
DOKTORITÖÖ
84/2026

Kiirekäiguliste liugkerede pardal viibijate ohutuse parandamine

FATEMEH ROSHAN

TAL TECH KIRJASTUS

Contents

List of Publications 7
Author's Contribution to the Publications 8
Abbreviations 10
1 Introduction 11
1.1 Background 11
1.2 Problem statement and scope 12
1.3 Literature review 13
1.3.1 High speed craft dynamics in wave conditions 13
1.3.2 Safety improvement using motion reduction devices 14
1.3.3 Safety improvement using shock mitigation seats 16
1.4 Motivation and research questions 17
1.5 Research objectives and tasks 18
1.6 Thesis outline 19
2 Research Methods 22
2.1 Systematic review 22
2.2 Numerical simulations 23
2.3 Experimental testing 29
2.4 Mathematical approach 32
2.4.1 Mathematical model for safety evaluation 32
2.4.2 Mathematical model for shock mitigation seat performance 34
3 Results 39
3.1 Human safety risks associated with HSPC operations 39
3.2 Interceptor performance in improving HSPC dynamics and occupant safety 46
3.3 Shock mitigation seat to enhance human safety 52
4 Discussion 57
4.1 Main novelties of the thesis 57
4.2 Discussion of the main findings 59
4.3 Limitations 61
4.3.1 Limitations in the systematic review 61
4.3.2 Limitations in CFD simulation study 61
4.3.3 Limitations in experimental investigations 62
4.3.4 Limitations in safety assessment analysis 62
4.3.5 Limitations in mathematical approach 62
5 Conclusion 64
List of Figures 66
List of Tables 68
References 69
Acknowledgements 78
Abstract 79
Lühikokkuvõte 81
Appendix 1 (Publication I) 83
Appendix 2 (Publication II) 113

Appendix 3 (Publication III) 147
Appendix 4 (Publication IV) 161
Appendix 5 (Publication V) 189
Appendix 6 (Publication VI) 217
Curriculum vitae 237
Elulookirjeldus 240

List of Publications

The list of author's publications, on the basis of which the thesis has been prepared:

I **Roshan, F.,** Dashtimanesh, A., & Kujala, P. (2024). Safety Improvements for High-Speed Planing Craft Occupants: A Systematic Review. Journal of Marine Science and Engineering, 12(5), 845. **https://doi.org/10.3390/jmse12050845**.

II **Roshan, F**., Tavakoli, S., Mancini, S., & Dashtimanesh, A. (2022). Dynamic of Tunneled Planing Hulls in Waves. Journal of Marine Science and Engineering, 10(8), 1038. **https://doi.org/10.3390/jmse10081038**.

III **Roshan, F**., Dashtimanesh, A., De Luca, F., Mancini, S. (2025). High-speed craft with double interceptor system in calm water: URANS Solution. Progress in Marine Science and Technology. **https://doi.org/10.3233/pmst250047.**

IV **Roshan, F.,** Niazmand Bilandi. R., De Luca, F., Mancini, S., Kõrgesaar, M., (2026). Numerical Investigation of Transom and Double Interceptor Systems on a High-Speed Planing Craft in Regular Waves with Experimental Validation. Ocean Engineering, 367, p. 128197. **https://doi.org/10.1016/j.oceaneng.2026.128197.**

V **Roshan, F**., Niazmand Bilandi, R., De Luca, F., Mancini, S., Kujalaa, P., Dashtimanesh, A., (2025). High Speed Planing Craft Dynamics in Irregular waves: Safety Improvement using Interceptor Systems. Applied Ocean Research. **https://doi.org/10.1016/j.apor.2025.104692.**

VI **Roshan, F.,** Garme, K., & Dashtimanesh, A. (2026). Acceleration effects in the horizontal plane on the safety assessment aboard a high-speed craft. *Proceedings of the Institution of Mechanical Engineers, Part M: Journal of Engineering for the Maritime Environment*, 14750902261440461. **https://doi.org/10.1177/14750902261440461.**

Author's Contribution to the Publications

The author's contributions to the publications included in this thesis are as follows:

I In Publication I, the author was responsible for the conceptualization and methodological development of the study. The author conducted investigations, data collection and curation, formal analysis, validation, and visualization. The author also prepared the original manuscript. A. Dashtimanesh contributed to the conceptualization, methodology, investigation, supervision, and review and editing of the manuscript. P. Kujala contributed to the methodology and review and editing of the manuscript.

II In Publication II, the author conducted the investigation and was responsible for the validation, software, and visualization. The author prepared the original manuscript. S. Tavakoli contributed to the conceptualization, methodology, formal analysis, visualization, and editing of the manuscript. S. Mancini contributed to the investigation and review and editing of the manuscript. A. Dashtimanesh contributed to the conceptualization, methodology, resources, formal analysis, supervision, and review and editing of the manuscript.

III In Publication III, the author was responsible for the conceptualization and methodological development of the study. The author conducted the software development, investigation, data curation, formal analysis, validation, and visualization. The author also prepared the original manuscript. A. Dashtimanesh contributed through supervision, formal analysis, and review and editing of the manuscript. F. De Luca contributed to data curation, resources, formal analysis, and review and editing of the manuscript. S. Mancini contributed to data curation, formal analysis, supervision, and review and editing of the manuscript.

IV In Publication IV, the author was responsible for the conceptualization and methodology of the study. The author conducted the software development, validation, formal analysis, investigation, experiments, numerical simulations, data curation, and visualization. The author also prepared the original manuscript. R. Niazmand Bilandi contributed to the conceptualization, software, data curation, experiments, validation, formal analysis, and review and editing of the manuscript. F. De Luca contributed to the conceptualization, hull form design and configuration, experimental setup, experiments, and review and editing of the manuscript. S. Mancini contributed to the conceptualization, experiments, supervision, and review and editing of the manuscript. M. Kõrgesaar contributed through supervision, formal analysis, and review and editing of the manuscript.

V In Publication V, the author was responsible for the conceptualization and methodology of the study. The author conducted the experimental work and investigation and was responsible for data curation, formal analysis, resources, and visualization. The author also prepared the original manuscript. R. Niazmand Bilandi contributed to the conceptualization, experimental work, data curation, formal analysis, investigation, resources, and review and editing of the manuscript. F. De Luca contributed to the experimental work, data curation, resources, formal analysis, and review and editing of the manuscript. S. Mancini contributed to the experimental work, data curation, formal analysis, supervision, and review and editing of the manuscript. P. Kujala contributed through supervision and review and

editing of the manuscript. A. Dashtimanesh contributed through supervision, formal analysis, and review and editing of the manuscript.

VI In Publication VI, the author was responsible for the conceptualization and methodology of the study, formal analysis, visualization, validation, and investigation. The author also prepared the original manuscript. K. Garme contributed to data curation, resources, supervision, and review and editing of the manuscript. A. Dashtimanesh contributed to the conceptualization, supervision, and review and editing of the manuscript.

Abbreviations

CFD	Computational Fluid Dynamics
CG	Centre of Gravity
DIS	Double Interceptor System
HSC	High Speed Craft
HSPC	High Speed Planing Craft
NSS	Naples Systematic Series
RAO	Response Amplitude Operator
RMSi	Root-Mean-Square of weighted acceleration in *i* direction
SAR	Search and Rescue
TIS	Transom Interceptor System
URANS	Unsteady Reynolds-Averaged Navier-Stokes
VDV_i	Vibration Dose Value in *i* direction
$VDV_{i,8h}$	Vibration Dose Value in *i* direction for 8 hours
WBV	Whole Body Vibration

1 Introduction

1.1 Background

High-speed planing craft (HSPCs) are extensively used in both military and civilian marine transportation, including military patrols, search and rescue missions, and recreational activities. These vessels are specifically designed to operate at high speeds over the water, making them highly efficient for tasks that require rapid response times.

Currently, the global number of high-speed boats is estimated at approximately 34 million, with Nordic and European countries leading in ownership (ICOMIA, 2023). In the Baltic Sea alone, around 3.5 million leisure boats are actively used, predominantly along coastal areas for recreational purposes (Moldanová et al., 2018). However, high-speed operations often expose these craft to challenging conditions that can significantly affect crews' performance and safety.

In the Baltic Sea region, maritime weather conditions can be highly unpredictable, and powerful storms can lead to the rapid development of waves and turbulence. These dynamic environmental factors, combined with operating at high speed, can greatly influence the vessel's dynamic performance and, consequently, the occupant's safety.

The safety risks associated with high-speed craft (HSC) operations are numerous and varied. These risks include, but are not limited to:

- **Loss of Hull Control or Capsizing:** In extreme cases, the combination of high-speed operations, rough seas, and inadequate vessel design or handling can lead to a loss of control, potentially resulting in capsizing or other catastrophic failures, with serious consequences for the occupant's safety.
- **Disorientation and Balance Issues:** High-speed operations over rough seas can cause occupants to lose balance or experience disorientation, increasing the risk of falls or improper posture.
- **Musculoskeletal Injuries:** Prolonged exposure to whole-body vibrations and sudden shocks can result in strains and injuries to muscles, joints, and spine.
- **Internal Injuries from Sudden Impacts:** Harsh hull impacts against waves or turbulence can cause serious internal injuries, particularly without proper shock mitigation systems or restraints.
- **Fatigue and Reduced Performance:** Continuous exposure to high-speed motion and acceleration can lead to significant fatigue, reducing the crew's operational efficiency and ability to perform critical tasks.
- **Psychological Stress and Anxiety:** The constant exposure to vibrations and shocks can lead to psychological stress, anxiety, and reduced mental resilience in crew members.

These safety concerns underscore the importance of considering human safety on board the HSC, which becomes more crucial with the development of HSCs and innovative hull forms to achieve higher speeds. Figure 1 shows the number of publications related to high-speed craft and safety for every five years from 1987 to 2024. The literature trends for the published documents using the terms "high-speed crafts" and "safety indicate increasing research attention to safety-related aspects of high-speed craft operations.

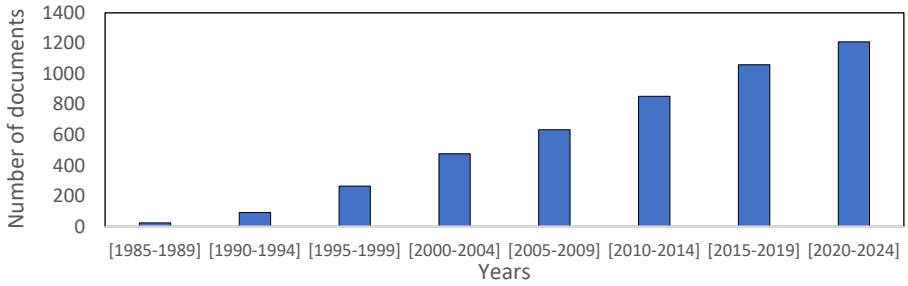


Figure 1. Trend of the number of published documents related to high-speed craft safety over the past 40 years.

However, the present thesis does not directly assess all of these safety outcomes or the broader safety aspects represented in the literature. Instead, it focuses on vessel motions and acceleration exposure experienced by occupants during high-speed planing craft operations, and on the potential relevance of this exposure to occupant safety. In particular, the thesis investigates acceleration exposure and associated human safety risks and evaluates approaches for reducing vessel motions and the vibrations and shocks transmitted to occupants. Other outcomes, such as capsizing, psychological stress, and fatigue, are considered only as broader contextual aspects of high-speed craft safety and are outside the direct scope of this thesis.

1.2 Problem statement and scope

Numerous studies have addressed the issues of human safety on board HSPCs, including Meyer et al. (1994), Ensign et al. (2000), Carvalho (2004), and de Alwis and Garme (2021). These safety risks are usually caused by whole-body vibration (WBV) and shock exposures. Therefore, national and international organizations have established various safety guidelines and standards aimed at minimizing the likelihood of adverse health effects and discomfort caused by WBVs and shocks. These standards are set by organizations such as the International Organization for Standardization (ISO), the European Union (EU), the British Standards Institution (BSI), the American National Standards Institute (ANSI), and the Japanese Industrial Standards Committee (JISC). Implementing these standards in the context of HSPCs allows for the prediction of safety-related issues, facilitating effective safety improvements.

The majority of safety assessment studies of HSPCs have considered ISO 2631-1:1997, ISO 2631-5:2004, and EU Directive 2002/44/EC as key measures, such as Allen et al. (2008), Dobbin et al. (2008), Garme et al. (2011), Taunton et al. (2011), and Folsø (2004). Their findings consistently confirm that vertical accelerations on board HSPCs significantly exceed the limits recommended by current safety standards, highlighting the critical requirement to minimize vertical accelerations to enhance crew safety. However, existing information on the effects of accelerations in other directions on the safety of HSPC occupants remains limited.

Key strategies to reduce hull accelerations, as explored in existing literature, include optimizing hull designs (e.g., deep-V hulls, stepped hulls, or tunnelled planing hulls), installing motion reduction devices to enhance dynamic performance, and mitigating vibrations and shocks transmitted to the occupant using suspension systems. Additionally, load and weight distribution, crew training, and the use of protective equipment have also been identified as critical considerations.

A significant aspect of these efforts has been directed toward minimizing hull motion and acceleration and mitigating the accelerations transmitted to seated occupants to reduce safety risks. To achieve this, the following strategies are recommended:

1. Adjusting operational speeds based on sea conditions to minimize hull motion and acceleration.
2. Using motion reduction devices, such as interceptors or trim tabs, to reduce hull motions and maintain better stability during high-speed operations.
3. Installing shock mitigation seats to absorb accelerations transmitted to the seated occupants.

These strategies can significantly improve safety on board HSPCs by mitigating the transmission of accelerations to occupants and reducing risks associated with WBV and shocks, such as musculoskeletal injuries, disorientation, balance issues, internal injuries from sudden impacts, and fatigue. Additionally, reducing hull motions through adjusted operational speeds and the implementation of motion reduction devices can efficiently lower the likelihood of loss of hull control or capsizing, thereby addressing associated safety concerns.

1.3 Literature review

1.3.1 High speed craft dynamics in wave conditions

Over the years, many designers have continuously tried to improve HSPCs performance with the aim of designing stronger, faster, and safer boats. The need for speed is driven by various applications, such as military operations, search and rescue (SAR) missions, and recreational boating, where short response times are crucial. However, it is important to consider that increasing operational speeds, especially in challenging sea conditions, also leads to higher hull motions and severe accelerations. These factors, in turn, contribute to a range of safety risks, including the probability of losing hull control or capsizing, human injuries as a result of sudden shocks, fatigue, discomfort, etc**.** As a result, predicting hull motions accurately at the designed operational speeds, considering wave conditions, is a critical aspect of HSPC design and operation.

Numerous studies have examined the effects of hull geometry, operational speeds, and wave characteristics on the performance of HSPCs in different regular head waves, including those by Fridsma (1969), Grigoropoulos et al. (2010), and Kim et al. (2013). Begovic et al. (2014a) conducted experiments on four hulls in ten different regular waves. They demonstrated that higher vertical acceleration occurs in waves with lengths from 1.5 to 3 times the hull length, with hull motions increasing significantly at higher speeds within this range. However, the effect of hull speed on hull motion diminished outside this wavelength range. The influence of hull speed on hull motions has also been presented by Seo et al. (2016) and Ma et al. (2015).

In contrast to these experimental studies, other researchers have used numerical simulations to investigate the effect of various parameters on hull motions in regular waves, including Judge et al. (2020), Ling and Wang (2019), Bilandi et al. (2019) and Tavakoli et al. (2020). Additionally, mathematical models have been widely used, such as those developed by Sun and Faltinsen (2011), and Tavakoli et al. (2020). These models, validated against experimental data, are particularly valuable in the early stages of design, enabling designers to predict performance and optimize hull configurations for specific operating conditions.

Despite the wealth of research conducted to date, as the design of high-speed crafts evolves, introducing more complex hull forms and higher operational speeds, new challenges emerge. For example, vessels designed to achieve higher speeds in increasingly difficult sea states will likely encounter more extreme wave-induced accelerations, which must be understood and mitigated to maintain both performance and safety. Consequently, analyzing complex hull forms in regular waves to predict hull motions and accelerations, and estimating critical wavelength associated with harsh motions, is still required for new complex hull forms. Additionally, as the real sea condition consists of a random wave, investigating dynamic performance in irregular waves is also crucial to explore hull dynamics in real seas.

Investigations of high-speed craft dynamics in irregular waves are often conducted experimentally to evaluate the effects of hull geometry and operational speeds on hull motions. For instance, Fridsma (1971) studied the effects of deadrise angle on hull performance in irregular waves and found that hulls with a higher deadrise angle have lower vertical acceleration. However, Begovic et al. (2014b) argued that the wave heights considered in Fridsma's (1971) experiments were excessively high, leading to severe hull motions that may not reflect realistic conditions. In response, Begovic et al. (2016) analyzed two different HSPC hull forms in irregular waves with $Hs/B > 0.3$ at different speeds. Their observations demonstrated the potential for vertical acceleration exceeding 3g, which is over the limit value for human safety and comfort. Following this, Rosén et al. (2017) examined hull motions, including heave and pitch, as well as vertical acceleration, and proposed operational speed limitations based on wave height to mitigate excessive hull motions. Additionally, De Luca and Pensa (2019) conducted towing tank tests on five Naples systematic series (NSS) hull forms in various sea states and speeds. Other experimental investigations of HSPC in irregular waves can be found in Zarnick and Turner (1981), Klosinski and Brown (1993), Taunton et al. (2011), and Grigoropoulos and Damala (2011). Their results indicate that vertical acceleration in irregular waves is strongly influenced by hull speed and the hull form slenderness ratio, underscoring the importance of geometric optimization and operational speeds in high-speed craft design.

Although experimental investigations are generally more reliable than mathematical and numerical modeling, they involve higher costs and require specialized instrumentation, which can present practical challenges. As a result, numerical and mathematical approaches can be employed during the pre-design process as cost-effective alternatives. Akers (1999), Garme (2005), and Sebastiani et al. (2008) presented some mathematical investigations of HSPC in irregular head waves, which are mostly based on Zarnick models (1978, 1979). However, due to the computationally intensive nature of numerical simulations in irregular waves, research in this area remains limited.

1.3.2 Safety improvement using motion reduction devices

In addition to reducing hull speeds when HSPCs are confronted with rough seas that cause harsh motions and impact shocks, some preventive strategies can be employed to reduce severe hull motions and accelerations, consequently minimizing human safety risks. One effective approach is to implement motion reduction devices. These devices are installed on HSPCs to improve hydrodynamics in calm water, such as minimizing trim angles, hull resistance, and the probability of porpoising. Furthermore, these devices are also efficient in wave conditions for reducing hull motions and accelerations.

Motion reduction devices can improve HSPC performance in two aspects: reducing fuel consumption and emissions (by minimizing hull resistance and undesired motions) and enhancing occupants' safety (by reducing extreme motions and accelerations). These two benefits make motion reduction devices a valuable solution for both dynamic efficiency and the safety of on board crews.

Researchers have proposed several types of motion reduction devices, including interceptors, trim tabs, transom wedges, and flaps (Katayama and Ikeda, 2004; Ashkezari and Moradi, 2021). Trim tabs and interceptors share a similar design; both contain a flap installed at the transom to generate additional lift and a bow-down torque, thus preventing excessive trim angles. Figure 2 shows the force distribution and torque effects of the bare hull in comparison to the hull equipped with a trim tab, a Transom Interceptor System (TIS), and a Double Interceptor System (DIS).

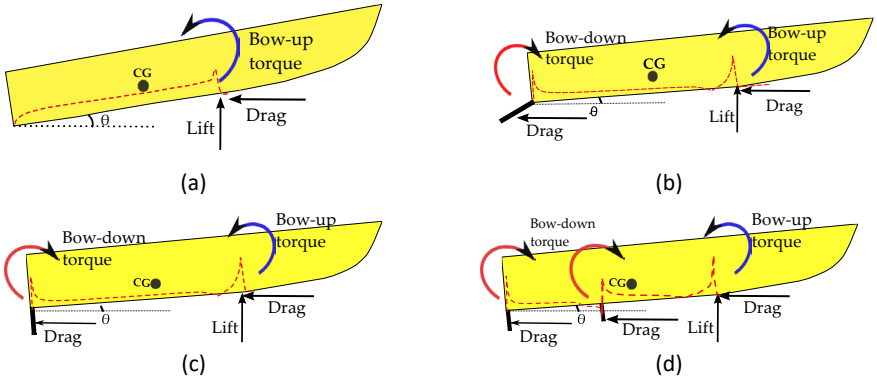


Figure 2. Schematic illustration of hydrodynamic forces acting on the HSPC for different configurations: a) bare hull, b) with trim tab, c) with Transom Interceptor System (TIS), and d) with Double Interceptor System (DIS). (Figures (a), (b), and (c) are adapted from Paper I, and Figure (d) is adopted from Paper IV)

As Figure 2(b) indicates, adding a trim tab at the transom generates a bow-down torque that counteracts the bow-up torque at the stagnation point. This adjustment lowers the trim angle, resulting in a flatter running attitude, which helps reduce wave impacts, slamming, and pitching motions compared to the bare hull. Consequently, this improvement enhances human comfort and safety. Furthermore, studies such as Wang (1998), Sakaki et al. (2019), and Mohebbi et al. (2020) have shown that a well-designed trim tab can ultimately reduce overall hull resistance, despite inducing some drag due to its deflection of water flow.

Although trim tabs offer numerous advantages, they may not significantly dampen hull motions in waves, and improper designs can cause unexpected instability and raise safety concerns in rough seas. The effectiveness of a trim tab depends on operational hull speeds and sea conditions, as well as trim tab dimensions and angle. Numerous research studies have been conducted to investigate the effect of these parameters on trim and drag reduction, aiming to determine the most efficient dimensions for optimal performance, such as those presented by Brown (1991), Yaakob et al. (2004), Ghadimi et al. (2014), Song et al. (2018), Wang (1985), Savitsky and Brown (1976), and Santos et al. (2005).

As Figure 2(c) shows, the Transom Interceptor System (TIS) is a vertical flap installed on the transom and acts as a dam in front of the fluid flow. TIS generates a high lift and

strong counter torque that efficiently reduces the hull trim angle. Numerous studies compared the performance of TIS and trim tabs in reducing hull trim angles, such as Villa and Brizzolara (2009), Tsai and Hwang (2004), Rijkens et al. (2012), and Seo et al. (2013). All of these studies confirm the superiority of TIS compared with the trim tab in controlling trim angles and reducing drag. Using TIS causes the bow to remain more stable, preventing porpoising and reducing hull motions in rough seas, which leads to enhanced human safety on board the HSPC.

The higher lift generated by TIS compared to the trim tab makes it more efficient in improving human safety and reducing the risk of adverse health effects, discomfort, loss of balance, and motion sickness. However, it should be considered that TIS performance is always a function of sea conditions, hull speed, and interceptor dimensions, as Song et al. (2018), Day and Cooper (2011), and Molini and Brizzolara (2005) demonstrated.

Moreover, several studies have demonstrated the effectiveness of installing TIS on the HSPC's transom to reduce vertical hull motions and accelerations in wave conditions (Luca and Pensa, 2014; Najafi et al., 2015; and Karimi et al., 2015). However, the efficiency of interceptors in wave conditions is influenced by factors such as hull speed and wave frequency, which may lead to a negative trim angle at certain wavelengths and speeds. To optimize interceptor performance under these conditions, the use of controllable or active systems has been proposed by Rijkens et al. (2011), Katayama et al. (2003), and Ertogan et al. (2016).

In addition to the conventional transom interceptor system, De Luca and Pensa (2011) introduced an unconventional interceptor configuration, a Double Interceptor System (DIS), which consists of a conventional transom interceptor (TIS) and an additional interceptor located in the middle of hull length, as shown in Figure 2(d). This innovative configuration is designed to generate an extra lift at the forward interceptor position, potentially leading to a greater reduction in hull motions. Furthermore, the DIS can create an air cavity behind the forward interceptor, contributing to a reduction in hull shear resistance. The performance of the DIS in calm water and regular waves was presented by De Luca and Pensa (2012), who observed that, while the DIS is effective in reducing resistance, it could lead to increased hull motions and accelerations in regular waves. However, the dynamic performance of a hull equipped with DIS in irregular waves remains unexplored, highlighting a gap that needs to be addressed for a comprehensive understanding of DIS behavior.

1.3.3 Safety improvement using shock mitigation seats

Shock mitigation seats are systems that consist of masses, springs, and dampers, designed to mitigate mechanical vibrations and shocks. These seats are widely used in various vehicles such as trains, cars, and ships, due to their potential to reduce the adverse effects of whole-body vibrations (WBVs) and shocks on human health and comfort. Mathematical modelling serves as a foundational approach to provide an efficient and repeatable means to predict the performance of shock mitigation seats under various dynamic conditions. Early validation efforts by Olausson and Garme (2015) and Marshall and Riley (2020) established the credibility of seat models by comparing simulated results with empirical data from sea trials and drop-tower tests.

Depending on the objective, researchers have employed a range of mathematical models for simulating a seat. For instance, a simplified seat model with a single mass and a vertical spring-damper system (1DOF) has been used to analyse vertical seat motions, neglecting the effects of the seat cushion and horizontal accelerations, by Wei and Griffin

(1998), Mayton et al. (2006), and Gannon (2017). Other studies have introduced models incorporating two mass-spring-damper systems to account for seat cushion effects, such as the models of Wei and Griffin (1998), Liam (2011), and Townsend et al. (2012). Additionally, some models consider non-vertical springs or non-vertical dampers, such as Choi et al. (2000), Ma et al. (2008), and Rakheja et al. (2003). In more complex scenarios, models have also integrated end-stop buffers to avoid "bottoming out" conditions that can occur during harsh impact shocks when seat travel length is limited (see Rebelle, 2000, 2004, and Ma et al., 2008).

Experimental testing complements modelling by providing real-world and accurate data on seat effectiveness. In the context of marine vehicles, sea trials remain one of the most direct methods for assessing acceleration exposure and its effect on occupants. As demonstrated by Allen et al. (2008) and Garme et al. (2011), prolonged exposure to vertical vibration can exceed safety thresholds, emphasizing the importance of seat design to reduce safety risks. Suspension seats have generally shown improvements in acceleration reduction, with some studies reporting reductions in peak accelerations by more than 50% (Dobbins et al., 2008). However, not all findings are consistent. Riley et al. (2013) noted that soft seat cushions might amplify vertical accelerations, complicating efforts to enhance ride comfort and safety through seat modifications alone.

To address the practical and financial limitations of sea trials, researchers have increasingly relied on laboratory-based drop-tower tests to evaluate seat dynamics under controlled impact conditions. These tests, as conducted by Alam et al. (2017) and Kearn (2001), simulate slamming impacts and measure parameters such as damping duration and acceleration transfer. A key observation from these experiments is the phase difference between seat base and seat pan responses—an insight essential for accurately modelling impact absorption (Riley et al., 2013; Reynolds et al., 2012; Wice, 2015). Drop tests offer reproducibility and adaptability, and Marshall and Riley (2020) stated that drop-tower experiments can closely align with shocks in sea conditions when properly designed. Integrating both methods enables a comprehensive assessment framework, facilitating the iterative improvement of seat systems to better safeguard marine personnel against the demanding conditions encountered during HSPC operations.

1.4 Motivation and research questions

The safety of occupants on board HSPCs is a crucial concern due to the dynamic and challenging operating conditions these vessels face, especially at high speeds in rough sea conditions that cause exposure to harsh accelerations in different directions. These severe accelerations can cause adverse health effects, discomfort, motion sickness, and long-term health issues for the occupants.

Despite existing efforts to mitigate vertical accelerations using motion reduction devices and shock mitigation seats, current human safety assessments still indicate that accelerations exceed the recommended limits set by safety standards. While much of the research has focused on reducing vertical accelerations, there is a lack of understanding regarding the dynamic effects of horizontal accelerations (forward and sideways) and their role in safety assessments. Additionally, there is limited exploration of novel systems like the Double Interceptor System (DIS) in irregular wave conditions, where their performance may differ significantly from calm water.

This research aims to examine the effects of multidirectional acceleration on the safety of HSPC occupants and explore opportunities for safety enhancement. By

assessing the effectiveness of current safety improvement strategies under various sea conditions, such as the effects of motion reduction devices (TIS and DIS) and shock mitigation seats, the study evaluates multiple approaches to improve occupant protection on board HSPCs.

The key research questions that guide this study are:

RQ1. How do acceleration exposure and hull dynamics affect occupant safety in high-speed planing craft (HSPC)?

RQ2. Which strategies for modifying hull dynamics and reducing acceleration exposure can be implemented in HSPCs, and how effective are they in improving occupant safety?

1.5 Research objectives and tasks

The main objective of this thesis is to improve human safety on board HSPC by reducing exposure to vibrations and shocks through an in-depth understanding of HSPC dynamics in wave conditions and evaluating the efficiency of innovative strategies for reducing hull accelerations and mitigating transmitted accelerations to the human body. The objectives are:

Objective 1: Conduct a comprehensive review of acceleration-related safety concerns on board HSPC and evaluate existing standards and safety enhancement strategies.

Task 1: Conduct a systematic literature review on acceleration exposure effects on human safety aboard HSPCs and existing safety standards and safety improvement strategies to identify current gaps and challenges. (Paper I)

Objective 2: Investigate how hull dynamics under different operational conditions affect the safety of HSPC crews.

Task 1: Simulate a high-speed planing hull in different regular waves at various speeds to assess the effect of operational speeds and wave characteristics on hull motions and acceleration. (Papers II and IV)

Task 2: Investigate the effect of operational speeds on hull dynamics and human safety under different irregular wave conditions. (Paper V)

Task 3: Study the effect of multidirectional acceleration on the safety of HSPC crews by analyzing measured accelerations in forward, vertical, and sideways directions. (Paper VI)

Objective 3: Examine the influence of proposed safety improvement strategies in enhancing the safety of HSPC occupants.

Task 1: Analyze the hydrodynamic performance of the double interceptor system in calm water and evaluate its potential as a motion reduction device. (Paper III)

Task 2: Investigate the effects of transom interceptor and double interceptor systems on hull dynamics under different regular wave conditions. (Paper IV)

Task 3: Investigate the impact of transom interceptors and double interceptor systems on occupant safety at varying speeds. (Paper V)

Task 4: Assess the performance of shock mitigation seating in reducing transmitted accelerations and improving the safety of seated occupants. (Paper VI)

To provide a structured overview of the research conducted in this thesis, Table 1 summarizes the included papers, their main focus areas, associated research questions, and corresponding objectives. The table demonstrates how each publication contributes to addressing the overall scope of the thesis. In addition, Figure 3 illustrates the relationships between the research objectives and the included publications, highlighting the coherence and progression of the research framework. This visual mapping clarifies how each objective is addressed across multiple studies, highlighting the coherence and progression of the research effort.

Table 1. Overview of the included papers, highlighting their main focus, related research questions and corresponding objectives.

Paper	Title	Relevant RQ	Related objective
I	Safety Improvements for High-Speed Planing Craft Occupants: A Systematic Review	1, 2	1
II	Dynamics of Tunnelled Planing Hulls in Waves	1	2
III	High-speed craft with double interceptor system in calm water: URANS Solution	2	3
IV	Numerical investigation of transom and double interceptor systems on a high-Speed planing craft in regular waves with experimental validation	1, 2	2, 3
V	Dynamic and Occupants' Safety Improvement of an HSPC in Irregular Waves Using Interceptor Systems	1, 2	2, 3
VI	Acceleration effects in the horizontal plane on the safety assessment aboard a high-speed craft.	1, 2	2, 3

1.6 Thesis outline

This thesis is structured into five chapters, providing a comprehensive overview of the research, followed by six appended papers:

- **Chapter 1:** Introduces the thesis topic, outlining the objectives, scope, and limitations of the research. It also explains how the included papers contribute to cohesive work and shows the logical relationships between the publications and the thesis objectives.
- **Chapter 2:** Details the methodologies used throughout the thesis, including systematic review, towing tank tests, numerical simulations, and mathematical approaches employed in this thesis.
- **Chapter 3:** Presents the key findings and results of the research, emphasizing the most important outcomes.
- **Chapter 4:** Provides a discussion of the results and suggests potential directions for future research.
- **Chapter 5:** Presents the main conclusions of the thesis, summarizing the key findings in relation to the research objectives and research questions.
- **Appendix 1 [PI]:** Safety Improvements for High-Speed Planing Craft Occupants: A Systematic Review
- **Appendix 2 [PII]:** Dynamics of Tunneled Planing Hulls in Regular Waves

• **Appendix 3 [PIII]:** High-speed craft with double interceptor system in calm water URANS Solution

• **Appendix 4 [PIV]:** Numerical investigation of transom and double interceptor systems on a high-Speed planing craft in regular waves with experimental validation

• **Appendix 5 [PV]:** High-Speed Planing Craft Dynamics in Irregular Waves: Safety Improvement Using Interceptor Systems

• **Appendix 6 [PVI]:** Acceleration effects in the horizontal plane on the safety assessment aboard HSC

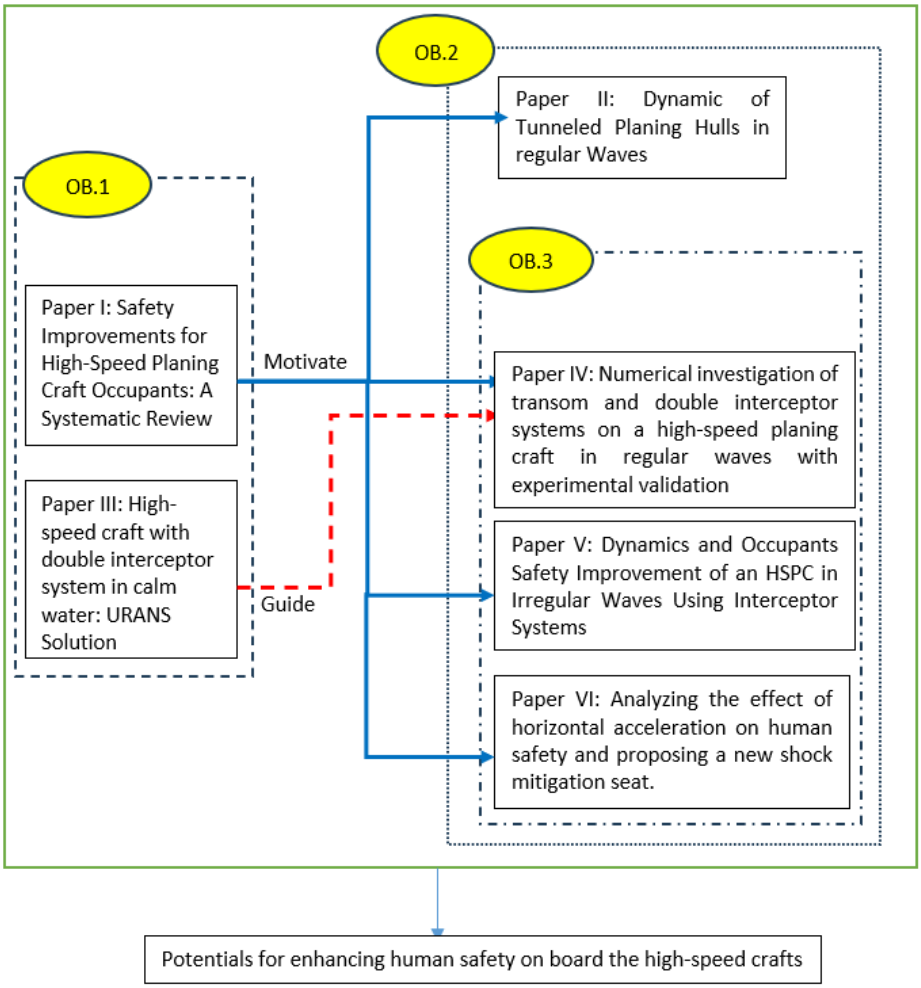


Figure 3. Logical relations between the research objectives and the publications included in this thesis.

2 Research Methods

The research methods used in this study are important for understanding how HSPC dynamics affect human safety, highlighting how motion reduction devices and suspension seats can improve safety for occupants. These methods include a systematic review incorporating meta-analysis, CFD simulations, towing tank tests, safety evaluation, and a mathematical model of the seat. These investigations provide valuable insights into different aspects of the problem, ensuring that the findings are comprehensive, reliable, and applicable for reducing safety risks for humans on board the HSPCs. Table 2 summarizes the methods used for each paper.

Table 2. Summary of the methods employed in each paper included in this thesis

Paper	Systematic review	Numerical simulations	Experimental testing	Mathematical approach	
				Safety evaluation	Seat model
I	Yes	-	-	-	-
II	-	Yes	-	-	-
III	-	Yes	-	-	-
IV	-	Yes	Yes	-	-
V	-	-	Yes	Yes	-
VI	-	-	-	Yes	Yes

The following sections provide a detailed description of the methods employed in this study and explain how each one contributes to addressing the research objectives.

2.1 Systematic review

This study begins with a comprehensive systematic review of safety improvements for HSPC occupants, as presented in Paper I. The paper reviews the literature on human safety on board HSPCs, focusing on issues associated with hull motions and accelerations in rough seas. In addition, current safety standards for humans exposed to acceleration are analyzed, and a detailed review of published documents on motion reduction devices (interceptors and trim tabs) and shock/vibration mitigation devices (shock mitigation seats) is conducted to estimate the potential for enhancing human safety on board the HSPCs.

As detailed in Paper I, the systematic review follows the revised guidelines of the Preferred Reporting Items for Systematic Reviews and Meta-Analyses (PRISMA), as proposed by Page et al. (2021). The document search process is carried out in multiple phases, using databases like Google Scholar, Scopus, and Web of Science. The search strategy for this review is shown in Figure 4.

The primary goal of this review, improving the safety of HSPC occupants, leads to defining four research questions. These questions are used to guide a search for relevant documents using various keywords across the selected databases. Further details of research questions, keywords, number of relevant documents in each database, and eligibility criteria are provided in Paper I.

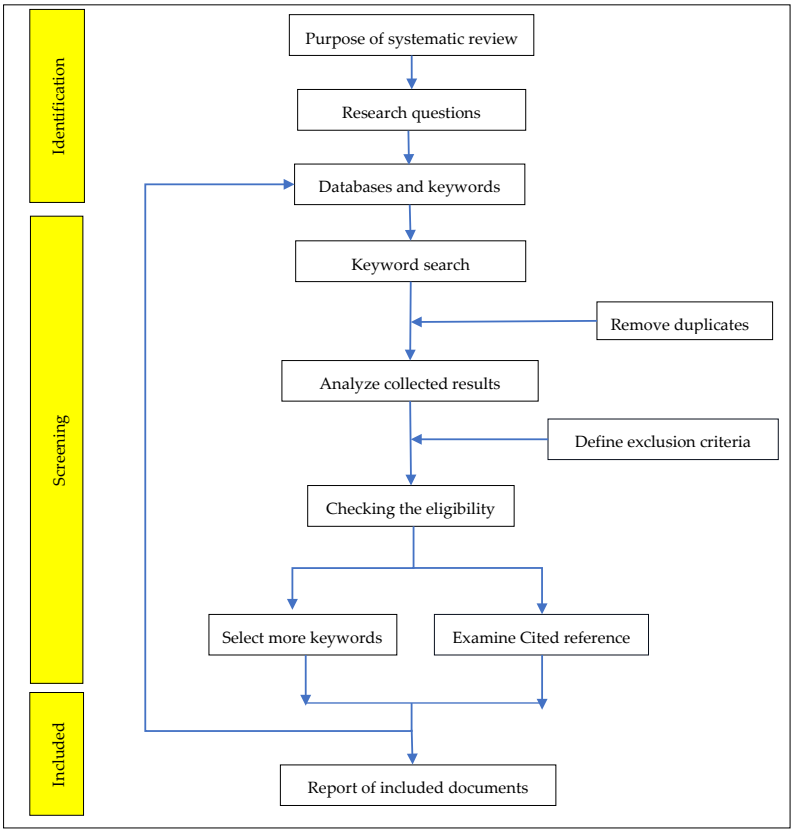


Figure 4. Search strategy in literature review. (Paper I)

This systematic review plays a crucial role in synthesizing the existing knowledge on human safety and motion reduction technologies for HSPCs to identify gaps and challenges in the current understanding, underscoring areas that require further investigation.

2.2 Numerical simulations

As summarized in Table 1, Papers II, III, and IV employ numerical approaches to address Objectives 2 and 3. Paper II investigates the dynamic behavior of a high-speed planing craft (HSPC) under different operational speeds and regular wave conditions. In addition, Paper IV investigates hull motions and acceleration reductions under regular wave conditions for three hull configurations, namely the bare hull, the TIS-equipped hull, and the DIS-equipped hull, at a constant Froude number of Fr_B = 3.0. The detailed hull geometry is presented in the corresponding papers, while the wave conditions for Papers II and IV are summarized in Tables 3 and 4, respectively.

Table 3. Regular wave properties used in Paper II.

Wave	Wave Steepness ($k_{tn}A_{tn}$) (–)	f_{tn} (Hz)	Fr_B (-)	λ/L (-)
1	0.10	1.00	3.1-3.9-4.7-5.6	0.65
2	0.07	0.80	3.1-3.9-4.7-5.6	1.0

Wave	Wave Steepness ($k_{tn}A_{tn}$) (–)	f_{tn} (Hz)	Fr_B (-)	λ/L (-)
3	0.06	0.66	3.1-3.9-4.7-5.6	1.4
4	0.06	0.57	3.1-3.9-4.7-5.6	2.0
5	0.05	0.50	3.1-3.9-4.7-5.6	2.6
6	0.04	0.44	3.1-3.9-4.7-5.6	4.3
7	0.03	0.40	3.1-3.9-4.7-5.6	4.0

Table 4. Regular wave properties used in Paper IV at Fr_B=3.0.

λ/L	K (rad/m)	TV(g/B)	H/B		
			ε=0.07	ε=0.1	ε=0.12
0.69	3.76	5.04	-	0.12	-
1	2.62	5.61	0.0546	0.17	-
1.5	1.75	6.87	0.0804	0.26	-
2	1.31	7.93	0.1072	0.35	0.417
3	0.87	9.71	0.1608	0.52	0.275
4	0.65	11.21	0.214	0.69	0.367

Additionally, Paper III presents calm water simulations to investigate the hydrodynamic performance of DIS and TIS at different hull speeds.

All numerical models in Papers II, III, and IV are developed using STAR-CCM+, a computational fluid dynamics (CFD) solver based on the Unsteady Reynolds-Averaged Navier-Stokes (URANS) equations. The fluid flow around the hull is assumed to be incompressible, homogeneous, and Newtonian. The URANS equations are formulated as follows:

$$\frac{\partial \rho}{\partial t} + \frac{\partial}{\partial x_i}(\rho u_i) = 0, \tag{1}$$

$$\frac{\partial (\rho u_i)}{\partial t} + \frac{\partial}{\partial x_j}\left(\rho u_i u_j\right) = -\frac{\partial P}{\partial x_i} + \frac{\partial}{\partial x_j}\left(\mu \frac{\partial u_i}{\partial x_j} - \rho \overline{\acute{u}_i \acute{u}_j}\right) + F_i\,, \qquad (i,j = 1,2,3) \tag{2}$$

where ρ represents the fluid density, t denotes time, μ indicates fluid viscosity, u_i and u_j refer to the velocity components, and P is pressure. In addition, F_i represents external forces.

Since HSPCs operate on the water surface, the Volume of Fluid (VOF) method is employed to capture the air–water interface. In this method, ρ and μ are defined as follows:

$$\rho_m = (1-\phi)\rho_w + \phi\rho_a, \tag{3}$$

$$\mu_m = (1-\phi)\mu_w + \phi\mu_a, \tag{4}$$

where ϕ represents the volume fraction, which varies between 0 and 1 ($\phi = 0$ for pure water, $\phi = 1$ for pure air, and $0 < \phi < 1$ for a mixture of water and air). The subscripts w and a correspond to water and air, respectively.

In numerical simulations, a computational domain is generated around the hull, as shown in Figure 5. The hull motions in heave and pitch, representing two degrees of freedom are modelled using DFBI morphing (discussed in Paper II). The defined boundary conditions for the computational domain are presented in Table 5.

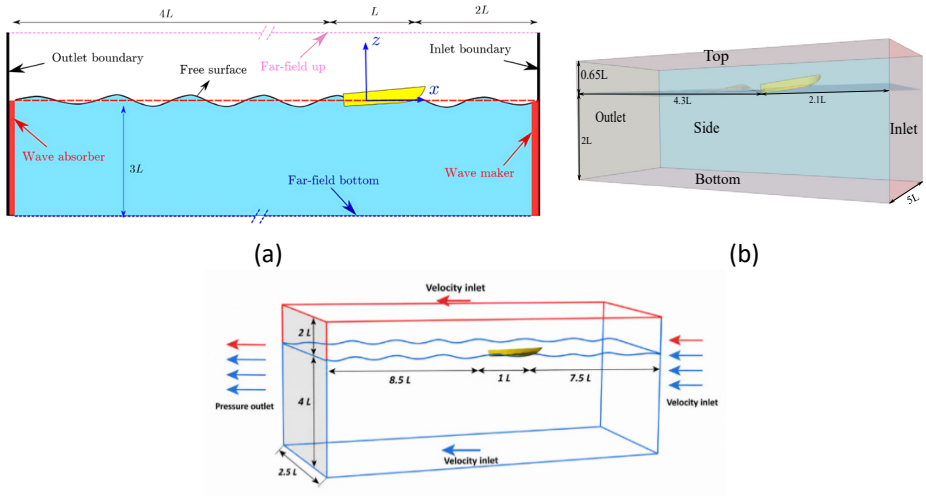
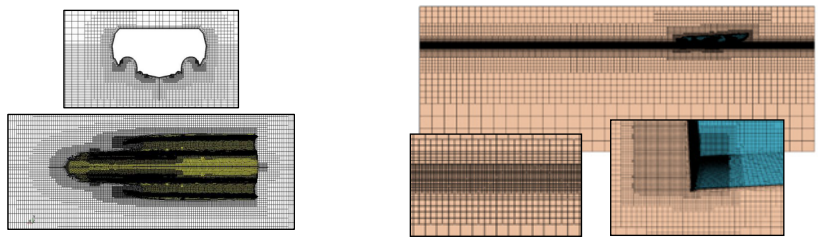


Figure 5. Computational domains used for numerical simulations in a) Paper II and b) Paper III, and c) Paper IV.

Table 5. Boundary conditions used in Papers II, III, and IV.

Boundary	**Condition**
Inlet	Velocity inlet
Outlet	Pressure outlet
Right side	Symmetry plane
Left side	Velocity inlet
Top	Velocity inlet
Bottom	Velocity inlet

Afterward, a 3D mesh is generated within the computational domain and over the hull surface to solve the governing flow and motion equations within each computational cell over time. Figure 6 shows the mesh structure used in Papers II, III, and IV. This mesh consists of a surface mesh over the hull and computational domain. The cell size increases as the distance from the hull increases. Additionally, six prism layers are generated around the hull to accurately resolve the boundary layer and the interaction between the hull and the surrounding flow.



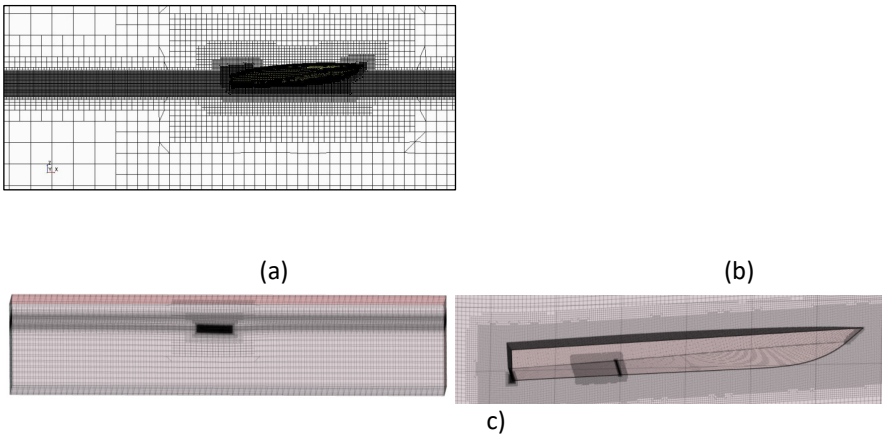


Figure 6. Mesh structure in the computational domain: a) Paper II, b) Paper III and c) Paper IV.

As shown in Figure 6, a trimmer mesh is generated around the free surface region to accurately capture the air and water interface and surface elevation.

To ensure that predicted heave and pitch motions are independent of mesh resolution, a mesh independence study is conducted using different grid resolutions in Papers II, III and IV. Figure 7 presents the results of the mesh independence studies for Paper II and Paper III (bare hull). As shown in Figure 7(a) and 7(b), the predicted heave and pitch responses converge towards the experimental results for a mesh containing 1.05 million cells. Similarly, the trim angle and resistance obtained in the simulations for Paper III show mesh convergence at approximately 1.04 million cells. At this mesh resolution, the error in the trim angle is 2.97%, while the resistance is underpredicted by 7.76% compared with the experimental measurement (Figures 7(c) and 7(d), respectively). Although the numerical results show convergence with respect to mesh refinement, a discrepancy remains between the predicted and measured resistance. This difference may be related to uncertainties in numerical modelling, including the turbulence model, the prediction of viscous and free-surface effects, and differences between the numerical and experimental conditions. Therefore, mesh convergence does not necessarily imply complete agreement with experimental data. Further details of the mesh independence study for HSPC simulations with DIS in calm water are provided in Paper III. Moreover, the mesh independence study for HSPC simulations with TIS and DIS under regular wave conditions is presented in Paper IV.

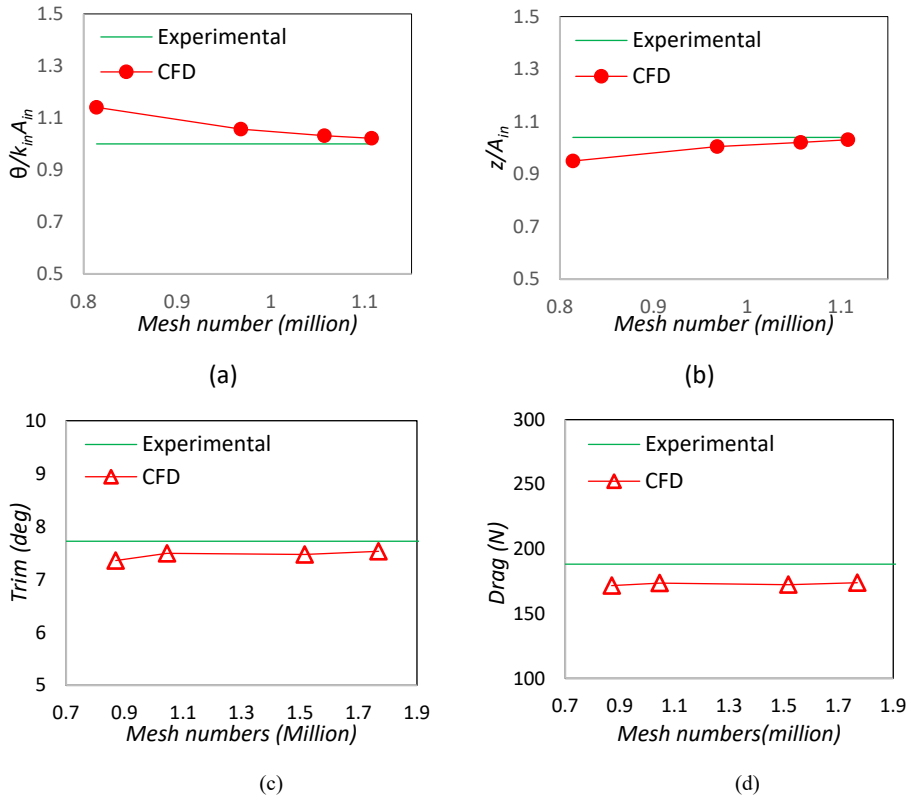


Figure 7. Mesh convergence study for: a) Pitch and b) Heave under λ/L= 2 at Fr_B = 4.7 (Paper II), and c) trim and d) Resistance for the bare hull in calm water in Paper III.

The accuracy of numerical results is evaluated by comparing them with experimental data. Since no experimental data are available for the hull model studied in Paper II under wave conditions, a similar hull form (another tunneled planing hull) is selected as a validation. A numerical simulation is performed using the same numerical setup, and heave and pitch motions results are compared with the available experimental data, as shown in Figure 8.

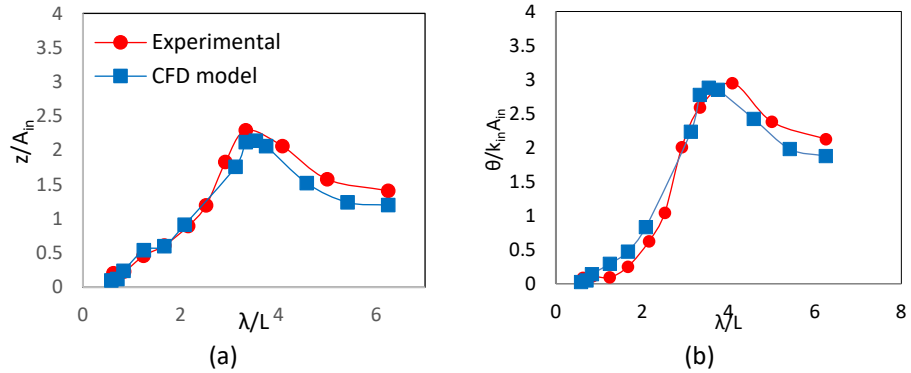


Figure 8. Validation of HSPC a) Heave and b) pitch motions in regular wave conditions (Paper II).

Further details of validation for tunneled planing hull simulations in both calm water and wave conditions are provided in Paper II.

In Paper III, the validation process involves comparing the trim angle and hull resistance with experimental measurements for the bare hull and the hull with DIS. Figure 9 presents the validation results for the bare hull.

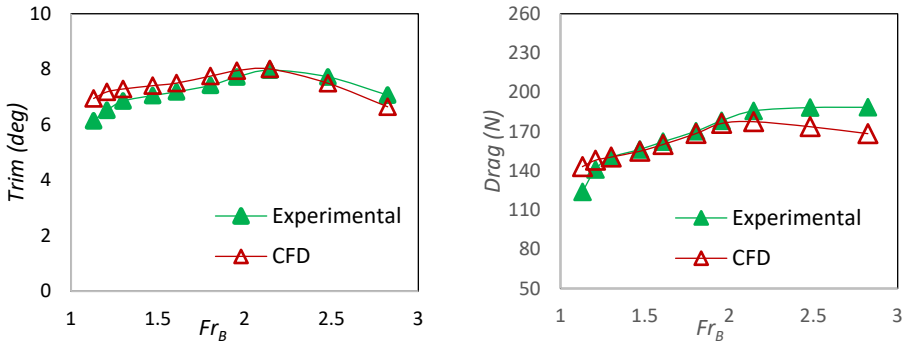
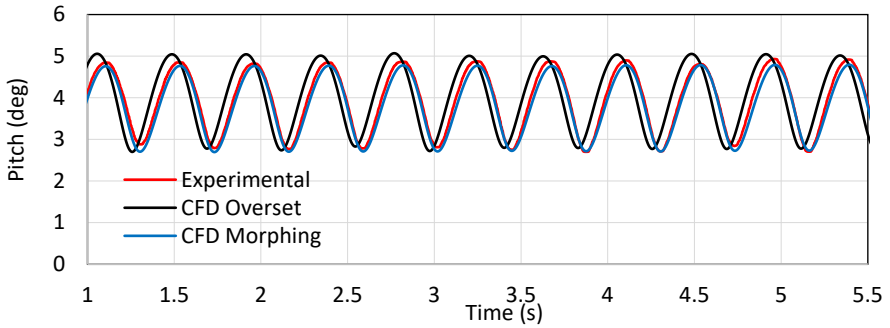


Figure 9. Validation of a) trim angle and b) resistance of the bare hull (Paper III).

Validation results for the hull with two DIS configurations, along with error details, are discussed in Paper III.

The validation study in Paper IV evaluates the numerical model under regular wave conditions for the bare hull, TIS-equipped hull, and DIS-equipped hull configurations. The validation is performed by comparing the time histories of hull heave, pitch, and vertical acceleration obtained from numerical simulations with the corresponding experimental measurements. A sample time series comparison of pitch motions is presented in Figure 10.



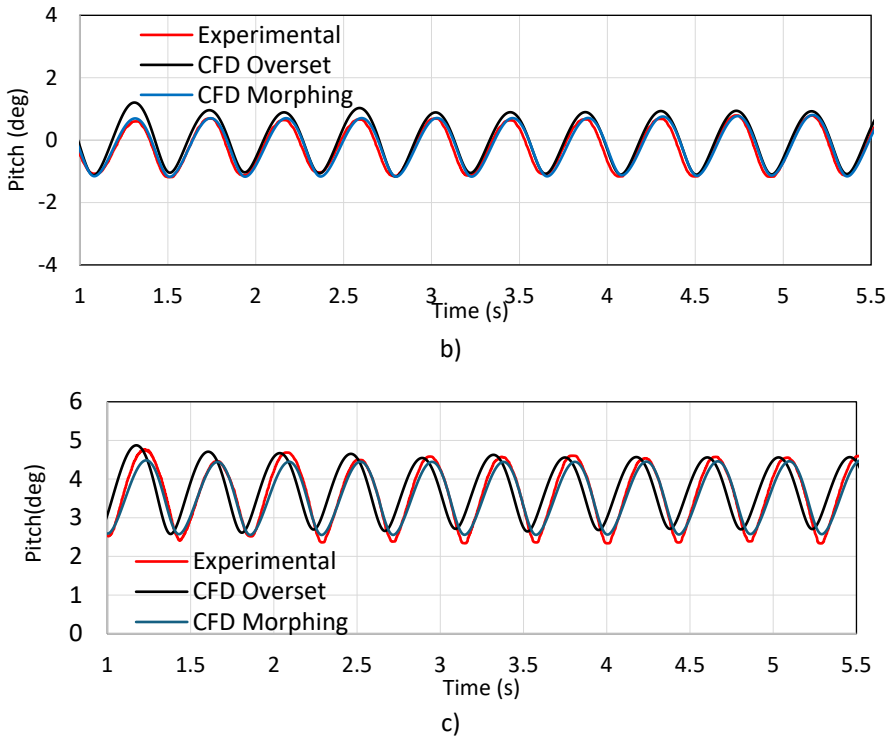


Figure 10. Experimental and CFD time histories of pitch motion for a) bare hull, b) TIS-equipped hull, c) DIS-equipped hull in regular waves (Paper IV).

In Paper IV, the RAOs of the bare hull, TIS-equipped hull, and DIS-equipped hull are also compared to further assess the capability of the numerical model in predicting frequency-dependent motion responses.

2.3 Experimental testing

Experimental tests are conducted to investigate the dynamic performance of an HSPC under a single regular wave at Fr=3.0 in Paper IV and under various irregular wave conditions and operational speeds in Paper V. During these experiments, a high-speed planing craft (HSPC), designated as Model C5, is tested to measure hull motions, vertical acceleration, and resistance to assess acceleration exposure and associated human safety aspects according to relevant safety standards. In addition, the potential for improving HSPC seakeeping performance and reducing the likelihood of adverse health effects is analyzed by testing different interceptor configurations across various wave conditions and hull speeds. The details of these experimental investigations are provided in Papers IV and V.

The experiments are carried out at the Department of Industrial Engineering (DII) of the Università degli Studi di Napoli “Federico II”, in a towing tank that measures 136.0 m in length, 9.0 m in width, and 4.5 m in depth. The tank is equipped with a carriage capable of reaching a maximum speed of 10.0 m/s.

In Paper IV, the bare hull, TIS-equipped hull and DIS-equipped hull are tested under regular head waves with a wave amplitude of 0.03 m and a period of 1.51 s at FrB = 3.0 to provide a validation case for the numerical model. Furthermore, towing tank tests are

conducted under three irregular wave conditions and four forward speeds corresponding to semi-planing, transient, and planing regimes. An overview of the test runs is provided in Table 6, while details of hull characteristics are available in Paper V.

Table 6. Towing tank test matrix for irregular wave conditions (Paper V).

Hull model	Wave conditions					Fr_B
	Wave condition	Spectrum	H_s (m)	γ	T_p (s)	
Bare hull	1	JONSWAP	0.075	3.3	1.52	1.2-1.7-2.2-3.0
	2	JONSWAP	0.060	3.3	1.356	1.2-1.7-2.2
	3	JONSWAP	0.045	3.3	1.176	1.2-2.2
TIS ($0.5B_{WL}$)	1	JONSWAP	0.075	3.3	1.52	1.7-2.2
	2	JONSWAP	0.060	3.3	1.356	1.7-2.2
TIS ($0.25B_{WL}$)	1	JONSWAP	0.075	3.3	1.52	3.0
Hull with DIS	1	JONSWAP	0.075	3.3	1.52	3.0

As shown in Table 6, three irregular wave conditions based on JONSWAP spectra are used in the experiments. To validate the accuracy of wave generation, wave elevations are recorded using capacitive wave probes and compared with the corresponding theoretical spectra. Figure 11 presents the comparison between the generated wave spectra and the target JONSWAP spectra.

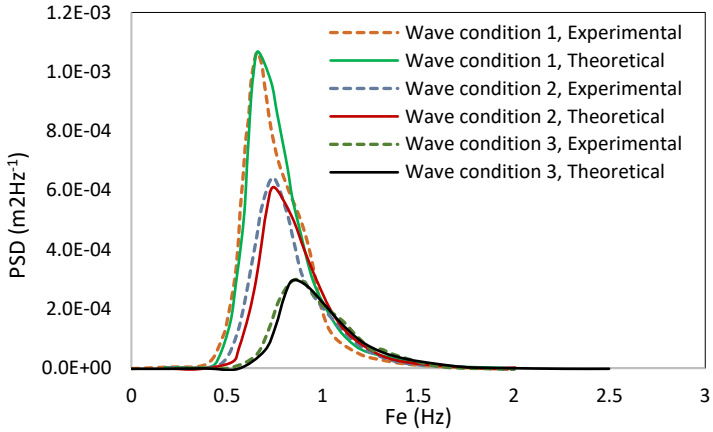


Figure 11. Generated wave spectra and theoretical JONSWAP wave spectra (Paper IV).

During all experimental tests, the hull is towed by the carriage and is free to move vertically (heave) and rotate around the transverse axis (pitch). Total resistance, heave and pitch motions, and vertical accelerations at both center of gravity (CG) and bow are measured. The measurement system and data acquisition setup are described in detail in Paper IV and V.

To ensure reliable statistical analyses for hull dynamics in irregular waves, a large number of repeated tests, typically 15 or more, are conducted, resulting in approximately 200 wave encounters per condition. The total duration of the repeated tests is approximately 250 seconds. Wave generation is initiated at different times to introduce

variability between repeated runs, while the wave sequences are generated using a fixed random seed in the time domain. Data is sampled at 500 Hz and processed using a Butterworth bandpass filter with a cutoff range of 0.05 to 20 Hz. Wave signals are synthesized using 256 (2^8) Fourier components to ensure adequate spectral resolution.

After the tests on the bare hull (as outlined in Table 5) are completed, a transom interceptor system with a length of 0.5 B_{WL} and a height of 2.0 mm is installed to assess the performance of TIS at transient speeds. The resulting motions and accelerations are compared with those of the bare hull to evaluate the effectiveness of TIS in improving seakeeping performance and reducing human safety risk caused by motion and acceleration.

To further investigate the TIS effectiveness in planing mode is compared with the Double Interceptor System (DIS). The DIS configuration includes a transom interceptor with a length of 0.5 B_{WL} and a height of 2 mm, and a forward interceptor located 0.8 L_{WL} from the transom with a length of B_{WL} and a height of 2.0 mm. However, calm water tests revealed that this configuration caused excessive bow-down pitching moment, resulting in negative trim angles. Consequently, the length of the transom interceptor is reduced to 0.25 B_{WL} to avoid overcorrection. The planing-mode tests were then repeated with the adjusted DIS setup.

In the final step, after completing the DIS tests, the forward interceptor is removed and the tests are repeated using only the transom interceptor system (length = 0.25 B_{WL}, height = 2.0 mm).

To analyze the efficiency of TIS and DIS in improving HSPC seakeeping, the highest significant amplitude of heave motions ($H_{1/3}$, $H_{1/10}$, and $H_{1/100}$), pitch motions ($\theta_{1/3}$, $\theta_{1/10}$, and $\theta_{1/100}$), and vertical acceleration in CG and bow ($a_{1/3}$, $a_{1/10}$, and $a_{1/100}$) are compared with those of the bare hull. Additionally, to assess the reliability of measured responses, a statistical uncertainty analysis is performed following ITTC Recommended Procedures 7.5-02-01-01.

The mean values of significant hull motions and accelerations, together with their uncertainties, are calculated using the following equation:

$$\bar{q} = \frac{1}{N}\sum_{t=0}^{T} q(t) \tag{5}$$

where $\bar{q}$ is the mean value of the highest *1/n* significant responses, *N* is the number of data points within the highest *1/n* portion of the data (e.g., *1/3*, *1/10,* or *1/100*), *T* is the measurement time, and *q(t)* represents a time series of a uniformly sampled quantity (e.g., heave, pitch, or acceleration) within the top *1/n* subset. Furthermore, the standard deviation of *q* is calculated as:

$$S = \sqrt{\frac{1}{N-1}\sum_{t=0}^{T}(q(t) - \bar{q})^2} \tag{6}$$

where *S* is the standard deviation of the selected data subset. Then, the standard uncertainty is estimated using:

$$u(\bar{q}) = \frac{S}{\sqrt{N}} \tag{7}$$

To account for a 95% confidence interval, the uncertainty is expressed as follows:

$$\bar{q} \pm 1.96.\, u(\bar{q}) \tag{8}$$

2.4 Mathematical approach

This study uses mathematical methods in Papers IV and V to evaluate the effect of HSPC accelerations on human safety and to simulate a shock mitigation seat to predict its performance in reducing safety risks. All of these models are developed in Python.

2.4.1 Mathematical model for safety evaluation

The safety evaluation for a human exposed to accelerations is performed based on ISO 2631-1:1997, ISO 2631-5:2004, and the EU Directive 2002/44/EC. It aligns with objectives 2 and 3, which aim to investigate the effects of hull dynamics on human safety on board HSPCs and analyse safety improvement strategies.

These standards define limits for vibration and shock exposure to avoid adverse health effects and discomfort. The primary measures used to assess human safety are Root Mean Square (RMS) and Vibration Dose Value (VDV) of acceleration, calculated using the following equations:

$$a_w = \left\{\frac{1}{T}\int_0^T a_w^2(t)dt\right\}^{1/2} \quad (9)$$

$$VDV = \left\{\int_0^T [a_w(t)]^4 dt\right\}^{\frac{1}{4}} \quad (10)$$

here, $a_w(t)$ refers to the frequency-weighted acceleration in each direction, and T is the measurement time. Figure 12 presents the process for evaluating human safety regarding RMS and VDV values as suggested by different guidance. In this figure, CF represents the maximum weighted acceleration divided by the RMS.

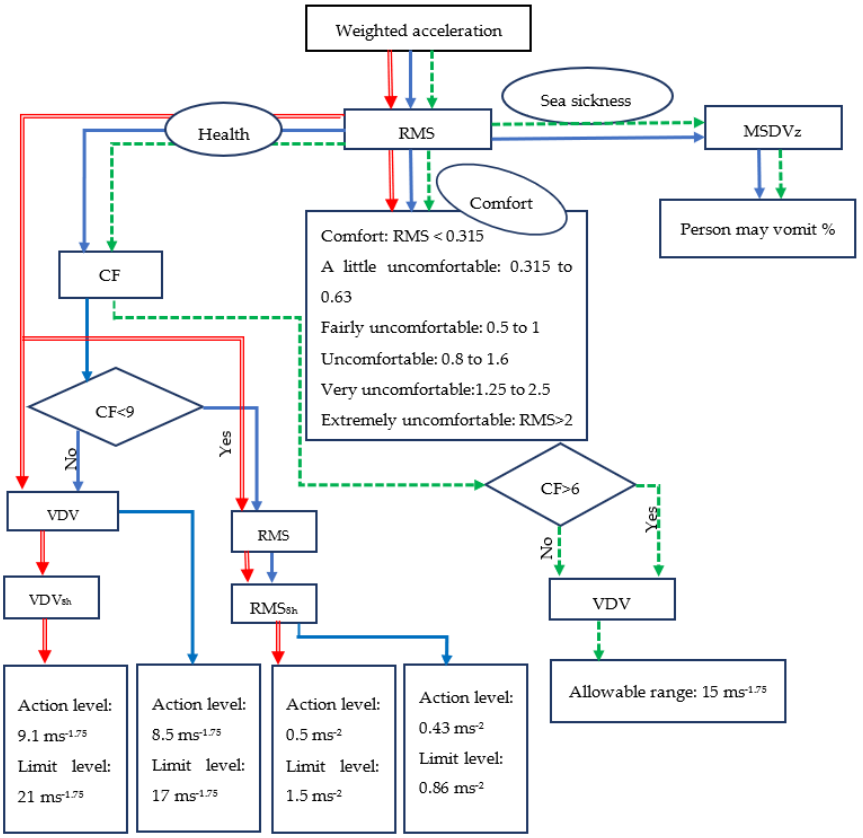


Figure 12. Safety evaluation methods according to the standards: the blue line represents ISO 2631-1:1997, the green dashed line represents BS 6841:1987, and the red double line represents Directive 2002/44 (Paper I).

A detailed analysis of the safety evaluation for humans exposed to multidirectional accelerations is provided in Paper VI. In Paper VI, the influence of forward, sideways, and vertical accelerations of an HSPC on human safety is analysed by employing recorded accelerations from Garme et al. (2011). Furthermore, safety assessments are conducted to evaluate the performance of a shock mitigation seat in minimizing RMS and VDV in the forward and vertical directions, consequently reducing the likelihood of adverse health risks for seated occupants (Paper VI).

Moreover, in Paper V, this method is applied to an experimental HSPC by analysing the measured acceleration for three configurations at different speeds: bare hull, TIS-equipped hull, and DIS-equipped hull. This analysis aims to investigate the effectiveness of interceptor systems in enhancing human safety.

Paper V also utilizes ISO 2631-5:2004 guidance to predict the potential influence of interceptor systems in reducing long-term adverse health effects. According to ISO 2631-5:2004, if S_{ed} exceeds 0.8 MPa, there is a high probability of health risks. S_{ed} is calculated using the following equations:

$$S_{ed} = \left[\sum_k (m_k D_k)^6 \frac{t_d}{T}\right]^{1/6} \quad (11)$$

$$D_k = (\sum_k A_{ik}^6)^{1/6} \quad (12)$$

where m_k is the weighting factor in k-directions, with ISO 2631-5 recommending values of m_x= 0.015MPa/(m/s^2), m_y= 0.035MPa/(m/s^2), and m_z= 0.032 MPa/(m/s^2). T represents measurement time, and t_d denotes the duration of daily work. Moreover, D_k is the acceleration dose, and A_{ik} is the *i-th* peak of the response acceleration.

2.4.2 Mathematical model for shock mitigation seat performance

One of the effective safety improvement strategies for enhancing human safety on board HSPCs is the use of shock mitigation seats. A shock mitigation seat is a mass-spring-damping system designed to reduce transmitted vibrations and shocks to the seated occupant. There are three methods for evaluating the performance of shock mitigation seats: sea trials, drop tower tests, and mathematical modelling. Given the available resources, this study utilizes mathematical modelling as a cost-effective and time-efficient approach to investigate shock mitigation seat performance for achieving research objective 3.

For this modelling approach, recorded acceleration data from an HSPC operating in 12 sea trial tests, each lasting approximately 10 minutes, are used. During these tests, the HSPC operated at a speed of 25.7 m/s, and hull acceleration was measured by Garme et al. (2011) using three accelerometers. Two accelerometers were mounted on the deck at different longitudinal positions to record vertical acceleration, while a third accelerometer was positioned on the seat cushion to measure vertical, forward, and sideways accelerations. Figure 13 shows the positions of the accelerometers on the hull.

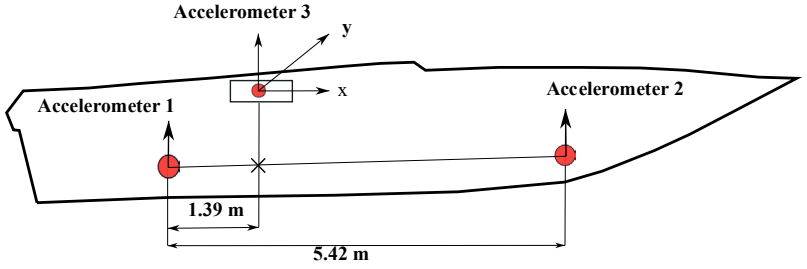


Figure 13. Location of each accelerometer on the hull (Paper VI).

Investigating the shock mitigation performance requires a comparison between seat base and seat cushion acceleration. Therefore, recorded acceleration data from accelerometers 1 and 2 are used to calculate vertical acceleration at the seat base using equation 13.

$$a_{z,base} = a_1 + 1.39.\frac{a_2 - a_1}{5.42} \quad (13)$$

a_1 and a_2 represent the vertical accelerations recorded by accelerometers 1 and 2, respectively. Since there is no acceleration mitigation system in the forward direction for the reference seat, and measurement data at the seat base in this direction are unavailable, it is assumed that the measured forward acceleration on the seat cushion is equal to that at the seat base.

Furthermore, a mathematical model is developed to analyse the performance of the shock mitigation seat. Figure 14 presents a schematic of the modelled seat, which incorporates both vertical and forward suspension systems. This seat is influenced by seat base (deck) vertical and forward acceleration, and the equations of motion for the seat can be expressed as

$$m\ddot{x}_r + K_2.x_r + C_2.\dot{x}_r = -m\ddot{x}_b \quad (14)$$

$$m\ddot{z}_r + K_1.z_r + C_1\dot{z}_r = -m\ddot{z}_b \quad (15)$$

All variables and parameters are defined in Table 7.

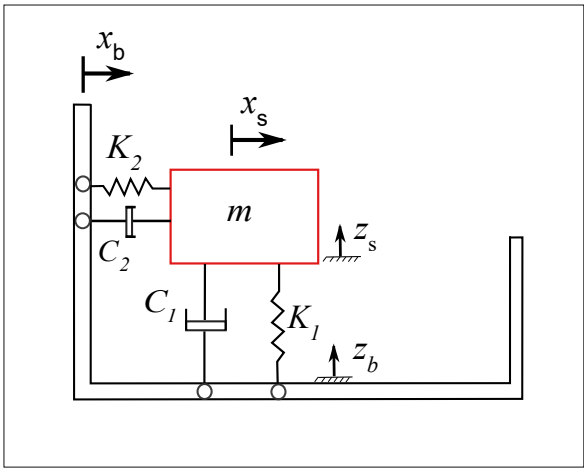


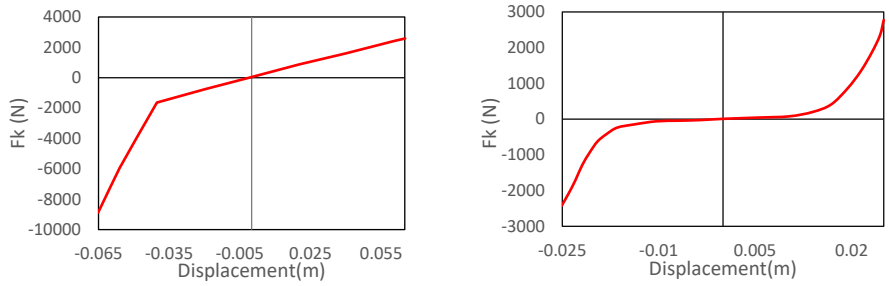
Figure 14. Schematic of the seat model and free body diagram (Paper VI).

Table 7. Definition and values of parameters used in the shock mitigation seat model (Paper VI).

parameter	definition	value
m	Mass (Seat+ Human thighs and upper body)	107.5 (Kg)
$\ddot{x}_r$	Relative forward accelerations of the seat	Variable
$\ddot{z}_r$	Relative vertical accelerations of the seat	variable
$\dot{x}_r$	Relative forward velocity of seat	Variable
$\dot{z}_r$	Relative vertical velocity of seat	Variable
x_r	Seat relative displacements in the forward direction	Variable
z_r	Seat relative displacements in the vertical direction	Variable
$\ddot{x}_b$	Forward acceleration at the seat (assumed equal to the seat base acceleration; not directly measured)	Measured in sea trial
$\ddot{z}_b$	Vertical acceleration on seat base	Measured in sea trial
K_1	Vertical Spring stiffness coefficient	Nonlinear, see Fig 15 a)
K_2	Horizontal Spring stiffness coefficient	Nonlinear, see Fig 15 b)

parameter	definition	value
C_1	Vertical damping coefficient	2200 Ns/m
C_2	Horizontal damping coefficient	1564.88 Ns/m

It is assumed that the seated human has a total mass of 85 kg, with the upper body accounting for 72.3% of the total weight (61.4 kg) and the thighs contributing 9.5% (8.1 kg) (see Olausson and Garme 2015). The nonlinear stiffness characteristics of the seat's vertical and forward suspension systems are shown in Figure 15.



a b

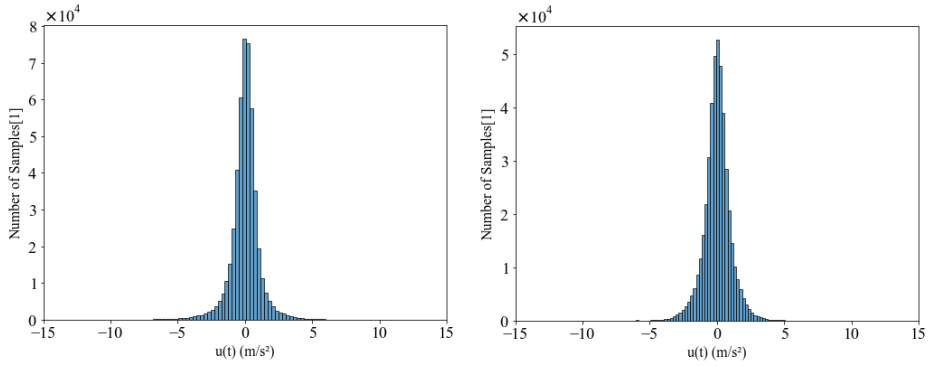
Figure 15. Nonlinear spring characteristics: a) Vertical direction (Olausson and Garme, 2015), and b) Forward direction (Stein and Múčka, 2011) (Paper V).

Equations (14) and (15) are solved numerically using the Runge-Kutta method in Python. A detailed description of the numerical implementation is provided in Paper VI.

To validate the seat model, the computed vertical acceleration on the seat cushion is compared with the recorded acceleration from the 12 sea trial tests (Garme et al., 2011). The difference between the model and the experimental vertical acceleration at each time step is calculated as

$$u(t) = \ddot{z}_1(t) - \ddot{z}_{1,exp}(t) \tag{16}$$

where $\ddot{z}_1(t)$ and $\ddot{z}_{1,exp}(t)$ represent computed vertical acceleration of the seat model and recorded accelerations on the seat cushion. The distribution of the difference between acceleration on the seat model and the experimental seat in test runs 2 and 3 is presented in Figure 16. The difference is predominantly centred around zero, indicating a strong agreement between the mathematical model and experimental results.



a b

Figure 16. Distribution of difference u(t) for a) test run 2, and b) test run 3 (Paper V).

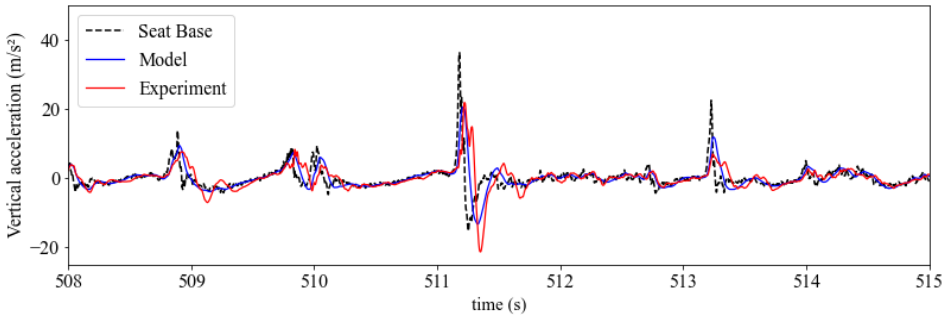


Figure 17. Computed and measured time history of vertical accelerations in test run 1.

Furthermore, the calculated RMS_z and $VDVz_{,8h}$ for the seat model are compared with the measured acceleration on the experiment seat, as shown in Figure 18. Detailed differences and comparisons are provided in Paper VI.

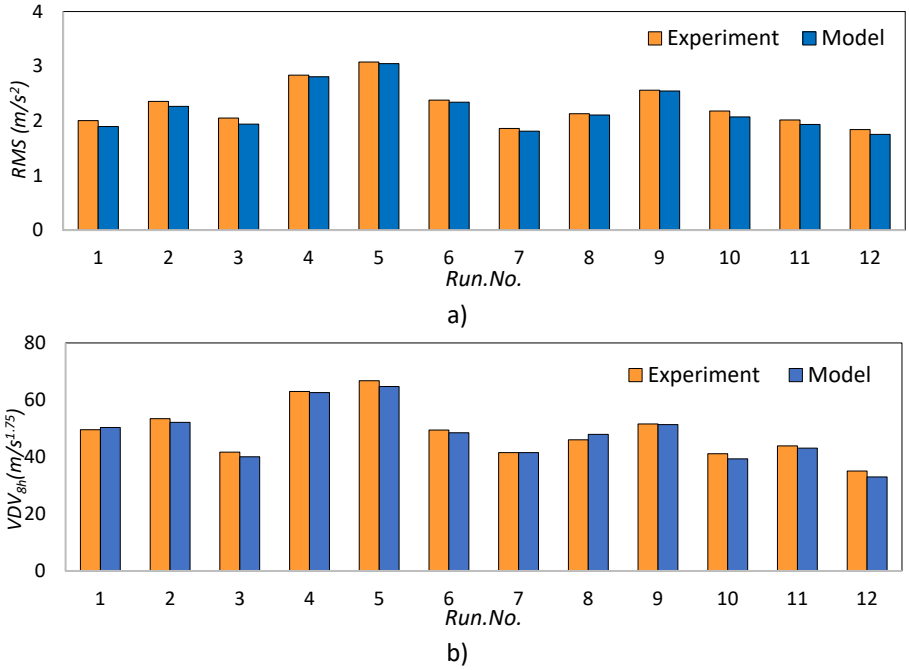


Figure 18. a) RMS_z and b) $VDV_{z,8h}$ of vertical acceleration on seat model and experiment seat (Paper VI).

The current difference in obtained results might be attributed to several simplifications and assumptions made in the model, such as neglecting the effects of the seat backrest, seatbelt, footrest, and assuming damping coefficients linear.

Previous studies on suspension seats for HSPC have predominantly focused on vertical acceleration, while horizontal acceleration has received comparatively limited attention. The systematic review conducted in this thesis, together with an evaluation of the measured forward and vertical acceleration in Paper VI, indicates that forward

acceleration can has important effects on occupant health risks and comfort and should also be considered in shock mitigation seat modelling. Therefore, as an initial modelling approach to investigate the potential for reducing forward acceleration, a simple shock mitigation seat with forward and vertical suspension systems was adopted. This simplified approach provides a tractable framework for examining the transmission and potential reduction of acceleration in each direction, without attempting to reproduce the complete biomechanical behaviour of a seated occupant.

The mathematical model provides a cost-effective and time-efficient approach for investigating shock mitigation seat performance under realistic acceleration inputs. The comparison with sea trial data provides a benchmark for the model's vertical response. However, because forward acceleration at the seat base was not directly measured and was instead assumed to be equal to the measured seat-cushion acceleration, the forward-direction results should be interpreted as conceptual predictions rather than experimentally validated results. Therefore, the model provides an initial framework for investigating the potential reduction of forward acceleration and for informing future shock mitigation seat development and optimization.

3 Results

This chapter presents the main findings of the research derived on six papers, each addressing one or more research objectives, as detailed in Table 1. The full manuscripts of these papers are provided in the Appendices.

First, the findings from the systematic review are presented, highlighting the human safety risks associated with acceleration exposure aboard HSPCs, current safety standards, and existing safety improvement strategies.

The numerical investigations provide insights into HSPC dynamic responses under different wave and operational conditions, as well as the influence of interceptor configurations on hydrodynamic performance.

The experimental results obtained from towing tank tests demonstrate the effects of wave conditions, operational speeds, and interceptor configurations on HSPC motions, accelerations, and occupant safety indicators.

Human safety assessment results based on relevant standards are presented, together with the predicted performance of a shock mitigation seat in reducing transmitted accelerations to seated occupants. In addition, a mathematical model of a shock mitigation seat is developed to predict its performance in reducing the acceleration transmitted to the seated occupant in vertical and forward directions and enhance human safety.

3.1 Human safety risks associated with HSPC operations

The assessment of human safety risks associated with HSPC operations, addressing Objectives 1 and 2, begins with the findings of Paper I. This paper summarizes previous investigations on safety evaluation of HSPC occupants, including reported acceleration levels and associated human safety criteria, as presented in Table 8.

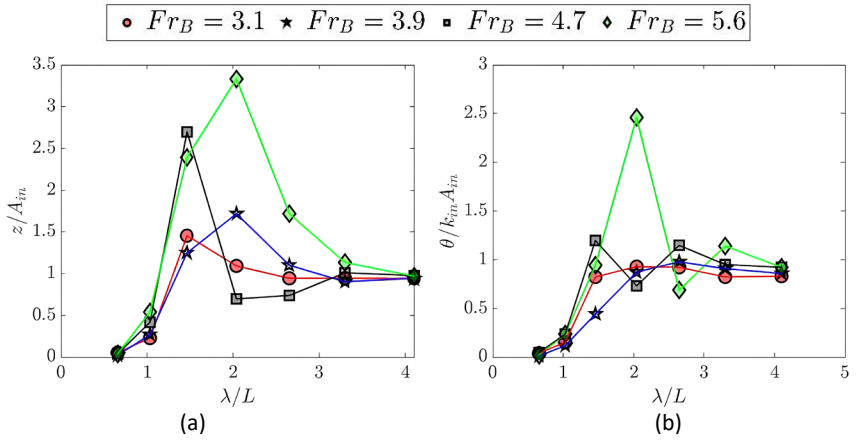
Table 8. Summary of previous studies on safety evaluation of HSPCs (Paper I).

Speed (m/s)	Sea state	RMS_z (m/s^2)	$VDV_{z,8h}$ ($m/s^{1.75}$)	$S_{ed\text{-}8h}$ (MPa)	Reference
7.72 to 10.3	1	-	62.03	-	Allen et al. (2008)
	2	-	35.15	-	
20.57	-	2.0	51	-	Dobbins et al. (2008)
25.7	1	1.9	65.2	5.7	Garme et al. (2011)
	2	2.2	63.1	4.2	
	3	1.9	49.5	3.8	
	4	2.8	79	6.3	
	5	3	81	6.1	
15.0	1	4.9	-	-	Taunton et al. (2011)
	2	8.5	-	-	
	3	9.4	-	-	
	4	7.7	-	-	
	5	4.9	-	-	
12.9	403	1.92	-	-	Folsø (2004)
	411	1.73	-	-	
15.4	404	2.35	-	-	
18.0	405	0.85	-	-	
	410	1.87	-	-	
	416	0.55	-	-	

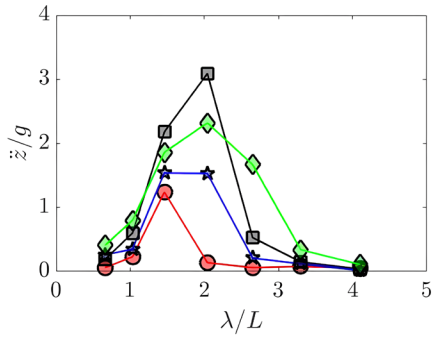
RMSz values reported in the reviewed studies correspond to the “very uncomfortable” to “extremely uncomfortable” categories. Moreover, RMS_z values in all reviewed studies are in the range of the "very uncomfortable" to "extremely uncomfortable" categories for humans. Similarly, the S_{ed} values reported by Garme et al. (2011) reveal a high prevalence of long-term adverse health effects due to HSPC accelerations. Additional results for other sea states can be found in Garme et al. (2011) and Taunton et al. (2011). According to these results, the vertical acceleration in all examined HSPCs exceeds the safe ranges suggested by standards. Therefore, these findings highlight the need for effective strategies to reduce acceleration exposure and improve occupant safety on board HSPCs. However, it should be considered that these safety assessment studies are conducted at high speeds and during the planing mode of operation.

Although previous studies demonstrate the severity of acceleration exposure during HSPC operation, the influence of operational conditions on the generation of excessive motions and accelerations requires further investigation. Therefore, Paper II investigates the effect of hull speed and wave characteristics on HSPC dynamics through numerical simulations.

Hull operating speed has a significant effect on hull motion and acceleration and, consequently, occupant safety. Therefore, the effect of operational speed on hull motion and acceleration in regular waves is investigated in Paper II through numerical simulations. In this study, a tunnelled high-speed planing hull is numerically investigated at four different speeds across three regular wave conditions, as presented in Section 2.2. The RAOs of hull motions and vertical accelerations are presented in Figure 19.



(a) (b)



(c)

Figure 19. Non-dimensional a) heave, b) pitch, and c) vertical acceleration of an HSPC at various speeds under different regular wave conditions (Paper II).

According to Figure 19, although hull speed has no significant effect on hull motions and accelerations when the wavelength is significantly longer or shorter than the hull length, it has a pronounced effect at critical wavelengths (when the wavelength is approximately 1.5 to 2.5 times the hull length). Once an HSPC operates at high speeds within this critical wavelength range, a "fly-over" phenomenon can occur, resulting in severe vertical impact acceleration.

The “fly-over” phenomenon occurs when an HSPC operates in rough head seas, partially loses contact with the water surface and subsequently impacts the water surface after a short airborne period. Figure 12 of Paper II shows resistance approaching zero during fly-over, together with vertical acceleration approaching −g. This indicates negligible water-related resistance; aerodynamic drag may persist on exposed hull surfaces. Separate air- and water-resistance contributions were not quantified. Then, the hull impacts the water surface with severe vertical acceleration, posing serious safety risks to on board crews. The snapshots of the vessel’s position relative to the water surface and volume fraction at different speeds are presented in Figure 20 to visualize the fly-over phenomenon that occurs at high speeds for a tunneled planing hull (Paper II). Similarly, Paper IV demonstrates the occurrence of the fly-over phenomenon for the C5 hull model under a critical regular wave condition at Fr_B = 3.0, as shown in Figure 21.

Fr				
3.1	$t = T/4$	$t = T/2$	$t = 3T/4$	$t = T$
3.9	$t = T/4$	$t = T/2$	$t = 3T/4$	$t = T$
	$t = T/8$	$t = T/4$	$t = 3T/8$	$t = T/2$

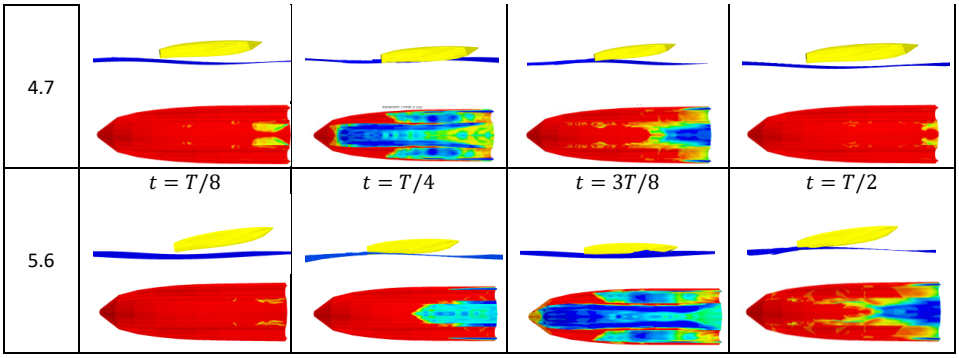


Figure 20. Snapshots of the hull position to the water surface and volume fraction at different speeds corresponding to the wavelengths of 2L (Paper II).

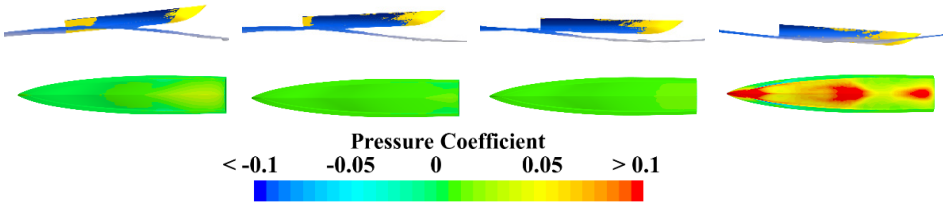


Figure 21. Fly-over phenomenon for the bare hull under the critical wave condition ε = 0.12 and λ/L = 3 (Paper IV).

Paper II highlights the importance of managing hull speed when operating in critical wave conditions to reduce human safety risks associated with severe impact shocks. Reducing hull speed in these waves helps reduce human safety risks; however, it may hinder the primary mission capabilities of HSPCs, which rely on high-speed performance. However, it should be considered that real sea conditions consist of irregular waves with various wavelengths, while this study indicates that for waves significantly longer or shorter than the critical wavelength, hull speed has no significant effect on hull motions and acceleration.

Since real operational environments consist of irregular seas with a broad range of wave frequencies, the influence of speed and sea conditions on occupant safety is further investigated experimentally in irregular waves in Paper V. In Paper V, a high-speed planing hull model C5 is tested in a towing tank under various irregular wave conditions to assess the effects of hull speed and sea conditions on human safety. The wave conditions are presented in Table 5 in Section 2.3. Figure 22 presents the RMS_z, $VDV_{z,8h}$, $S_{edz,1h}$, and $S_{edz,8h}$ of the bare hull at the CG for comparison with safety standards. More details of hull heave and pitch motions can be found in Paper V.

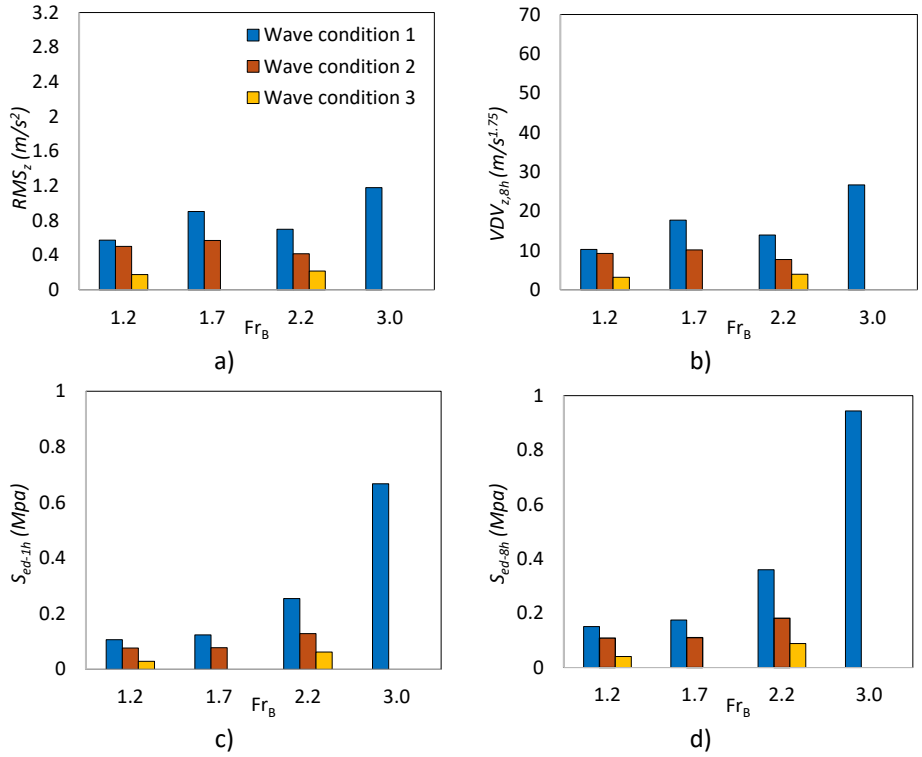


Figure 22. a) RMS_z, b) $VDV_{z,8h}$, c) $S_{ed\text{-}1h}$ and d) $S_{ed\text{-}8h}$ of a bare hull at different Froude numbers across various wave conditions (Paper V).

The RMS_z values measured at the CG indicate that increasing hull speeds from semi-planing to transient mode causes an increase in RMS_z (Fr_B = 1.2 to Fr_B = 1.7) and occupants' discomfort. However, a further increase in speed to Fr_B = 2.2 results in a reduction in RMS_z compared with Fr_B = 1.7. Furthermore, by entering the planing mode, the vertical acceleration rises significantly, causing an increase in human discomfort.

Figure 22 (b) shows that $VDV_{z,8h}$ of vertical acceleration recorded at the CG under wave condition 1 consistently exceeds the action threshold across all examined Froude numbers. It even exceeds the limit threshold at Fr_B = 3, corresponding to planing mode. Also, $VDV_{z,8h}$ is higher than the action value at Fr_B = 1.2 and 1.7 in wave condition 2, whereas wave condition 3 exhibits a lower $VDV_{z,8h}$, potentially reflecting a decreased likelihood of health issues due to lower vertical acceleration exposure.

According to ISO 2631–5:2004, for crew members aged between 20 and 65 years who operate 220 days annually, S_{ed} values exceeding 0.8 MPa indicate a high likelihood of adverse health effects, and values below 0.5 MPa suggest a low health risk. Figures 22(c) and 22(d) present the full-scale $S_{ed\text{-}1h}$ and $S_{ed\text{-}8h}$ estimates based on CG vertical accelerations for daily operations aboard this HSPC. As shown in Figures 22(c) and 22(d), both $S_{ed\text{-}1h}$ and $S_{ed\text{-}8h}$ values remain under the risk threshold during semi-planing and transient mode across wave conditions 1, 2, and 3. However, in planing mode (Fr_B = 3), $S_{ed\text{-}1h}$ rises to 0.67 MPa, and $S_{ed\text{-}8h}$ increases to 0.94 MPa, indicating a high risk of adverse health effects and highlighting the need for effective acceleration reduction strategies.

The human safety assessment is also conducted based on the recorded acceleration at the bow, as detailed in Paper V.

Besides the vertical acceleration effects on human safety, forward and sideways accelerations also play a critical role. According to Griffin (1990), various directions of shock and vibration are linked to distinct health concerns: forward impacts may compress the spinal column, sideways shocks can affect nerve pathways, potentially causing conditions like back pain or sciatica, and vertical vibration may induce disorientation effects such as the "elevator illusion". Since lumbar pain is widely recognized as a common injury among marine personnel (Ensign et al., 2000; Carvalhais, 2004; de Alwis and Garme, 2021) and can be affected by non-vertical acceleration, it becomes essential to investigate the recorded acceleration in different directions on board HSPCs and quantitatively assess their effects on human safety risk, using the current safety standards.

Therefore, Paper VI analyses hull acceleration data collected by Garme et al. (2011) in multiple directions for an HSPC operating under 12 sea states. Figure 23 presents a comparative analysis of RMS and VDV values across the various acceleration directions.

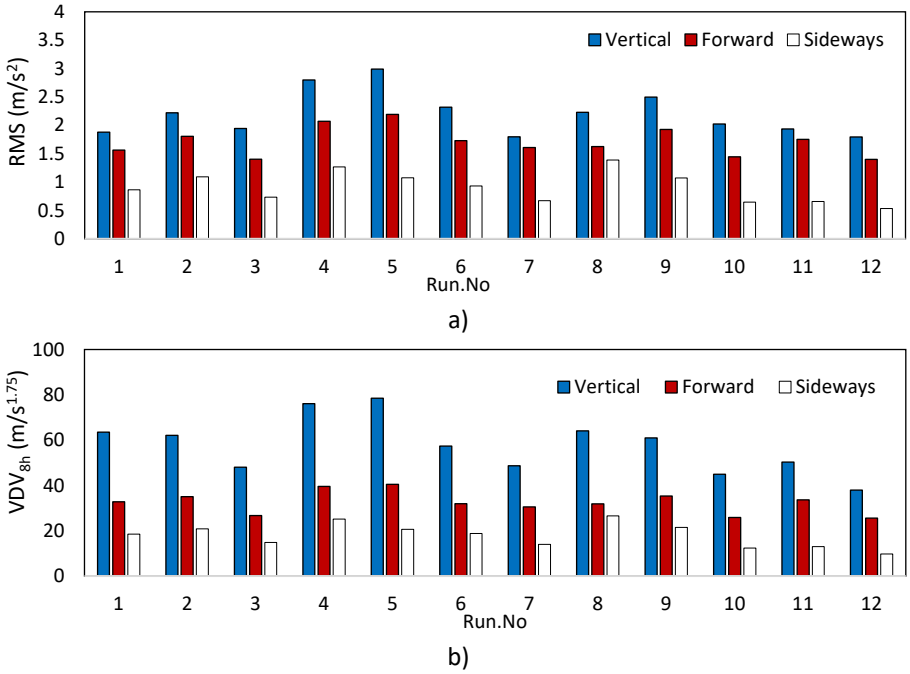


Figure 23. a) RMS and b) VDV_{8h} for different directions of acceleration in 12 sea conditions at V=25.5 m/s (Paper VI).

Across the 12 test runs, forward acceleration RMS_x values ranged from 1.4 m/s² to 2.2 m/s², corresponding to grades of “Uncomfortable” to “Extremely uncomfortable.” Sideways acceleration values varied between 0.53 m/s² and 1.4 m/s², demonstrating a comfort perception between “a little uncomfortable” and “very uncomfortable.” Meanwhile, the vertical RMS acceleration spans 1.8 m/s² to 3.0 m/s². Assuming no contribution from forward or sideways accelerations, these values represent conditions classified as “Very uncomfortable” to “Extremely uncomfortable.”

As shown in Figure 23(b), the vertical accelerations consistently exceed the recommended limit value specified in EU directive 2002/44 (21.0 $m/s^{1.75}$). These accelerations range from 37.92 to 78.5 $m/s^{1.75}$, indicating considerable potential for

negative health effects on crew members. In addition, VDV_{8h} values in the forward direction emphasize the necessity for focused strategies to reduce forward accelerations over prolonged operational durations, as they range from 25.6 to 40.5 $m/s^{1.75}$, exceeding the EU Directive 2002/44 limit value. Sideways VDV_{8h} values, which range from 9.8 to 26.5 $m/s^{1.75}$, frequently exceed the EU Directive's action level, and in some instances, even surpass the limit safety threshold.

Although this study exposes forward, sideways, vertical accelerations as well as their potential impact on human health, it is essential to explore their combined effects. This is because in real-world environments, vibrations and shocks typically occur in a simultaneous and multidirectional manner.

Figure 24 shows the effect of incorporating multidirectional accelerations on the RMS and VDV_{8h} values measured on the HSPC, using three test cases as examples. Among these, vertical acceleration consistently emerges as the dominant component in all runs. However, combining forward and vertical accelerations results in a 22.9% to 35.2% (across 12 test runs) increase in RMS compared to vertical acceleration alone. Similarly, combining vertical and sideways accelerations leads to a 4.4% to 17.8% increase over the vertical component. When all three directions—forward, sideways, and vertical—are included, RMS rises by 27.0% to 39.3% compared to the vertical RMS alone. These findings highlight the substantial role of forward and sideways accelerations in overall acceleration exposure, despite being largely overlooked in earlier research.

The influence of combined directional accelerations on VDV_{8h} is indicated in Figure 24. The results indicate that including all three directional components causes an increase in VDV_{8h} ranging from 1.8% to 4.9% compared to $VDV_{z,8h}$. It is worth noting that the contribution of sideways acceleration to total VDV_{8h} is minimal, with the combination of vertical and sideways components increasing VDV_{8h} by only 0.1% and 0.7%.

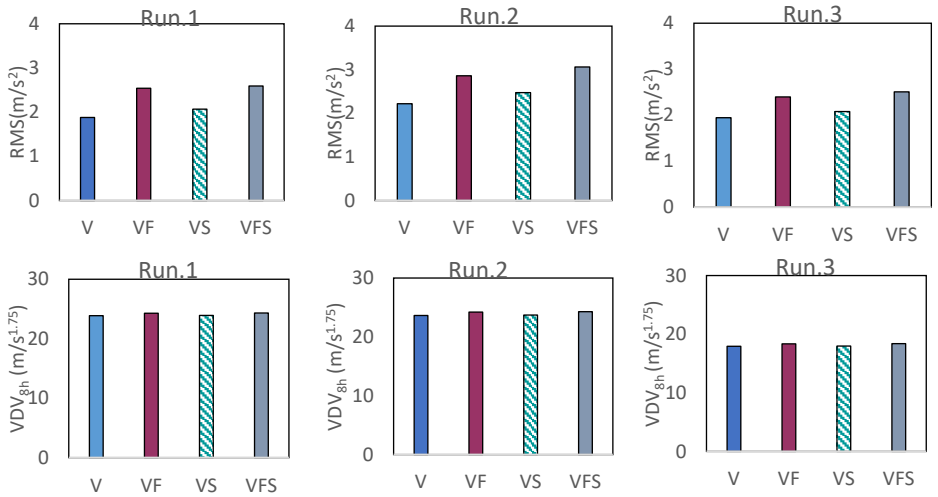


Figure 24. A sample comparison of RMS and VDV_{8h} values based on acceleration in different directions (V: Vertical, VF: Vertical and Forward, VS: Vertical and Sideways, VFS: Vertical, Forward, and Sideways) (Paper V).

3.2 Interceptor performance in improving HSPC dynamics and occupant safety

The primary strategy for preventing severe hull motions and accelerations in rough sea conditions involves the use of motion control devices such as trim tabs and interceptors (objective 3). Previous investigations summarized in Paper I indicate that motion reduction devices, particularly trim tabs and interceptors, can reduce hull motions and acceleration responses under wave conditions, as summarized in Table 9.

Table 9. Effects of trim tabs on motion reduction for various HSPCs (Paper I).

FrL	Wave	Result	References
1.2	Regular wave	50% reduction in pitch amplitude in resonance wave	Wang (1985)
		17% reduction in heave amplitude in high wavelengths	
		22% reduction in CG acceleration in high wavelengths	
		22% increase in CG acceleration in short wavelengths	
		26% bow acceleration reduction	
1.4	Regular wave	60% reduction in pitch amplitude	Wang (1985)
		30% reduction in heave amplitude in high wavelengths	
		20% reduction in CG acceleration in high wavelengths	
		35% increase in CG acceleration in short wavelengths	
		40% bow acceleration reduction	
1.06	Irregular wave	25% reduction in vertical bow acceleration	Rijkens et al. (2011)
2.3	Irregular wave	26.1% reduction in pitch acceleration	Santos et al. (2004)
		35.5% reduction in motion sickness incidence	
3.1	Irregular wave	41.1% reduction in pitch acceleration	Santos et al. (2004)
		56.14% reduction in motion sickness	
7.8	Regular wave	10-25% reduction in pitch amplitude	Kim et al. (2020)

While trim tabs significantly reduce hull motions, accelerations, and related human safety risks, transom interceptor systems demonstrated even better efficiency. Several comparative studies have demonstrated the interceptor's superiority in reducing the hull trim angle in calm water, such as Tsai and Hwang (2004) and Song et al. (2018). Further details on these findings can be found in Paper I.

In addition, there is evidence supporting the effectiveness of TIS in reducing hull motions and accelerations in wave conditions, as reported by Karimi et al. (2013), Luca and Pensa (2014), and Najafi et al. (2015). These findings can be directly linked to improvements in human safety.

Following advancements in TIS, researchers have introduced a novel motion control concept known as the double interceptor system (DIS). As shown in Figure 2, this system has the potential to enhance the hydrodynamic and dynamic performance of HSPCs in wave conditions. Despite its promising concept, research on DIS is still limited. To address this gap, a preliminary numerical study is conducted to evaluate the hydrodynamic effects of DIS on the HSPC. This analysis focuses on the trim angle, drag force, and pressure distribution for four cases: the bare hull, the hull equipped with a TIS, and the hull equipped with two different DIS configurations. A comparison of the pressure distributions on the hull bottom is presented in Figure 25. The origin of the longitudinal axis (x=0) corresponds to the transom, while the forward interceptor in the DIS i3 y3 and DIS i4 y3 configurations is located 1.25 m forward of the transom. As shown in Figure 25, the addition of the transom increases the wetted length and produces high-pressure

regions at the transom and forward interceptor locations. Furthermore, negative-pressure regions are observed immediately behind the forward interceptor in the DIS i3 y3 and DIS i4 y3 configurations, between x=1.0 m and x=1.25 m.

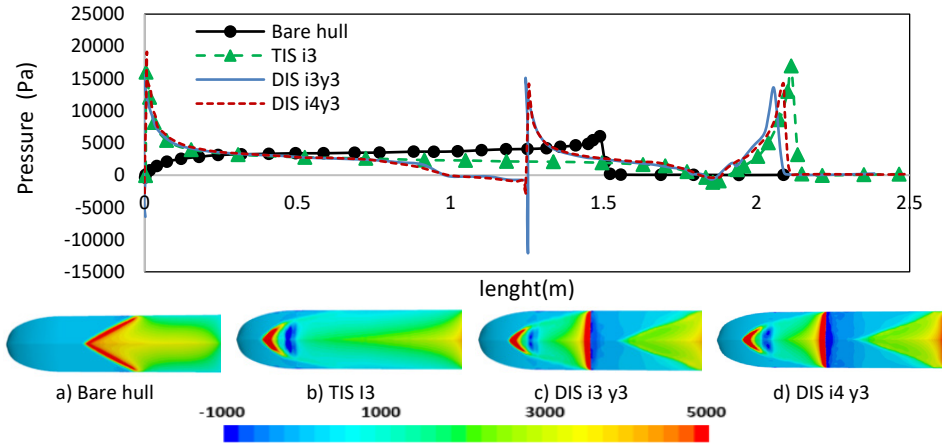


Figure 25. Effect of using TIS and DIS in pressure distribution on hull centerline at Fr= 2.8 (Paper III).

According to the obtained pressure distribution, both the DIS and the TIS influence the pressure distribution on the hull bottom, which in turn affects the trim angle under calm water and hull motion in wave conditions. However, the performance of the DIS and TIS in reducing hull motions under different wave conditions, requires further investigation.

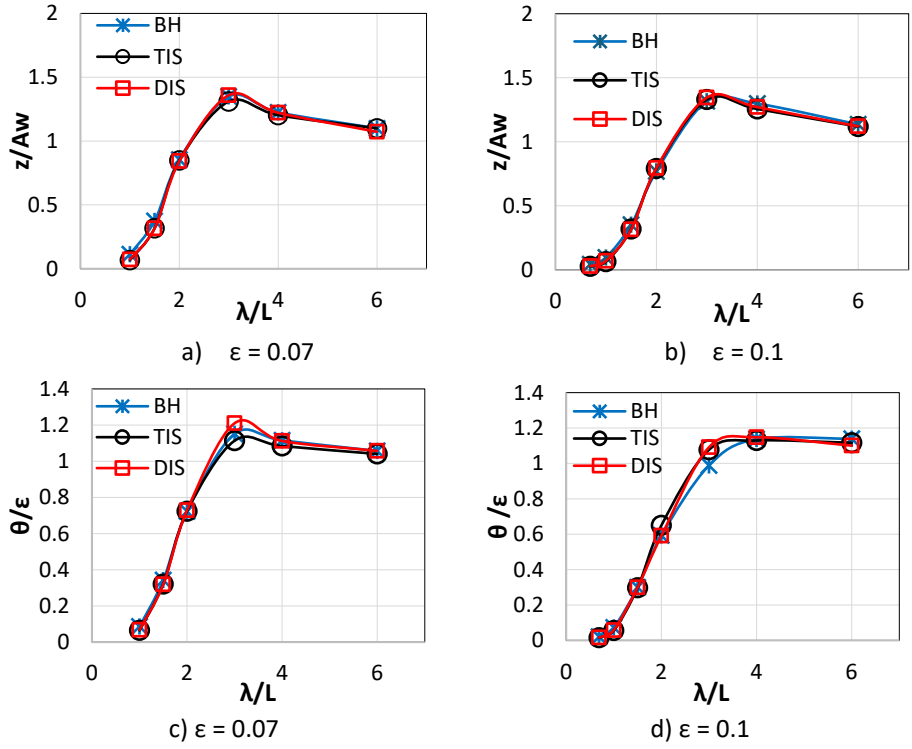
Following the preliminary hydrodynamic assessment of TIS and DIS in calm water, their influence on the dynamic responses of the HSPC under regular wave conditions is investigated in Paper IV. The effects of both TIS and DIS on heave, pitch, and vertical acceleration responses are evaluated by comparing their RAOs with those of the bare hull as indicated in Figure 26. RAOs of hull motions and acceleration in wave steepness 0.12 are presented in Paper IV for transom interceptor 0.5 B_{WL} and forward interceptor B_{WL} and height 2.0 mm.

For heave motion, the effect of interceptor installation remains relatively limited under the examined wave conditions. At a wave steepness of ε = 0.07, the TIS reduces the heave RAO by approximately 3.0% at the critical wavelength (λ/L = 3) compared with the bare hull, while the heave response of the DIS remains almost unchanged. Increasing the wave steepness to ε = 0.10 results in similar heave responses among the bare hull, TIS-equipped hull, and DIS-equipped hull over the investigated wavelength range. These results indicate that the influence of interceptor systems on heave motion is mainly confined to specific critical wave conditions rather than representing a general reduction across all wavelengths.

A similar trend is observed for pitch motion. Under ε = 0.07, the TIS decreases the pitch RAO by approximately 3.3% at λ/L = 3, whereas the DIS increases the pitch RAO by approximately 5.12% compared with the bare hull. At the higher wave steepness (ε = 0.10), both interceptor-equipped configurations exhibit pitch responses slightly higher than the bare hull, while remaining close to each other. Overall, the results suggest that the effectiveness of interceptor systems in controlling pitch motion is limited, with only minor improvements observed for the TIS under lower wave steepness conditions.

The influence of interceptor systems becomes more evident when considering vertical acceleration responses. Under the lower wave steepness condition (ε = 0.07), only minor differences are observed among the three configurations, indicating a limited effect of TIS and DIS on acceleration reduction. However, as wave steepness increases, the contribution of interceptor systems becomes more significant. At ε = 0.10 and λ/L = 3, the TIS and DIS reduce the peak vertical acceleration by approximately 15% and 5.6%, respectively, compared with the bare hull. Under the most severe wave condition investigated (ε = 0.12 and λ/L = 4), the TIS achieves a 28.9% reduction in vertical acceleration RAO relative to the bare hull. Although the DIS also reduces acceleration at this wavelength, it increases the acceleration RAO by approximately 10.5% at λ/L = 3.

Overall, the results demonstrate that the effectiveness of interceptor systems in reducing vertical acceleration is highly dependent on wave steepness and wavelength. While their influence is negligible under mild wave conditions, they can provide meaningful acceleration mitigation under severe waves. Among the investigated configurations, the TIS provides the most consistent improvement in dynamic responses, suggesting greater potential for reducing occupant exposure to severe acceleration events.



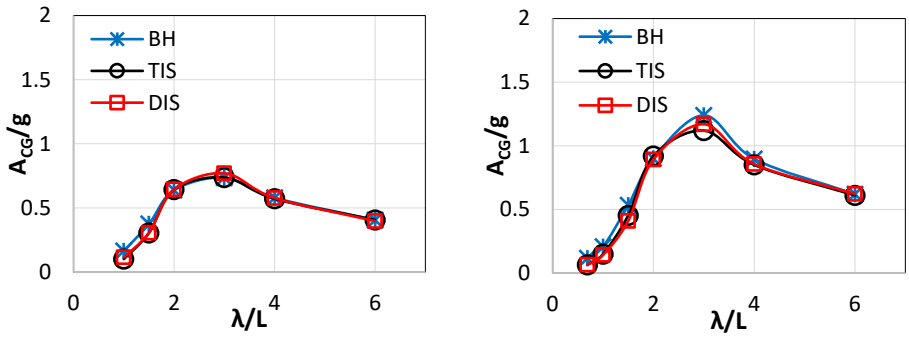


Figure 26. RAOs of heave, pitch, and vertical acceleration for the bare hull (BH), TIS-equipped hull (TIS), and DIS-equipped hull (DIS) under regular wave conditions with wave steepnesses of ε = 0.07 and ε = 0.10 at Fr_B= 3.0 (Paper IV).

Beyond the frequency-domain analysis of motion and acceleration responses, Paper IV further examines the influence of TIS and DIS on the severity of fly-over events under critical wave conditions. Figure 27 compares the time histories of vertical acceleration for the three hull configurations under ε = 0.12 and λ/L = 3. For all configurations, the acceleration decreases toward -g, indicating the separation of the hull from the water surface, followed by subsequent re-entry. The re-entry process generates a sharp positive acceleration peak due to the slamming impact.

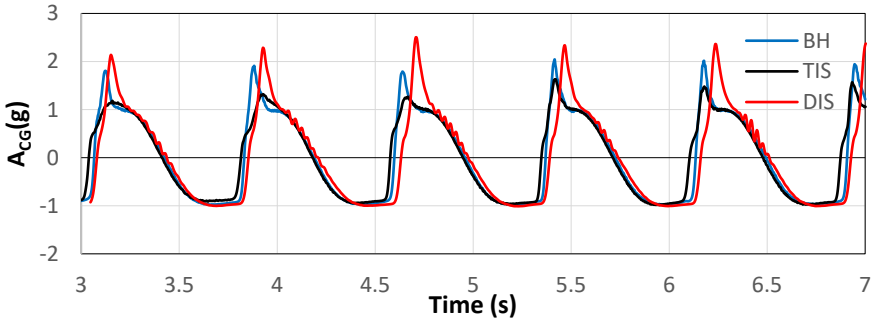


Figure 27. Time history of vertical acceleration for the hull configurations under ε = 0.12 and λ/L = 3 (Paper IV).

Although fly-over occurs for all configurations, differences are observed in both the airborne duration and the magnitude of the impact acceleration. The airborne duration is defined as the time interval between hull separation from the water surface and re-entry, during which the vertical acceleration approaches -g. The TIS-equipped hull exhibits the shortest airborne duration and the lowest impact acceleration, indicating that the interceptor improves hydrodynamic support during the separation and reduces the severity of the subsequent water impact. In contrast, the DIS-equipped hull remains in a near free-fall condition for a longer duration and experiences a higher impact acceleration after re-entry, resulting in a more severe fly-over event compared with the bare hull.

The results obtained from regular wave simulations demonstrate that interceptor systems can influence hull motions and acceleration responses; however, their

effectiveness depends strongly on wave severity and operating conditions. Since real operational environments are characterized by irregular waves with a broad range of frequencies and random wave elevations, the performance of these motion-reduction devices should also be evaluated under more realistic sea conditions.

Therefore, experimental investigations in irregular waves are conducted to assess the capability of TIS and DIS configurations in reducing acceleration exposure and improving occupant safety during different operational modes.

Initially, a TIS with a length of 0.5 B_{WL} and a height of 2.0 mm is tested at Froude numbers Fr_B = 1.7 and 2.2 to simulate the transient operational mode of the HSPC. The results are compared with those of the bare hull to evaluate improvements in human safety, as presented in Figure 28. The TIS effect on hull seakeeping in transient mode (heave and pitch motions and CG and bow accelerations) is presented in Paper IV.

The effect of the TIS on reducing RMS_z acceleration in transient conditions is clearly observed when compared to the bare hull, as shown in Figure 28(a). In wave conditions 1 and 2 at Fr_B = 1.7, RMS_z values at the CG reduce significantly by 40.1% and 36.8%, respectively. At a higher speed (Fr_B = 2.2), although the reduction is less, the TIS still contributes to noticeable improvements, with RMS_z at the CG reduced by 9.6% and 9.5%. The TIS performance in reducing RMS_z of bow acceleration is presented in Paper IV.

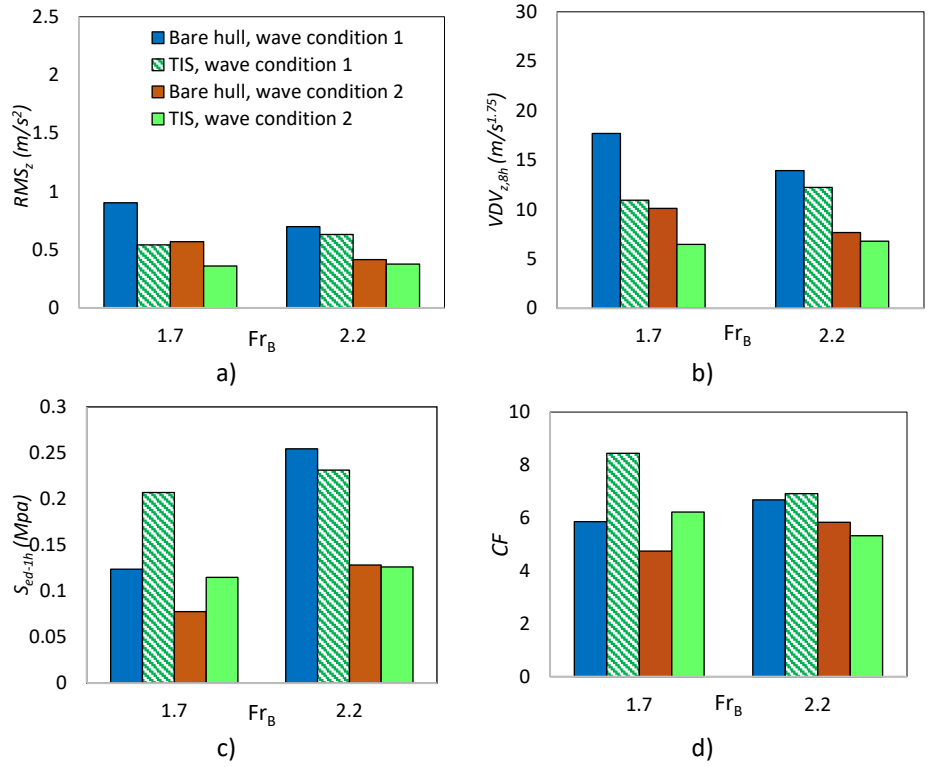


Figure 28. Key safety metrics: a) RMS_z, b) $VDV_{z,8h}$, c) Sed-1h, and d) CF for the bare hull and hull with TIS (0.5 B_{WL}) at transient mode under wave conditions 1 and 2 (Paper IV).

An evaluation of the full-scale $VDV_{z,8h}$ values demonstrate that TIS has considerable effectiveness in lowering acceleration peaks. In wave condition 1 at Fr_B = 1.7, the $VDV_{z,8h}$ at the centre of gravity (CG) is reduced by 38.2%, while in wave condition 2, a reduction of 36.0% is observed. These results confirm the TIS's efficiency in reducing acceleration

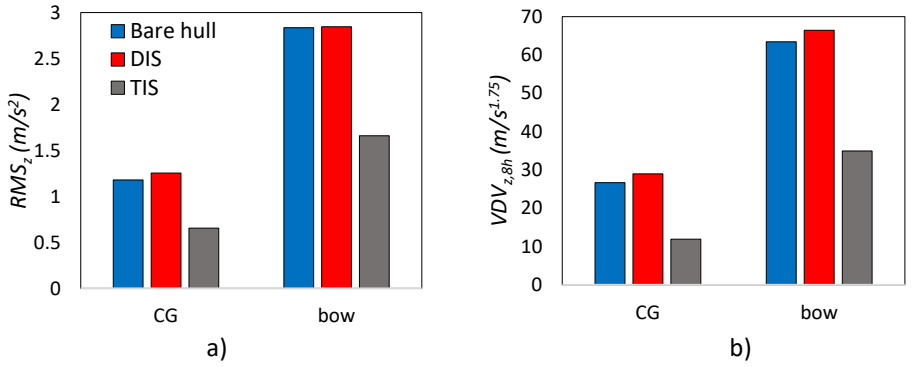
exposure at lower speeds. However, its performance declines at higher operational speeds.

As presented in Figure 28(c), implementing the TIS at Fr_B = 1.7 leads to a substantial increase in $S_{ed\text{-}1h}$ at the CG of 67.2% and 47.9% for wave conditions 1 and 2, respectively compared with the bare hull. Nevertheless, the $S_{ed\text{-}1h}$ values remain under 0.5 MPa, which falls within the "low risk" category for long-term health effects according to ISO 2631-5:2004. At a higher speed (Fr_B = 2.2), the TIS causes a decrease in $S_{ed\text{-}1h}$, with reductions of 9.1% and 1.6% in wave conditions 1 and 2, respectively. These results suggest better performance of the TIS in mitigating spinal stress at higher speeds.

The Crest Factor (CF) is a dimensionless parameter calculated as the ratio between the maximum weighted acceleration peak and the RMS_z value, reflecting the intensity of shocks. As shown in Figure 28(d), using the TIS at Fr_B = 1.7 results in a noticeable increase in CF for both wave conditions. This is attributed to higher acceleration peaks, which align with the observed rise in S_{ed} values. Despite this, the reductions in RMS_z and $VDV_{z,8h}$ suggest lower vertical acceleration exposure and moderate peak values. In contrast, at Fr_B = 2.2, the TIS contributes to overall reductions in CF, S_{ed}, $VDV_{z,8h}$, and RMS_z across both wave conditions 1 and 2, demonstrating better human safety outcomes under higher-speed conditions.

Comprehensive results, including bow acceleration and uncertainties, are presented in Paper V.

Subsequently, in planing mode, an additional interceptor is added to the existing system. This allows comparison of the performance of TIS and DIS and to determine the more effective device. The configurations of both DIS and TIS used in the planing mode are described in Section 2. The safety measures for planing mode, based on the measured CG acceleration during the towing tank tests at Fr_B = 3.0 across wave condition 1, are presented in Figure 29.



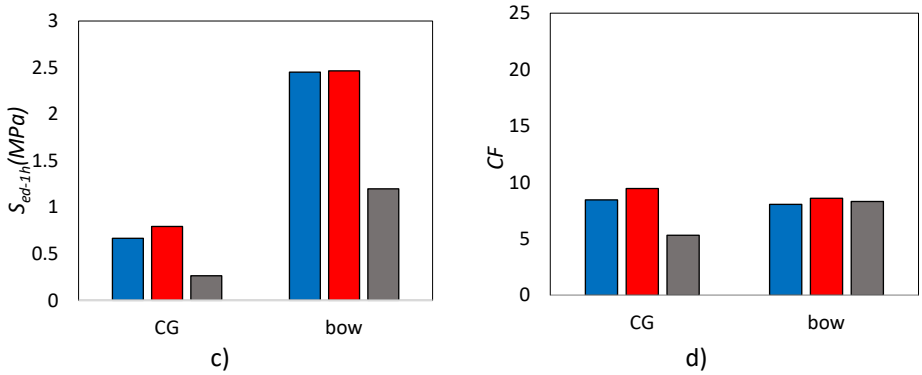


Figure 29. Key safety metrics: a) RMS_z, b) $VDV_{z,8h}$, c) $S_{ed\text{-}1h}$, and d) CF for bare hull and hull with TIS and DIS at planing mode in wave conditions 1 and 2 (Paper IV).

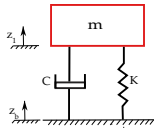
As shown in Figure 29 (a) and (b), the DIS leads to increases in both RMS_z and $VDV_{z,8h}$ of the CG acceleration, by 6.4% and 8.7%, respectively, compared to the bare hull. These increases indicate that DIS may be ineffective in enhancing occupants' safety and could also contribute to a higher likelihood of discomfort in planing mode. However, the TIS demonstrates significant effectiveness, reducing RMS_z and $VDV_{z,8h}$ by 44.4% and 55.3%, respectively, relative to the bare hull.

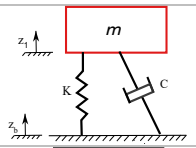
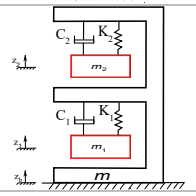
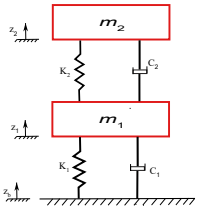
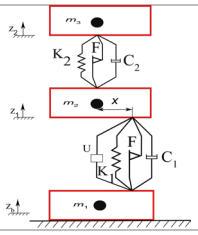
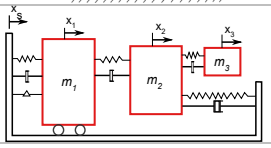
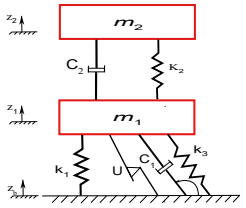
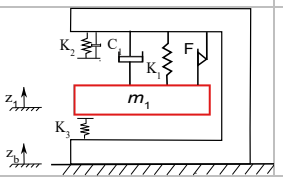
Furthermore, Figure 29(c) shows that the DIS results in an 18.8% increase in $S_{ed\text{-}1h}$ at the CG, while the TIS successfully reduces $S_{ed\text{-}1h}$ by 60.6% at the CG, confirming its superior ability to mitigate vertical acceleration and improve human safety during planing mode operations.

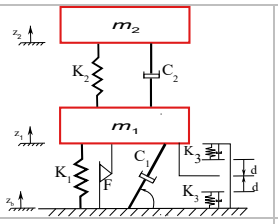
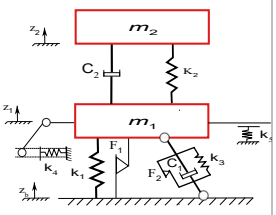
3.3 Shock mitigation seat to enhance human safety

Although the investigation of TIS performance in irregular waves demonstrates a significant reduction in vertical acceleration and an improvement in human safety, whole body vibrations and shocks on board the HSPC may still exceed the limit values, resulting in adverse health effects and discomfort for the occupant. As an additional safety improvement strategy, a shock mitigation seat can be implemented to reduce the transmission of deck acceleration to the seated occupants. As mentioned in Section 2, a mathematical model is developed to evaluate the effectiveness of a shock mitigation seat in enhancing human safety on board the HSPC (Objective 3). Prior to this analysis, a review of existing mathematical models for various shock mitigation seat designs developed by previous researchers is presented in Paper I. Table 10 summarizes several seat models used in previous studies.

Table 10. A summary of various mathematical models for shock mitigation seats (Paper I).

Seat model	Modelling schematic	Description	References
A1		Single degree of freedom Ignoring the cushion effects	Gannon (2017), Wei and Griffin (1998), Mayton et al. (2006), Riley and Coats (2015), Chen et al. (2021)

A2		Capability to study vertical and longitudinal vibrations.	Chen et al. (2021)
B1		Considering cushion effects Considering rigid support	Wei and Griffin (1998), Coe et al. (2008)
B2		Eliminating rigid support Considering cushion effects	Wei and Griffin (1998), Liam (2011), Townsend et al. (2012), Zuneid Alam (2013), Olausson (2012, 2015), Olausson and Garme (2015), Ereq (2018), Ekstrom (2019), Abdelkareem et al. (2021)
B3		Considering fixed frame and cushion effects Considering friction and active components Capability to study angular acceleration mitigation	Wice (2015)
C1		Considering longitudinal acceleration	Maciejewski et al. (2023)
C2		Considering seat and cushion effects Considering oblique damper and spring Considering active controller (u) for seat Capability to study lateral motion mitigation Proposed for trucks	Choi et al. (2000)
D1		Suggested for truck seat Considering top and bottom buffers Ignoring cushion effects proposed for truck	Rebelle (2000, 2004)

D2		Considering seat and cushion effects Considering top and bottom buffers Considering oblique damper Proposed for road and off-road vehicles	Ma et al. (2008) Rakheja et al. (2003)
D3		Considering seat and cushion effects Considering top and bottom buffer Considering oblique spring, damper, and friction component Capability to mitigate lateral motion Considering end-stop buffer for lateral motions Proposed for off-road vehicles	Gunston et al. (2004)

According to the literature on shock mitigation seat research for HSPCs, most studies focus on vertical suspension systems designed to reduce vertical acceleration, as it is the dominant direction of acceleration during HSPC operation. However, the comparative analysis in Section 3.1 (referenced in Paper VI) reveals that forward acceleration on board the HSPC is important and could also enhance comfort and reduce the risk of adverse health issues. While certain injuries caused by forward acceleration may be attributed to occupants being thrown from their seats—a risk that can be mitigated through the use of seat belts—a seat incorporating a forward suspension system could also enhance comfort and reduce the risk of adverse health issues.

To address this, Paper VI proposes and analyses a shock mitigation seat model equipped with both forward and vertical suspension systems, aimed at enhancing human safety on board HSPCs. The schematic of the seat model is provided in Figure 14 within Section 2.4. Additionally, Figures 30 to 32 present comparative analysis of RMS and VDV values measured at the seat base and the seat cushion, demonstrating the system's effectiveness in reducing transmitted acceleration.

Figure 30 presents a comparison of RMS_z and $VDV_{z,8h}$ values for the measured vertical acceleration at the seat base, predicted by the seat model, and experimentally measured on the seat cushion during 12 sea trial runs reported by Garme et al. (2011). In the majority of tests, both the modelled and measured RMS_z values on the seat cushion exceed those at the seat base, a trend consistent with previous findings by Garme et al. (2011). Conversely, the $VDV_{z,8h}$ values on the seat are observed to be 14.3% to 33.8% lower than those at the seat base. Despite this, $VDV_{z,8h}$ levels still surpass the limit value defined by the EU Directive 2002/44/EC. These findings underscore the seat's capability to mitigate intense vertical acceleration, thereby lowering the likelihood of acceleration-related health effects.

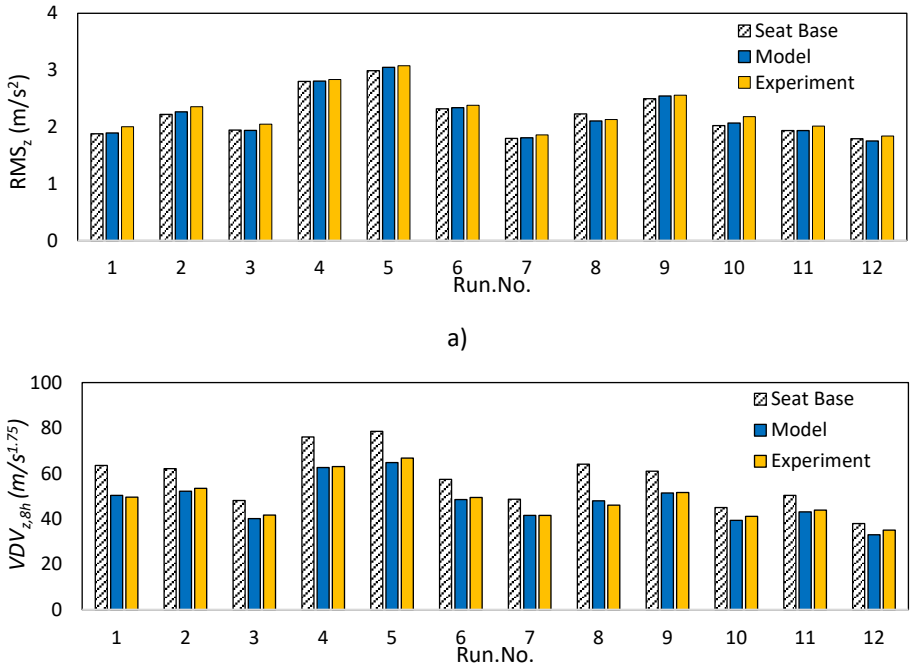
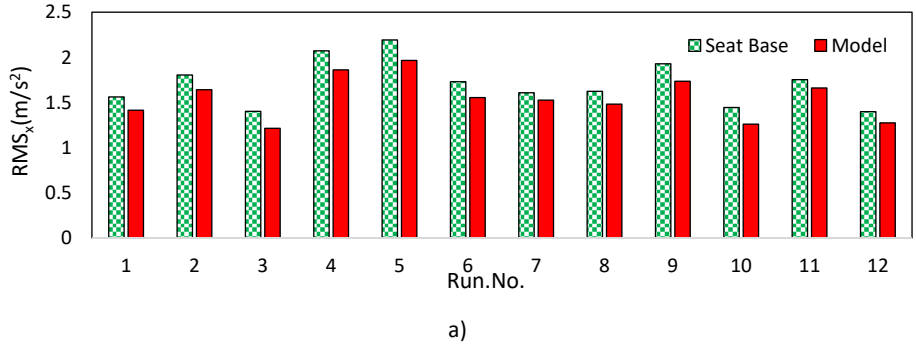
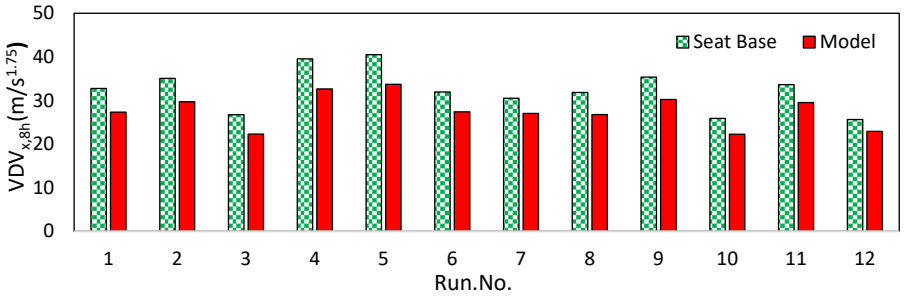


Figure 30. a) RMSz and b) $VDV_{z,8h}$ for the seat base, experimental seat cushion, and seat model in 12 sea trials (Paper VI).

The RMS_x and $VDV_{x,8h}$ obtained from the seat model using the measured forward acceleration of the seat cushion are compared (assumed to be equivalent to the seat base forward acceleration) with experimental measurements recorded at the seat cushion during 12 sea trials, as shown in Figure 31. The seat model demonstrates a reduction in RMS_x ranging from 5.4% to 15.3%, which indicates an improvement in occupant comfort. Similarly, the seat model predicts a decrease in $VDV_{x,8h}$ values ranging from 11.8% to 21.2%. Although all values remain above the limit value recommended by the EU Directive 2002/44/EC for minimizing potential health risks, the implementation of multidirectional suspension systems effectively mitigates acceleration exposure.



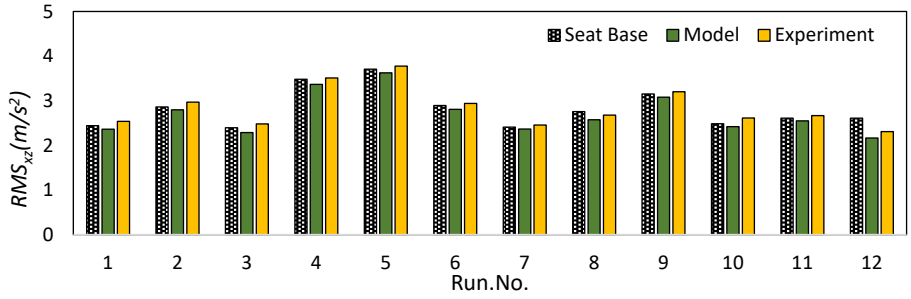


b)

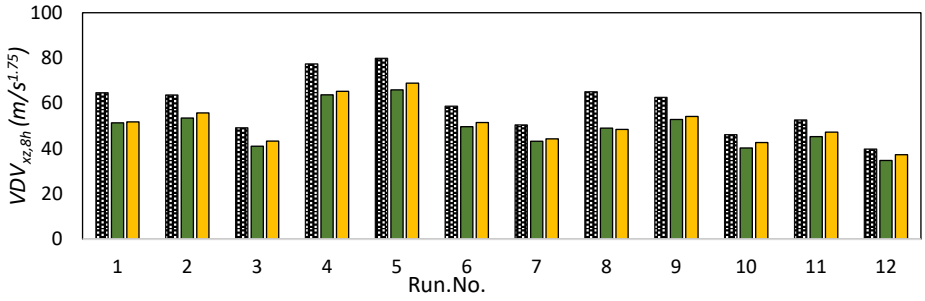
Figure 31. a) RMS$_x$ and b) VDV$_{x,8h}$ for seat base and seat model in 12 sea tests (Paper VI).

Figure 32 shows the RMS$_{xz}$ and VDV$_{xz,8h}$ values for the seat base, the experimental seat, and the modelled seat. The RMS$_{xz}$ values predicted by the modelled seat are between 1.9% and 20.5% lower than those measured at the seat base. Nevertheless, acceleration exposure remains classified as "extremely uncomfortable" in accordance with ISO 2631-1:1997. Additionally, the integration of a forward suspension system and the vertical suspension results in a further reduction in RMS$_{xz}$, ranging from 3.7% to 7.8%, relative to the experimental measurements on the seat cushion.

Moreover, the VDV$_{xz,8h}$ values at the modelled seat cushion are between 14.3% and 33.8% lower than those recorded at the seat base. In comparison to the sea trial measurements, the VDV$_{xz}$ values predicted by the proposed seat model are 0.7% to 6.8% lower than those measured at the experimental seat cushion during the sea trials. An exception occurs in test run 8, where a slight increase of 1.2% is observed.



a)



b)

Figure 32. a) RMS$_{xz}$ and b) VDV$_{xz,8h}$ for seat base, experimental seat cushion, and seat model in 12 sea tests (Paper VI).

4 Discussion

4.1 Main novelties of the thesis

This thesis investigates occupant exposure to hull motions and accelerations in HSPCs, with particular emphasis on the vertical, forward, and sideways acceleration components. Based on the gaps identified through the systematic review in Paper I, the main contributions of the thesis are summarized below. The novelty of each contribution is defined in relation to the specific prior work addressed in the corresponding publication and is limited to the craft configurations, operating conditions, and datasets investigated in this thesis.

The main novel contributions of this research are:

1. **Effects of Multidirectional accelerations on occupants' safety**
   Data and comparison: Paper VI uses acceleration measurements from 12 sea trials of an HSPC to evaluate vertical, forward, and sideways accelerations. In contrast to studies that primarily report vertical acceleration for occupant exposure assessment, the dataset allows the three directional components to be evaluated under the same operating conditions.
   Finding: The comparison of HSPC accelerationn measurements with ISO 2631-1:1997, ISO 2631-5:2004, and EU Directive 2002/44/EC shows that the forward and sideways accelerations can exceed the corresponding exposure criteria associated with occupant health and comfort.
   Scope and novelty: This contribution extends the assessment beyond vertical acceleration by providing a multidirectional evaluation based on full-scale measurements. The finding applies to the tested HSPC, operating conditions, and measurement configuration, and should not be interpreted as evidence that forward or sideways acceleration influences occupant safety for all HSPCs and sea conditions.
2. **Numerical and experimental analysis of HSPC in waves at different speeds**
   Data and comparison: Paper II investigates the effects of different operating speeds on the motion and acceleration responses of a tunneled HSPC in different regular head waves using numerical simulations. Paper IV investigates the motion and acceleration responses of an HSPC in different regular head waves at a constant operating speed. In addition, Paper V presents experimental towing-tank tests of an HSPC in irregular head waves at different speeds. These studies are used to investigate the effect of hull speed and wave conditions on HSPC motions and accelerations.
   Finding: For the investigated tunneled HSPC and the simulated regular-wave conditions in Paper II, high impact accelerations were observed within a critical wavelength range of approximately 1.5–2.5 times the hull length. In Paper IV, a similar high response region was observed for wavelengths of approximately 3.0–4.0 times the hull length at the investigated speed. Outside these investigated wavelength ranges, the influence of wave conditions and hull speed on vertical acceleration was less pronounced. Experimental observations under irregular waves and transient-speed operation further showed that acceleration did not consistently increase with increasing vessel speed.
   Novelty and scope: These results provide an extension of previous speed- and wave-response studies by demonstrating that the relationship between speed

and occupant-relevant acceleration is dependent on wave conditions and operating speeds. The conclusions are limited to the investigated hull configurations, wave conditions, and operating speeds, and experimental and numerical setups.

3. **Evaluation of interceptor effects on improving occupants' safety**
   Data and comparison: Previous studies have extensively investigated the influence of interceptor systems on the hydrodynamic performance and motions of HSPCs. Papers III, IV and V extend this line of investigation by examining the implications of a transom interceptor system (TIS) and a double interceptor system (DIS) in calm water, regular waves and irregular waves, with respect to hull dynamics, acceleration exposure, and related occupant-safety indicators.
   Finding: Although both TIS and DIS can improve HSPC hydrodynamics in calm water, they show different performance in wave conditions under investigated speeds and wave conditions. The investigated TIS configuration reduced hull acceleration and fly-over severity under, whereas the investigated DIS configuration did not provide the same reduction and, under the conditions, resulted in increased acceleration and fly-over severity. Moreover, Paper V indicated the possibility of amplifying some vertical acceleration which seriously affects occupant safety, for the investigated DIS- equipped hull.
   Scope and novelty: The contribution is therefore an extension of interceptor-performance research from hull dynamics toward occupant-relevant acceleration exposure. The findings are specific to the TIS and DIS configurations, hull geometry, speeds, and wave conditions investigated in Papers III, IV, and V and should not be generalized to all interceptor configurations, hull forms, or sea conditions.
4. **Development of a shock mitigation seat model with forward and vertical suspension systems**
   Data and comparison: Previous shock mitigation seat studies for HSPC have predominantly focused on vertical acceleration. Building on the multidirectional acceleration assessment in this thesis, Paper IV develops a mathematical seat model incorporating both vertical and forward suspension systems.
   Finding: The model demonstrates the potential for reducing the forward and vertical acceleration transmitted to the seated occupant under the assumed input conditions. The vertical response of the model is benchmarked against sea-trial measurements, whereas forward seat-base acceleration was not directly measured and was therefore assumed to be equal to the measured seat cushion acceleration.
   Novelty and applicability: The contribution is an initial modelling framework for considering forward acceleration in addition to vertical acceleration in the analysis of an HSPC shock-mitigation seat. The forward-direction results are conceptual predictions rather than experimentally validated results. The model is intended as an initial framework for investigating acceleration transmission and potential mitigation, rather than as a comprehensive biomechanical model of the seated occupant.

In summary, the thesis extends the assessment of occupant exposure in HSPCs beyond vertical acceleration by incorporating forward and sideways acceleration measurements, examining the dependence of acceleration response on speed and wave conditions,

evaluating the occupant relevant effects of the investigated interceptor configurations, and developing an initial shock-mitigation seat model that includes forward and vertical suspension. These contributions collectively provide a framework for relating HSPC motions and multidirectional acceleration exposure to occupant safety considerations. The findings are bounded by the specific hull configurations, operating conditions, experimental datasets, and modelling assumptions investigated in the thesis.

4.2 Discussion of the main findings

Previous studies on human safety assessment on board HSPCs, comprehensively reviewed in Paper I, indicate a high risk of adverse health effects and discomfort when evaluated according to ISO 2631-1 and EU Directive 2002/44. These studies are often conducted at high speeds in planing mode, where speed significantly affects hull motions and accelerations. Therefore, this thesis utilizes an HSPC, designed to achieve high speeds with Froude numbers (Fr) up to 5.6, to investigate the relationship between hull dynamics and occupant safety under different operating conditions (Paper II).

Paper II numerically investigates the influence of operational speed on hull motions and vertical accelerations in regular head waves. The results show that hull speed has the greatest influence when the wavelength is approximately 1.5–3.0 times the hull length. Within this critical wavelength range, increasing speed considerably amplifies hull motions and vertical accelerations and may trigger the fly-over phenomenon, during which the hull separates from the water surface and re-enters the water with a severe slamming impact. In contrast, for wavelengths considerably shorter or longer than the critical range, changes in operational speed have only a limited influence on the dynamic response.

As real sea conditions consist of irregular waves, and the results suggest that in wavelengths shorter or longer than the critical wavelength, the effect of hull speeds is not significant, a series of towing tank tests are conducted to investigate the effect of hull speeds on motion and acceleration across three different irregular wave conditions in semi-planing, transient, and planing modes (Paper V). The results show an increase in the vertical acceleration peaks as the hull speed increases from the semi-planing to the transient mode and from the transient mode to the planing mode. However, in transient mode, increasing Fr from 1.7 to 2.2 reduces RMS_z and $VDV_{z,8h}$ values, while S_{ed} increases. This indicates that increasing speed in transient mode produces higher acceleration peaks, which increases S_{ed} because this metric is strongly influenced by the fourth power of acceleration peaks. However, some moderate acceleration peaks decrease, resulting in reductions in RMS_z and VDV_z in $Fr_B = 2.2$ compared to $Fr_B = 1.7$.

The numerical and experimental investigations presented in Papers II and V primarily consider heave and pitch motions. However, occupants on board HSPCs are exposed to multidirectional accelerations under real operating conditions.

To address this, recorded accelerations in 12 sea trial tests are analysed to identify the most harmful acceleration direction considering forward, vertical, and sideways accelerations. Calculated RMS and VDV for different directions of acceleration indicate that each of these acceleration directions alone can lead to human discomfort, with the highest acceleration values being associated with vertical, forward, and sideways directions, respectively. Additionally, both vertical and forward accelerations exceed the VDV_{8h} limit value suggested by the EU Directive 2002/44/EC to avoid the human health risks. Therefore, considering multidirectional acceleration is essential in evaluating human safety on HSPCs.

The results obtained in Papers II and V indicate that reducing operational speed is an effective method for mitigating hull accelerations, particularly near critical wavelengths. However, for many HSPC applications, such as military, patrol, and rescue missions, reducing speed may compromise operational effectiveness. Consequently, improving hull dynamics through motion-control devices provides a more practical approach for enhancing human safety while maintaining high-speed capability.

Paper I reviewed existing motion reduction strategies and highlighted interceptors as one of the most promising solutions. Previous studies demonstrated that trim tabs effectively reduce hull motions and accelerations, while comparative investigations in calm water reported superior trim-control performance for transom interceptor systems (TIS). Nevertheless, limited information was available regarding the influence of interceptor systems on human safety, particularly under wave conditions.

To address this research gap, Paper III first investigates the hydrodynamic behaviour of conventional TIS and the novel Double Interceptor System (DIS) under calm-water conditions. The results demonstrate that both systems modify the pressure distribution on hull bottom and reduce the trim angle. In particular, the DIS generates two distinct high-pressure regions beneath the hull, producing additional trimming moments compared with the conventional TIS. These findings suggest that both TIS and DIS have the potential to alter hull motions in waves and therefore require further investigation under realistic operating conditions.

Based on these observations, Paper IV numerically evaluates the dynamic performance of the bare hull, TIS-equipped hull, and DIS-equipped hull in regular waves at a constant planing speed. The results indicate that the effectiveness of the interceptor systems strongly depends on wave steepness. Under mild wave conditions, both systems produce only limited changes in hull motions and vertical accelerations. As wave steepness increases, however, the TIS provides noticeable reductions in vertical acceleration, whereas the DIS generally offers smaller improvements and, under certain critical wave conditions, even increases the acceleration response. Paper IV also demonstrates that TIS shortens the airborne duration during fly-over and reduces the impact acceleration upon water re-entry, whereas the DIS tends to prolong the airborne phase and produce more severe impacts. These findings show that interceptor performance cannot be evaluated solely from calm water characteristics and highlight the importance of assessing their behaviour under severe wave conditions.

To verify these observations under realistic sea states, Paper V experimentally investigates the effects of TIS and DIS in irregular waves using towing tank tests. The results confirm that the TIS effectively reduces RMS, VDV, and Sed in both transient and planing operating modes, thereby improving occupant safety. However, in transient mode, although TIS reduces overall acceleration exposure, it also increases several extreme acceleration peaks, leading to higher Sed and Crest Factor values under certain operating conditions. In contrast, the DIS generally increases acceleration exposure during planing operation and provides no consistent improvement in occupant safety. The combined numerical and experimental investigations therefore demonstrate that for the specific configurations and operating conditions investigated in this thesis, the conventional TIS generally showed more favourable performance than the investigated DIS configuration with respect to occupant-relevant acceleration and fly-over responses..

Besides reducing hull motions, another practical approach for improving occupant safety is to isolate the occupants from the remaining vibrations and shocks through shock mitigation seats. The literature review presented in Paper I revealed that most existing

suspension-seat models focus exclusively on vertical vibration isolation despite the significant contribution of forward acceleration identified in this thesis. Therefore, Paper VI develops a mathematical shock mitigation seat model incorporating both vertical and forward suspension systems. The results demonstrate that the proposed seat reduces the accelerations transmitted to the occupant in both directions compared with the seat base, leading to lower RMS and VDV values and improved occupant comfort. Although acceleration levels may still exceed recommended exposure limits under severe operating conditions, the results indicate that multidirectional suspension systems represent a promising complementary strategy for further improving human safety on board HSPCs.

4.3 Limitations

While this study provides valuable insights into safety improvements for high-speed small boats, certain limitations must be acknowledged, as they could have influenced the findings. These limitations arise from the methodological approach, data availability, computational constraints, and practical considerations. Recognizing these limitations enhances research transparency and provides a foundation for future studies to build upon.

To provide a structured overview, the limitations are categorized based on the research methods used in this study:

4.3.1 Limitations in the systematic review

A systematic literature review was conducted in Paper I, focusing on safety standards for humans exposed to whole-body vibrations and shocks, published safety assessment studies on human safety on board the HSPC, and safety improvement strategies suggested to reduce hull motions and accelerations and consequently reduce safety risks. Despite the extensive nature of this review, a limitation should be noted:

- Limited availability and unpublished research: Some relevant studies, especially from industry and defense sectors, remain inaccessible due to confidentiality restrictions.

4.3.2 Limitations in CFD simulation study

Numerical simulations presented in Papers II, III and IV were employed to investigate the influence of operational speed, wave characteristics, and interceptor configurations on HSPC hydrodynamic performance and dynamic behaviour. Although these simulations provide valuable insights into hull motions and hydrodynamic effects, several limitations remain:

- Simplified physical assumptions: CFD models involve simplifications in representing real-world flow phenomena, including turbulence, wave breaking, and hull flexibility.
- Computational constraints: High-fidelity simulations require extensive computational resources, limiting the number of scenarios that can be tested. For example, the DIS analyses in Paper III and IV were restricted to selected interceptor configurations and operating conditions, while other geometries, interceptor heights, or locations may result in different performances. Similarly, the simulations in Paper II were limited to selected regular wave conditions and Froude numbers.

- Limited validation range: Although numerical results were validated against available experimental data, validation was limited to the investigated hull forms and operating conditions. Further experimental validation under additional wave conditions and interceptor configurations would improve confidence in numerical predictions.

4.3.3 Limitations in experimental investigations

Towing tank experiments conducted in Papers IV and V were used to investigate HSPC dynamics under regular and irregular wave conditions and to evaluate the effectiveness of TIS and DIS in reducing acceleration exposure and improving human safety. However, several limitations should be considered:

- Scale effects: Towing tank tests are conducted on scaled models, which may not fully replicate real-world hydrodynamic and acceleration responses.
- Towing tank length and carriage maximum speed: The length of the towing tank and the maximum speed of the carriage impose some limitations on the range of conditions that can be tested.
- Controlled test conditions: The tests are performed in controlled environments, which may not fully capture the randomness and variability of real sea states. This includes environmental factors, such as wind power and wave directions.
- Limited range of conditions tested: Due to time and cost constraints, only a subset of operational scenarios could be tested, potentially missing critical conditions.

4.3.4 Limitations in safety assessment analysis

Human safety assessment in this thesis was conducted using acceleration measurements obtained from towing tank experiments (Paper V) and full-scale sea trials (Paper VI). The final results are used to indicate the effectiveness of motion reduction devices TIS and DIS in enhancing human safety on board the HSPC. Furthermore, accelerations in three different directions (vertical, forward, and sideways) on board an HSPC, recorded by previous researchers during 12 sea trials, have been analyzed to assess the effect of different directions of acceleration on human safety, considering current safety standards. However, there are some limitations:

- Generalization of results: The assessment is based on specific operational conditions and hull configurations, which may not be universally applicable to all high-speed craft across different speeds and sea conditions.
- Uncertainties in human tolerance levels: Safety thresholds are based on existing standards, which may not fully account for individual variations in injury susceptibility and responses to acceleration exposure.
- Limited full-scale data availability: The multidirectional acceleration analysis was based on available full-scale sea trial data, and additional measurements from different vessels and operational scenarios are required to further generalize the findings.

4.3.5 Limitations in mathematical approach

In Paper VI, a mathematical approach has been used to model a shock mitigation seat's performance in reducing transmitted vibrations to the seated occupants. However, there are some limitations:

- Idealized seat behaviour: The model assumes predictable seat damping and suspension behaviour, while real-world performance can vary due to wear, environmental factors, and human weight.
- Simplified seat model: Certain aspects, such as the seat backrest, footrest effects, human posture, and seatbelt influence, have been neglected to simplify the modelling process.
- Numerical and modelling uncertainties: The accuracy of the mathematical approach depends on the assumptions, parameter values, and numerical solution methods, which may introduce uncertainties into the predicted seat performance.

5 Conclusion

This study aimed to improve occupants' safety on board high-speed planing crafts by investigating acceleration exposure and developing strategies to reduce safety risks. To achieve this goal, the research addressed two main aspects: (1) evaluating human safety risks associated with HSPC acceleration and (2) investigating potential strategies for reducing acceleration exposure and improving occupant safety.

The first research question focused on evaluating human safety risks on board HSPCs. Paper I presented a systematic review of existing safety assessments, demonstrating that acceleration exposure on board HSPCs frequently exceeds the recommended limits defined by current standards, potentially resulting in discomfort and adverse health effects. Numerical simulations conducted in Paper II investigated the influence of operational speed and wave characteristics on HSPC dynamics. The results showed that severe impact accelerations and fly-over phenomena are likely to occur at critical wavelengths (approximately 1.5–3.0 times the hull length), particularly at high speeds, highlighting the significant safety risks associated with high-speed operation in specific wave conditions.

The effect of operational conditions on human safety was further investigated experimentally in Paper V through towing tank tests in irregular waves. The results demonstrated that planing mode operation generally leads to higher acceleration exposure and increased risks of discomfort and adverse health effects compared with semi-planing and transient modes. However, the relationship between speed and safety risk is not always straightforward, as increasing speed in transient mode reduced some acceleration-based indicators, such as RMS and VDV, due to changes in hull-wave interaction.

Furthermore, Paper VI analysed multidirectional acceleration exposure using previously recorded full-scale sea trial data. The results showed that vertical, forward, and sideways accelerations can all contribute to occupant discomfort and safety risks. Although vertical acceleration remains the dominant component, forward acceleration also exceeded the limit values defined by EU Directive 2002/44/EC in several operating conditions, demonstrating the importance of considering multidirectional acceleration in future HSPC safety assessments.

The second research question focused on identifying strategies to improve human safety on board HSPCs. A systematic review in Paper I showed that motion reduction devices, including trim tabs and interceptors, and shock mitigation seats have significant potential for reducing hull motions and acceleration. Since previous studies have demonstrated the superior capability of interceptors in controlling hull trim compared with conventional trim tabs, interceptor systems were selected for further investigation.

Numerical simulations of DIS and TIS performance in calm water in Paper III showed that DIS can generate two high-pressure regions, providing two bow-down moments that help control trim angles. However, the TIS provides one high-pressure region around the transom and one bow-down torque. This hydrodynamic effect influences hull trim angle in calm water and may influences hull motions in wave conditions, which are linked to human safety on board the HSPC.

Therefore, Paper IV numerically investigated the performance of TIS and DIS under regular wave conditions, focusing on their effects on hull motions, accelerations, and fly-over behaviour. The results indicated that the effectiveness of interceptor systems depends strongly on wave steepness and response characteristics. TIS generally provided

improved dynamic behaviour by reducing acceleration responses under severe wave conditions, while DIS did not consistently improve the dynamic response and, in some cases, increased acceleration exposure and fly-over severity.

The safety benefits of interceptor systems were further evaluated in Paper V under irregular wave conditions. The results showed that TIS effectively reduced acceleration exposure and improved safety indicators in both transient and planing modes. However, in transient mode, although TIS reduced moderate acceleration levels, it could increase extreme acceleration peaks, resulting in higher S_{ed} and Crest Factor values under some conditions. In planing mode, TIS demonstrated superior performance compared with both the bare hull and DIS by reducing RMS, VDV, and S_{ed} values. Conversely, DIS increased acceleration exposure and did not provide safety improvements under the investigated conditions.

Furthermore, the potential safety improvement using shock mitigation seats was investigated in Paper VI. In Paper VI, a mathematical model of a seat with combined vertical and forward suspension systems was developed. The results demonstrated that the proposed seat configuration can reduce transmitted acceleration in both directions compared with a conventional vertical-only suspension system, indicating its potential for improving occupant comfort and safety.

Despite the contributions of this study, several challenges remain for future research:

1. Current information on the effects of acceleration in different directions is limited. Measuring acceleration in all directions during sea trial tests of HSPCs and considering all directions of vibration and shock in safety evaluations are required to evaluate the effect of fore-and-aft and sideways vibrations on human safety. Although this study analysed the effect of forward and sideways acceleration on human health and comfort, it was conducted at one speed, and further studies at other speeds are required.
2. There are numerous studies of motion reduction devices, whereas only a few of them analysed their effects on human safety. In addition, the effects of these devices on forward and sideways acceleration are limited. Although this study investigated the effect of interceptors on safety improvement on board the HSPC, it was limited to the vertical acceleration effects.
3. Existing studies on shock mitigation seats mainly focus on vertical motion and overlook the effects of lateral and fore-and-aft accelerations, which are significant factors for occupants' safety. Although there are some new types of shock mitigation seats that manufacturers believe are effective in reducing vibrations in other directions, there are no academic publications to confirm this. This study developed a shock mitigation seat with forward and vertical suspension systems by a mathematical model. However, this is a simplification of the seat model, neglecting the backrest, footrest, and linearized damping coefficient. Future studies on the shock mitigation seat model can improve the current model to achive more accurate results.

These advanced studies are essential for achieving more effective human safety improvements and enhancing the efficiency of HSPCs in high-speed operations, particularly for missions that demand optimal performance.

List of Figures

Figure 1. Trend of the number of published documents related to high-speed craft safety over the past 40 years. 12
Figure 3. Logical relations between the research objectives and the publications included in this thesis. 21
Figure 4. Search strategy in literature review.(Paper I) 23
Figure 5. Defined computational domain for HSPC a) Paper II and b) Paper III, and c) Paper IV 25
Figure 6. Mesh structure in the computational domain: a) Paper II and b) Paper III. 26
Figure 7. Mesh convergence study for: a) Pitch and b) Heave across wavelength = 2L at Fr_B = 4.7 (Paper II), and c) trim and d) Resistance for the bare hull in calm water in Paper III. 27
Figure 8. Validation of HSPC a) Heave and b) pitch motions in regular wave conditions (Paper II). 27
Figure 9. Validation of a) trim angle and b) resistance of the bare hull (Paper III). 28
Figure 10. Generated wave spectra and theoretical JONSWAP wave spectra (Paper IV). 30
Figure 11. Safety evaluation methods according to the standards: the blue line represents ISO 2631-1:1997, the green dashed line represents BS 6841:1987, and the red double line represents Directive 2002/44 (Paper I). 33
Figure 12. Location of each accelerometer on the hull (Paper V). 34
Figure 13. Schematic of the seat model and free body diagram (Paper V). 35
Figure 14. Nonlinear spring characteristics: a) Vertical direction (Olausson and Garme, 2015), and b) Forward direction (Stein and Múčka, 2011) (Paper V). 36
Figure 15. Distribution of difference u(t) for a) test run 2, and b) test run 3 (Paper V). 37
Figure 16. Computed and measured time history of a) vertical and b) forward accelerations in test run 1. 37
Figure 17. a) RMS_z and b) $VDV_{z,8h}$ of vertical acceleration on seat model and experiment seat (Paper V). 37
Figure 18. Non-dimensional a) heave, b) pitch, and c) vertical acceleration of an HSPC at various speeds under different regular wave conditions (Paper II). 41
Figure 19. Snapshots of the hull position to the water surface and volume fraction at different speeds corresponding to the wavelengths of 2L (Paper I). 42
Figure 20. a) RMS_z, b) $VDV_{z,8h}$, c) $S_{ed\text{-}1h}$ and d) $S_{ed\text{-}8h}$ of a bare hull at different Froude numbers across various wave conditions (Paper IV). 43
Figure 21. a) RMS and b) VDV_{8h} for different directions of acceleration in 12 sea conditions at V=25.5 m/s (Paper V). 44
Figure 22. A sample comparison of RMS and VDV_{8h} values based on acceleration in different directions (V: Vertical, VF: Vertical and Forward, VS: Vertical and Sideways, VFS: Vertical, Forward, and Sideways) (Paper V). 45
Figure 23. Effect of using TIS and DIS in pressure distribution on hull centerline at Fr= 2.8 (Paper III). 47
Figure 24. Key safety metrics: a) RMS_z, b) $VDV_{z,8h}$, c) Sed-1h, and d) CF for the bare hull and hull with TIS (0.5 B_{WL}) at transient mode under wave conditions 1 and 2 (Paper IV). 50
Figure 25. Key safety metrics: a) RMS_z, b) $VDV_{z,8h}$, c) $S_{ed\text{-}1h}$, and d) CF for bare hull and hull with TIS and DIS at planing mode in wave conditions 1 and 2 (Paper IV). 52

Figure 26. a) RMSz and b) $VDV_{z,8h}$ for the seat base, experimental seat cushion, and seat model in 12 sea tests (Paper V)..... 55
Figure 27. a) RMS_x and b) $VDV_{x,8h}$ for seat base and seat model in 12 sea tests (Paper V). 56
Figure 28. a) RMS_{xz} and b) $VDV_{xz,8h}$ for seat base, experimental seat cushion, and seat model in 12 sea tests (Paper V)..... 56

List of Tables

Table 1. Overview of the included papers, highlighting their main focus, related research questions and corresponding objectives. 19
Table 2. Summary of the methods employed in each paper included in this thesis 22
Table 3. Regular wave properties used in Paper II. 23
Table 4. Boundary conditions used in Papers II,III, and IV. 25
Table 5. Towing tank test matrix for irregular wave conditions. 30
Table 6. Definition and values of parameters used in the shock mitigation seat model. 35
Table 7. Summary of previous studies on safety evaluation of HSPCs (Paper I). 39
Table 8. Effects of trim tabs on motion reduction for various HSPCs (Paper I). 46
Table 9. A summary of various mathematical models for shock mitigation seats (Paper I). 52

References

Abdelkareem, M. A., Zhang, R., Jing, X., Wang, X., & Ali, M. K. A. (2022). Characterization and implementation of a double-sided arm-toothed indirect-drive rotary electromagnetic energy-harvesting shock absorber in a full semi-trailer truck suspension platform. Energy, 239, 121976, https://doi.org/10.1016/j.energy.2021.121976.

Akers, R. H. (1999). Dynamic analysis of planing hulls in the vertical plane. Proceedings of the society of naval architects and marine engineers, New England Section.

Alam, Z., Afagh, F., & Langlois, R. (2017). Efficient identification of naval high-speed craft shock mitigation seat modal parameters from drop-test data. Journal of Dynamic Systems, Measurement, and Control, 139(3), 031009, https://doi.org/10.1115/1.4035018.

Allen, D. P., Taunton, D. J., & Allen, R. (2008). A study of shock impacts and vibration dose values onboard highspeed marine craft. Transactions of the Royal Institution of Naval Architects Part A: International Journal of Maritime Engineering, 150(A3), 1-10, http://eprints.soton.ac.uk/id/eprint/64778.

Ashkezari, A. Z., & Moradi, M. (2021). Three-dimensional simulation and evaluation of the hydrodynamic effects of stern wedges on the performance and stability of high-speed planing monohull craft. Applied Ocean Research, 110, 102585, https://doi.org/10.1016/j.apor.2021.102585.

Begovic, E., Bertorello, C., & Pennino, S. (2014a). Experimental seakeeping assessment of a warped planing hull model series. Ocean Engineering, 83, 1-15, https://doi.org/10.1016/j.oceaneng.2014.03.012.

Begovic, E., Bertorello, C., & Pennino, S. (2014b). Planing hull seakeeping in irregular head seas. Transactions of FAMENA, 38(3), 1-12, https://hrcak.srce.hr/129604.

Begovic, E., Bertorello, C., Pennino, S., Piscopo, V., & Scamardella, A. (2016). Statistical analysis of planing hull motions and accelerations in irregular head sea. *Ocean Engineering*, *112*, 253-264, https://doi.org/10.1016/j.oceaneng.2015.12.012.

Bilandi, R. N., Mancini, S., Dashtimanesh, A., Tavakoli, S., & De Carlini, M. (2019). A numerical and analytical way for double-stepped planing hull in regular wave. In MARINE VIII: proceedings of the VIII International Conference on Computational Methods in Marine Engineering (pp. 417-427). CIMNE. and Grigoropoulos et al. (2010)

Brizzolara, S., & Villa, D. (2009, October). A systematic CFD analysis of flaps/interceptors hydrodynamic performance. In Proceedings 10th International Conference on Fast Sea Transportation (FAST 2009), Athens.

Brown, P. W. (1971). An experimental and theoretical study of planing surfaces with trim flaps. Report No. SIT-DL-71-1463; Stevens Institute of Technology, Davidson Laboratory: Hoboken, NJ, USA, 1971.

Carvalhais, A. (2004, October). Incidence and Severity of Injuries to Surf Boat Operators. In *75th Shock and Vibration Symposium, Virginia Beach, VA* (Vol. 37).

Chen, Q., Zhang, Y., Zhu, C., Wu, J., & Zhuang, Y. (2021). A sky-hook sliding mode semiactive control for commercial truck seat suspension. Journal of Vibration and Control, 27(11-12), 1201-1211, https://doi.org/10.1177/1077546320940972.

Choi, S. B., Nam, M. H., & Lee, B. K. (2000). Vibration control of a MR seat damper for commercial vehicles. Journal of intelligent material systems and structures, 11(12), 936-944. https://doi.org/10.1106/AERG-3QKV-31V8-F250.

Coe, T., Shenoi, R. A., & Xing, J. T. (2008, September). Human body vibration response models in the context of high speed planing craft and seat isolation systems. In Proceedings of the Sixth International Conference on High-performance marine vehicles (HIPER'08), Naples, Italy (pp. 18-19).

Day, A. H., & Cooper, C. (2011). An experimental study of interceptors for drag reduction on high-performance sailing yachts. Ocean Engineering, 38(8-9), 983-994, https://doi.org/10.1016/j.oceaneng.2011.03.006.

de Alwis, M. P., & Garme, K. (2021). Effect of occupational exposure to shock and vibration on health in high-performance marine craft occupants. Proceedings of the Institution of Mechanical Engineers, Part M: Journal of Engineering for the Maritime Environment, 235(2), 394-409. https://doi.org/10.1177/1475090220981187.

De Luca, F., & Pensa, C. (2011). Experimental data on Interceptor's effectiveness. ITA. https://www.iris.unina.it/handle/11588/401517.

De Luca, F., & Pensa, C. (2012). Experimental investigation on conventional and unconventional interceptors. Transactions of the Royal Institution of Naval Architects Part B: International Journal of Small Craft Technology, 154, B65–B72. https://doi.org/10.3940/rina.ijsct.2012.b2.129.

De Luca, F., & Pensa, C. (2019). The Naples Systematic Series – Second part: Irregular waves, seakeeping in head sea. Ocean Engineering, 194, 106620. https://doi.org/10.1016/j.oceaneng.2019.106620.

Directive 2002/44/EC. (2002). Directive 2002/44/EC of the European Parliament and of the Council of 25th June 2002 on the Minimum Health and Safety Requirements Regarding the Exposure of Workers to the Risks Arising from Physical Agents (vibration).

Dobbins, T., Myers, S., Withey, W., Dyson, R., Gunston, T., & King, S. (2008, September). High speed craft motion analysis: Impact count index (ici). In 43rd UK Conference on Human Response to Vibration, Leicester.

Ekstrom, V.(2019). Semi-active suspension seats in High speed crafts, degree project in mechanical engineering, Master Thesis, KTH Royal institute of technology, second cycle, 30 credits Stockholm, Sweden, 2019, Available from: 2019-12-17, URN: urn:nbn:se:kth:diva-265586.

Ensign, W., Hodgdon, J. A., Prusaczyk, W. K., Ahlers, S., Shapiro, D., & Lipton, M. (2000). A survey of self-reported injuries among special boat operators. Naval Health Research Centre, 00-48.

Ereq, K. (2018) Active Suspension Seat for High-Speed Craft, Master thesis, degree project in mechanical engineering, second cycle, KTH Royal institute of technology, 30 credits Stockholm, Sweden, Available from 2018-09-11, URN: urn:nbn:se:kth:diva-234825

Ertogan, M., Wilson, P. A., Tayyar, G. T., & Ertugrul, S. (2017). Optimal trim control of a high-speed craft by trim tabs/interceptors Part I: Pitch and surge coupled dynamic modelling using sea trial data. Ocean Engineering, 130, 300-309. https://doi.org/10.1016/j.oceaneng.2016.12.007.

Folsø, R. (2004). Comfort Monitoring of High Speed Passenger Ferries. Technical University of Denmark: Copenhagen, Denmark.

Fridsma, G. (1969). A systematic study of the rough-water performance of planing boats.

Fridsma, G. (1971). A Systematic Study of the Rough-Water Performance of Planing Boats. Irregular Waves-Part II (No. SIT-DL-71-1495 Final Rpt).

Gannon, L. (2017). Single impact testing of suspension seats for high-speed craft. Ocean Engineering, 141, 116-124. https://doi.org/10.1016/j.oceaneng.2017.06.017.

Garme, K. (2005). Improved time domain simulation of planing hulls in waves by correction of the near-transom lift. International Shipbuilding Progress, 52(3), 201-230, https://doi.org/10.3233/SHP-2005-52.3_1.

Garme, K., Burström, L., & Kuttenkeuler, J. (2011). Measures of vibration exposure for a high-speed craft crew. Proceedings of the Institution of Mechanical Engineers, Part M: Journal of Engineering for the Maritime Environment, 225(4), 338-349, https://doi.org/10.1177/1475090211418747.

Ghadimi, P., Loni, A., Nowruzi, H., Dashtimanesh, A., & Tavakoli, S. (2014). Parametric study of the effects of trim tabs on running trim and resistance of planing hulls. Advances in shipping and Ocean Engineering, 3(1), 1-12.

Griffin, K., Knight, J. (Eds.). (1990). *Human Development and the International Development Strategy for the 1990s*; Macmillan: 1990, London, UK, Volume 8, 258p.

Grigoropoulos, G. J., & Damala, D. P. (2011, September). Dynamic performance of the NTUA double-chine series hull forms in random waves. In 11th international conference on Fast Sea Transportation FAST, Honolulu, Hawaii, USA.

Grigoropoulos, G. J., Damala, D. P., & Loukakis, T. A. (2010, March). Dynamic Performance of the NTUA Double-Chine Series Hullforms in Regular Waves. In SNAME Chesapeake Power Boat Symposium (p. D021S002R005). SNAME, https://doi.org/10.5957/CPBS-2010-019.

Gunston, T. P., Rebelle, J., & Griffin, M. J. (2004). A comparison of two methods of simulating seat suspension dynamic performance. Journal of Sound and Vibration, 278(1-2), 117-134, https://doi.org/10.1016/j.jsv.2003.09.063.

ICOMIA. (2023). Recreational boating industry statistics 2022. Surrey: International Council of Marine Industry Associations (ICOMIA.org).

International Standard Organization (ISO) (2004). Shock–Evaluation of Human Exposure to Whole Body Vibration–Part 5: Method for Evaluation of Vibration Containing Multiple Shocks. Geneva: ISO, 2631-5.

International Standard Organization (ISO), (1997). Shock—evaluation of human exposure to whole-body vibration—part 1: General requirements. International Organization for Standardization, ISO, 2631-1.

Judge, C., Mousaviraad, M., Stern, F., Lee, E., Fullerton, A., Geiser, J., ... & Ikeda, C. (2020). Experiments and CFD of a high-speed deep-V planing hull–part II: Slamming in waves. Applied ocean research, 97, 102059, https://doi.org/10.1016/j.apor.2020.102059.

Karimi, M. H., Seif, M. S., & Abbaspoor, M. (2015). A study on vertical motions of high-speed planing boats with automatically controlled stern interceptors in calm water and head waves. Ships and Offshore Structures, 10(3), 335-348, https://doi.org/10.1080/17445302.2013.867647.

Katayama, K. S. T., & Ikeda, Y. (2004) A Study on Performance of a Hydrofoil Assisted High-Speed Planing Mono-hull. Proc. of the 2nd Asia-Pacific Workshop on Hydrodynamics (APHydro2004), pp.177-184, Busan, KOREA(2004,6).

Katayama, K., Suzuki, K., & Ikeda, Y. (2003, October). A new ship motion control system for high-speed craft. In Proceedings of the FAST 2003 The 7th International Conference on Fast Sea Transportation, Ischia, Italy (pp. 7-10).

Kearns, S. D. (2001). Analysis and mitigation of mechanical shock effects on high speed planing boats, Master of Science in Mechanical Engineering, Massachusetts Institute of Technology): Cambridge, MA, USA.

Kim, D. J., Kim, S. Y., You, Y. J., Rhee, K. P., Kim, S. H., & Kim, Y. G. (2013). Design of high-speed planing hulls for the improvement of resistance and seakeeping performance. International Journal of Naval Architecture and Ocean Engineering, 5(1), 161-177, https://doi.org/10.2478/IJNAOE-2013-0124.

Klosinski, W. E., & Brown, P. W. (1993). ADDITIONAL SEAKEEPING MODEL TESTS OF TWO US COAST GUARD NOTIONAL DESIGNS OF 110 FT AND 120 FT WPB HULLS; FINAL REPT (No. USCG-D-18-93).

Liam, C. C. (2011). Testing and modeling of shock mitigating seats for high speed craft, Master theses of Science in Mechanical Engineering,,http://hdl.handle.net/10919/32874.

Ling, H., & Wang, Z. (2019). Numerical prediction and analysis of motion response of high speed planing craft in regular waves The school of naval architecture and ocean engineering, Jiangsu University of Science and Technology. Ed, 33, 1-8.

Luca, F., & Pensa, C. (2014). The prediction of the interceptor performances based on towing tank test data: Ship-model correlation and hull form influence. positions, 9707, C0301.

Ma, W., Sun, H., Sun, H., Zou, J., & Zhuang, J. (2015). Test studies of the resistance and seakeeping performance of a trimaran planing hull. Polish Maritime Research, 22(1 (85)), 22-27, https://doi.org/10.1515/pomr-2015-0004.

Ma, X. Q., Rakheja, S., & Su, C. Y. (2008). Damping requirement of a suspension seat subject to low frequency vehicle vibration and shock. International Journal of Vehicle Design, 47(1-4), 133-156, https://doi.org/10.1504/IJVD.2008.020884.

Maciejewski, I., Blazejewski, A., Pecolt, S., & Krzyzynski, T. (2023). A sliding mode control strategy for active horizontal seat suspension under realistic input vibration. Journal of Vibration and Control, 29(11-12), 2539-2551, https://doi.org/10.1177/10775463221082716.

Marshall, J. T., & Riley, M. R. (2020). A comparison of the mechanical shock mitigation performance of a shock isolation seat subjected to laboratory drop tests and at-sea seakeeping trials. NAVSEA Carderock.

Mayton, A. G., DuCarme, J. P., Jobes, C. C., & Matty, T. J. (2006, January). Laboratory investigation of seat suspension performance during vibration testing. In ASME International Mechanical Engineering Congress and Exposition (Vol. 47675, pp. 177-183), https://doi.org/10.1115/IMECE2006-14146.

Meyer, L. T., Moore, J., & Sopchick-Smith, T. (1994). Naval Special Warfare Sports Medicine Conference Proceedings, Held in Coronado, California on 4-6 May 94. NAVAL HEALTH RESEARCH CENTER SAN DIEGO CA.

Mohebbi, M., Ghassemi, M. A., & Ghassemi, H. (2020). Obtaining the Practical Formula for the Trim-tab Dimensions to Reach the Minimum Drag for Planing Boat. American Journal of Mechanical Engineering, 8(4), 163-171, doi:10.12691/ajme-8-4-3.

Moldanová, J., Fridell, E., Matthias, V., Hassellöv, I.-M., Jalkanen, J.-P., Tröltzsch, J., Quante, M., Johansson, L., Karl, M., Malutenko, I., Ytreberg, E., Eriksson, M., Sigray, P., Karasalo, I., Peltonen, H., Hasenheit, M., Granhag, L., Mawdsley, I., Aulinger, A., … Piotrowicz, J. (2018). Sustainable Shipping and Environment of the Baltic Sea region: Final Report. In Sustainable Shipping and Environment of the Baltic Sea region [Report]. SHEBA.

Molini, A., & Brizzolara, S. (2005). Hydrodynamics of interceptors: a fundamental study. In Proceeding of the International Conference on Marine Research and Transportation, ICMRT, Italy, (Vol. 1).

Najafi, A., Alimirzazadeh, S., & Seif, M. S. (2015). RANS simulation of interceptor effect on hydrodynamic coefficients of longitudinal equations of motion of planing catamarans. Journal of the Brazilian Society of Mechanical Sciences and Engineering, 37(4), 1257-1275, doi:10.1007/s40430-014-0256-6.

Olausson, K. (2012). Vibration Mitigation for High Speed Craft. Master's Thesis, Centre for Naval Architecture Royal Institute of Technology: Stockholm, Sweden.

Olausson, K. (2015). On Evaluation and Modelling of Human Exposure to Vibration and Shock on Planing High-Speed Craft. Ph.D. Thesis, KTH Royal Institute of Technology: Stockholm, Sweden.

Olausson, K., & Garme, K. (2015). Prediction and evaluation of working conditions on high-speed craft using suspension seat modelling. Proceedings of the Institution of Mechanical Engineers, Part M: Journal of Engineering for the Maritime Environment, 229(3), 281-290, https://doi.org/10.1177/1475090213515641.

Olausson, K., & Garme, K. (2015). Prediction and evaluation of working conditions on high-speed craft using suspension seat modelling. Proceedings of the Institution of Mechanical Engineers, Part M: Journal of Engineering for the Maritime Environment, 229(3), 281-290, https://doi.org/10.1177/1475090213515641.

Page, M. J., McKenzie, J. E., Bossuyt, P. M., Boutron, I., Hoffmann, T. C., Mulrow, C. D., ... & Moher, D. (2021). The PRISMA 2020 statement: an updated guideline for reporting systematic reviews. *bmj*, *372*, https://doi.org/10.1136/bmj.n71.

Rakheja, S., Boileau, P. É., Wang, Z., & Politis, H. (2003). Performance analysis of suspension seats under high magnitude vibration excitations: Part 1: Model development and validation. Journal of low frequency noise, vibration and active control, 22(4), 225-252, https://doi.org/10.1260/0263092041456792.

Rakheja, S., Boileau, P. É., Wang, Z., & Politis, H. (2003). Performance analysis of suspension seats under high magnitude vibration excitations: Part 1: Model development and validation. Journal of low frequency noise, vibration and active control, 22(4), 225-252, https://doi.org/10.1260/026309203323022599.

Rebelle, J. (2000, September). Development of a numerical model of seat suspensions to optimize the end-stop buffers. In UK Conference on Human Responses to Vibration, University of Southampton.

Rebelle, J. (2004). Methodology to improve the performance of the end-stop buffers of suspension seats. Vehicle System Dynamics, 42(4), 211-233. https://doi.org/10.1080/00423110412331289826.

Reynolds, D., Ayyad, E. A., & Hachem, M. (2012). Evaluation of a Pneumatic-Seat-Bladder-System Designed for Shock and Vibration Isolation. University of Nevada: Las Vegas, NV, USA.

Rijkens, A. A. K., Keuning, J. A., & Huijsmans, R. H. M. (2011). A computational tool for the design of ride control systems for fast planing vessels. International shipbuilding progress, 58(4), 165-190, https://doi.org/10.3233/ISP-2012-0074.

Rijkens, A. A. K., Keuning, J. A., & Huijsmans, R. H. M. (2011). A computational tool for the design of ride control systems for fast planing vessels. International shipbuilding progress, 58(4), 165-190, https://doi.org/10.3233/ISP-2012-0074.

Riley, M. R., Murphy, H. P., & Coats, T. W. (2013). Initial Investigation of Wave Impact Load Transfer Through Shock Isolation Seats in High Speed Craft. Naval Surface Warfare Center carderock Division Virginia Beach United States.

Rosén, A., Begovic, E., Razola, M., & Garme, K. (2017). High-speed craft dynamics in waves: challenges and opportunities related to the current safety philosophy. In 16th International Ship Stability Workshop (ISSW 2017), Belgrade, Serbia, 2017.

Sakaki, A., Ghassemi, H., & Keyvani, S. (2019). Evaluation of the hydrodynamic performance of planing boat with trim tab and interceptor and its optimization using genetic algorithm. Journal of Marine Science and Application, 18(2), 131-141, doi:10.1007/s11804-018-0040-6.

Santos, M., López, R., & De la Cruz, J. M. (2005). Fuzzy control of the vertical acceleration of fast ferries. *Control Engineering Practice*, *13*(3), 305-313, https://doi.org/10.1016/j.conengprac.2004.03.012.

Savitsky, D., & Brown, P. W. (1976). Procedures for hydrodynamic evaluation of planing hulls in smooth and rough water. Marine Technology and SNAME News, 13(04), 381-400, https://doi.org/10.5957/mt1.1976.13.4.381.

Sebastiani, L., Bruzzone, D., Gualeni, P., Rambaldi, G., Ruscelli, D., & Viviani, M. (2008, January). A practical method for the prediction of planing craft motions in regular and irregular waves. In *International Conference on Offshore Mechanics and Arctic Engineering* (Vol. 48210, pp. 687-696).

Seo, J., Choi, H. K., Jeong, U. C., Lee, D. K., Rhee, S. H., Jung, C. M., & Yoo, J. (2016). Model tests on resistance and seakeeping performance of wave-piercing high-speed vessel with spray rails. *International Journal of Naval Architecture and Ocean Engineering*, *8*(5), 442-455, https://doi.org/10.1016/j.ijnaoe.2016.05.010.

Seo, K.C.; Gopakumar, N.; Atlar, M. Experimental investigation of dynamic trim control devices in fast speed vessel. J. Navig. Port Res. 2013, 37, 137–142. https://doi.org/10.5394/KINPR.2013.37.2.137.

Song, K. W., Guo, C. Y., Gong, J., Li, P., & Wang, L. Z. (2018). Influence of interceptors, stern flaps, and their combinations on the hydrodynamic performance of a deep-vee ship. Ocean Engineering, 170, 306-320, https://doi.org/10.1016/j.oceaneng.2018.10.048.

Stein, G. J., & Múčka, P. (2011). Study of simultaneous shock and vibration control by a fore-and-aft suspension system of a driver's seat. International Journal of Industrial Ergonomics, 41(5), 520-529, https://doi.org/10.1016/j.ergon.2011.03.003.

Sun, H., & Faltinsen, O. M. (2011). Dynamic motions of planing vessels in head seas. *Journal of marine science and technology*, *16*, 168-180.

Taunton, D. J., Hudson, D. A., & Shenoi, R. A. (2011). Characteristics of a series of high speed hard chine planing hulls-part II: performance in waves. International Journal of Small Craft Technology, 153, B1-B22, https://doi.org/10.3940/rina.ijsct.2011.b1.97.

Tavakoli, S., Niazmand Bilandi, R., Mancini, S., De Luca, F., & Dashtimanesh, A. (2020). Dynamic of a planing hull in regular waves: Comparison of experimental, numerical and mathematical methods. Ocean Engineering, 217, 107959, https://doi.org/10.1016/j.oceaneng.2020.107959.

Townsend, N. C., Coe, T. E., Wilson, P. A., & Shenoi, R. A. (2012). High speed marine craft motion mitigation using flexible hull design. Ocean Engineering, 42, 126-134, https://doi.org/10.1016/j.oceaneng.2012.01.007.

Tsai, J. F., & Hwang, J. L. (2004, November). Study on the compound effects of interceptor with stern flap for two fast monohulls. In Oceans' 04 MTS/IEEE Techno-Ocean'04 (IEEE Cat. No. 04CH37600) (Vol. 2, pp. 1023-1028). IEEE, doi:10.1109/OCEANS.2004.1405650.

Wang, L. W. (1985). A study on motions of high-speed planing boats with controllable flaps in regular waves. International shipbuilding progress, 32(365), 6-23, https://doi.org/10.3233/ISP-1985-3236502.

Wei, L., & Griffin, M. J. (1998). Mathematical models for the apparent mass of the seated human body exposed to vertical vibration. Journal of sound and vibration, 212(5), 855-874, https://doi.org/10.3233/ISP-1985-3236502.

Wice, A. M. (2015). Spatial dynamic modelling of high-speed craft suspension seating (Doctoral dissertation, Carleton University), Carleton University, Ottawa, Ontario, Canada.

Yaakob, O., Shamsuddin, S., & Koh, K. K. (2004). Stern flap for resistance reduction of planing hull craft: a case study with a fast crew boat model. Journal Teknologi, 43â-52, https://doi.org/10.11113/jt.v41.689

Zarnick, E. (1978). A Nonlinear Mathematical Model of Motions of a Planing Boat in Regular Waves (Technical Report DTNSRDC-78/032,). David Taylor Naval Ship 73 Research and Development Center, https://apps.dtic.mil/sti/citations/ADA052039.

Zarnick, E. (1979). A Nonlinear Mathematical Model of Motions of a Planing Boat in Irregular Waves (Technical Report DTNSRDC/SPD-0867-01). David Taylor Naval Ship Research and Development Center, https://apps.dtic.mil/sti/citations/ADA078605.

Zarnick, E. E., & Turner, C. R. (1981). Rough water performance of high length to beam ratio planing boats, Maritime Technical Information Facility, (No. DTNSRDC/SPD-0973-01).

Zuneid Alam, S. (2013). Implementation of a drop test impact rig for dynamic testing of high speed craft shock mitigation seats and extraction of modal parameters (Doctoral dissertation, Carleton University), https://hdl.handle.net/20.500.14718/32864.

Acknowledgements

The completion of this doctoral thesis marks the end of a rewarding and transformative academic journey at the Estonian Maritime Academy, Tallinn University of Technology. I am sincerely thankful to the Academy for its financial support and for offering an encouraging environment that has made this research possible.

I gratefully acknowledge the Erasmus+ scholarship for Doctoral Students, which provided the opportunity to conduct a short-term research visit at the Department of Engineering Mechanics, KTH Royal Institute of Technology, and a long-term study stay at the Department of Industrial Engineering at the University of Naples "Federico II." These international collaborations greatly enriched my academic and professional development.

My deepest appreciation goes to my main supervisor during the thesis writing process, **Assistant Professor Abbas Dashtimanesh** for his invaluable guidance, insightful feedback, and continued support throughout every stage of this research. I am also deeply thankful to my co-supervisors, **Professor Pentti Kujala** (Estonian Maritime Academy) and **Professor Karl Garme** (KTH Royal Institute of Technology), for their expert advice, constructive input, and dedicated mentorship. I want to acknowledge **Associate Professor Mihkel Kõrgesaar** for accepting the role of main supervisor to finalize the thesis in TalTech and for his feedback to final version of the thesis.

I would like to extend special thanks to my co-authors: **Associate Professor Simone Mancini**, **Dr. Fabio De Luca, Dr. Rasul Niazmand Bilandi,** and **Dr. Sasan Tavakoli**. Their collaboration, knowledge, and commitment significantly contributed to the outcomes of the research included in this thesis.

I am also grateful to my colleagues, academic staff, and administrative personnel at the Estonian Maritime Academy for their continuous support and cooperation throughout my doctoral studies.

On a personal note, I am profoundly thankful to my spouse for his unwavering love, patience, and support. I also wish to express my heartfelt gratitude to my parents, sister, and brother, whose encouragement and belief in me have played a vital role in reaching this milestone.

“What we know is a drop; what we don’t know is an ocean.”
— Isaac Newton

Abstract

Improving Occupant Safety on Board High-Speed Planing Craft

High-speed craft (HSCs) are widely used for special missions that require fast operations, such as rescue and military missions. However, their high-speed performance in rough sea conditions poses significant safety concerns for the occupants. Severe hull motions and accelerations at high speed in wave conditions often cause pilots to reduce the hull speed to avoid occupant safety risks. However, this compromises the HSC mission effectiveness. Therefore, improving occupant safety on board the HSCs is crucial to maintaining high-speed operations with minimal need to reduce hull speed.

This thesis addresses two main research questions: (1) How do changes in hull dynamics and acceleration exposure affect the motion and acceleration levels experienced by occupants of high-speed planing craft (HSPC)? and (2) To what extent can the investigated hull and appendage-based strategies reduce vessel motions and acceleration exposure and thereby improve occupant safety in high-speed planing craft?

To answer the first research question, occupant safety was investigated through a comprehensive review of previous research, numerical simulations, towing tank tests, and analysis of full-scale sea trial data in accordance with the safety guidance from ISO 2631-1:1997, EU Directive 2002/44/EC, and ISO 2631-5:2004. The review presented in Paper I showed that hull accelerations in planing mode often exceed the limit values recommended by current safety standards.

Numerical simulations of two HSPCs in regular head waves (Papers II and IV) demonstrated the potential for fly-over with harsh impact shocks at high speeds at critical wavelengths (1.5 to 3 times the hull length), which can significantly affect occupant safety. Experimental tests in the towing tank of the Dipartimento di Ingegneria Industriale at the University of Naples “Federico II”, under different irregular waves, revealed that acceleration exposure increases when hull speed increases from semi-planing to transient mode and from transient mode to planing mode. However, within the speed range corresponding to the transient mode, hull acceleration decreases as operational speed increases.

Since occupants are exposed to multidirectional accelerations in real operating conditions, Paper VI also analysed full-scale measurements of vertical, forward, and sideways accelerations from 12 sea trials. The results showed that, although vertical acceleration remains the dominant component, forward acceleration also frequently exceeds recommended exposure limits, while forward and sideways accelerations contribute substantially to occupant discomfort. These findings indicate that safety assessments based solely on vertical acceleration may underestimate the overall safety risk.

To address the second research question, potential safety improvement strategies were investigated. The literature review in Paper I identified motion reduction devices and shock mitigation seats as promising approaches. Numerical simulations in calm water (Paper III) showed that the conventional Transom Interceptor System (TIS) creates a single high-pressure region near the transom, whereas the Double Interceptor System (DIS) generates two high-pressure regions associated with the transom and forward interceptors, producing different trimming moments.

The performance of TIS and DIS was then investigated under regular head waves through validated numerical and experimental analysis (Paper IV). The results demonstrated that the effectiveness of interceptor systems strongly depends on wave

steepness and wavelength. TIS generally provided improved dynamic behaviour and reduced impact acceleration under severe wave conditions, whereas DIS did not consistently improve the response.

Further experimental evaluation in irregular waves (Paper V) showed that TIS reduced RMS, VDV, and S_{ed} values and improved occupant safety in both transient and planing operating modes. However, under some transient conditions, TIS increased several extreme acceleration peaks. In contrast, DIS generally increased acceleration exposure during planing operation, indicating that further optimisation is required before practical implementation.

As a complementary strategy, Paper VI developed a mathematical model of a shock-mitigation seat incorporating both vertical and forward suspension systems. The results showed that the proposed seat configuration can reduce transmitted accelerations in both directions and improve occupant comfort and safety compared with a conventional vertical-only suspension system.

In conclusion, this thesis highlights the importance of improving occupant safety on board HSPCs. Although TIS and shock mitigation seats offer potential improvements, further reduction of transmitted accelerations to the occupants is still required to avoid safety risks. Moreover, comprehensive safety assessments must consider multidirectional accelerations, which are often overlooked in both motion reduction devices and shock mitigation seat studies.

Lühikokkuvõte
Kiirekäiguliste liugkerede pardal viibijate ohutuse parandamine

Kiirekäigulisi aluseid (HSC) kasutatakse laialdaselt eriotstarbelistes ülesannetes, kus on vajalik kiire tegutsemine, näiteks pääste- ja sõjalistes operatsioonides. Suurel kiirusel karmides mereoludes liikumisega kaasnevad aga olulised ohutusriskid pardal viibijatele. Tugevad kere liikumised ja suured kiirendused lainetuses sunnivad juhte sageli vähendama aluse kiirust, et vältida pardal viibijate ohutusega seotud riske. See vähendab aga kiirekäigulise aluse missiooni tõhusust. Seetõttu on pardal viibijate ohutuse parandamine oluline, et säilitada suurel kiirusel tegutsemise võime võimalikult vähese kiiruse vähendamise vajadusega.

Käesolevas doktoritöös käsitletakse kahte peamist uurimisküsimust: (1) kuidas mõjutavad kere dünaamika ja kiirenduskoormuse muutused kiirekäiguliste liugkerede pardal viibijate kogetavaid liikumisi ja kiirendustasemeid ning (2) mil määral võimaldavad uuritud kere- ja lisaseadmepõhised lahendused vähendada aluse liikumisi ja kiirenduskoormust ning seeläbi parandada pardal viibijate ohutust kiirekäigulistel liugkeredel?

Esimesele uurimisküsimusele vastamiseks uuriti pardal viibijate ohutust varasemate teadusuuringute põhjaliku ülevaate, numbriliste simulatsioonide, katsebasseini katsete ning täismõõtkavas merekatsete andmete analüüsi abil, lähtudes standardite ISO 2631-1:1997 ja ISO 2631-5:2004 ning Euroopa Liidu direktiivi 2002/44/EÜ ohutusjuhistest. Artiklis I esitatud kirjanduse ülevaade näitas, et liugrežiimis ületavad kere kiirendused sageli kehtivates ohutusstandardites soovitatud piirväärtusi.

Kahe kiirekäigulise liugkere numbrilised simulatsioonid regulaarsetes vastulainetes (artiklid II ja IV) näitasid, et suurel kiirusel ja kriitiliste lainepikkuste korral, mis vastavad ligikaudu 1,5–3 kere pikkusele, võib tekkida kere ulatuslik veest lahtitõusmine ehk fly-over, millele järgnevad tugevad löökkoormused. Need võivad oluliselt mõjutada pardal viibijate ohutust. Napoli Federico II Ülikooli tööstustehnika osakonna katsebasseinis erinevates ebaregulaarsetes lainetingimustes tehtud katsed näitasid, et kiirenduskoormus suureneb, kui aluse kiirus kasvab poolliugrežiimist üleminekurežiimi ning üleminekurežiimist liugrežiimi. Samas väheneb üleminekurežiimile vastavas kiirusvahemikus kere kiirendus töökiiruse suurenedes.

Kuna tegelikes töötingimustes puutuvad pardal viibijad kokku mitmesuunaliste kiirendustega, analüüsiti artiklis VI ka 12 täismõõtkavas merekatse käigus mõõdetud vertikaal-, ettepoole suunatud ja külgsuunalisi kiirendusi. Tulemused näitasid, et kuigi vertikaalkiirendus jääb domineerivaks komponendiks, ületab ka ettepoole suunatud kiirendus sageli soovitatud kokkupuute piirväärtusi ning nii ettepoole suunatud kui ka külgsuunalised kiirendused suurendavad märkimisväärselt pardal viibijate ebamugavust. Need tulemused näitavad, et üksnes vertikaalkiirendusel põhinev ohutuse hindamine võib alahinnata tegelikku üldist ohutusriski.

Teise uurimisküsimuse käsitlemiseks uuriti võimalikke pardal viibijate ohutuse parandamise strateegiaid. Artiklis I esitatud kirjanduse ülevaates tuvastati paljulubavate lahendustena aluse liikumisi vähendavad seadmed ja lööke leevendavad istmed. Vaikse vee numbrilised simulatsioonid (artikkel III) näitasid, et tavapärane ahtriinterseptorite süsteem (TIS, Transom Interceptor System) tekitab ahtri lähedale ühe kõrgrõhuala, samas kui topeltinterseptorite süsteem (DIS, Double Interceptor System) tekitab kaks kõrgrõhuala, mis on seotud vastavalt ahtri- ja eespool paikneva interseptoriga ning põhjustavad seetõttu erinevaid trimmimomente.

Seejärel uuriti TIS-i ja DIS-i toimivust regulaarsetes vastulainetes valideeritud numbriliste ja eksperimentaalsete analüüside abil (artikkel IV). Tulemused näitasid, et interseptorisüsteemide tõhusus sõltub tugevalt laine järskusest ja lainepikkusest. TIS parandas üldiselt dünaamilist käitumist ja vähendas löökkiirendusi rasketes lainetingimustes, samas kui DIS ei parandanud aluse dünaamilist vastust järjepidevalt.

Täiendavad katsed ebaregulaarsetes lainetes (artikkel V) näitasid, et TIS vähendas RMS-, VDV- ja Sed-väärtusi ning parandas pardal viibijate ohutust nii ülemineku- kui ka liugrežiimis. Mõnes üleminekurežiimi tingimuses suurendas TIS siiski mitut äärmuslikku kiirendustippu. Seevastu DIS suurendas liugrežiimis üldiselt kiirenduskoormust, mis näitab, et enne praktilist rakendamist on vajalik süsteemi täiendav optimeerimine.

Täiendava ohutuse parandamise strateegiana töötati artiklis VI välja lööke leevendava istme matemaatiline mudel, mis sisaldas nii vertikaal- kui ka ettepoole suunatud vedrustussüsteemi. Tulemused näitasid, et pakutud istmekonfiguratsioon võib vähendada pardal viibijale ülekanduvaid kiirendusi mõlemas suunas ning parandada mugavust ja ohutust võrreldes tavapärase, ainult vertikaalsuunalise vedrustussüsteemiga.

Kokkuvõttes rõhutab käesolev doktoritöö pardal viibijate ohutuse parandamise tähtsust kiirekäigulistel liugkeredel. Kuigi TIS ja lööke leevendavad istmed pakuvad võimalusi ohutuse parandamiseks, on ohutusriskide vähendamiseks vaja pardal viibijatele ülekanduvaid kiirendusi veelgi vähendada. Lisaks peavad terviklikud ohutushinnangud arvestama mitmesuunaliste kiirendustega, mida sageli ei käsitleta piisavalt ei aluse liikumisi vähendavate seadmete ega lööke leevendavate istmete uuringutes.

Appendix 1 (Publication I)

Paper I

Roshan, F., Dashtimanesh, A., & Kujala, P. (2024). Safety Improvements for High-Speed Planing Craft Occupants: A Systematic Review. Journal of Marine Science and Engineering, 12(5), 845. https://doi.org/10.3390/jmse12050845.

Journal of *Marine Science and Engineering*

MDPI

Review

Safety Improvements for High-Speed Planing Craft Occupants: A Systematic Review

Fatemeh Roshan [1,*], Abbas Dashtimanesh [2] and Pentti Kujala [1]

[1] Estonian Maritime Academy, Tallinn University of Technology, 11712 Tallinn, Estonia; pentti.kujala@taltech.ee
[2] Center of Naval Architecture, Department of Engineering Mechanics, School of Engineering Science, KTH Royal Institute of Technology, 11428 Stockholm, Sweden; abbasda@kth.se
* Correspondence: fatemeh.roshan@taltech.ee

Abstract: Moving fast by high-speed planing craft (HSPC) is advantageous for some special missions, though it causes severe hull vibrations and shocks that can transfer to the human body and increase health and comfort risks. This study reviews the current safety standards to avoid human safety risks affected by whole-body vibrations (WBVs), as well as the safety status of HSPC occupants. In addition, the efficiency of motion-reduction devices (trim tab and interceptor) and shock/vibration-mitigation devices (shock-mitigation seat) in improving the safety of HSPC occupants is examined according to existing documents. The research methodology was based on the Preferred Reporting Items for Systematic Reviews and Meta-Analyses (PRIS-MA) method, and published papers in the Scholar, Scopus, and Web of Science databases were analyzed. Because most of these publications are academic research, issues of bias in the eligible publications were not of particular interest. During this systematic review, many gaps and challenges in current information on safety improvement devices were found that need to be addressed in future studies, such as a lack of information on motion-reduction devices and shock-mitigation seat performance in reducing lateral and fore-and-aft motions. Referring to these gaps and challenges can be valuable as a suggestion to improve current knowledge in research and reduce safety risks.

Keywords: literature study; high-speed craft; motion-reduction device; shock-mitigation seat; whole-body vibration; onboard crew safety

check for updates

Citation: Roshan, F.; Dashtimanesh, A.; Kujala, P. Safety Improvements for High-Speed Planing Craft Occupants: A Systematic Review. *J. Mar. Sci. Eng.* **2024**, *12*, 845. https://doi.org/10.3390/jmse12050845

Academic Editors: Chenxu Wang, Jiaxuan Yang, Bin Xue and Degang Xu

Received: 16 April 2024
Revised: 15 May 2024
Accepted: 17 May 2024
Published: 19 May 2024

Copyright: © 2024 by the authors. Licensee MDPI, Basel, Switzerland. This article is an open access article distributed under the terms and conditions of the Creative Commons Attribution (CC BY) license (https://creativecommons.org/licenses/by/4.0/).

1. Introduction

High-speed planing crafts (HSPCs) are types of small high-speed crafts with length Froude numbers higher than 1 that can skim over the water surface. Although operation at high speeds by HSPCs offers significant advantages, it can also result in severe hull motions and intense shocks when encountering rough waters. These conditions pose safety concerns, leading to potential human injuries and disabilities for HSPC crews, as observed in previous studies [1–3]. Therefore, it is essential to improve HSPC occupants' safety by understanding the performance of the safety improvement devices and implementing them more effectively.

Figure 1 shows the literature trend for published documents using the terms "high-speed craft" and "human safety" in their abstracts for every five years from 1987 to 2023. Since the entirety of 2024 annual data is not yet available, it was not considered in this annual output. According to Figure 1, before 1992, safety on board HSPCs was not given as much attention, while the number of publications indicates an upward trend with time. Considering various reports of health risks on board these vessels [4–6], this upward trend demonstrates the increasing importance of the safety improvements of HSPCs.

There is numerous evidence demonstrating that the main reason for safety risks on board HSPCs is severe hull motions in different directions [7–13]. As hull motions occur in different directions with varying acceleration magnitudes and frequencies, HSPC occupants

might experience intense shocks and vibrations in all directions. These kinds of mechanical vibrations that can transfer to the human body and lead to safety risks and discomfort are known as whole-body vibrations (WBVs). WBVs can cause various safety risks for humans, such as pain in different parts of the human body, chronic stress, musculoskeletal problems, and nervousness [14–18].

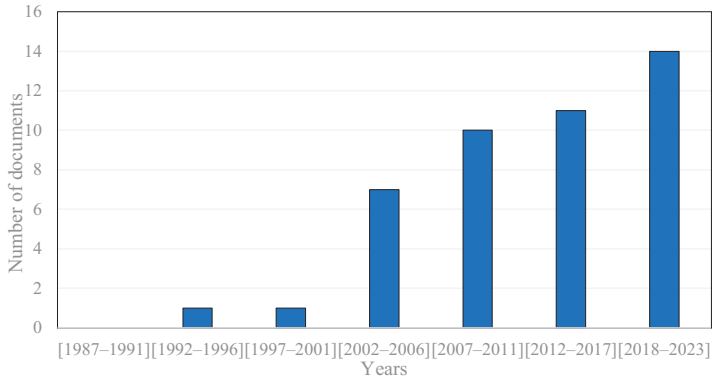


Figure 1. Annual scientific outputs contain "high-speed craft" and "human safety" in their abstracts.

During high-speed operations, fly-over phenomena with harsh impact shocks are probable [19], which lead to harsh shocks in both vertical and fore-and-aft directions. In these conditions, having a small roll angle during the impact causes severe lateral acceleration with serious effects on human nerve fibers, precipitating back pain and sciatica [20]. Figure 2 shows some examples of HSPC accelerations provided in previous research on an Atlantic 75 RIB boat operating in a mixture of head, beam, and following seas at speeds between 7.7 and 10.3 ms^{-1}.

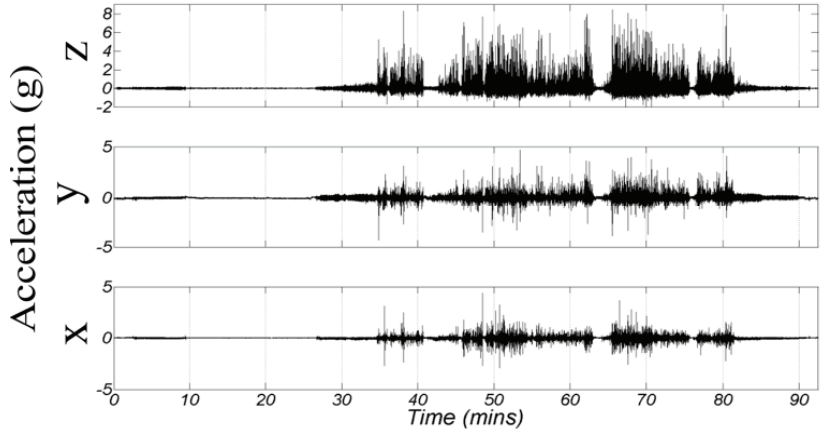


Figure 2. Examples of accelerations time series of HSPCs in vertical, lateral and fore–and–aft directions [21].

According to Figure 2, the highest acceleration is related to the vertical direction, with a maximum impact acceleration of $8\times\ g$ (here, g represents gravitational acceleration). In addition, maximum impact acceleration in fore-and-aft and lateral directions is $3\times\ g$ and $4\times\ g$, respectively. These high fore-and-aft and lateral acceleration peaks occur at the same time with high vertical acceleration. Therefore, it is expected that high vertical impact shocks could cause impact shocks in fore-and-aft and also lateral directions. The

effect of vertical vibrations recorded by Allen et al. [21] on human safety are analyzed later, considering the current safety standards.

Although vertical impact shocks are associated with impact shocks in fore-and-aft and lateral directions, the highest value of vibrations is in the vertical direction, which can even exceed $20\times g$ [22].

Hull motions in different directions can be transmitted to the human body and cause various safety risks. The effects of WBVs on the human body exposed to vibrations can be evaluated using current safety standards. These standards recommend a safe range for WBVs, considering the vibration direction, magnitude, and frequency, to avoid human health and discomfort risks. There are various published studies to evaluate human safety by comparing vibrations on board these vessels against the standard allowable ranges [23,24]. Although they have focused on vertical vibration and ignored other directions of vibrations, their results demonstrate that WBVs on board HSPCs are often higher than allowable safe ranges. Therefore, again, it implies the importance of the safety improvement of HSPCs to reduce human health issues.

1.1. Classification of Previous Studies on Safety Improvement of High-Speed Crafts

Generally, the preceding step to safety improvement is safety assessment. The previous studies on the safety assessment of humans on board HSPCs have been conducted by collecting crews' self-reports or safety evaluations using existing standards. The results of self-reported studies are qualitative, and they do not determine which kinds of vibrations and directions cause reported risks. However, the results of safety evaluations by employing safety standards are quantitative in terms of RMS and VDV values, which could be useful in finding the main reason for health issues and appropriate methods to avoid them. Consequently, the first part of this literature study will focus on safety standards and a summary of their applications to provide a basis for further discussions on motion reduction and shock-mitigation devices.

Since the main cause of human health risks are vibrations and shocks resulting from hull motions in rough water, two approaches are reviewed to improve human safety on board HSPCs: reducing hull motions (motion-reduction devices) and mitigating shock/vibration (shock-mitigation seats).

1.1.1. Standards

As mentioned before, some HSPC motions can be transferred to the human body and cause various health risks. Therefore, some national and international organizations have defined various safety guidelines and standards that can be used for the evaluation of the safety risks for humans exposed to WBVs. Some of these standards are defined by the International Standard Organization (ISO), European Union (EU), British Standards Institute (BSI), American National Standards Institute (ANSI), and Japanese Industrial Standards Committee (JISC). By implementing these standards in the context of HSPCs, safety-related issues can be accurately identified, enabling effective safety improvements.

Current safety standards for safety assessments consider different weighting factors for acceleration in each direction according to their frequency. Then, the root mean square (RMS) and vibration dose value (VDV) of weighted frequency accelerations should be calculated to compare against the allowable range for human health and comfort. In cases where RMS or VDV exceeds the allowable range recommended by standards, reducing WBVs is essential to avoid human health risks and discomfort.

Hull parameters such as deadrise angle, L/B ratio, and displacement have an impact on the hydrodynamic performance of an HSPC, including hull motions and accelerations [25–27]. Consequentially, when designing an HSPC, the consideration the safety issues is very important. However, for existing hulls, other safety improvement methods need to be considered.

Although reducing hull speeds may be the first action taken for crew safety, it is crucial to prioritize the well-being of the entire human–machine system and the mission. In

addition to reducing operation speeds, the use of various motion and vibration reduction tools and devices on HSPCs can be introduced as a preventive measure to reduce human health and comfort risks on board the HSPC.

1.1.2. Motion-Reduction Devices

HSPCs can be equipped with motion reduction equipment that actively or passively modulates body motion and improves not only crew safety but also calm water performance [28–31]. Although there are various types of motion-reduction devices, trim tabs and interceptors are used most commonly on HSPCs due to numerous published documents emphasizing their performance in reducing hull motions. Therefore, this study reviews current published studies on the effect of using these devices in HSPC motions to provide a deeper understanding of their performance and efficiency in safety improvements.

1.1.3. Vibration/Shock-Mitigation Devices

In addition, WBVs can be reduced by mitigating vibrations to avoid transferring them to the human body [32,33]. Shock-mitigation seats are effective devices for mitigating vibrations and shocks to improve the safety of seated humans. This study reviews the various studies that examine the efficiency of shock-mitigation seats in reducing WBVs using sea trial tests, drop-tower tests, and mathematical simulations.

1.2. Paper Ojective and Structure

This paper aims to provide a systematic review of occupant safety on board HSPCs and the performance of safety improvement devices and methods that can be implemented to reduce safety risks. This systematic review plays an important role in identifying existing gaps and challenges that need to be addressed in future studies to enhance current knowledge of the safety improvement of high-speed crafts. This aim can be achieved through the following objectives:

- Analyzing the current safety standards, considering the occupants' safety on board HSPCs.
- Investigating the influence of motion-reduction devices on the safety improvement of HSPC occupants.
- Examining shock-mitigation seat performance for the safety improvement of HSPC occupants.
- Identifying current research gaps and challenges in the safety improvement of small high-speed crafts.

This study is categorized into eight sections. Section 1 contains an introduction to the importance of safety improvements of HSPCs, considering the effects of WBVs on human safety risks. The literature review methodology for reviewing the safety of HSPC occupants is described in Section 2. In Sections 3–5 the selected documents are reviewed to answer the research questions and identify existing gaps and challenges. Section 3 reviews current safety standards to avoid human health risks, discomfort, and motion sickness as well as previous safety evaluations of HSPCs conducted by previous researchers. If vibrations on board an HSPC exceed the allowed range recommended by safety standards, it is crucial to reduce WBVs to avoid human safety risks. Therefore, Section 4 investigates motion-reduction devices and their effects on safety improvement. Additionally, the effectiveness of shock-mitigation seats in mitigating WBVs is analyzed in Section 5 by considering published studies based on seat trials, drop-tower tests, and mathematical simulations. Finally, Section 6 presents identified gaps and challenges in the safety improvement of HSPCs. The last section, Section 7, gives a summary of current information and future outlooks regarding required information that should be prioritized in future studies based on the identified gaps and challenges. Through this analysis, the paper strives to foster the implementation of effective safety measures to ensure a safer and more comfortable environment for HSPC crew members.

2. Literature Review Methodology

This systematic review follows the updated version of the Preferred Reporting Items for Systematic Reviews and Meta-Analyses (PRISMA) method, presented by Page et al. [34], based on a 27-item checklist. Figure 3 indicates the searching strategy for this review, which was a multi-step process of searching in different databases. The main research questions, inclusion and exclusion criteria, and defined keywords will be discussed later.

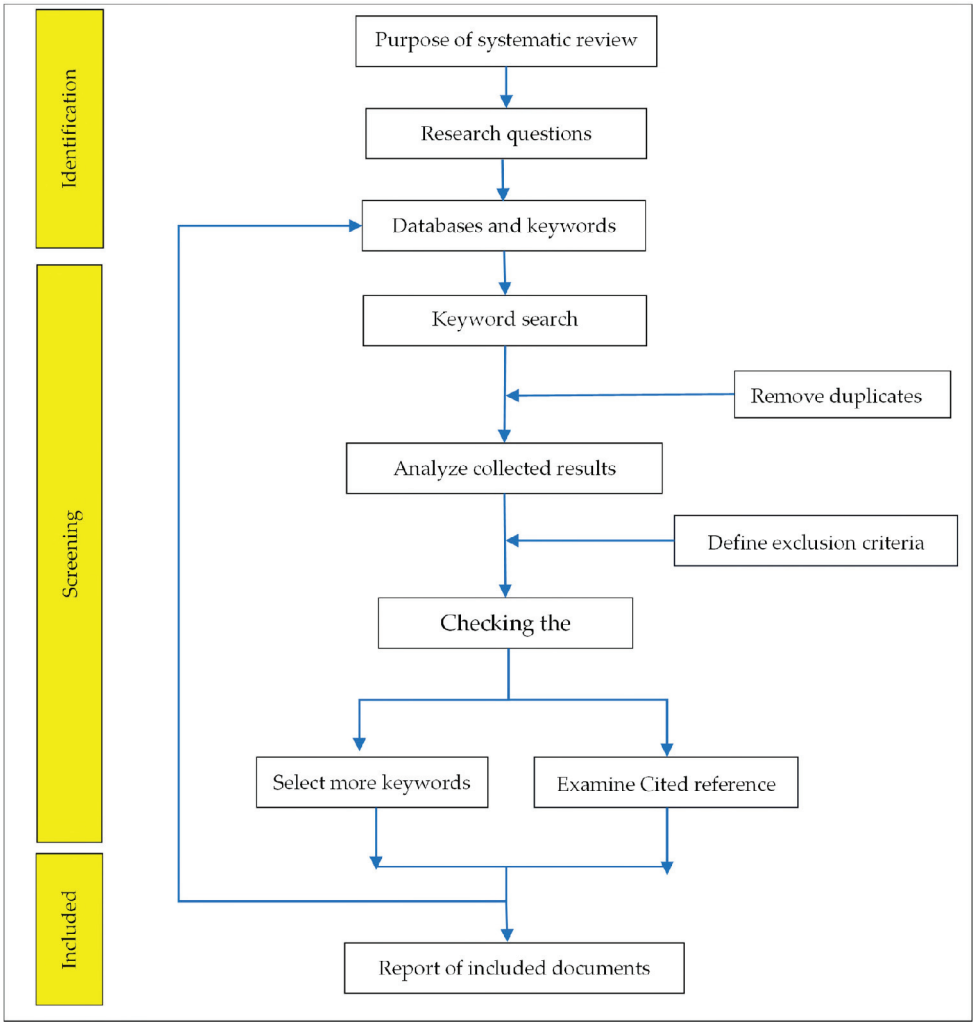


Figure 3. Search strategy.

According to Figure 3, from the collected relevant documents found for selected keywords, a search procedure on their cited references and keywords is conducted to find other documents that might not have been indexed in considered databases and defined keywords. The last step involves studying and analyzing all the collected references to provide appropriate answers to each research question.

2.1. Main Research Questions

There are many questions that might be raised by HSPC researchers, designers, and users regarding human safety that could cover a wide range of studies from various perspectives. In this paper, four main research questions are provided considering the objectives of this systematic review on the effects of WBVs on humans, as follows:

- RQ1. What are the current safety standards considering human safety on board HSPCs?
- RQ2. What is the effect of motion-reduction devices on improving the safety of HSPC occupants?
- RQ3. What is the effect of shock-mitigation seats on improving the safety of HSPC occupants?
- RQ4. What gaps and challenges exist in the current knowledge of safety improvement devices and methods that need to be addressed in future studies?

Regarding these questions and previous studies, appropriate keywords were selected that will be explained in Section 2.2. The next step involved exploring published studies containing selected keywords in their text in several scientific databases, including Google Scholar, Scopus, and Web of Science.

2.2. Search Keywords

Table 1 shows the initial research keywords selected according to the previous background, and the number of papers found in databases for each keyword combination. These results were found until February 2024, and some papers were repeated in two or three databases and even in two keyword groups. The first chosen keyword was "high-speed craft," specified by "whole-body vibration", because numerous documents confirmed that the main reason for human health risk on board HSPCs are WBVs. It could be useful to gather current evidence on WBVs on board HSPCs and their effect on human safety. In this step, some papers that studied the effect of WBVs on HSPCs' structure were excluded because they did not correspond to the aim of this study. Analyzing the results found revealed that most of them referred to using specific safety standards, including ISO 2631-1 [15], ISO 2631-5 [35], Directive 2002 [36], and BS 6841 [37]. Therefore, in the next stage, the guidance for these standards and their combination with "high-speed craft" was searched. Most of the papers found in this stage demonstrated that WBVs on HSPCs exceed the allowable range suggested by these standards. In such cases, it is necessary to minimize WBVs. Thus, various WBV reduction devices on board HSPCs were investigated using two approaches: reducing hull motions with motion-reduction devices and mitigating vibration with shock-mitigation seats, which both reduce the vibrations transmitted to the human body.

Motion-reduction devices introduced for high-speed crafts included transom flaps (interceptor and trim tab). Hence, the combination of "high-speed craft" with "interceptor" and "trim tab" was searched to find their efficiency in reducing hull motion and, consequently, WBV. In addition, the keywords "high-speed craft" combined with "shock-mitigation seat" were investigated as an effective means for mitigating WBVs and improving safety for a seated person. Shock-mitigation seats on board a vessel can be examined using sea trial tests, drop-tower tests (also called impact tests), and mathematical simulations. These keywords were searched in combination with "shock-mitigation seat" to ensure that no article was missed. Although the most reliable results for shock-mitigation seats on vessels are sea trial tests, Table 1 shows that current published studies in this field are limited. Hence, the combination of "shock-mitigation seat" with "drop-tower test", "impact test", and "mathematical model" were also examined. Using these keywords caused us to find some research on shock-mitigation seats in other vehicles, which were not excluded because we believe that these mathematical models and drop tests can be developed for HSPCs and sea states. Consequently, papers that contained those keywords were included in this study, even for other vehicles.

Table 1. Results of searching for keywords in different databases.

Keyword Group	Keywords Searches	Google Scholar	Scopus	Web of Science
Safety evaluation	High-speed craft, whole-body vibration	243	16	4
	High-speed craft, ISO 2631-1	128	3	2
	High-speed craft, ISO 2631-5	80	4	3
	High-speed craft, BS 6841	61	0	0
	High-speed craft, Directive 2002	61	1	1
Motion reduction	High-speed craft, trim tab	153	6	3
	High-speed craft, interceptor	269	53	16
	High-speed craft, transom flap	53	8	0
Shock/Vibration reduction	High-speed craft, shock-mitigation seat	34	9	2
	High-speed craft, suspension seat	76	11	1
	Shock-mitigation seat, sea trial	5	1	1
	Shock-mitigation seat, drop-tower test	2	1	4
	Shock-mitigation seat, impact test	11	10	12
	Shock-mitigation seat, mathematical model	13	4	5

Figure 4 presents the percentage of documents found in each section of this review. According to this figure, 31% of existing research on HSPC safety evaluates human safety using current standards, and 46% focuses on improving safety. From all of the published studies on safety evaluations, the majority (39%) considered the ISO 2631-1 [15] standard as a safety regulation for humans exposed to WBVs.

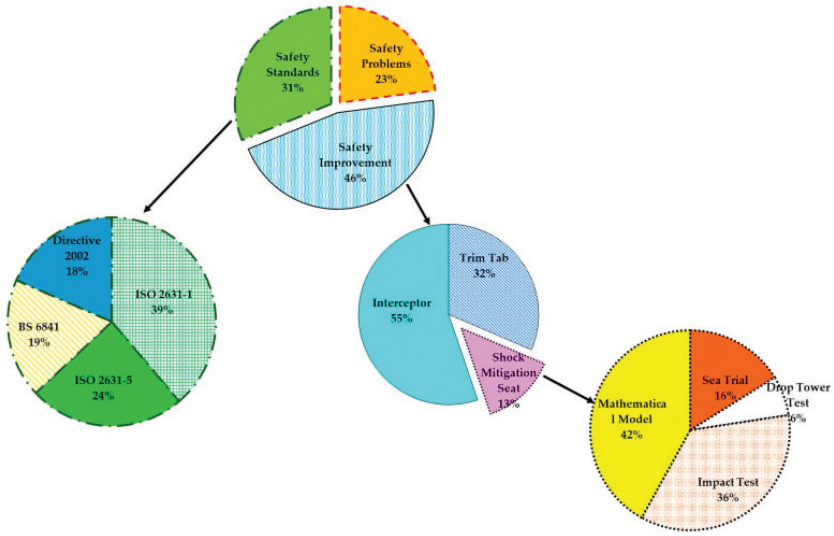


Figure 4. Percentage of studies included in each stage of this study.

To improve the safety of HSPCs, most researchers studied motion-reduction devices (55% interceptor and 32% trim tabs), while current information on shock-mitigation seats is limited (13%) because motion-reduction devices are also efficient in drag reduction. Figure 4 shows that investigating shock-mitigation seat performance is usually conducted mathematically (42%), which might be due to the lower cost and time associated with this approach. In addition, there are no CFD simulations of HSPCs containing a shock-mitigation seat. For instance, there are numerous hydrodynamic simulations of HSPCs in wave conditions using the Star CCM+. In addition, Star CCM+ has the opportunity to model mass, spring, and damper, though there are no CFD simulations of HSPCs combined with the shock-mitigation seat model.

2.3. Eligibility Criteria

After removing duplicates from the documents found for the search keywords, they were analyzed to exclude ineligible documents, considering defined exclusion criteria. Ineligibility criteria for this research included (a) some documents studied high-speed crafts that did not implement planning characteristics, (b) safety risk assessment documents related to other reasons than WBVs, (c) documents that studied the effects of vibration on structure, and (d) documents published by manufacturers of motion-reduction devices and shock-mitigation seats that could affect this research's bias.

Eligible papers for this review were (a) safety assessments of HSPC occupants considering the effects of WBVs, (b) hydrodynamic investigations of motion-reduction device performance on HSPCs, and (c) analyses of performance of various shock-mitigation seat models. Notably, the current studies of shock-mitigation seat performance in other vehicles, which were conducted using drop-tower tests or mathematical simulations, were also included because they can be useful to identify the lack of information in the marine environment.

3. Existing Safety Standards

Various transportation vehicles, including high-speed crafts (HSPCs), operate at different speeds and encounter environmental vibrations that can affect human health. To evaluate the effects of these vibrations on occupants, national and international committees have developed guidelines for human safety [15,35–40]. These guidelines consider factors such as vibration magnitude, frequency, direction, duration, and the individual characteristics of the occupants' bodies based on previous studies [41,42]. By measuring vibrations in different vehicles, such as trains, planes, cars, helicopters, and vessels, the potential risks for occupant health, comfort, and motion sickness can be assessed. Some of these standards are ISO 2631-1 [15], ISO 2631-5 [35], BS 6841 [37], and EU Directive 2002 [36], as well as ISO 2041 [38] and ISO 5805 [39] for vibration and shock terminology, and ISO 10326-1 [40] for vehicle seat vibration evaluation.

ISO 2631-1 [15] and BS 6841 [37] play a crucial role in guiding the measurement of WBV effects on human health, performance, comfort, perception, and motion sickness. These standards consider motion frequencies in the range of 0.1 to 80 Hz as effective vibrations on human bodies, while vibrations outside of this range have insignificant effects. Moreover, since vibrations can occur in different directions and have varying effects on the human body, weighted frequency signals are used to amplify hazardous frequencies and suppress non-hazardous ones in the time history of acceleration. Then, the effect of WBVs on human health, comfort, and motion sickness can be evaluated by calculating RMS and VDV for weighted accelerations in each direction. The RMS and VDV formulations can be found in Equations (1) and (2), considering ISO 2631-1 [15]:

$$\mathrm{RMS} = \left\{ \frac{1}{T} \int_0^T a_w^2(t) dt \right\}^{\frac{1}{2}} \tag{1}$$

$$\mathrm{VDV} = \left\{ \int_0^T [a_w(t)]^4 dt \right\}^{\frac{1}{4}} \tag{2}$$

where $a_w(t)$ is the frequency-weighted acceleration and T is the time period of the measurement. Figure 5 presents the safety evaluation process for different standards regarding the RMS and VDV values.

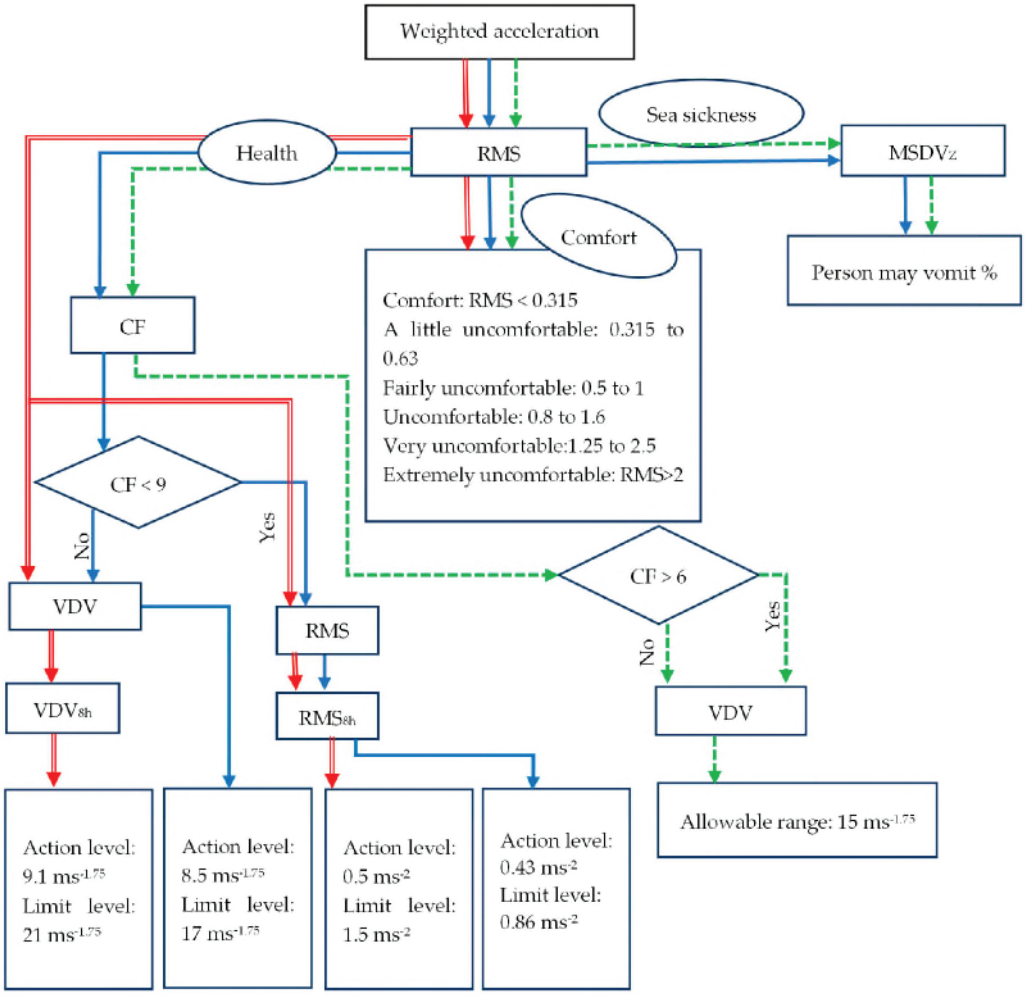


Figure 5. Safety evaluation methods according to the standards' (blue line is ISO 2631-1 [15], green dashed line is BS 6841 [37], and red double line is Directive 2002/44 [36]) guidance.

3.1. Human Health Assessment

Current safety standards consider human health problems as any injury to different parts of the body resulting from WBVs and use RMS and VDV for evaluating the possibility of human safety risks. ISO 2631-1 [15] suggests RMS as a criterion to assess human health risks and introduces a caution zone when the crest factor (maximum peak/weighted RMS) is lower than 9. The crest factor (CF) is a dimensionless parameter that is calculated by dividing the maximum instantaneous peak of the frequency-weighted acceleration by its RMS value.

A higher CF indicates harsh impact shocks in acceleration time history. In the case of using RMS individually to estimate human risks, impact shocks might be underestimated because occasional shocks can have a serious effect on the human body. Therefore, studying CF is as important as RMS to estimate human health risks.

According to ISO 2631-1 [15], $RMS_{8h} > 0.43\ ms^{-2}$ demonstrates a potential health risk, and if it exceeds $0.86\ ms^{-2}$, the likelihood of health risks escalates. Moreover, for CF > 9 with severe slam impact, using eVDV (estimated VDV; see the equation in [15]) or

VDV has been suggested. In this case, VDV > 8.5 $ms^{-1.75}$ indicates an action level, and VDV > 17.0 $ms^{-1.75}$ is a limitation level for human health risks. Similarly, BS 6841 [37] proposes VDV < 15 $ms^{-1.75}$ as allowable ranges to avoid human health injuries, which can be used for CFs lower and higher than 6.

The EU Directive 2002 [36] considers a wider range for RMS and VDV_{8h} to avoid human health risks. As is shown in Figure 5, RMS > 0.5 ms^{-2} demonstrates the action level, and RMS > 1.15 ms^{-2} the limitation range for human health. It also specifies VDV_{8h} > 9.1 $ms^{-1.75}$ as an action value and VDV_{8h} > 21 $ms^{-1.75}$ as a limitation value for vibration.

3.2. Human Comfort Assessment

Improving the comfort of occupants on board an HSPC is another crucial aspect of safety enhancement. According to current standards, an RMS value below 0.315 ms^{-2} indicates a comfortable condition for the crew. However, this comfort level changes to an uncomfortable situation when the RMS ranges from 0.8 to 1.8 ms^{-2} and becomes extremely uncomfortable for RMS values greater than 2.0 ms^{-2}. Similar to the health limitation ranges, these comfort criteria apply only for CF values less than 6.0 in BS 6841 [37] and less than 9.0 in ISO 2631-1 [15]. However, both standards do not provide predictions for crew comfortability for higher CF values, emphasizing the importance of considering these factors when assessing occupant comfort on HSPCs.

3.3. Motion Sickness Assessment

Motion sickness is a common issue faced by crews on board HSPCs, particularly within the motion frequency range from 0.1 to 0.5 Hz (BS 6841 [37] and ISO 2631-1 [15]). Both standards provide a similar prediction method for motion sickness, aiming to assess the likelihood of vomiting during vertical motions by calculating the motion sickness dose value (MSDVz) of vertical vibrations (see the equation in ISO 2631-1 [15]).

ISO 2631-1 [15] states that the possibility of motion sickness may be higher in children and women compared to adult individuals and men. Therefore, it is crucial to consider individual human characteristics when evaluating the occurrence of motion sickness. However, human gender and age are not considered in evaluating the motion sickness dose value. Additionally, MSDVz is calculated for vertical accelerations, and the effect of vibrations in other directions is neglected, while various studies showed the high possibility of motion sickness during pitch and roll and lateral vibrations [43–45].

3.4. Assessing Long-Term Effects of WBVs

In addition to the effects of WBVs on human health, comfort, and motion sickness, it is crucial to consider the long-term effects of vibration over an individual's lifetime. To address this, ISO 2631-5 [35] introduced a method to measure the effect of environmental vibrations on the bony vertebral endplate, considering the daily acceleration dose.

In ISO 2631-5 [35], two factors, Sed and R, are utilized to predict the effects of environmental vibrations on human health over a lifetime. Sed is used to assess adverse health effects based on the daily acceleration dose, while R evaluates these effects over a specific number of years of exposure. The equations for Sed and R can be found in ISO 2631-5 [35].

According to ISO 2631-5 [35], adverse health effects are less likely for Sed values lower than 0.5 MPa, whereas they become more prevalent for Sed values higher than 0.8 MPa. Similarly, R values lower than 0.8 indicate a lower possibility of health problems over the specified exposure time, while R values higher than 1.2 suggest a higher likelihood of adverse health effects during an individual's lifetime.

3.5. Safety Evaluations of HSPCs

There is some evidence from the safety assessment of HSPCs that indicates the high possibility of human health risks on board these vessels. Table 2 presents the measured RMS_z and $VDV_{8h,z}$ for conventional HSPCs in various sea states provided by previous

researchers. It is worth mentioning that conventional HSPC, in this study, refers to the common hull form employed for monohull high-speed planing crafts, because there are special types of HSPCs that are designed especially to be more comfortable with lower WBVs, such as catamarans, trimarans, and some HSPCs with suspension decks.

Table 2. Safety evaluation of conventional HSPCs.

Speed (ms^{-1})	Sea State	RMS(ms^{-2})	VDV($ms^{-1.75}$)	$S_{ed\text{-}8h}$ (Mpa)	Reference
7.72 to 10.3	1	-	62.03	-	[21]
	2	-	35.15	-	
20.57	-	2.0	51	-	[23]
25.7	1	1.9	65.2	5.7	[24]
	2	2.2	63.1	4.2	
	3	1.9	49.5	3.8	
	4	2.8	79	6.3	
	5	3	81	6.1	
15.0	1	4.9	-	-	[46]
	2	8.5	-	-	
	3	9.4	-	-	
	4	7.7	-	-	
	5	4.9	-	-	
12.9	403	1.92	-	-	[47]
	411	1.73	-	-	
15.4	404	2.35	-	-	
18.0	405	0.85	-	-	
	410	1.87	-	-	
	416	0.55	-	-	

According to Table 2, in all considered sea states and speeds, $VDV_{8h,z}$ is extremely higher than the range recommended by standards. In addition, the RMS_zs presented in all case studies are in "very uncomfortable" to "extremely uncomfortable" zones, which can cause discomfort issues for the occupants. Similarly, the S_{ed} calculated by Garme et al. [24] demonstrates a high prevalence of adverse health effects (additional results for other sea states can be found in [24,46]). According to these results, WBVs in the vertical direction in all investigated HSPCs are higher than the safe ranges suggested by standards. Therefore, there is a high possibility of safety risks for the occupants, and improving the safety of conventional HSPCs is essential to avoid safety risks.

It is also worth noting that most previous studies on safety evaluations of HSPCs have focused on vertical vibrations, and current information on the effects of other directions of vibration on human safety is limited. Therefore, current information is not enough to provide a general view of how much other directions of vibration could affect human safety. However, Ullman et al.'s [6] survey indicated that most of the human injuries occurred during the impact shock, which contained fore-and-aft and lateral accelerations.

4. Safety Improvement with Motion-Reduction Devices

The effects of WBVs on human safety can be assessed using current safety standards; thus, in the case of exceeding the recommended allowable range to avoid human injuries, it is essential to improve safety by reducing WBVs. To enhance human safety and comfort on board HSPCs, the focus lies on reducing WBVs through the implementation of various WBV reduction devices. For an HSPC, WBVs have a hydrodynamic source resulting from hull motions in rough water that are associated with severe accelerations. As a result, decreasing WBVs in HSPCs can be accomplished by reducing hull motions using motion-reduction devices such as trim tabs and interceptors.

In this section, we will focus on motion-reduction devices designed to mitigate the adverse effects of hull motions and vertical/lateral accelerations experienced by HSPC occupants, even during straight-line navigation in calm water conditions. These devices aim to suppress undesirable motions and accelerations to improve crew safety. The arrangement and general effect of these motion-reduction devices on the boat's hydrodynamics can be understood from Figure 6. To provide a comprehensive understanding, we will review previous studies on the implementation of these devices and compare their performance and effectiveness in reducing WBVs and enhancing the overall riding experience for onboard crews. The focus will be on the trim tab and interceptor.

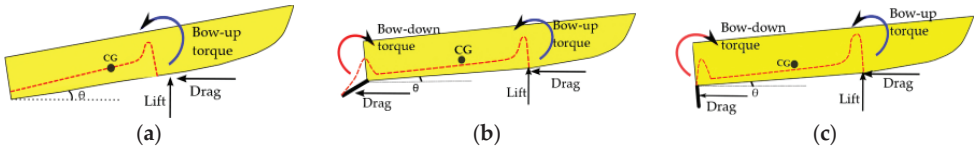


Figure 6. Hydrodynamic force around the HSPC for (**a**) bare hull, (**b**) with trim tab, and (**c**) with interceptor.

4.1. Trim Tab

The trim tab is a motion-reduction device that reduces hull motions by creating an additional lift force at the transom. Figure 6a,b illustrate the comparison of hydrodynamic force distribution over the hull bottom with and without the trim tab. Without the trim tab, the high-pressure region in the stagnation line creates a high lift force acting at $\times 1$ distance from the CG (Center of Gravity), resulting in a bow-up torque that increases the trim angle and leads to severe slamming. However, when a trim tab is added at the transom, it creates another high-pressure region near the transom and generates a bow-down torque to reduce the trim angle [30]. This implementation of the trim tab helps in reducing hull motions and, consequently, acceleration to enhance crew safety and comfort on HSPCs.

Various studies have investigated the effects of trim tabs on reducing the trim angle [45–51] and avoiding porpoising in calm water [52–55]. These studies collectively demonstrate the significant role of trim tabs in improving hull stability and reducing motion in various water conditions. Furthermore, it should be considered that trim tab efficiency is influenced by factors such as trim tab geometry, dimension, and angle [56–59]. Careful consideration of these factors is crucial for achieving optimal results in WBV reduction and the overall safety enhancement for HSPCs.

Indeed, while reducing trim angle and avoiding porpoising in calm water may be effective in reducing vertical motions and acceleration in waves, when using a fixed trim tab, designing an optimal trim tab for every wave condition is challenging, even when assuming a constant speed. Wang [52] demonstrated that a fixed trim tab can effectively reduce vertical hull acceleration in certain wave conditions. However, in scenarios with higher wave frequencies or lower speeds, it can result in excessive pitch motion and increased vertical acceleration. This limitation highlights the need for adaptive or controllable trim tab systems that can dynamically adjust to varying wave conditions and vessel speeds to ensure the optimal reduction of vertical acceleration and improve overall crew comfort and safety during HSPC operations. Such adaptive systems can play a vital role in mitigating the effects of hull acceleration and enhancing the onboard experience for the crew in a variety of sea states.

The implementation of a controllable trim tab, where the tab can rotate around the connection point while maintaining constant span and chord length, has shown promising results in reducing vertical motions in wave conditions. Previous studies revealed that a controllable trim tab can effectively reduce the amplitude, velocity, and impact acceleration of vertical motions [52,60]. Katayama et al. [61] demonstrated a significant reduction in pitch motion, with a 25% decrease in wavelength at 1.3 L_{OA} (the overall length of the hull) and an approximately 70% reduction in pitch amplitude in irregular waves.

Moreover, Santos et al. [62] employed a fuzzy controller system for transom trim tabs and a T-foil near the bow to address vertical motions and enhance safety at different speeds. Their study showed that the control system led to a remarkable reduction in vertical acceleration, with an approximately 67% decrease in pitch acceleration, thereby reducing the possibility of motion sickness.

Table 3 provides a concise summary of previous research findings on the efficiency of trim tabs in reducing various HSPC motions and accelerations in waves. These studies collectively indicate that controllable trim tabs offer a promising solution to effectively mitigate the adverse effects of hull motions in different sea states, enhancing crew comfort and safety on board high-speed crafts.

Table 3. Effects of trim tab on motion reduction of various HSPCs.

Fr_L	Wave	Result	References
1.2	Regular wave	50% reduction in pitch amplitude in resonance wave 17% reduction in heave amplitude in high wavelengths 22% reduction CG acceleration in high wavelengths 22% increase CG acceleration in short wavelengths 26% bow acceleration reduction	[52]
1.4	Regular wave	60% reduction in pitch amplitude 30% reduction in heave amplitude in high wavelengths 20% reduction in CG acceleration in high wavelengths 35% increase CG acceleration in short wavelengths 40% bow acceleration reduction	[52]
2.9	Irregular wave	25% reduction in vertical bow acceleration	[29]
2.3	Irregular wave	26.1% reduction in pitch acceleration 35.5% reduction in motion sickness incident	[62]
3.1	Irregular wave	41.1% reduction in pitch acceleration 56.14% reduction in motion sickness	[62]
7.8	Regular wave	10–25% reduction in pitch amplitude	[55]

While vertical accelerations are a significant concern for onboard crew injuries in HSPC, it is essential to acknowledge that longitudinal and lateral accelerations also play crucial roles in influencing human safety. Studies have primarily focused on the trim tab's efficiency in reducing HSPC roll motion, as demonstrated by Hughes and Weems [63]. However, there is still limited information available on the trim tab's effect on reducing longitudinal and lateral accelerations.

Addressing the reduction of longitudinal and lateral accelerations is vital, as they can lead to discomfort, motion sickness, and potential injuries for the crew. Further research and studies are required to explore and quantify the trim tab's impact on minimizing longitudinal and lateral accelerations. Understanding these effects will be valuable in designing more comprehensive and effective solutions to enhance crew safety and comfort on board HSPCs.

4.2. Interceptor

The interceptor is a vertical transom flap installed symmetrically in the transom to reduce hull motion and acceleration. Similar to the trim tab, the interceptor creates a high-pressure region near the transom, as shown in Figure 6c, resulting in a large lift force that helps reduce vertical hull motions and acceleration, thereby improving HSPC safety and fuel consumption [64].

Numerous studies have demonstrated the interceptor's effectiveness in reducing the trim angle and hull motions [65–67]. While the interceptor's behavior resembles that of the trim tab, researchers have compared the two devices to identify the most effective solution for reducing hull motions.

Some studies demonstrated that interceptors are superior in trim reduction [68], while others showed that trim tabs result in more trim reduction [56]. These differences could be attributed to variations in the dimensions and configurations of the trim tab and interceptor used in each study. Similar to trim tabs, the performance of interceptors is highly influenced by their geometry, including position, span, and height. As a result, the effect of interceptors on reducing hull trim angle may vary significantly depending on their specific dimensions, even when applied to the same hull at the same speed [69].

Increasing the height of interceptors can lead to a reduction in trim and resistance in calm water conditions [70–76]. However, caution is necessary, as using an interceptor height exceeding 60% of the boundary layer thickness around the hull may induce negative trim angles, increase hull resistance, and pose safety concerns [30,71].

Furthermore, Avci and Barlas [77,78] explored the impact of interceptor position on trim reduction and found that a full-length interceptor, covering the entire width of the transom, is more effective. Nevertheless, they noted that a full-length interceptor with a height-to-waterline length ratio (h/L) greater than 0.15 could lead to negative trim angles at high speeds. To address these issues and optimize performance, the use of controllable or active systems for interceptors has been suggested by researchers such as Katayama et al. [61] and Park et al. [79]. With a controllable system, the interceptor height can be adjusted based on the operating speed and sea conditions, providing an efficient and adaptable solution for trim reduction and enhanced safety on HSPCs.

Several studies have demonstrated the effectiveness of installing interceptors on the HSPC's transom in reducing vertical hull motions and acceleration in wave conditions [80–82]. However, it should be noted that the efficiency of interceptors in wave conditions is influenced by hull speed and wave frequency, which can lead to a negative trim angle at certain wavelengths and speeds. To address this issue and optimize the interceptor's performance, the use of a controllable or active system has been suggested [29,61,83].

The superiority of an active interceptor over a fixed interceptor in reducing heave and pitch motions has been demonstrated by Park et al. [79]. By employing a controllable system, the interceptor's height can be adjusted dynamically, allowing for better adaptability to different sea waves and avoiding adverse effects that could arise with fixed interceptors. Overall, using a controllable or active system for interceptors provides a more versatile and efficient solution to reduce vertical hull motions and acceleration to enhance the safety and comfort of occupants on board HSPCs during wave conditions.

5. Safety Improvement by Shock/Vibration-Mitigation Devices

Despite using motion-reduction devices, hull motions of high-speed crafts (HSPCs) in rough waves cannot be entirely eliminated, subjecting onboard crews to vibrations. To enhance human safety, shock-mitigation seats are employed to mitigate WBVs transmitted to the human body.

Shock-mitigation seats have been developed and widely adopted in various modes of transportation like aircraft, trains, and marine vehicles. These seats utilize a combination of mass, spring, and damper systems to absorb vibrations and ensure comfort for the seated person. There are four main types of suspension seats designed to mitigate accelerations exceeding 0.001 ms^{-2}: passive, adaptive, semi-active, and active suspension seats. Each type differs in energy source, cost, maintenance, fixability, and efficiency across different frequency ranges. For further details, see [84–86].

When selecting a suitable suspension seat for high-speed crafts (HSPCs), several factors, such as lateral stability constraints, foot strap cost, and efficiency in the marine environment, must be considered [22]. To identify the most effective models for HSPCs, researchers have compared the efficiency of different seats. McMorris et al. [17] highlighted the advantages of suspension seats over fixed seats in reducing fatigue and sleepiness in HSPCs. The efficiency of suspension seats in mitigating WBVs compared to fixed seats can also be found in [8,23,86,87]. Various approaches can be used to examine shock-mitigation seat efficiency, considering the most dangerous vibrations for humans.

Human injuries on board HSPCs can result from repeated continuous vibrations and slam impact shocks. For repeated continuous vibration, typically, sea trial tests are conducted to evaluate human safety. On the other hand, slam impact shocks are studied using drop-tower tests, which allow researchers to predict the seat response to transient pulses. In addition, the mathematical model of shock-mitigation seats can also be used to simulate both repeated continuous vibration and drop-tower tests to predict seat efficiency with lower cost and time. These distinct approaches enable a comprehensive understanding of the effects of both mechanisms on reducing vibrations and shocks. Therefore, in the next subsections, previous studies on shock-mitigation seats are discussed, considering their investigation methods.

5.1. Sea Trial Tests

To estimate the effects of vibrations on human response, safety standards emphasize considering the time duration of exposure as a critical parameter. Sea trial tests have emerged as a well-established method for studying this aspect, extensively used by numerous researchers. For instance, Allen et al. [21] conducted two sea trials on an HSPC, varying speed and duration, and measured the VDV. Their findings revealed that the VDV exceeded the proposed standard ranges, indicating potential safety concerns. Dobbin et al. [23] analyzed the VDV and crest factors for both fixed and suspension seats in the vertical direction. While both seat types showed considerably higher values than the standards, suspension seats demonstrated the ability to reduce peak impact acceleration by up to 57%. Additionally, Garme et al. [24] conducted 12 sea trial tests, studying human response to vibration. These studies demonstrated that shock-mitigation seats effectively reduce the vertical VDV and human health risks across different sea states, highlighting the benefits of implementing such seats in HSPC operations.

Indeed, there are different perspectives on shock-mitigation seats. Riley et al. [88] presented an alternative view based on their sea trial studies. Surprisingly, they found that using a soft seat cushion could lead to vertical acceleration amplification [89], resulting in an increased number of acceleration peaks or impacts. As it has been mentioned, shock-mitigation seat performance in absorbing slam impact shock can be investigated with drop-tower tests.

5.2. Drop-Tower Tests

Indeed, while sea trials are highly effective for studying shock-mitigation seat performance, they come with significant costs and time requirements. Additionally, sea trials may not adequately address harsh impact shocks and accidental conditions. To address these limitations, researchers have proposed laboratory drop-tower tests as an alternative method for predicting seat performance in absorbing slam impact shocks and determining damping duration.

Various studies have explored the use of drop-tower tests for this purpose, such as [90–96]. These laboratory-based tests offer a controlled and repeatable environment for simulating transient pulses like slam impacts, providing valuable insights into seat performance, and enhancing their design for improved passenger safety in challenging conditions. In the drop-tower test method, the shock-mitigation seat is raised to a certain height and then released to impact a surface on the ground. This test measures the seat's response and the time duration for damping vertical acceleration. For more details, refer to [97].

According to Kearn's investigations in a drop-test study from 2001, when the seat is released, the seat base experiences vertical acceleration due to the gravity force, while the seat cushion has no acceleration [97]. The seat pan acceleration begins when the seat base reaches maximum negative acceleration. As a result, there is a phase difference between the seat base and seat pan responses. This phase difference has also been confirmed by other researchers [88,98,99]. Understanding these dynamics is crucial for accurately assessing

the shock-mitigation seat's performance and optimizing its design to effectively absorb impacts during marine operations.

The experiments conducted by Kearn [97] and Alam et al. [95] were replicated at different drop heights, and they demonstrated significant shock reduction using suspension seats in all considered conditions. However, contrary opinions have been expressed, stating that suspension seats could sometimes result in the amplification of relative acceleration between the deck and the occupant [88,98,100–102].

Drop test studies conducted by Petersen and Riley [103] revealed the challenge of absorbing long-duration wave impact shocks (ranging from 100 to 450 milliseconds) for HSPC seats, and the possibility of dynamic amplification. Shock amplification by a suspension seat during slamming impact depends on the specific seat characteristics and can be predicted by selecting an appropriate drop height in the drop-test study.

Indeed, careful assessment and understanding of suspension seat dynamics in various scenarios are crucial for ensuring optimal design and performance, ultimately enhancing passenger safety during high-speed marine operations. Choosing the appropriate drop height for drop-tower tests is a critical parameter that should be determined by considering the wave impact data obtained from sea trials, as highlighted in [89,102]. Predicting the possibility of shock amplification that may lead to bottom impacts and human injuries is essential for improving occupant safety in HSPCs under different sea states.

Other studies on shock-mitigation seats using drop-tower tests have been presented in [104–106]. Although Gunston et al. [107] believed that this method might not accurately match high-impact and stochastic conditions, Marshall and Riley [96] conducted a comparative study between a shock-mitigation seat's performance in a laboratory drop test and real sea trials. Their findings showed good accuracy in predicting the seat's mitigation capabilities for shock impacts.

By combining sea trial data with well-designed drop-tower tests, researchers can gain valuable insights into shock-mitigation seat behavior, enabling improvements in seat design and enhancing passenger safety in HSPCs under varying environmental conditions.

5.3. Mathematical Modeling of Shock-Mitigation Seat

Mathematical modeling is a reliable approach for predicting shock-mitigation seat performance in mitigating repeated continual vibrations and impact shocks. The studies by Olausson and Garme [108] and Marshall and Riley [96] have compared mathematical results with both sea trials and drop-tower tests, confirming the acceptable accuracy of the models. Other researchers have also conducted sea trial tests on shock-mitigation seats to verify mathematical models against real sea states [87,104,109].

Selecting an appropriate seat model is a crucial step in using mathematical models for dynamic studies of shock-mitigation seats. As mentioned earlier, shock-mitigation seats comprise a system of mass, spring, and damper with various configurations and properties. Therefore, considering the seat configurations and the study aim, various mathematical models can be suggested for studying seat efficacy. For instance, to study the seat cushion's influence on vibrations, a model with two DOFs is required. However, the seat cushion effect might not be the aim of some other studies, and others prefer to use a 1DOF seat model and ignore the cushion effect to simplify the problem. The choice of the seat model should be carefully considered to ensure that it accurately reflects the seat's behavior and response to different dynamic conditions, thereby providing valuable insights for improving seat design and enhancing passenger safety in high-speed marine operations. Table 4 shows some of the different types of shock-mitigation seat models that have been used by previous researchers for mathematical modeling. These models are categorized based on their complexity. It is also worth mentioning that some seat models in Table 4 have been designed for other vehicles; however, there are two reasons for including them: current seat models for HSPCs are still limited, and these seat models can also be employed to investigate the effects of fore-and-aft and lateral vibrations, which are significant in

HSPCs. Therefore, it is suggested to consider these kinds of seat models for HSPCs in future studies.

The seat model A1, with its single degree of freedom (1DOF), is the simplest representation used by researchers to simulate the slam impact test [102,110–113]. In this seat model, K and C are spring stiffness and damping coefficients that are used for the seat by the manufacturer, and m_1 is a summation of seat weight + cushion weight + the weight of the upper body and thighs of the seated human body. The weight of the upper body and thighs is 72.3% and 9.5% of the total human weight, respectively [114].

Although seat model A1 can simply model the shock-mitigation seat, it is important to consider that Riley et al. [88] found that seat cushions may amplify vertical acceleration, a factor that is not accounted for in this basic model. Moreover, the effects of longitudinal and lateral acceleration cannot be studied using this model, while, according to the Ullman et al.'s [6] study, most of the human injuries are related to impacts that contain lateral force. As a result, more complex seat models with additional degrees of freedom are suggested to better understand and predict the behavior of shock-mitigation seats under various dynamic conditions.

To study the effects of both longitudinal and vertical vibrations, seat model A2 can be used. Chen et al. [115] adopted this model, which consists of an oblique damper with longitudinal and vertical elements to absorb vibrations in these directions. This model is the simplest model and it can be developed to consider the effects of seat cushions.

Seat models B1 to B4, which incorporate 2 degrees of freedom (2DOFs), are recommended for studying shock-mitigation seat performance with a cushion and focus on vertical acceleration. In this model, m_1 is the weight of the seat mass, and m_2 is a summation of seat cushion weight (if the cushion effect is ignored) and the weight of the seated human's upper body and thighs. In addition, K_1 and C_1 are the seat model parameters, which are the same as seat model A1. If this seat model is considered to simulate the seat cushion, K_2 and C_2 can refer to the cousin parameters defined by the manufacturer. In some studies that ignored the seat cushion, K_2 and C_2 have been used as human parameters. According to Olausson and Garme, K_2 is 869.40 m_2 and C_2 is 21.25 m_2.

Model B1 was used to compare foam and suspension seats in waves, with an emphasis on mitigating vertical acceleration [116]. In this model, the occupant's mass (m_2), cushion stiffness (K_2), and damper (C_2) are considered, along with seat characteristics (m_1, k_1, and c_1).

Following the introduction of model B1, Alam et al. [95], Townsend et al. [16], Ereq [109], and Ekstrom [86] used model B2 to predict seat performance in absorbing slam impacts. Additionally, model B2 was applied by other researchers to study HSPCs in different sea states [84,86,108,109,117,118]. In previous research, seat model B2 garnered more interest among researchers compared to model B1. However, Wei and Garffin [119] conducted a comparison between these two models and recommended using model B1 as it was found to be more accurate.

Another seat model that considers the seat cushion effect, introduced by Wice [99], is known as model B3. Wice [99] used this model to study slamming impacts and simulating sea states, achieving good agreement with experimental results. As is shown in Table 4, the active component force (fu), friction force, and also the pitch moment have been considered in this model.

These 2DOFs seat models (B1 to B3) offer a more comprehensive representation of shock-mitigation seat behavior, incorporating both cushion properties and seat characteristics, thereby providing a more accurate understanding of the seat's performance in various dynamic conditions compared to seat model A.

Although vertical vibration is usually associated with the highest weighted acceleration in HSPCs, longitudinal and lateral acceleration are also relevant and can influence human health and comfort. Therefore, different directions of vibration should be addressed in designing and evaluating shock-mitigation seat performance. Seat model C1 is a mathematical model developed by Maciejewski et al. [120] to investigate the effects of

longitudinal acceleration on a seated person. However, this model cannot investigate the effects of vertical vibrations.

Seat model C2, introduced by Choi et al. [121] considers two degrees of freedom (2DOFs) for shock-mitigation seats. In this model, m_1, m_2, K_1, K_2, C_1, and C_2 are the same as seat model B, and also, K_3, C_3, and u refer to seat properties defined by the manufacturer. Although this seat model has been designed for trucks due to its high vertical and horizontal accelerations, it can also be used for studying shock-mitigation seats in marine environments, which have high accelerations in different directions, similarly to trucks. This model is capable of mitigating both vertical and longitudinal acceleration as it incorporates an x-direction component. In contrast, seat models A, B, and C (Table 4) are free to move upward, and their travel length is not defined.

The travel length of shock-mitigation seats is an essential parameter for predicting the occurrence of the "Bottom impact" phenomenon. A few previous studies have presented the maximum displacement obtained during their research to predict the possibility of bottom impact, such as Olausson and Garme [108]. However, other studies on shock-mitigation seats on trucks, roads, and off-road vehicles have preferred to use seat models D1 to D3, which are limited in travel length, to avoid bottom impact. By incorporating these limitations, seat models D1 to D3 provide a more accurate representation of the seat's behavior during extreme dynamic events, particularly when the seat might reach its travel limit and experience bottom impacts. These seat models can also be used for HSPCs that have a high possibility of bottom impact.

The choice of seat model depends on the research objectives and the specific scenario being studied. Models with limited travel length are especially useful for simulating harsh impacts and avoiding the potential risks associated with bottom impacts.

Rebelle [122,123] proposed the simplest seat model, considering vertical motion with restrictive components, which was initially designed as a lift truck seat model. This basic concept was further developed into the D2 model in [124–126]. Model D2 not only incorporates longitudinal components but also has a limitation on vertical motion.

In response to the limitations of D2, Gunston et al. [107] decided to use seat model D3, which includes restrictive components in both the x- and z-directions. By adding restrictions in two directions, model D3 provides a more comprehensive representation of shock-mitigation seat behavior, particularly in situations involving multi-directional impacts and dynamic forces.

These seat models (D1 to D3) with restrictive components are especially valuable for studying shock mitigation in extreme conditions where the seat's motion may be constrained, providing insights into the seat's performance under challenging dynamic events and helping to ensure passenger safety in high-speed marine operations. It is worth mentioning that these seat types have not been employed on board marine vehicles so far.

Table 4. Various mathematical models for shock-mitigation seats.

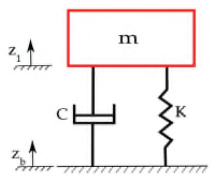
Seat Model	Modeling Schematic	Description	References
A1		Single degree of freedom Ignoring the cushion effects	[102,110–112,115,119]

Table 4. *Cont.*

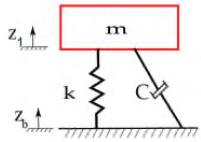
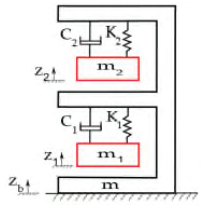
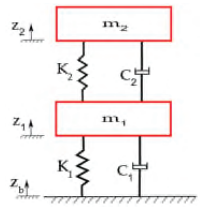
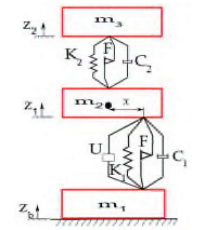
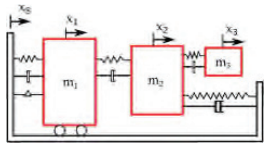
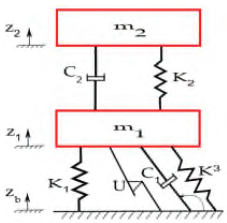
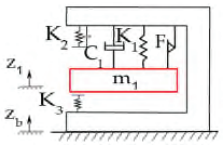
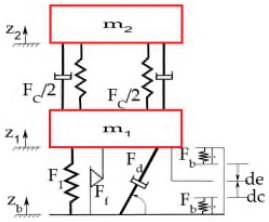
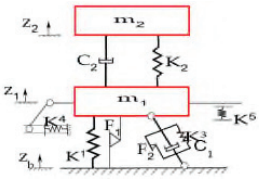
Seat Model	Modeling Schematic	Description	References
A2		Capability to study vertical and longitudinal vibrations	[115]
B1		Considering cushion effects Considering rigid support	[116,119]
B2		Eliminating rigid support Considering cushion effects	[16,85,86,94,108,109,117–119,127]
B3		Considering fixed frame and cushion effects Considering friction and active components Capability to study angular acceleration mitigation	[98]
C1		Considering longitudinal acceleration	[120]
C2		Considering seat and cushion effects Considering oblique damper and spring Considering active controller (u) for seat Capability to study lateral motion mitigation Proposed for trucks	[121]
D1		Suggested for truck seats Considering top and bottom buffers Ignoring cushion effects Proposed for trucks	[122,123]

Table 4. *Cont.*

Seat Model	Modeling Schematic	Description	References
D2		Considering seat and cushion effects Considering top and bottom buffer Considering oblique damper Proposed for on-road and off-road vehicles	[124–126]
D3		Considering seat and cushion effects Considering top and bottom buffer Considering oblique spring, damper, and friction component Capability to mitigate lateral motion Considering end-stop buffer for lateral motions Proposed for off-road vehicles	[107]

Once the most suitable seat model is selected for mathematical simulation, seat component parameters such as stiffness, damping coefficient, mass, etc., can be determined through laboratory tests, as demonstrated in [99,105,128]. These laboratory tests provide valuable data to accurately represent the behavior and response of the shock-mitigation seat under different dynamic conditions.

To study more about human safety on board HSPCs, the results of the seat's performance in mitigating vibrations can then be utilized in a biodynamic study to predict the potential for human injuries. By considering the interactions between the seat and the human body, the biodynamic study helps assess the seat's effectiveness in reducing vibration-related health risks for onboard crews during high-speed marine operations.

The integration of mathematical modeling, laboratory tests, and biodynamic studies forms a comprehensive approach to designing and evaluating shock-mitigation seats, ultimately leading to improved passenger safety and reduced risks of injury during marine operations.

6. Gaps and Challenges

This paper has addressed the current standards related to human safety in vibrated environments and analyzed the safety of HSPCs regarding these safety standards. Safety evaluations of HSPCs demonstrate the high possibility of safety risks though safety improvement devices can efficiently improve human safety. Therefore, the efficiency of motion-reduction devices (such as trim tabs and interceptors) and vibration/shock-reduction devices (shock-mitigation seats) in reducing hull acceleration has been investigated. During this systematic review of current studies, many gaps and challenges in the safety assessment of HSPC occupants and safety improvement devices have been identified that are required to be addressed in future studies:

Identified Gaps and Challenges

1. Current information on the effects of vibrations in different directions is limited. Measuring vibration in all directions during sea trial tests of HSPCs and considering all directions of vibration in safety evaluations is required to evaluate the effect of fore-and-aft and lateral vibrations on human safety. In addition to the sea trial tests, numerical approaches might be applicable in predicting impact shocks in other directions, as [19] demonstrate their capability in predicting vertical impact shocks.

2. Current information on motion-reduction devices' performance in reducing fore-and-aft and lateral acceleration is limited. Therefore, it is required to investigate the efficiency of trim tabs and interceptors in reducing lateral and fore-and-aft accelerations, as well as the effect of their dimensions. This study could be useful to implement them more efficiently, with the aim of improving the safety of HSPC occupants.
3. Although numerous studies confirm the efficiency of using active control systems to improve the efficiency of motion-reduction devices, current information is still limited. Therefore, more research is needed to optimize the design and efficiency of active control systems for motion-reduction devices in HSPCs, especially in wave conditions.
4. There are some studies that show promise in reducing hull motions and acceleration using combined motion-reduction devices, for instance, interceptor–trim tab, but there are few published studies, and their performance in waves and lateral acceleration reduction requires exploration. Combined motion-reduction devices can be studied in future work using mathematical models, CFDs, and experimental approaches.
5. Existing studies on shock-mitigation seats mainly focus on vertical motion and overlook the effects of lateral and fore-and-aft accelerations, which are significant factors for occupants' safety. Although there are some new types of shock-mitigation seats that manufacturers believe are effective in reducing vibrations in other directions, there are no academic publications to confirm this. Future studies can provide an important step toward improving seated human safety by studying the efficiency of these seat models in mitigating vibrations in other directions.
6. There are numerous studies that demonstrate the effects of footrests on transmitted vibrations to the human body in other vehicles. However, in most of the current studies on safety evaluations and shock-mitigation seat performance for HSPCs, the effect of footrests has been ignored. In addition, the seat backrest is also effective in mitigating fore-and-aft acceleration and rotational vibrations, which are ignored in current studies. Therefore, it is required to develop the current mathematical seat models to consider the effect of backrests and footrests in future studies.
7. There is a lack of appropriate human models for HSPC occupants. Numerous studies have simulated the seated human body using a system of masses, springs, and dampers. These studies are useful to predict the transmitted vibrations to each part of the human body and estimate the probability of injury to that part. These models can also be employed for a standing position, which is a common work position on HSPCs.

7. Summary and Future Outlook

This paper addressed the current standards related to human safety in vibrated environments and safety improvement methods for reducing HSPC motions (trim tab and interceptor) and reducing vibration/shock transmitted to seated humans (shock-mitigation seat). Reviewing published documents is an efficient way to determine the safety status of HSPCs, safety improvement device performance, and existing gaps and challenges in current information. As an example, most studies on safety evaluations of HSPCs and motion-reduction devices have focused on reducing vertical motions, with limited information on their effectiveness in reducing other directions of motion. In addition, active control systems for these devices have been proposed as a superior solution, but more research is needed to optimize their design and efficiency, especially in wave conditions.

Regarding shock-mitigation seats, numerous studies have evaluated their performance in absorbing vibrations for various vehicles. However, the use of CFD models for shock-mitigation seat studies in HSPCs is still limited. Additionally, existing studies have mainly focused on vertical motion and neglected the effects of other motions, such as lateral and fore-and-aft accelerations. The consideration of seat backrests, footrests, and buffers to control bottom impacts is also lacking in current seat models.

Future Outlook

To address the identified gaps and challenges in safety improvement devices and implement them more efficiently, future research should focus on developing a criterion to assess the effects of vibration in different directions on motion sickness (see Section 3.3). This criterion can be achieved through statistical investigations in various sea states that measure vibration in different directions and human responses to the vibration. Moreover, epidemiologic research on the effects of vibration direction, magnitude, and duration can provide the necessary information for defining this criterion (see [43]). These epidemiologic studies can also assist in predicting the type of human injury and its location by installing sensors on different parts of the human body affected by WBVs and presenting the critical vibration that causes injuries in each part. Afterward, in marine environments, mathematical modeling of the human body can be employed to predict the vibration transmitted to each part of the human body, such as the pelvis, back, and legs, and compare the results against the provided criteria to estimate the most vulnerable part of the human body to injury. Some mathematical modeling of the human body can be found in [129–133].

In the safety improvement strategies, the effects of trim tabs and interceptors (passive, controllable, and active systems) in reducing hull motions in different directions should be explored during sea trial tests, towing tank tests, numerical simulation, or mathematical modeling. This is an important subject to address in designing motion-reduction devices to improve human safety, because most human injuries are caused by lateral and forward impacts. Furthermore, shock-mitigation seats for HSPCs should mitigate vibrations in more than one direction. Although there are some new types of shock-mitigation seats for HSPCs with new configurations to absorb forward and lateral vibrations, there is no published evidence regarding their efficiency in safety improvement compared to the previous seat models. Therefore, future studies on these types of shock-mitigation seats by measuring and comparing vibration in different directions on the deck and seat through sea trial tests are required to investigate their efficiency. This investigation can also be achieved using mathematical modeling of these kinds of seats.

By addressing these gaps and challenges, the future outlook for human safety in vibrated environments, particularly HSPCs, will be significantly improved. This will lead to more effective design strategies, optimized motion-reduction devices, and safer conditions for occupants during high-speed marine operations.

Author Contributions: Conceptualization, F.R. and A.D.; methodology, F.R., A.D., and P.K.; formal analysis, F.R.; investigation, F.R. and A.D.; resources, F.R.; data curation, F.R.; writing—original draft preparation, F.R.; writing—review and editing, F.R., A.D., and P.K.; visualization, F.R.; supervision, A.D.; project administration, A.D. All authors have read and agreed to the published version of the manuscript.

Funding: This research received no external funding.

Institutional Review Board Statement: Not applicable.

Informed Consent Statement: Not applicable.

Data Availability Statement: Data are contained within the article.

Conflicts of Interest: The authors declare no conflict of interest.

References

1. Bovenzi, M.; Hulshof, C.T.J. An updated review of epidemiologic studies on the relationship between exposure to whole-body vibration and low back pain. *J. Sound Vib.* **1998**, *215*, 595–611. [CrossRef]
2. Meyer, L.T.; Moore, J.; Sopchick-Smith, T. Proceedings of the Naval Special Warfare Sports Medicine Conference Proceedings, Report number: NHRC-TD-95-4D, Accession Number: ADA299974. Coronado, CA, USA, 4–6 May 1994; p. 0149. Available online: https://apps.dtic.mil/sti/tr/pdf/ADA299974.pdf (accessed on 24 February 2022).
3. Bazrgari, B.; Shirazi-Adl, A.; Kasra, M. Seated whole body vibrations with high-magnitude accelerations—Relative roles of inertia and muscle forces. *J. Biomech.* **2008**, *41*, 2639–2646. [CrossRef] [PubMed]

4. Ensign, W.; Hodgdon, J.A.; Prusaczyk, W.K.; Ahlers, S.; Shapiro, D.; Lipton, M. *A Survey of Self-Reported Injuries among Special Boat Operators*; Naval Health Research Centre: San Diego, CA, USA, 2000; 48p.
5. Carvalhais, A. Incidence and Severity of Injuries to Surf Boat Operators. In Proceedings of the 75th Shock and Vibration Symposium, Virginia Beach, VA, USA, 24–26 October 2004; Volume 37.
6. Ullman, J.; Hengst, D.; Carpenter, R.; Robinson, Y. Does military high-speed boat slamming cause severe injuries and disability? *Clin. Orthop. Relat. Res.* **2022**, *480*, P2163–P2173. [CrossRef] [PubMed]
7. Wikström, B.O.; Kjellberg, A.; Landström, U. Health effects of long-term occupational exposure to whole-body vibration: A review. *Int. J. Ind. Ergon.* **1994**, *14*, 273–292. [CrossRef]
8. Leung, A.W.; Chan, C.C.; Ng, J.J.; Wong, P.C. Factors contributing to officers' fatigue in high-speed maritime craft operations. *Appl. Ergon.* **2006**, *37*, 565–576. [CrossRef] [PubMed]
9. Myers, S.D.; Dobbins, T.D.; King, S.; Hall, B.; Holmes, S.R.; Gunston, T.; Dyson, R. Effectiveness of suspension seats in maintaining performance following military high-speed boat transits. *Hum. Factors* **2012**, *54*, 264–276. [CrossRef] [PubMed]
10. Martire, R.L.; de Alwis, M.P.; Äng, B.O.; Garme, K. Construction of a web-based questionnaire for longitudinal investigation of work exposure, musculoskeletal pain and performance impairments in high-performance marine craft populations. *BMJ Open* **2017**, *7*, e016006. [CrossRef]
11. de Alwis, M.P.; Garme, K.; Lo Martire, R.; Kåsin, J.I.; Äng, B. Crew acceleration exposure, health and performance in high-speed operations at sea. In Proceedings of the 11th Symposium on High-Speed Marine Vehicles (HSMV 2017), Naples, Italy, 25–26 October 2017.
12. de Alwis, M.P.; Garme, K. Effect of occupational exposure to shock and vibration on health in high-performance marine craft occupants. *Proc. Inst. Mech. Eng. Part M J. Eng. Marit. Environ.* **2021**, *235*, 394–409. [CrossRef]
13. Burström, L.; Nilsson, T.; Wahlström, J. Whole-body vibration and the risk of low back pain and sciatica: A systematic review and meta-analysis. *Int. Arch. Occup. Environ. Health* **2015**, *88*, 403–418. [CrossRef]
14. Guruguntla, V.; Lal, M.; Ghantasala, G.S.P.; Vidyullatha, P.; Alqahtani, M.S.; Alsubaie, N.; Abbas, M.; Soufiene, B.O. Ride comfort and segmental vibration transmissibility analysis of an automobile passenger model under whole body vibration. *Sci. Rep.* **2023**, *13*, 1–13. [CrossRef]
15. *ISO 2631–1*; Shock—Evaluation of Human Exposure to Whole-Body Vibration—Part 1: General Requirements. International Organization for Standardization: Geneva, Switzerland, 1997.
16. Townsend, N.C.; Coe, T.E.; Wilson, P.A.; Shenoi, R.A. High speed marine craft motion mitigation using flexible hull design. *Ocean Eng.* **2012**, *42*, 126–134. [CrossRef]
17. McMorris, T.; Myers, S.; Dobbins, T.; Hall, B.; Dyson, R. Seating type and cognitive performance after 3 hours travel by high-speed boat in sea states 2–3. *Aviat. Space Environ. Med.* **2009**, *80*, 24–28. [CrossRef] [PubMed]
18. Myers, S.D.; Dobbins, T.D.; King, S.; Hall, B.; Ayling, R.M.; Holmes, S.R.; Dyson, R. Physiological consequences of military high-speed boat transits. *Eur. J. Appl. Physiol.* **2011**, *111*, 2041–2049. [CrossRef] [PubMed]
19. Roshan, F.; Tavakoli, S.; Mancini, S.; Dashtimanesh, A. Dynamic of Tunneled Planing Hulls in Waves. *J. Mar. Sci. Eng.* **2022**, *10*, 1038. [CrossRef]
20. Griffin, K.; Knight, J. (Eds.) *Human Development and the International Development Strategy for the 1990s*; Macmillan: London, UK, 1990; Volume 8, 258p.
21. Allen, D.P.; Taunton, D.J.; Allen, R. A study of shock impacts and vibration dose values onboard highspeed marine craft. *Trans. R. Inst. Nav. Archit. Part A: Int. J. Marit. Eng.* **2008**, *150*, 1–10. Available online: http://eprints.soton.ac.uk/id/eprint/64778 (accessed on 24 February 2022).
22. ABCD Group. High Speed Craft Human Factors Engineering and Design Guide, ABCD TR-08-01 V1.0 Edition. 2008. Available online: https://www.ullmandynamics.com/wp-content/uploads/2011/02/hsc-human-factors-design-guide_2mg.pdf (accessed on 24 February 2022).
23. Dobbins, T.; Myers, S.; Withey, W.; Dyson, R.; Gunston, T.; King, S. High speed craft motion analysis: Impact count index (ici). In Proceedings of the 43rd UK Conference on Human Response to Vibration, Leicester, UK, 15–17 September 2008.
24. Garme, K.; Burström, L.; Kuttenkeuler, J. Measures of vibration exposure for a high-speed craft crew. *Proc. Inst. Mech. Eng. Part M J. Eng. Marit. Environ.* **2011**, *225*, 338–349. [CrossRef]
25. Fridsma, G. *A Systematic Study of the Rough-Water Performance of Planing Boats*; Davidson Laboratory, Stevens Institute of Technology: Hoboken, NJ, USA, 1969.
26. De Luca, F.; Pensa, C. The Naples Systematic Series–Second part: Irregular waves, seakeeping in head sea. *Ocean. Eng.* **2019**, *194*, 106620. [CrossRef]
27. Tavakoli, S.; Zhang, M.; Kondratenko, A.A.; Hirdaris, S. A review on the hydrodynamics of planing hulls. *Ocean Eng.* **2024**, *303*, 117046. [CrossRef]
28. Turner, T.; McKillop, J. *Calm Water Resistance of a 1: 25 Scale Model of the Armidale Class Patrol Boat*; Defense Science and Technology Organization: Melbourne, Australia, 2012.
29. Rijkens, A.A.K.; Keuning, J.A.; Huijsmans, R.H.M. A computational tool for the design of ride control systems for fast planing vessels. *Int. Shipbuild. Prog.* **2011**, *58*, 165–190. [CrossRef]
30. Mansoori, M.; Fernandes, A.C.; Ghassemi, H. Interceptor design for optimum trim control and minimum resistance of planing boats. *Appl. Ocean Res.* **2017**, *69*, 100–115. [CrossRef]

31. Ashkezari, A.Z.; Moradi, M. Three-dimensional simulation and evaluation of the hydrodynamic effects of stern wedges on the performance and stability of high-speed planing monohull craft. *Appl. Ocean Res.* **2021**, *110*, 102585. [CrossRef]
32. Atindana, V.A.; Xu, X.; Kwaku, N.J.; Akayeti, A.; Jiang, X. A novel semi-active control of an integrated chassis and seat quasi-zero stiffness suspension system for off-road vehicles. *J. Vib. Control.* **2024**, 1–24. [CrossRef]
33. Davoodi, E.; Safarpour, P.; Pourgholi, M.; Khazaee, M. Design and evaluation of vibration reducing seat suspension based on negative stiffness structure. *Proc. Inst. Mech. Eng. Part C J. Mech. Eng. Sci.* **2020**, *234*, 4171–4189. [CrossRef]
34. Page, M.J.; McKenzie, J.E.; Bossuyt, P.M.; Boutron, I.; Hoffmann, T.C.; Mulrow, C.D.; Shamseer, L.; Tetzlaff, J.M.; Akl, E.A.; Brennan, S.E.; et al. The PRISMA 2020 statement: An updated guideline for reporting systematic reviews. *Int. J. Surg.* **2021**, *88*, 105906. [CrossRef] [PubMed]
35. *ISO 2631–2635:2004*; Shock–Evaluation of Human Exposure to Whole Body Vibration–Part 5: Method for Evaluation of Vibration Containing Multiple Shocks. ISO: Geneva, Switzerland, 2004.
36. *DIRECTIVE 2002/44/EC*; Directive 2002/44/EC of the European Parliament and of the Council of 25th June 2002 on the Minimum Health and Safety Requirements Regarding the Exposure of Workers to the Risks Arising from Physical Agents (vibration), 2002. European Union: Luxembourg, 2002.
37. *British Standards Institution 6841*; Measurement and Evaluation of Human Exposure to Whole-Body Mechanical Vibration. BSI: London, UK, 1987.
38. *ISO 2041/TC 108*; Mechanical Vibration, Shock and Condition Monitoring—Vocabulary. ISO: Geneva, Switzerland, 2009.
39. *ISO 5805/TC 108/SC*; Mechanical Vibration and Shock—Human Exposure—Vocabulary—Vocabulary. ISO: Geneva, Switzerland, 1997.
40. *ISO 10326-1/TC 108/SC 4*; Mechanical Vibration—Laboratory Method for Evaluating Vehicle Seat Vibration—Part 1: Basic Requirements. ISO: Geneva, Switzerland, 2016.
41. Griffin, M.J.; Whitham, E.M.; Parsons, K.C. Vibration and comfort I. Translational seat vibration. *Ergonomics* **1982**, *25*, 603–630. [CrossRef] [PubMed]
42. Griffin, M.J.; Parsons, K.C.; Whitham, E.M.W. Vibration and comfort IV. Application of experimental results. *Ergonomics* **1982**, *25*, 721–739. [CrossRef] [PubMed]
43. Joseph, J.A.; Griffin, M.J. Motion sickness: Effect of changes in magnitude of combined lateral and roll oscillation. *Aviat. Space Environ. Med.* **2008**, *79*, 1019–1027. [CrossRef] [PubMed]
44. Howarth, H.V.; Griffin, M.J. Effect of roll oscillation frequency on motion sickness. *Aviat. Space Environ. Med.* **2003**, *74*, 326–331. [PubMed]
45. McCauley, M.E.; Royal, J.W.; Wylie, C.D.; O'Hanlon, J.F.; Mackie, R.R. *Motion Sickness Incidence: Exploratory Studies of Habituation, Pitch and Roll, and the Refinement of a Mathematical Model*; Technical Report; Human Factors Research Division, Canyon Research/Group Inc.: Goleta, CA, USA, 1976; pp. 1733–2000.
46. Taunton, D.J.; Hudson, D.A.; Shenoi, R.A. Characteristics of a series of high speed hard chine planing hulls-part II: Performance in waves. *Int. J. Small Craft Technol.* **2011**, *153*, B1–B22.
47. Folsø, R. Comfort Monitoring of High Speed Passenger Ferries. Ph.D. Thesis, Technical University of Denmark, Copenhagen, Denmark, 2004.
48. Brown, P.W. *An Experimental and Theoretical Study of Planing Surfaces with Trim Flaps*; Report No. SIT-DL-71-1463; Stevens Institute of Technology, Davidson Laboratory: Hoboken, NJ, USA, 1971.
49. Seo, K.C.; Gopakumar, N.; Atlar, M. Experimental investigation of dynamic trim control devices in fast speed vessel. *J. Navig. Port Res.* **2013**, *37*, 137–142. [CrossRef]
50. Ghadimi, P.; Loni, A.; Nowruzi, H.; Dashtimanesh, A.; Tavakoli, S. Parametric study of the effects of trim tabs on running trim and resistance of planing hulls. *Adv. Shipp. Ocean Eng.* **2014**, *3*, 1–12.
51. Mansoori, M.; Fernandes, A.C. Interceptor and trim tab combination to prevent interceptor's unfit effects. *Ocean Eng.* **2017**, *134*, 140–156. [CrossRef]
52. Wang, L.W. A study on motions of high-speed planing boats with controllable flaps in regular waves. *Int. Shipbuild. Prog.* **1985**, *32*, 6–23. [CrossRef]
53. Xi, H.; Sun, J. Feedback stabilization of high-speed planing vessels by a controllable transom flap. *IEEE J. Ocean. Eng.* **2006**, *31*, 421–431. [CrossRef]
54. Jokar, H.; Zeinali, H.; Tamaddondar, M.H. Planing craft control using pneumatically driven trim tab. *Math. Comput. Simul.* **2020**, *178*, 439–463. [CrossRef]
55. Kim, S.; Oshima, N.; Lee, S.; Lee, G.; Seo, K. Hydrodynamic performance and appendage considerations of wave-piercing planing craft overlapping waves and porpoising. *J. Fluid Sci. Technol.* **2020**, *15*, JFST0013. [CrossRef]
56. Song, K.W.; Guo, C.Y.; Gong, J.; Li, P.; Wang, L.Z. Influence of interceptors, stern flaps, and their combinations on the hydrodynamic performance of a deep-vee ship. *Ocean Eng.* **2018**, *170*, 306–320. [CrossRef]
57. Yaakob, O.; Shamsuddin, S.; Koh, K.K. Stern flap for resistance reduction of planing hull craft: A case study with a fast crew boat model. *J. Teknol.* **2004**, *41*, 43–52. [CrossRef]
58. Brizzolara, S.; Villa, D. A systematic CFD analysis of flaps/interceptors hydrodynamic performance. In Proceedings of the 10th International Conference on Fast Sea Transportation (FAST 2009), Athens, Greece, 5–8 October 2009.

59. Mohebbi, M.; Ghassemi, M.A.; Ghassemi, H. Obtaining the Practical Formula for the Trim-tab Dimensions to Reach the Minimum Drag for Planing Boat. *Am. J. Mech. Eng.* **2020**, *8*, 163–171. [CrossRef]
60. Savitsky, D.; Brown, P.W. Procedures for hydrodynamic evaluation of planing hulls in smooth and rough water. *Mar. Technol. SNAME News* **1976**, *13*, 381–400. [CrossRef]
61. Katayama, K.; Suzuki, K.; Ikeda, Y. A new ship motion control system for high-speed craft. In Proceedings of the FAST 2003 the 7th International Conference on Fast Sea Transportation, Ischia, Italy, 7–10 October 2003; pp. 7–10.
62. Santos, M.; López, R.; De la Cruz, J.M. Fuzzy control of the vertical acceleration of fast ferries. *Control. Eng. Pract.* **2005**, *13*, 305–313. [CrossRef]
63. Hughes, M.J.; Weems, K.M. Time-domain seakeeping simulations for a high speed catamaran with an active ride control system. In Proceedings of the 11th International Conference on FAST2011, Honolulu, HI, USA, 26–29 September 2011.
64. Ekman, F.; Rydelius, F. Model for Predicting Resistance and Running Attitude of High-Speed Craft Equipped with Interceptors: A Comparative Study Including Validation on Swedish Coast Guard Patrol Boat KBV 315. Bachelor's Thesis, KTH Royal Institute of Technology, Stockholm, Sweden, 2016.
65. Praveen, P.C.; Khan, M.K. Interceptor for better Hydrodynamic Performance of a Planing Hull. In Proceedings of the International Workshop Conference & Expo in Engineering and Marine Applications, Auckland, New Zealand, 21–24 February 2010.
66. John, S.; Kareem Khan, M.D.; Praveen, P.C.; Manu, K.; Panigrahi, P.K. *Hydrodynamic Performance Enhancement Using Stern Wedges, Stern Flaps and Interceptors*; Naval Science & Technological Laboratory: Visakhapatnam, India, 2011.
67. Putra AM, F.; Suzuki, H. Experimental and numerical study on the high-speed ship hydrodynamics influenced by an interceptor with varied angle of attack. *Int. J. Nav. Archit. Ocean Eng.* **2024**, *16*, 100566. [CrossRef]
68. Tsai, J.F.; Hwang, J.L. Study on the compound effects of interceptor with stern flap for two fast monohulls. In Proceedings of the Oceans'04 MTS/IEEE Techno-Ocean'04, 2004, Kobe, Japan, 9–12 November 2004; Volume 2, pp. 1023–1028. [CrossRef]
69. Ghassemi, H.; Mansouri, M.; Zaferanlouei, S. Interceptor hydrodynamic analysis for handling trim control problems in the high-speed crafts. *Proc. Inst. Mech. Eng. Part C J. Mech. Eng. Sci.* **2011**, *225*, 2597–2618. [CrossRef]
70. Molini, A.; Brizzolara, S. Hydrodynamics of interceptors: A fundamental study. In Proceedings of the International Conference on Marine Research and Transportation, Napels, Italy, 28–30 June 2005; Volume 1.
71. Day, A.H.; Cooper, C. An experimental study of interceptors for drag reduction on high-performance sailing yachts. *Ocean Eng.* **2011**, *38*, 983–994. [CrossRef]
72. Karimi, M.H.; Seif, M.S.; Abbaspoor, M. An experimental study of interceptor's effectiveness on hydrodynamic performance of high-speed planing crafts. *Pol. Marit. Res.* **2013**, *20*, 21–29. [CrossRef]
73. Seok, W.; Park, S.Y.; Rhee, S.H. An experimental study on the stern bottom pressure distribution of a high-speed planing vessel with and without interceptors. *Int. J. Nav. Archit. Ocean Eng.* **2020**, *12*, 691–698. [CrossRef]
74. Mansoori, M.; Fernandes, A.C. Hydrodynamics of the interceptor on a 2-D flat plate by CFD and experiments. *J. Hydrodyn. Ser. B* **2015**, *27*, 919–933. [CrossRef]
75. Mansoori, M.; Fernandes, A.C. The interceptor hydrodynamic analysis for controlling the porpoising instability in high speed crafts. *Appl. Ocean Res.* **2016**, *57*, 40–51. [CrossRef]
76. Deng, R.; Zhang, Z.; Luo, F.; Sun, P.; Wu, T. Investigation on the Lift Force Induced by the Interceptor and Its Affecting Factors: Experimental Study with Captive Model. *J. Mar. Sci. Eng.* **2022**, *10*, 211. [CrossRef]
77. Avci, A.G.; Barlas, B. The usage of interceptors in high speed crafts. In Proceedings of the 1st International Congress on Ship and Marine Technology, İstanbul, Turkey, 8–9 December 2016; Volume 1.
78. Avci, A.G.; Barlas, B. An experimental investigation of interceptors for a high speed hull. *Int. J. Nav. Archit. Ocean Eng.* **2019**, *11*, 256–273. [CrossRef]
79. Park, J.Y.; Choi, H.; Lee, J.; Choi, H.; Woo, J.; Kim, S.; Kim, N. An experimental study on vertical motion control of a high-speed planing vessel using a controllable interceptor in waves. *Ocean. Eng.* **2019**, *173*, 841–850. [CrossRef]
80. Najafi, A.; Alimirzazadeh, S.; Seif, M.S. RANS simulation of interceptor effect on hydrodynamic coefficients of longitudinal equations of motion of planing catamarans. *J. Braz. Soc. Mech. Sci. Eng.* **2015**, *37*, 1257–1275. [CrossRef]
81. Luca, F.; Pensa, C. The prediction of the interceptor performances based on towing tank test data: Ship-model correlation and hull form influence. *Positions* **2014**, *9707*, C0301.
82. Karimi, M.H.; Seif, M.S.; Abbaspoor, M. A study on vertical motions of high-speed planing boats with automatically controlled stern interceptors in calm water and head waves. *Ships Offshore Struct.* **2015**, *10*, 335–348. [CrossRef]
83. Ertogan, M.; Wilson, P.A.; Tayyar, G.T.; Ertugrul, S. Optimal trim control of a high-speed craft by trim tabs/interceptors Part I: Pitch and surge coupled dynamic modelling using sea trial data. *Ocean Eng.* **2017**, *130*, 300–309. [CrossRef]
84. AuCoin, C. *Shock Mitigating Seat Single Impact Program*; Naval Engineering Test Establishment: Montreal, QC, Canada, 2014.
85. Liam, C.C. Testing and Modeling of Shock Mitigating Seats for High Speed Craft. Master's Thesis, Faculty of the Virginia Polytechnic Institute and State University in Partial Fulfillment of the Requirements, Blacksburg, VA, USA, 2011.
86. Ekstrom, V. Semi-Active Suspension Seats in High Speed Crafts, Degree Project in Mechanical Engineering. Master's Thesis, KTH Royal Institute of Technology, Second Cycle, 30 Credits, Stockholm, Sweden, 2019. Available online: http://kth.diva-portal.org/smash/record.jsf?pid=diva2:1379727&dswid=9823 (accessed on 17 December 2019).

87. Coats, T.W.; Riley, M.R. *A Comparison of Shock Isolated Seat and Rigid Seat Acceleration Responses to Wave Impacts in a High-Speed Craft*; Technical Report; Naval Surface Warfare Center Carderock Division, Naval Architecture and Engineering Department: Carderock, VA, USA, 2018; NSWCCD-80-TR-2018/010, Accession Number: AD1055641.
88. Riley, M.R.; Murphy, H.P.; Coats, T.W. *Initial Investigation of Wave Impact Load Transfer Through Shock Isolation Seats in High Speed Craft*; Naval Surface Warfare Center Carderock Division: Virginia Beach, VA, USA, 2013.
89. Riley, M.R.; Coats, T.W. *The Simulation of Wave Slam Impulses to Evaluate Shock Mitigation Seats for High-Speed Planing Craft*; Naval Surface Warfare Center Carderock Division: Virginia Beach, VA, USA, 2013.
90. Reed, W.H.; Carroll, D.F.; Rothe, V.E. *Armored Crew Seat Drop Test Program*; Bell Helicopter Textron Inc.: Fort Worth, TX, USA, 1966.
91. Harris, K.; Melotik, J. *TARDEC Occupant Protection Seat*; Army Tank Automotive Research Development and Engineering Center: Warren, Mi, USA, 2012.
92. Murphy, H.P.; Riley, M.R.; Coats, T.W. *A Consistent Wave Impact Load Model for Studying Structure, Equipment Ruggedness, Shock Isolation Seats, and Human Comfort in Small High Speed Craft*; Naval Surface Warfare Center Carderock Division: Virginia Beach, VA, USA, 2016.
93. Li, K.; Darby, A.P. Modelling a buffered impact damper system using a spring–damper model of impact. *Struct. Control Health Monit. Off. J. Int. Assoc. Struct. Control Monit. Eur. Assoc. Control Struct.* **2017**, *16*, 287–302. [CrossRef]
94. Zuneid Alam, S. Implementation of a Drop Test Impact Rig for Dynamic Testing of High Speed Craft Shock Mitigation Seats and Extraction of Modal Parameters. Ph.D. Thesis, Carleton University, Ottawa, ON, Canada, 2013.
95. Alam, Z.; Afagh, F.; Langlois, R. Efficient Identification of Naval High-Speed Craft Shock Mitigation Seat Modal Parameters From Drop-Test Data. *J. Dyn. Syst. Meas. Control.* **2017**, *139*, 031009. [CrossRef]
96. Marshall, J.T.; Riley, M.R. *A Comparison of the Mechanical Shock Mitigation Performance of a Shock Isolation Seat Subjected to Laboratory Drop Tests and at-Sea Seakeeping Trials*; NAVSEA Carderock: Bethesda, MD, USA, 2020.
97. Kearns, S.D. Analysis and Mitigation of Mechanical Shock Effects on High Speed Planing Boats. Master's Thesis, Massachusetts Institute of Technology, Cambridge, MA, USA, 2001.
98. Reynolds, D.; Ayyad, E.A.; Hachem, M. *Evaluation of a Pneumatic-Seat-Bladder-System Designed for Shock and Vibration Isolation*; University of Nevada: Las Vegas, NV, USA, 2012.
99. Wice, A.M. Spatial Dynamic Modelling of High-Speed Craft Suspension Seating. Ph.D. Thesis, Carleton University, Ottawa, ON, Canada, 2015.
100. Coltman, J.W. *Design and Test Criteria for Increased Energy-Absorbing Seat Effectiveness*; Simula, Inc.: Tempe, AZ, USA, 1983.
101. Olivares, D. *Dynamic Seat Certification by Analysis: Volume III–Comparison of Hybrid II Versus Hybrid III ATD Dynamic Evaluation NIAR Test Series*; NIAR Technical Report FAA-003D; NIAR: Wichita, KS, USA, 2009.
102. Gannon, L. Single impact testing of suspension seats for high-speed craft. *Ocean. Eng.* **2017**, *141*, 116–124. [CrossRef]
103. Petersen, S.M.; Riley, M.R. *The Use of Shock Isolation mounts in Small High-Speed Craft to Protect Equipment from Wave Slam Effects*; Naval Surface Warfare Center Carderock: West Bethesda, MD, USA, 2017.
104. Sorensen, F.W.A. Development of Control Strategies and Testing Procedures for Suspension Seats Used in High Speed Craft. Ph.D. Thesis, Carleton University, Ottawa, ON, Canada, 2020.
105. Wang, M.; Chen, Z.; Wereley, N.M. Adaptive magnetorheological energy absorber control method for drop-induced shock mitigation. *J. Intell. Mater. Syst. Struct.* **2021**, *32*, 449–461. [CrossRef]
106. Jin, S.; Deng, L.; Yang, J.; Sun, S.; Ning, D.; Li, Z.; Li, W.H. A smart passive MR damper with a hybrid powering system for impact mitigation: An experimental study. *J. Intell. Mater. Syst. Struct.* **2021**, *32*, 1452–1461. [CrossRef]
107. Gunston, T.P.; Rebelle, J.; Griffin, M.J. A comparison of two methods of simulating seat suspension dynamic performance. *J. Sound Vib.* **2004**, *278*, 117–134. [CrossRef]
108. Olausson, K.; Garme, K. Prediction and evaluation of working conditions on high-speed craft using suspension seat modelling. *Proc. Inst. Mech. Eng. Part M J. Eng. Marit. Environ.* **2015**, *229*, 281–290. [CrossRef]
109. Ereq, K. Active Suspension Seat for High-Speed Craft. Master Thesis, Degree Project in Mechanical Engineering, Second Cycle,. KTH Royal Institute of Technology, 30 Credits, Stockholm, Sweden, 2018. Available online: http://www.diva-portal.se/smash/get/diva2:1247182/FULLTEXT01.pdf (accessed on 11 September 2018).
110. Mayton, A.G.; DuCarme, J.P.; Jobes, C.C.; Matty, T.J. Laboratory investigation of seat suspension performance during vibration testing. In Proceedings of the ASME International Mechanical Engineering Congress and Exposition, Chicago, IL, USA, 5–10 November 2006; Volume 47675, pp. 177–183. [CrossRef]
111. Cheng, M.; Bueley, D.; Dionne, J.P.; Makris, A. Survivability evaluation of blast mitigation seats for armored vehicles. In Proceedings of the 26th International Symposium on Ballistics, Miami, FL, USA, 12–16 September 2011.
112. Riley, M.R.; Coats, T.W. *Quantifying Mitigation Characteristics of Shock Isolation Seats in a Wave Impact Environment*; Naval Surface Warfare Center: Carderock, MD, USA, 2015.
113. Roberts, O.C. Development of the High-Speed Craft Slam Impact Seat Test Rig. Master's Thesis, Carleton University Ottawa, Ottawa, ON, Canada, 2015.
114. Fairley, T.E.; Griffin, M.J. The apparent mass of the seated human body: Vertical vibration. *J. Biomech.* **1989**, *22*, 81–94. [CrossRef]
115. Chen, Q.; Zhang, Y.; Zhu, C.; Wu, J.; Zhuang, Y. A sky-hook sliding mode semiactive control for commercial truck seat suspension. *J. Vib. Control* **2021**, *27*, 1201–1211. [CrossRef]

116. Coe, T.; Shenoi, R.A.; Xing, J.T. Human body vibration response models in the context of high speed planing craft and seat isolation systems. In Proceedings of the Sixth International Conference on High-performance marine vehicles (HIPER'08), Naples, Italy, 18–19 September 2008; pp. 18–19.
117. Olausson, K. Vibration Mitigation for High Speed Craft. Master's Thesis, Centre for Naval Architecture Royal Institute of Technology, Stockholm, Sweden, 2012.
118. Olausson, K. On Evaluation and Modelling of Human Exposure to Vibration and Shock on Planing High-Speed Craft. Ph.D. Thesis, KTH Royal Institute of Technology, Stockholm, Sweden, 2015.
119. Wei, L.; Griffin, M.J. Mathematical models for the apparent mass of the seated human body exposed to vertical vibration. *J. Sound Vib.* **1998**, *212*, 855–874. [CrossRef]
120. Maciejewski, I.; Blazejewski, A.; Pecolt, S.; Krzyzynski, T. A sliding mode control strategy for active horizontal seat suspension under realistic input vibration. *J. Vib. Control* **2023**, *29*, 2539–2551. [CrossRef]
121. Choi, S.B.; Nam, M.H.; Lee, B.K. Vibration control of a MR seat damper for commercial vehicles. *J. Intell. Mater. Syst. Struct.* **2000**, *11*, 936–944. [CrossRef]
122. Rebelle, J. Development of a numerical model of seat suspensions to optimize the end-stop buffers. In Proceedings of the UK Conference on Human Responses to Vibration, Southampton, UK, 17–19 September 2000.
123. Rebelle, J. Methodology to improve the performance of the end-stop buffers of suspension seats. *Veh. Syst. Dyn.* **2004**, *42*, 211–233. [CrossRef]
124. Ma, X.Q.; Rakheja, S.; Su, C.Y. Damping requirement of a suspension seat subject to low frequency vehicle vibration and shock. *Int. J. Veh. Des.* **2008**, *47*, 133–156. [CrossRef]
125. Rakheja, S.; Boileau, P.É.; Wang, Z.; Politis, H. Performance analysis of suspension seats under high magnitude vibration excitations: Part 1: Model development and validation. *J. Low Freq. Noise Vib. Act. Control.* **2003**, *22*, 225–252. [CrossRef]
126. Rakheja, S.; Boileau, P.É.; Wang, Z. Performance analysis of suspension seats under high magnitude vibration excitations: II. Design parameter study. *J. Low Freq. Noise Vib. Act. Control.* **2004**, *23*, 7–25. [CrossRef]
127. Abdelkareem, M.A.; Zhang, R.; Jing, X.; Wang, X.; Ali, M.K.A. Characterization and implementation of a double-sided arm-toothed indirect-drive rotary electromagnetic energy-harvesting shock absorber in a full semi-trailer truck suspension platform. *Energy* **2022**, *239*, 121976. [CrossRef]
128. Fouad, Y.H. An Experimental Methodology for Characterizing High Speed Craft Seat Suspension Components. Master's Thesis, Carleton University, Ottawa, ON, Canada, 2015.
129. Zhao, Y.; Bi, F.; Shu, H.; Guo, L.; Wang, X. Prediction of the driver's head acceleration and vibration isolation performance of the seating suspension system using the time and frequency domain modeling. *Appl. Acoust.* **2021**, *183*, 108308. [CrossRef]
130. Zhao, Y.; Bi, F.; Khayet, M.; Symonds, T.; Wang, X. Study of seat-to-head vertical vibration transmissibility of commercial vehicle seat system through response surface method modeling and Genetic Algorithm. *Appl. Acoust.* **2023**, *203*, 109216. [CrossRef]
131. Singh, H.J.; Wereley, N.M. Mitigation of Biodynamic Response to Shock Loads Using Semi-Active Vertically Stroking Crew Seats. In Proceedings of the Smart Materials, Adaptive Structures and Intelligent Systems, Philadelphia, PA, USA, 1 September 2010; Volume 44168, pp. 481–490. [CrossRef]
132. Singh, H.J.; Wereley, N.M. Model-based optimal control of biodynamic response to vertical crash loads for an occupant seated in a helicopter. In Proceedings of the AHS 69th Annual Forum, Phoenix, AZ, USA, 23–26 May 2013.
133. Singh, H.J.; Wereley, N.M. Influence of occupant compliance on a vertically stroking helicopter crew seat suspension. *J. Aircr.* **2015**, *52*, 1286–1297. [CrossRef]

Disclaimer/Publisher's Note: The statements, opinions and data contained in all publications are solely those of the individual author(s) and contributor(s) and not of MDPI and/or the editor(s). MDPI and/or the editor(s) disclaim responsibility for any injury to people or property resulting from any ideas, methods, instructions or products referred to in the content.

Appendix 2 (Publication II)

Paper II

Roshan, F., Tavakoli, S., Mancini, S., & Dashtimanesh, A. (2022). Dynamic of Tunneled Planing Hulls in Waves. Journal of Marine Science and Engineering, 10(8), 1038. https://doi.org/10.3390/jmse10081038.

Journal of
Marine Science and Engineering

MDPI

Article

Dynamic of Tunneled Planing Hulls in Waves

Fatemeh Roshan [1], Sasan Tavakoli [2,3], Simone Mancini [4] and Abbas Dashtimanesh [5,*]

[1] Estonian Maritime Academy, Tallinn University of Technology, 11712 Tallinn, Estonia; fatemeh.roshan@taltech.ee
[2] Department of Mechanical Engineering, Aalto University, 02150 Espoo, Finland; sasan.tavakoli@aalto.fi
[3] Department of Infrastructure Engineering, The University of Melbourne, Parkville, VIC 3052, Australia
[4] Force Technology, Division for Maritime Industry, Hydro and Aerodynamics Department, 2800 Kongens Lyngby, Denmark; simo@forcetechnology.com
[5] Department of Engineering Mechanics, KTH Royal Institute of Technology, 11428 Stockholm, Sweden
* Correspondence: abbasda@kth.se

Abstract: A tunneled planing craft is a high-speed boat with two tunnels over the hull bottom that are designed to improve the vessel's performance. Hydrodynamic performance of tunneled planing hulls in calm-water is well-known, however, current information on wave conditions is limited. In this study, two different tunneled planing hulls with two degrees of freedom in heave and pitch motions are studied in regular waves by using the computational fluid dynamics (CFD) method based on the Unsteady Reynolds Averaged Navier-Stokes Equations (URANSE) in conjunction with $k-\epsilon$ turbulence model. The results demonstrate that tunneled planing hull motions in waves are nonlinear. In addition, it is found that the dynamic responses of heave and pitch motions as well as occurrence portability of the fly-over phenomenon significantly increases as the Froude number grows. Fly-over motions resulted in vertical motions and acceleration up to $5g$, high impact pressure, and large induced drag. At a very high planing speed, after flying over the water surface, when the vessel re-enters the water, the resulting hydrodynamic load leads to a second fly-over motion. Since the fly-over is an unwanted movement with adverse effects, these results can provide a better understanding of the fly-over motion that one may consider in future design for improving the planing hull performance.

Keywords: tunneled planing hulls; dynamic in waves; fly-over motion; head sea; computational fluid dynamics (CFD)

check for updates

Citation: Roshan, F.; Tavakoli, S.; Mancini, S.; Dashtimanesh, A. Dynamic of Tunneled Planing Hulls in Waves. *J. Mar. Sci. Eng.* **2022**, *10*, 1038. https://doi.org/10.3390/jmse10081038

Academic Editors: Jialong Jiao and Tahsin Tezdogan

Received: 2 July 2022
Accepted: 25 July 2022
Published: 28 July 2022

Publisher's Note: MDPI stays neutral with regard to jurisdictional claims in published maps and institutional affiliations.

Copyright: © 2022 by the authors. Licensee MDPI, Basel, Switzerland. This article is an open access article distributed under the terms and conditions of the Creative Commons Attribution (CC BY) license (https://creativecommons.org/licenses/by/4.0/).

1. Introduction

Tunneled planing hulls are marine vehicles that use aerodynamic pressure to reduce the drag-over-lift ratio of the lifting surface by trapping the airflow in tunnels. The entrapped air increases the dry area of the bottom surface, decreases the wetted area, and gives rise to aerodynamic lift, which partially supports the weight of the vessel. All these factors together enable the boat to operate at higher speeds with less fuel consumption. The use of these vessels has been accelerated in the recent decade and has sparked up some new experimental and numerical research, which has provided a fundamental understanding of their hydrodynamics in calm-water conditions. The use of these vessels is widespread, and there is an urgent need to evaluate their performance in waves, yet very few studies are conducted in this realm.

Generally, planing problems, either steady or unsteady, refers to the advancement of a marine vehicle under the support of hydrodynamic pressure that is generated by the water flowing toward the bottom surface [1–3]. When a high-speed vessel that is operating in planing mode is exposed to water waves, motions in vertical and traverse planes occur [4] and hydrodynamic pressure, which dominantly supports the weight [5], gives rise to nonlinear forces. Consequently, the restoring forces and moments that are generated

by hydrostatic pressure decrease. In addition, the vessel skims on the water surface [6], which is wetting its surface and the area that is washed by water is small and narrow [7]. Moreover, the wetted surface of a planing vessel operating in waves might vary over time. This makes the physics of the problem more complicated. In this condition, the wetted surface is response-dependent, and the added mass along with damping forces/moments is time-dependent.

There is accumulating evidence that wave-induced motions of planing hulls are nonlinear (e.g., [8]). The contribution of hydrodynamic force in support of the weight force is likely to be the reason underlying nonlinearities. The energy corresponding to the motions, including heave and pitch, can be shifted to second and third harmonics, even in the case where the wave steepness is gentle. The nonlinearity of the motions has been seen to occur at wavelengths ranging between $2L$ to $4L$ in head sea conditions (here L refers to the length of the boat). The motion of the vessel resonates over the aforementioned range of wavelengths. The natural frequencies of heave and pitch motions are observed to decrease by increasing the speed of the vessel, while the larger dynamic response is expected to occur by increasing the speed [9]. A wide range of datasets that were measured in towing tanks and the sea has shown that the vertical acceleration of the vessel at its bow is highly increased by the increase of speed [4]. The bow acceleration can reach up to $2g$, where g is the gravitational acceleration, leading to an uncomfortable riding situation for the crew of the vessel. In addition, under the force that is caused by the large vertical acceleration, the structure of the vessel may significantly vibrate, which might get damaged over time.

A vessel operating in the planing mode in rough water can exit the water and re-enter it in a short period, being nearly half of a cycle [10]. Such a phenomenon, identified as fly-over motion, gives an account of large impact forces. The added resistance of the vessels at a higher speed can significantly increase since an induced drag can be influenced by the water waves [11] (i.e., extra hydrodynamic pressure can act on the vessel). The riders of planing hulls frequently prefer to de-accelerate in rough water conditions, preventing extreme responses.

Historically, the seakeeping of planing hulls has attracted the attention of researchers for six decades. The general knowledge regarding the dynamic of planing hulls in waves has been shaped through experimental research that was conducted in towing tanks. Some systematic studies can be found in the literature. While the body of knowledge regarding the dynamic response of the hard-chine boat is strong enough, the dynamic response of the tunneled hull form is poorly understood. We are still not sure about the method that can be used to model the dynamic responses and our understanding of the physics of the problem is immature at the present stage. This is while our knowledge regarding the calm-water performance of these vessels, as mentioned earlier, has been formed through experimental and numerical observations [12–16]. The designers in particular, need modeling of the dynamics of these boats, which can help them to fill the gaps in the design of fast tunneled boats. At the present stage, it is required to find out the effects of the aerodynamic pressure on forces, including damping and added mass ones. In addition, the very small wetted surface of the boat can increase the occurrence probability of fly-over motion.

While there is a strong experimental dataset for hydrodynamics of hard-chine hulls [17], the dataset regarding the hydrodynamic of tunneled planing hulls are scant, which forces us to employ a mathematical and numerical method for the replication of their unsteady planing motion in waves. The solution of the ideal fluid field around a structure has been widely used for modeling dynamic responses of ships/structures. In the case of planing hulls, such a methodology is mostly used for modeling steady motion. It is very complicated to implement nonlinear boundary conditions along with Kutta conditions, which govern the side edges and transom of the vessel. More importantly, aerodynamic pressure generates a significant force, which necessitates consideration of the two-phase flow around the body.

The mathematical methods are well known for their significant contribution to modeling the dynamic motions of planing hulls in waves and calm-water conditions [18,19].

However, in the case of a tunneled planing hull, the transverse section of the vessel does not have a simple shape, and as mentioned, the air flows in the tunnels. These two make the 2D + t method useless. In simple words, we need a unique theoretical simulation for a tunneled section entering the water, which is not presently available. Readers that are interested in the water entry problem can refer to [20].

The appropriate method to simulate the wave-induced motions of the high-speed tunneled hull is to solve the Navier–Stokes equations, which govern the viscous fluid field around the vessel. Turbulent two-phase flow, a mixture of air and water, is assumed to flow in a virtual water tank, and the solution of the fluid field around the vessel can be achieved. Computational fluid dynamics, CFD, provides the numerical solution of the Navier–Stokes equations. The popularity of the CFD codes in the numerical reapplication of different problems that are linked to ocean/offshore engineering can be seen in a wide range of studies that have been conducted in the last two decades [21,22]. The key strong point about CFD is that it can be used to solve the two-phase viscous flow in the fluid domain. In this condition, some physical aspects of the flow, which are neglected when an ideal flow is embarked, are considered. For example, we can model the shear stresses and turbulent development around the vessel [23], which are skipped under an ideal fluid assumption.

Going back to the last two decades, with the advances in computational mechanics and parallel processing, the application of CFD methods in simulating the planing problems has increased. The proper accuracy of CFD models in the simulation of the steady flow around planing hulls has been observed in a wide range of CFD studies (e.g., in [24,25]) which has directed boat designers to count on CFD as a promising hydrodynamic tool. Specifically, CFD models have been observed to provide a high level of accuracy in the modeling motions of the special designs of high-speed planing hulls [26–31]. CFD models have also demonstrated the ability to model the vertical motions of planing boats [32–35]. As mentioned earlier, the dynamic responses of tunneled planing hulls are not understood clearly. The numerical simulation of Navier–Stokes equations can help us to simulate the problem.

Current seakeeping studies of tunneled planing hull are conducted experimentally which has a limitation in presenting some physical details, i.e., pressure distribution, pressure and shear resistance, streamlines, etc., that are provided in the present paper. Therefore, in the present paper, the dynamic motions of tunneled planing hulls operating in head sea conditions are numerically replicated by employing state-of-the-art CFD simulations. It is aimed at providing a clear understanding regarding the dynamic motion of a tunneled planing hull that is advancing in waves at high speeds, which is lacking presently. Predicting the dynamic motions of tunneled planing hulls in waves as well as providing some insight regarding fly-over phenomenon can be applicable in designing the next generation of high-speed boats considering the vessel structure and crew safety. The rest of the present paper is structured as follows. Following the Introduction section, the equations governing the motions of the vessel and fluid motion are presented. The CFD model that was used for the numerical reproduction of the problem is described in Section 3. The model is then compared against experimental data in Section 4 of the present paper. In Section 5, the results are presented and discussed. Finally, the concluding remarks and the scope of future works are presented in Section 6.

2. Formulation of the Problem

Considering a three-dimensional spatial domain that is filled with water and air, a right-handed coordinate system that is denoted with Oxyz is placed in the domain. The domain represents the fluid field around a vessel that is operating in planing mode in a rough-water condition, as displayed in Figure 1. The interface between liquid and gas is the water surface. Gravity waves can propagate in the fluid domain causing the free surface to oscillate around its equilibrium condition. The water waves propagate in the longitudinal direction from one side to the other, transporting energy. They can, therefore, cause vertical motion for the vessel.

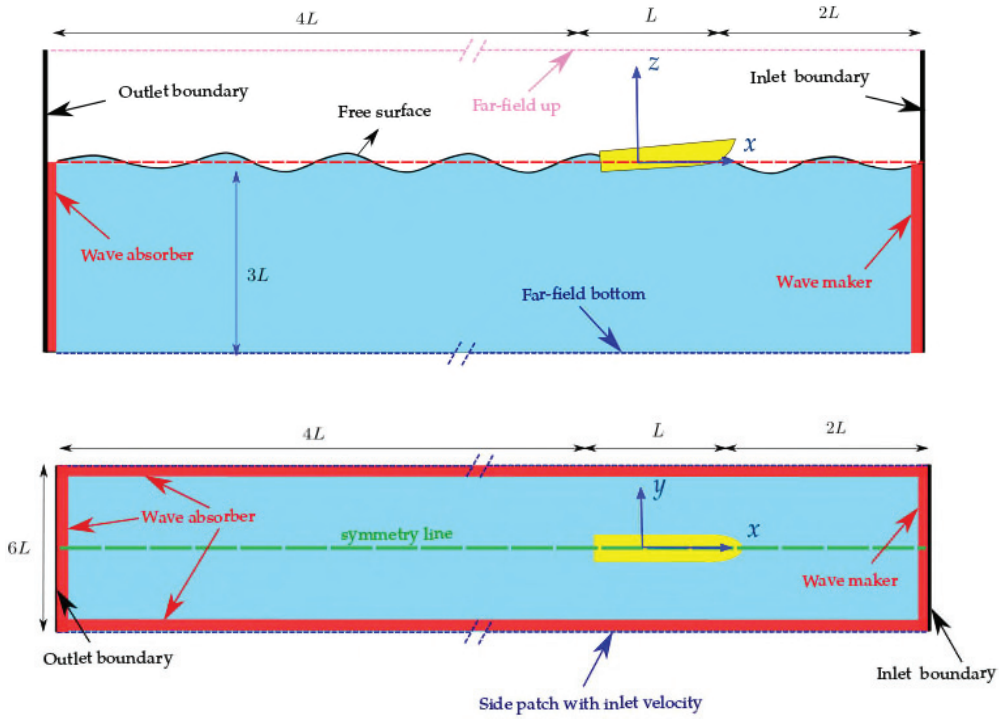


Figure 1. A sketch showing the problem domain. A tunneled planing craft is subjected to gravity waves that are generated by the numerical wave-maker that is located at the right end of the domain. The upper and lower panels show the longitudinal and top views of the problem. The dimensions of the domain are chosen based on the previous CFD simulations and recommendations, and their values are mentioned in Section 3 of the paper where the CFD model is described.

The fluid domain contains six patches, including two vertical, two horizontal, and two laterals. The vertical patches are the inlet and outlet boundaries. The lateral ones are the side boundaries. The bottom and upper patches are the far-field water and air boundaries. Since the fluid motion is symmetrical to the x-z plane passing through the centerline of the vessel, one of the side boundaries can be dropped, and the problem domain can be divided into two symmetric sub-domains. Thus, the symmetry lateral boundary can be used.

The dynamic motions of the vessel and wave motion in the fluid domain together cause changes in the linear momentum from one point to another. Therefore, the fluid problem is expected to be coupled with the dynamic motion of the vessel. See examples of the wave-induced motions that are caused by waves in [36].

The fluid motion of the air-water flow is hypothesized to be rotational, i.e., viscosity can cause vortex generation, deformations, and energy damping within the fluid domain. The flow is expected to be strongly turbulent near the walls of the vessel as the fluid velocity near its walls is relatively high. Note that the speed of the vessel, u, which is normalized using Froude's number, as per:

$$Fr_B = u/\sqrt{(gB)} \quad (1)$$

is greater than 2.0. Here, g is the gravity acceleration constant, and B is the beam of the vessel.

Assuming that the fluid flow is incompressible, homogeneous, and Newtonian, the equations governing the fluid motion can be formulated. In this condition, Navier–Stokes equations, which relate to the pressure field and the velocity field, given by: $\nabla \cdot \mathbf{v} = 0$

$$\partial_t(\rho_m \mathbf{v}) + \rho_m \mathbf{v} \cdot \nabla \mathbf{v} = -\nabla p + \nabla \cdot \mathbf{T}\mathbf{f} \tag{2}$$

govern the fluid motion. In Equation (2), $\mathbf{v}$ is the velocity vector and p is the fluid pressure. Both the velocity and pressure are unknown and need to be computed over time. $\mathbf{T}$ and $\mathbf{f}$ refer to the normal tensor and the body force vectors. The normal tensor is generated by viscosity and the body force is caused by gravity acceleration. $\mathbf{T}$ and $\mathbf{f}$ are given by

$$\mathbf{T} = (\mu_m + \mu_t)\left(\nabla \mathbf{v} + (\nabla \mathbf{v})^{\mathbf{T}}\right) \tag{3}$$

$$\mathbf{f} = \rho_m \mathbf{g}$$

In Equations (2) and (3), ρ_m and μ_m are the density and dynamic viscosity of the air-water mixture at any point. μ_t is the dynamic turbulent viscosity that can be computed through turbulent flow modeling. $\mathbf{g} = [0,\ 0,\ g]$ is the gravity acceleration vector.

The density and dynamic viscosity of the mixed air-water flow are computed by:

$$\rho_m = (1 - \phi)\rho_w + \phi\rho_a \tag{4}$$

$$\mu_m = (1 - \phi)\mu_w + \phi\mu_a.$$

In Equation (4), ϕ is the volume fraction. Subscripts w and a refer to the values of air and water. The volume fraction varies between 0 to 1. This value is employed to model the two-phase, non-reacting, fluid motion. $\phi = 0$ refers to pure water, and $\phi = 1$ refers to pure air. This helps us to model the two-phase flow [37], and capture the water surface properly, especially for the case of the fluid flow around the section of high-speed boats (e.g., in [38]).

The volume fraction is transmitted within the domain. A conservation law governs the flux of ϕ, as per:

$$\partial_t \phi + \mathbf{v} \cdot \nabla \phi = 0 \tag{5}$$

The boat is exposed to unidirectional monochromatic gravity waves that are generated at a numerical wave-maker, with an encounter angle of π. This wave-maker is located at the right side of the domain, the inlet boundary. The waves that are generated at the wave-maker lead to a head-sea condition.

As explained earlier, the wave steepness ($k_{in}A_{in}$) is set to be gentle, and thus Airy Theory governs the wave motion. No modulation instability, wave-induced turbulence, wave breaking, and wave–wave interaction is developed as the waves propagate along with the fluid domain.

The water surface elevation, ζ, is given by:

$$\zeta_{in} = A_{in}\cos(k_{in}x - \omega_{in}t + \epsilon) \tag{6}$$

In Equation (6), ω_{in} and k_{in} are the wave frequency and wave number, which are connected under the dispersion relation of deep-water, as:

$$\omega_{in}^2 = g k_{in} \tag{7}$$

The values of wave frequency and wavenumber are computed by:

$$\omega_{in} = 2\pi / T_{in}, \tag{8}$$

$$k_{in} = 2\pi / \lambda_{in},$$

where T_{in} and λ_{in} are the wave period and wavelength. Note that a far-field boundary condition is assumed for the bottom. Therefore, the deep-water dispersion relationship is valid.

The dynamic motion of the vessel is coupled with the first-order wave motion in the fluid domain. Two motions, heave and pitch, are assumed to be induced by the waves.

These are the vertical motions that are expected to be significant when a planing vessel is exposed to water waves.

The vertical motions of the vessel obey the rigid body law, as:

$$m\ddot{z} = \mathbf{F}.\mathbf{k} + mg \tag{9}$$

$$I\ddot{\theta} = \mathbf{M}.\mathbf{j}.$$

Here, m and I refer to the mass and the pitch moment of inertia of the boat. $\mathbf{F}$ and $\mathbf{M}$ are the force and moment vectors that can be computed using:

$$\mathbf{F} = \int_S (p + \sigma)\boldsymbol{n}\, dS, \tag{10}$$

$$\mathbf{M} = \int_S (p + \sigma)\boldsymbol{n} \times \mathbf{r}\, dS$$

Here, σ is the normal stress tensor. $\boldsymbol{n}$ and $\mathbf{r}$ are the normal vector and distance vector. The force and moment contain the contribution of pressure, added mass, damping, and restoring mechanisms [39].

Note that the wave-induced motions are identified as the displacement of the centre of gravity (CG) of the vessel concerning the considered coordinate system.

3. CFD Model Setup

3.1. Numerical Technique

Fluid equations are solved over time by employing the commercial CFD code SIEMENS PLM Star-CCM+ [40]. The upstream and downstream lengths are set to be $2L$ and $4L$. The tank is filled with water up to a height of $3L$. The side patch is set to be $3L$ far from the side edge of the vessel.

The water and air are set to flow in the domain from the right end and flow out from the left end of it. The bottom and top patches of the domain are set to be the velocity inlet to replicate an open-sea condition with no bottom effect. No slip condition is prescribed for the body of the vessel. The wave absorption condition is activated at all non-horizontal boundaries except the inlet to cancel out the wave energy reflection. Also, a symmetry boundary condition is set for the symmetry surface.

The $k - \epsilon$ turbulence model with a wall function is applied. The second-order upwind scheme is used to discrete the governing equations to reduce the transaction errors All $y+$ wall treatments of wall functions are selected, the $y+$ value is set to vary between 30 to 300 near the surface of the solid body addressing the requirement of the all wall $y+$ approach [40].

As indicated in the previous paragraph, the Volume of Fluid (VOF) method is used to trace the free surface. The VOF method is combined with the High-Resolution Interface Capturing (HRIC) approach.

The time-step that is used for simulation is set to be 0.0004 s, which gives a Courant number that is lower than 0.5 during the numerical simulations. For all speeds with the same time step, the Courant number was lower than 1. This ensures the convergence of CFD simulations. The convection terms are discretized by using a second-order upwind scheme. The unsteady terms are turned into algebraic equations by employing a three-dimensional segregated implicit unsteady scheme. The Navier–Stokes equations are solved using a Pressure-Implicit with Splitting of Operators (PISO) algorithm. The dynamic motions of the vessel are computed over physical time through the dynamic fluid body interaction (DFBI) module by setting heave and pitch motions to be free. The simulations are run over 6 time periods. More than 15 cycles occur during this time period, which satisfies the recommendations of the ITTC [41].

3.2. Spatial Discretization

The spatial domain is discretized into small volumes, in each of which the Navier–Stokes equations are solved at every single time step. An unstructured mesh is generated as the geometry of the vessel is not simple.

To model the dynamic motions of the vessel, an inverse distance weighted mesh technique that is called morphing mesh, is used and the Morpher solver is applied in a region-wise manner. This means that each region that is associated with this motion is morphed independently. This approach is considered to be the most suitable method that can be used for modeling the fluid-solid interaction, where the solid region has a rigid displacement motion and the fluid region has a morphing motion [40].

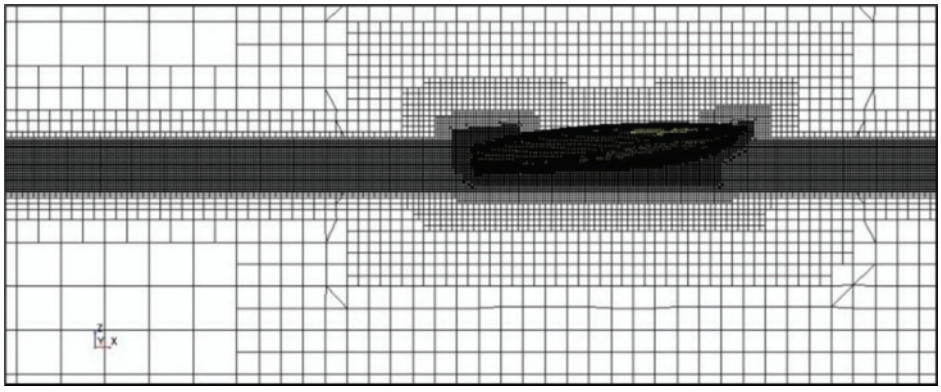
Using the morphing approach, the body of the vessel is moved every time step under the action of fluid forces and then the motions of cells that are located near the vessel are computed.

The Surface Mesh technique is used to generate cells in the whole domain. Trimmer Mesh and Prism Mesh methods are employed to generate cells near the free surface and the rigid surface of the vessel. Finer cells are generated in the vicinity of the vessel and free surface to capture the gas-liquid interface with high resolution. Coarser cells are generated near the lower and upper patches of the domain, where the fluid motion is weakly affected by the vessel and the wave motion.

A total fo four different grids with a refinement ratio of $\sqrt{2}$. are generated. The number of cells that are generated for each case is presented in Table 1. A mesh independence study is performed to detect the most proper grid, which is presented later. A view of the generated mesh, Grid C, is shown in Figure 2.

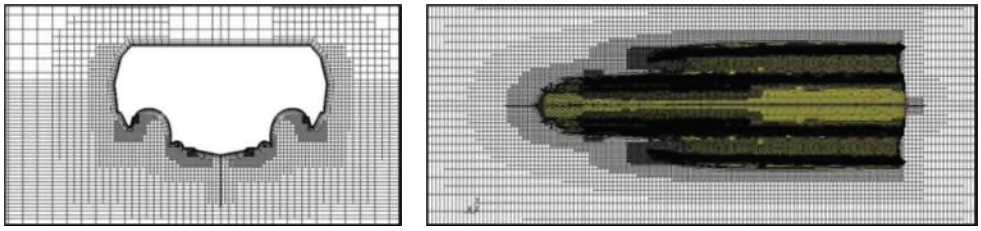
Table 1. The number of cells that are generated for each case.

Mesh	Number of Cells
Grid A	912,343
Grid B	1,050,045
Grid C	1,291,035
Grid D	1,484,532



(**a**) side

Figure 2. *Cont.*



(**b**) front (**c**) top

Figure 2. Generated mesh. The upper row shows the longitudinal view of the cells around the body from a longitudinal view. The lower panels show the generated cells from side, front, and top views. The vessel that is shown here is named Model B, which is introduced in Section 3.4. The generated mesh has 1,291,035 cells (Grid C).

3.3. Computation of Parameters

The dynamic responses of the vessel are computed over time. The time history of the heave, pitch, and vertical acceleration at CG are sampled. The heave (z) and pitch (θ) responses are computed by the downward zero-crossing method. The vertical acceleration ($\ddot{z}_{CG}$) is defined to be half of the difference between the crest and trough of the $\ddot{z}$ in each cycle. Note that the heave and pitch responses are normalized by dividing their values over the wave amplitude and wave steepness. Numerical data are sampled by using a frequency of 2500 Hz, which enables us to capture the data properly.

3.4. Planing Models and Forcing Condition

As explained earlier, two planing models are studied in the present paper. Both models have a tunneled body form and have been previously tested in towing tank experiments by researchers. The related information about these two planing designs can be found in [12,42]. The main hulls of both of the considered planing models have deadrise angles ranging between 10 to 13 degrees.

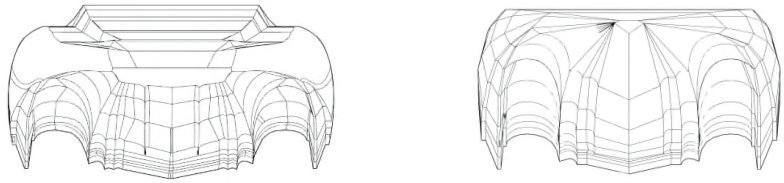
The reason for studying these two planing models is the lack of experimental data, highlighting the dynamic motions of tunneled planing hulls in waves. To the best of the authors' knowledge, no systematic experimental study has been conducted to measure the dynamic response of tunneled planing hulls in waves. There are two famous experimental studies that were carried out in the high-speed hydrodynamic tank of China Special Vehicle Research Institute, a subsidiary of the Aviation Industry Corporation of China (AVIC).

The first set of experiments was carried out by [12] in calm-water conditions. The calm-water performance of a tunneled planing hull is measured through towing tank tests. The vessel was later equipped with one, two, and three steps. It was reported that the non-stepped design had the best performance among all the cases, i.e., the resistance of the non-stepped planing trimaran hull was smaller than the other designs.

Later, another set of experiments was performed to evaluate whether air injections or a bilge keel can modify the performance of a tunneled planing vessel having large resistance [42]. The body form of this vessel is different from the one that was studied in [12]. Ma et.al. [42] also carried out a limited number of experimental tests to measure the dynamic response of the vessel in regular water waves. The experimental data they provided is the only available published research, highlighting the seakeeping of trimaran planing hulls. Importantly, the calm-water performance of the vessel that was studied in the second series of experiments is not as good as the one that was studied in the first set of experiments. The non-dimensional resistance force is larger for the case of the second set of experiments. This can be due to the different body forms, which can lead to the generation of a larger volume of water spray, and also the development of a stronger turbulent air-water mixture in the tunnels.

Resulting from our explanation, the experimental data of [42] can be used for evaluating the accuracy of the numerical model in the reproduction of the wave-induced motion of a trimaran planing hull. However, numerical simulations that are used to model the wave-induced motion of the vessel have better performance in calm-water conditions.

The wave-induced motions of the first model, Model A, are computed to evaluate the validity of the CFD model, as explained (experiments [42]). The dynamic motions of the second planing model, Model B, are simulated to understand the unsteady planing motion of the tunneled vessels (experiments performed in [12]). The calm-water performance of this model is also reported in Appendix A. The results that are presented in this Appendix A confirm the capability of the CFD model in simulations of the steady motion of Model B as well. The body plans of these models and their principal characteristics are shown in Figure 3 and Table 2. It can be seen that the dimensions of both vessels are very similar. However, their bottom shapes are different; the bottom of Model B has a convex shape.



(**a**) Model A (**b**) Model B

Figure 3. Body plans of the studied planing trimaran hulls [12,42].

Table 2. Principal characteristics of the studied models [12,42].

Parameter	Model A [42]	Model B [12]
L (m)	2.4	2.4
L/B	3.2	3.75
L_{CG}/L	0.305	0.2625
V_{CG}/B	0.17	0.156
k_{xx}/B	0.36	0.32
k_{yy}/L	0.31	0.27
Average deadrise angle (°)	11	13
$m/\rho B^3$	0.116	0.149

3.5. Tests

There are two different forcing conditions that are used to induce the vertical motions of boats. The first set of conditions corresponds to the waves that are generated to trigger motions for Model A, which is used to reproduce the experiments of [42]. The data are reported in Table 3. The second forcing condition that is used in the present research is shown in Table 4. The reported waves are used to numerically generate gravity waves to induce motions to Model B.

3.6. Grid Independence and Uncertainty Study

A mesh independence study is performed to find the optimum number of cells of the computational domain that can be used for numerical simulation of the problem. To this end, the vertical motions of Model B are numerically simulated for Fr_B of 4.7. An incoming water wave with a frequency of 0.57 Hz and a steepness of 0.03 (see Table 4) is numerically generated at the right end of the domain. The heave and pitch responses of the vessel are computed, showing that the results converge for the mesh size of 1.05 M (Grid C). A summary of the mesh independence study is shown in Figure 4, where the left

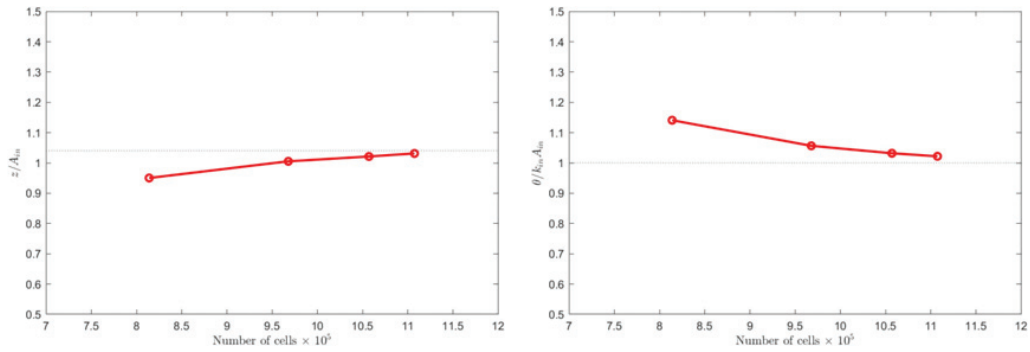
and right panels show the mesh convergence for heave and pitch responses. As seen, the coarse mesh may lead to the under-prediction of the heave and an over-prediction of the pitch responses.

Table 3. Forcing condition of the first set of numerical experiments.

Wave	Wave Steepness ($k_{in}A_{in}$) (-)	f_{in} (Hz)	Fr_B (-)	λ/L (-)
1	0.10	1.06	2.1	0.6
2	0.09	0.95	2.1	0.7
3	0.07	0.75	2.1	0.8
4	0.05	0.72	2.1	1.2
5	0.04	0.62	2.1	1.7
6	0.03	0.55	2.1	2.0
7	0.02	0.45	2.1	3.1
8	0.02	0.44	2.1	3.2
9	0.02	0.42	2.1	3.5
10	0.02	0.41	2.1	3.7
11	0.01	0.37	2.1	4.5
12	0.01	0.34	2.1	5.4
13	0.01	0.32	2.1	6.2

Table 4. Forcing condition of the second set of numerical experiments.

Wave	Wave Steepness ($k_{in}A_{in}$) (-)	f_{in} (Hz)	Fr_B (-)	λ/L (-)
1	0.10	1.00	3.1-3.9-4.7-5.6	0.65
2	0.07	0.80	3.1-3.9-4.7-5.6	1.0
3	0.06	0.66	3.1-3.9-4.7-5.6	1.4
4	0.06	0.57	3.1-3.9-4.7-5.6	2.0
5	0.05	0.50	3.1-3.9-4.7-5.6	2.6
6	0.04	0.44	3.1-3.9-4.7-5.6	4.3
7	0.03	0.40	3.1-3.9-4.7-5.6	4.0



(**a**) Heave response (**b**) Pitch response

Figure 4. A mesh independence study is performed to find the optimum grid size. The left and right panels show the data corresponding to the heave and pitch responses. The results correspond to the heave and pitch motions of Model B. The wavelength is 2*L*, and the Froude number is 4.7.

Also, the uncertainty analysis of the grid is presented in Table 5. Here, R_G is the grid refinement ratio. Furthermore, P_G is the estimated order of accuracy. GCI refers to the grid

convergence index. U_G is the uncertainty of grids and U_{SN} is the numerical simulation uncertainty. $|E|$ is the absolute value of the comparison error between the experimental and numerical results (of the finest grid). However, the values of P_G that are less than 1 or greater than the theoretical order of accuracy (P_{G_th}) determine an unreliable estimation of δ_{RE}, as shown by [42]. Specifically, when $P_G < 1$, δ_{RE} is over-conservatively estimated. Instead, when $P_G > P_{G_th}$, δ_{RE} is not reliable because U_G is underestimated.

Table 5. Grid uncertainty analysis.

Parameter	Grids	Grid Refinement Ratio	R_G	P_G	P_{G_LSR}	%U_G GCI	%U_G LSR-GCI	% |E|
$\theta/k_{in}A_{in}$	A-B-C	$\sqrt{2}$	1.300	−0.756	0.56	22.907	21.63	7.07
	B-C-D	$\sqrt{2}$	0.197	4.698		0.256		6.18
z/A_{in}	A-B-C	$\sqrt{2}$	2.400	−2.522	0.829	12.149	20.12	7.48
	B-C-D	$\sqrt{2}$	0.250	4.004		0.581		6.17

For the abovementioned reasons, Table 5 provides the results of the grid uncertainty based on the LSR (least square root) approach that was proposed by [43]. This approach is based on a least squares root version of the GCI method. Details of this method are provided in [44] and an example of application in the marine hydrodynamics field is available in [45].

4. Numerical Results vs. Experimental Measurements

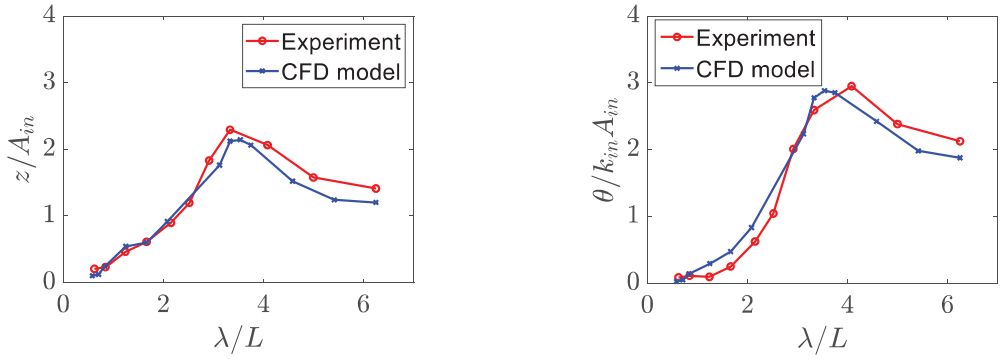
As mentioned earlier, the objective of the present paper is to provide an understanding of the vertical motions of a tunneled planing hull operating in a head sea. There were two tunneled planing hull models, Model A and Model B, that were designed earlier and the towing tank test results have been carried out in [12,42]. Although the calm-water performance of Model B was seen to be much better compared to Model A, no experimental data highlighting the seakeeping of Model B has been published yet. Therefore, the accuracy of the CFD model in the numerical modeling of the wave-induced motion of a tunneled planing vessel is evaluated by comparing the numerical results against the experimental measurements of [42] (Model A). As mentioned earlier, the resistance of this model is higher than the other one (Model B). In addition, the calm-water performance of Model B was previously simulated by using the CFD model and compared against experimental data. The calm-water results of Model B are presented in Appendix A.

The wave-induced motions of Model A are numerically simulated over time. The forcing condition that is presented in Table 2 is used to trigger the unsteady vertical motions. Note that all the numerical tests correspond to the experiments, i.e., the experiments are numerically reproduced. All the simulations are performed at the speed of 5.7 m/s, corresponding to Fr_B of 2.1.

The heave and pitch responses are computed. The results are compared against the experimental data in Figure 5. The results that were obtained using the CFD model, are seen to follow the experimental data in both panels. The numerically-predicted heave responses are in fair agreement with the experimental results of [42] at short wavelengths.

The resonance of the heave motion is seen to occur at the wavelength of ~3.5L, where the error of the CFD model is around ~10.15%. The heave response is seen to converge to 1.0 by the increase in the wavelength. Errors of the numerical model in computing the heave response are around ~10% in the resonance zone. The errors are around 15% at long waves. The pitch motion is seen to be resonated at the wavelength of ~4.5L. The CFD model has captured the peak value at a nearly shorter wavelength. Overall, the computed values of pitch response are seen to be close to the experimental data at most of the wavelengths, and they follow the experimental data. The values of errors vary between 0.08% to 5.14% at wavelengths that are shorter than 3.34L. For the case of longer wavelengths, where

resonance occurs, the pitch response reaches up to $3k_{in}A_{in}$, and the error of the CFD model is around ~11.54%. Overall, the results that are shown in Figure 4 prove that the present CFD model has proper accuracy in the simulation of the wave-inducted motion of a tunneled vessel that is operating in planing mode.



(**a**) Heave Response (**b**) Pitch response

Figure 5. Heave and pitch responses of Model A. Circle and cross markers correspond to experimental and CFD data. Experimental data are presented in [42].

5. Results and Discussion

The wave-induced motions of Model B are computed for different wave conditions that are reported in Table 4. The longitudinal force resisting against the vessel forward movement is also computed. The rest of the results and discussions that are presented in the present paper correspond to this set of simulations. Note that the data corresponding to the calm-water performance of Model B is presented in Appendix A. In this Appendix A, the CFD data and experimental data are compared against each other. It is shown that the CFD method can have a relatively great level of accuracy in the replication of the advancement of the vessel in calm-water. The accuracy of the CFD model in the replication of the unsteady motion of a tunneled planing hull is also evaluated in the previous section (Figure 5). Overall, the method has been seen to be accurate enough to be employed for replication of the advancement of Model B in head sea conditions. In addition, supplementary files are presented, containing recorded videos for unsteady motions of Model B, operating in water waves. Details of the videos are explained in the Supplementary Material Section.

A sample of the recorded responses of the vessel over five-wave periods, that are induced by the wavelength of $2L$ is shown in Figure 6. The results correspond to the condition the vessel advances with a Froude number of 4.7. As it can be seen, the period of the induced motion is shorter than that of the incoming wave, which agrees with the Doppler effects and the physics of the problem. The heave and pitch of the vessel are observed to have cyclic motions. The vertical motions are expected to be nonlinear. Every single cycle of heave and pitch motions is not symmetric with respect to a vertical line crossing the average point of that cycle.

The vertical acceleration is strongly nonlinear. The peak of each cycle is highly sharp. The peak value is seen to reach up to $5g$ in some cycles, which is relatively high for a vessel that is operating in the sea. Note that the wave steepness value is 0.02, which is identified as a very gentle wave condition. The minimum value of the vertical acceleration in each cycle is $-g$. This shows that the vessel experiences a $6g$ change in its vertical acceleration over a very short time. The vessel has a vertical acceleration of $-g$ over a very short time. This means that no vertical force, except the weight force, is acting on the vessel. Such a motion only occurs in the condition that the vessel comes out of the water. In this situation, the bottom surface is dry. A large acceleration occurs soon after. It occurs as the vessels re-enter the water and a large vertical impact force is generated. The center of this force is

behind the center of gravity. Thus, a large negative pitching moment emerges and pitches the vessel bow down. As a result, the pitch angle of the vessel decreases. Videos of the motions of the vessel are presented in the Supplementary Material. The file, named LF_47, includes a video of the motion of the vessel. The video demonstrates that the unsteady heave and pitch motions occur, and the vessel comes out of the water and then re-enters it. As is obvious in the video, the noticeable decrease of the pitching displacement occurs just after entering the water. In the videos, it can be seen that the rear part of the vessel enters the water first.

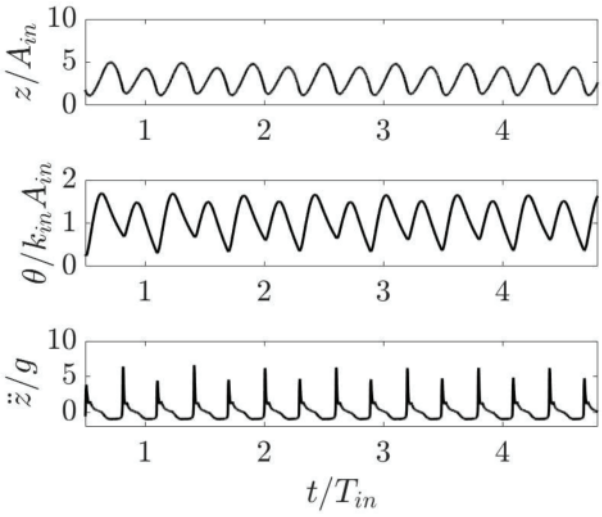


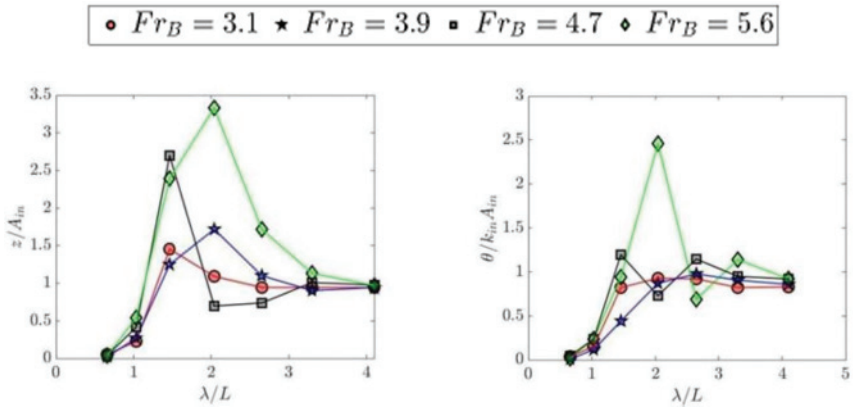
Figure 6. A sample of the responses of Model B to waves. The presented data correspond to 2*L* and a beam Froude number of 4.7.

Readers who are interested in an additional technical discussion on the time histories of heave and pitch responses of the hard-chine planing hulls are referred to [46].

5.1. Responses

The heave and pitch responses of the vessel are computed and reported in Figure 7. As seen, the resonance in the heave response occurs for all cases at wavelengths ranging between 1.4*L* to 2*L*. As it is observed, at the three lower speeds, resonance occurs at a wavelength of 1.4*L*, while it occurs at a longer wavelength at the highest Froude number (5.6). The wetted surface pattern of the vessel is expected to be the main reason for such behavior which needs to be studied in the future. The response is intensified by the increase in the speed and can reach up to $3.2A_{in}$ in the resonance zone. For all cases, long waves induce the non-dimensional response of ~1.0., which agrees with physics, i.e., at very long waves, the vessel follows the wave motion of the water. When the incident waves are much shorter than the length of the vessel, insignificant motion is induced.

Compared to Model A, the heave response of Model B is smaller. A simulation was run for Model A for the case of a smaller beam Froude number (2.1). The resonance of heave motion was seen to occur at a wavelength of ~3.8*L*. But the heave response, corresponding to the resonance of Model A, was seen to be ~$2A_{in.}$ For the case of Model B, the heave response, corresponding to beam Froude numbers of 3.1 and 3.9 is smaller than ~$2A_{in.}$ It confirms that Model B performs better in water waves compared with Model A. This may be due to the different designs of these two hulls. As it was mentioned before, Model B has a convex bottom shape which can direct the water toward the transom by decreasing the pressure. This can decrease the pressure near the transom of the vessel and modifies the heave response.



(**a**) Heave response (**b**) Pitch response

Figure 7. Heave (**a**) and pitch (**b**) responses of Model B in different forcing conditions.

The pitch response of Model B, right panel, is seen to be overdamped at the small Froude numbers, i.e., no resonance occurs at the two smaller speeds, showing that the entrapped air can strongly damp the pitch motions of a vessel at a mild planing speed. At a higher speed, the wetted surface of the vessel remarkably decreases, and the volume of air supporting the vessel decreases noticeably. As a result, less pitching moment damps the angular motion of the vessel. When the speed of the vessel reaches the highest value, the pitch response emerging in the resonance zone exceeds $2k_{in}A_{in}$. The vessel has been seen following the wave slope at long waves, while short waves cannot induce any noticeable motion.

The pitch response of Model A was previously presented in Figure 5. The pitch of Model A was seen to resonate at a wavelength of ~4.5L. The maximum pitch response of Model A was observed to be ~$3k_{in}A_{in}$. The results of the tests that are presented in Figure 5 correspond to the Froude number of 2.1. For the case of Model B, it was seen that the pitch response is overdamped at the Froude numbers of 3.1 and 3.9, both of which are greater than 2.1. This provides evidence that the pitch responses of Model B are smaller than that of Model A. These observations demonstrate that Model B has a greater level of performance in head sea conditions. The pressure distribution pattern over the bottom surface of Model B is the likely reason for its better performance in water waves. It is interesting to note that the performance of Model A may be modified by adding one step, which can distribute the pressure over the surface by balancing its value between the front and rear body. However, it is not the aim of the present paper to investigate the effects of steps on wave-induced motion of a planing trimaran vessel. Readers who are interested in the stepped design of planing trimarans are referred to [16].

The time-averaged values of the heave and pitch motions of the vessel are computed. These values inform the mean heave/pitch displacement around which the vessel oscillates. Figure 8 shows the mean value of the heave and pitch of Model B in different wave conditions. The error bars show the amplitudes of the motion.

The mean heave of the vessel is seen to be larger than that of the calm-water condition, the dashed red line, in all cases. This means that when a tunneled planing vessel operates in waves, the nonlinear effects of water waves give rise to an extra hydrodynamic force, which pushes the vessel up. Under the action of this force, the vessel is positioned at a mean heave value, which is higher than the CG rise-up of the vessel in the calm-water conditions.

The mean values of pitch displacement are seen to be smaller than the dynamic trim angles of the vessel in the calm-water conditions. As seen, the mean pitch angle is significantly affected in the resonance zone. Interestingly, the value of pitch turns negative in some cases. For example, when the vessel operates with a Froude number of 5.6 in waves

with $\lambda = 2L$, the lower error bar reaches a negative value. In some cases, the negative value for the pitch displacement is likely to be caused by the occurrence of fly-over motion. When the planing vessel re-enters the water, a large negative pitching moment occurs, leading to a pitched-down motion. Note that after flying over the air-water interface, the stern of the vessel enters the water, causing a large negative pitching moment. An example can be observed in the Supplementary File named LF_56. In the related video, the negative pitch displacement, pitched-down motion, can be viewed after the re-entry phase.

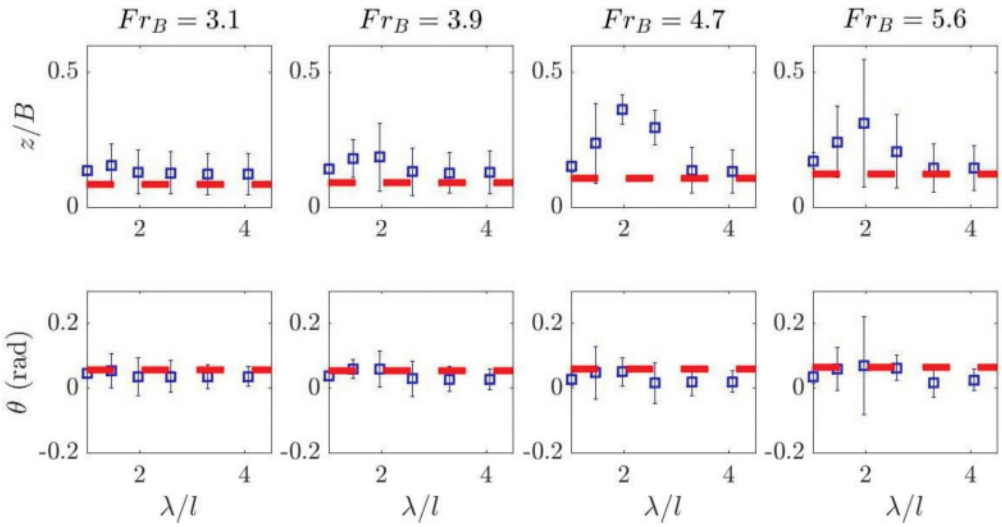


Figure 8. Mean values of the heave and pitch motions of Model B operating in a head sea. The dashed red line shows the calm-water performance of the model in calm-water conditions. The error bars are the amplitude of the heave and pitch motions.

In addition, it can be seen that in some other cases, the pitch angle turns negative however, the fly-over motion is not observed. For example, the pitch angle of the vessel might turn negative when its Froude number is 3.1 and the waves are 2L long. No fly-over motion occurs in this condition. This can be seen in the related video file (LF_31). Also, the time history of vertical acceleration of this case is presented later, showing that no fly-over motion occurs. When the vessel advances in waves with a wavelength of 2L, a large negative pitching moment emerges. The tunneled design of a planing hull distributes the pressure over the bottom of the vessel in a way that a large negative pitch moment might emerge when the wave crest reaches the stern of the vessel. Thus, the negative pitching moment pushes the bow of the vessel down. Note that the pressure distribution over the bottom surface of the vessel is discussed in Section 5.3.

The vertical acceleration at CG is computed for different wave conditions and is reported in Figure 9. The vertical acceleration that is caused by the long and short waves, is seen to increase by the increase in the Froude number from 2.8 to 4.3. The speed of the vessel is higher, and thus, larger vertical forces may act on its bottom surface, resulting in a larger acceleration. The amplitude of acceleration is seen to reach up to 3g at a Froude number of 4.7. This peak value, corresponding to a beam Froude number of 4.7, occurs when the waves are 2L long. In the case where the vessel operates at the highest Froude number, 5.6, the acceleration is seen to be smaller compared to the Froude number of 4.7 in some forcing conditions. The example can be seen in the case of the peak value of vertical acceleration.

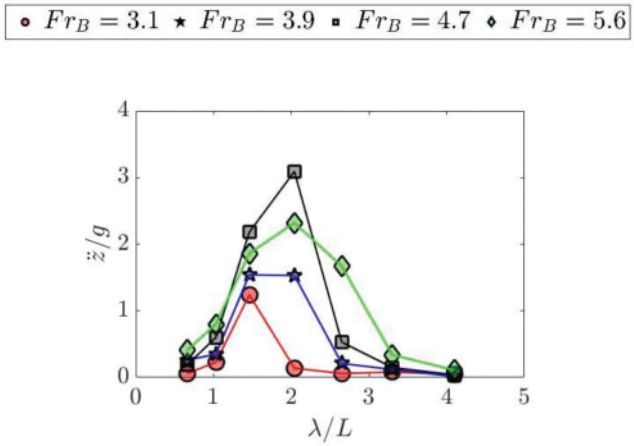


Figure 9. Vertical acceleration of Model B at CG.

The maximum values of acceleration are seen to occur under the excitation of waves that are 2L Froude number, 5.6. However, the acceleration that us related to the smaller Froude Number, 4.7, is larger when waves are 2L long. This is linked to the dynamic behavior of the vessel when fly-over motion occurs. For the case of the highest speed, the second harmonic pitch motion is relatively energetic causing two consecutive fly-over movements with different periods. This modifies the amplitude of the vertical acceleration of the boat at the highest speed. However, the vessel experienced a greater number of fly-over motions in this condition. Note that it is later shown that two consecutive fly-over motions occur at the highest speed when the incoming waves are 2L long.

The maximum value of acceleration emerges at longer waves as the speed is increased. At very long waves and very short waves, the vertical acceleration of the vessel converges to zero.

5.2. Resistance in Waves

The resistance of the vessel is sampled over time, and its amplitude is computed through a zero-crossing method. The data corresponding to resistance is displayed in Figure 10.

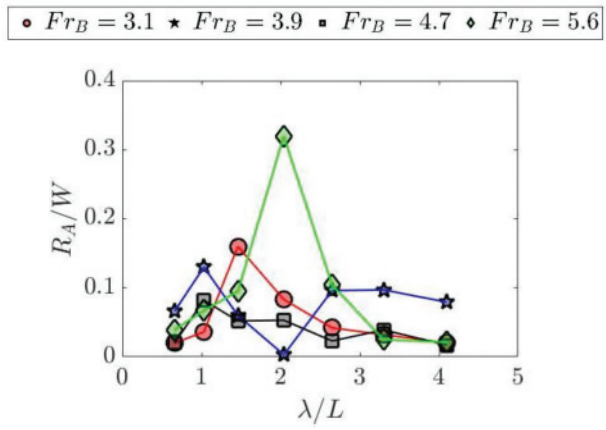


Figure 10. Resistance of Model B in waves.

Resistance reaches a peak value at all speeds. This value emerges at a wavelength of ~1L at Froude numbers of 3.9 and 4.7. The peak values of resistance at these two Froude numbers are around ~0.2W. Interestingly, the peak value of the resistance at the highest speed is ~0.38W, which is nearly two times larger than that of Froude numbers of 3.9 and 4.7. Furthermore, the peak value of the resistance corresponding to the Froude number of 5.6 emerges at a wavelength of 2L. The reason for such behavior needs to be investigated. In the rest of the paper, the time histories of the drag force and its components are presented to provide more understanding of such behavior.

The time history of resistance force is sampled and presented to understand the mechanisms that are causing this force. It is attempted to calculate the amount of drag that is caused by the shear stresses and pressure, separately. The time history of data, corresponding to Froude number of 4.7, and a wavelength of 2L, is presented in Figure 10.

As seen previously, the resistance force has a strong non-linear behavior over time. Over an exciting period, it reaches a sharp crest and then its values drop and reach zero. The zero-drag condition lasts for a period of $\sim 0.1T$. This implies that the vessel is not washed by the water, and it is above the air-water interface. Such a condition occurs when the vessel comes out of the water. This phenomenon, as defined earlier, is known as the fly-over movement and is more probable when the speed increases.

There are two different components for the resistance that are identified and presented in Figure 11 for Model B at a Froude number 4.7 in a wavelength of 2L. The first one is the induced drag, which is computed by integrating the hydrodynamic pressure over the wetted surface. The second one is the frictional drag which is caused by the shear stresses that is acting on the bottom surface of the vessel.

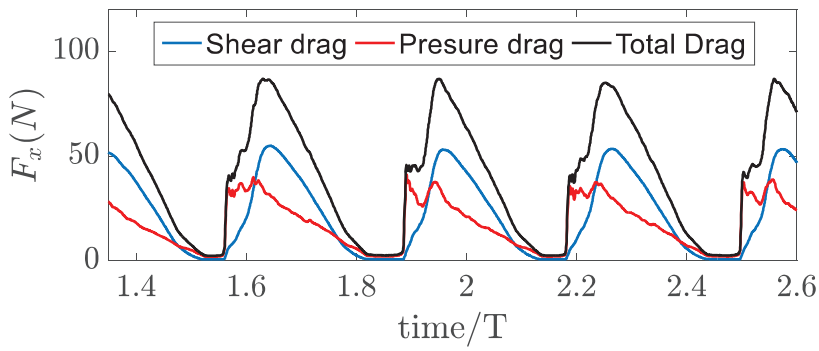


Figure 11. Time history of drag force, and its different components when the tunneled vessel Model B operate in waves with a beam Froude number of 4.7. The vertical motion of the body is caused by waves with a wavelength of 2L.

The drag force drastically increases and reaches a peak value. The sudden increase is observed to be linked to the sudden increase of the induced drag, the solid red curve (Figure 11). This confirms that as the vessel re-enters water and slams the free surface, a large drag force emerges. Simply stated, the solid body is impacted by the water. Thus, a larger force that is generated by hydrodynamic pressure acts on the surface in this condition. Afterwards, the contribution of the pressure drag highly decreases and converges to zero. The zero-value condition only lasts for ~0.1T.

Compared to the induced drag, the contribution of shear drag is seen to increase at a lower rate. However, at the instant the shear drag force reaches its peak value, the total drag force reaches its maximum value as well. When the peak drag force emerges, the value of the induced drag is notifiable. It is nearly half of the shear stress drag.

The shear drag force is expected to be dependent on the wetted area of the vessel. When the vessel reaches its lower vertical position, the shear drag is larger. Overall, the

presented results demonstrate that when the fly-over movement occurs, a very large drag force that is caused by the impact pressure emerges.

5.3. Fly-Over Motion

As was discussed earlier, the fly-over motion may occur when the tunneled vessel advances in a head sea condition. It was observed that the fly-over motion may lead to the generation of large induced drag forces as the vessel penetrates the water. To understand this problem more deeply, time histories of vertical acceleration are sampled and plotted. When the vessel comes out of the water, its CG has a constant vertical acceleration, which equals $-g$ as weight is the only force that is acting on it. Also, time histories of drag force are plotted to check whether the fly-over motion-induced extra drag force emerges or not.

Time histories of the resistance as well as the vertical acceleration of the vessel's left panels, and drag force, right panels, operating in waves with a length of $2L$ are displayed in Figure 12. The data that are shown in Figure 12 demonstrates that the vertical acceleration of the vessel reaches $-g$ at three higher speeds, corresponding to Froude numbers of 3.9, 4.7, and 5.6. When the vertical acceleration reaches $-g$, it does not vary over time for a very short period, e.g., $\sim 0.2T$ for a beam Froude number of 3.9. This confirms that the vessel is above the water surface, and fly-over motion has occurred, and thus only the weight force acts on it. Therefore, the vertical acceleration at CG is $-g$. Besides, the presented data for resistance confirms the occurrence of fly-over motion. It can be seen that when vertical acceleration is $-g$, the drag force is zero, i.e., the vessel is above the water and water cannot cause any friction/pressure force.

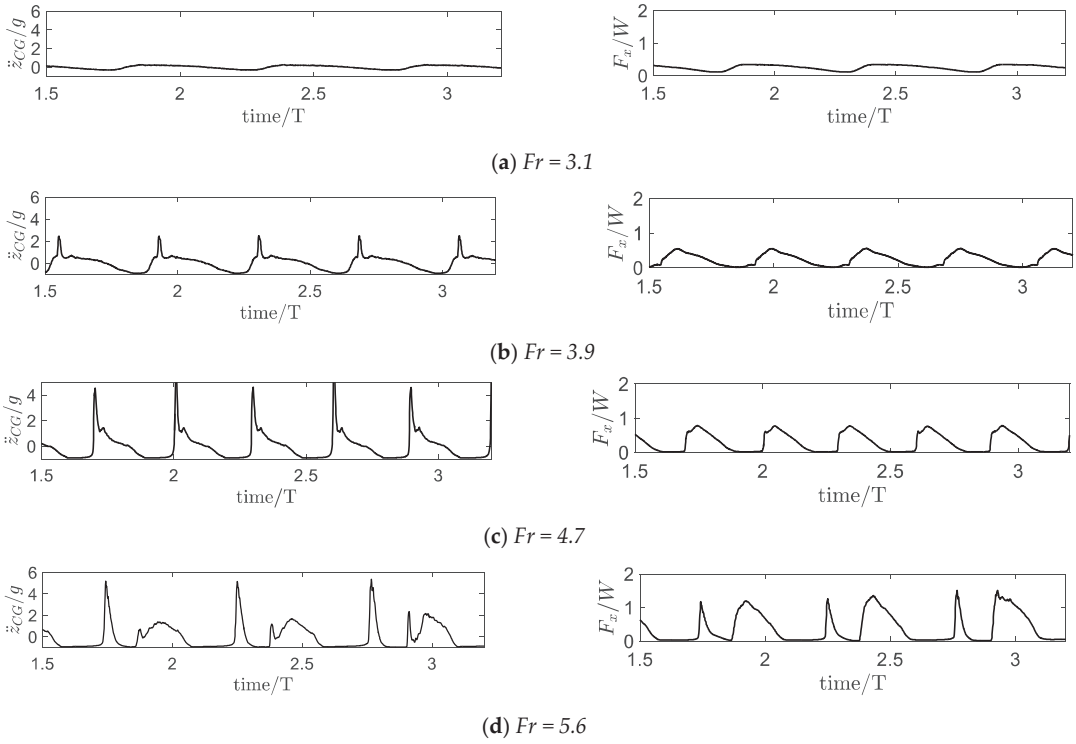


Figure 12. Time histories of the vertical acceleration of Model B at CG and the resistance of the tunneled planing hull in waves. (**a**–**d**) respectively denote the data corresponding to beam Froude numbers of 3.1, 3.9, 4.7, and 5.6. Note that all the motions are induced by regular waves with wavelengths of $2L$ and a wave amplitude $0.0187L$.

Interestingly, when the vessel operates at the highest speed, it has two different fly-over motions. One fly-over motion occurs just after a very large acceleration, which is around ~5g, and the second one occurs soon after when the vessel experiences a vertical acceleration of ~2g. The second fly-over motion is seen to last for a shorter time. This means that a higher frequency, which can be identified as the second harmonic, strongly involves the motion.

It seems that a higher speed can strongly affect the nonlinear behavior of the vessel that is operating in waves, and thus the acceleration energy is narrowed around two different harmonics. When the vessel operates at the highest speed (Fr = 5.6), the crest to trough distance of the first fly-over motion is near ~5g, and the crest to trough distance of the first fly-over motion is near ~3g. Therefore, the average value of the CG acceleration that is found through the zero-crossing method gives a value of ~2g, which is smaller compared to what was found for a Froude number of 4.7. It was previously observed that the vertical acceleration corresponding to a beam Froude number of 5.6, is smaller than that of a Froude number of 4.7 when the waves are 2L long. It was explained that the reason for it is the two consecutive fly-over motions that are occurring in a single exciting period.

In addition, the resistance force is affected, and thus, the pressure drag can cause two sudden increases in the time-history of the resistance. A comparison between the resistance forces of the highest speed with the other ones, confirms that the two-consecutive fly-over motions occur over a period of time.

It is very interesting to investigate the flow pattern around the vessel as it goes through the fly-over motion. It can help us to understand the physics of this phenomenon in detail. Therefore, the wetted area of the vessel, skin friction coefficient, and the pressure coefficient distribution over the bottom surface of the vessel is sampled at four different time steps. These time steps cover the different stages. The sampling is performed for four different speeds, corresponding to beam Froude numbers of 3.1, 3.9, 4.7, and 5.6. All of the results are related to the wavelength of 2L. Note that for the case of the lowest speed, fly-over does not occur.

Figures 13–16 show the results corresponding to beam Froude numbers of 3.1, 3.9, 4.7, and 5.6, respectively. The first row of each figure shows the position of the vessel. The second row shows the wetted area. The wetted surface pattern is identified by the distribution of volume fraction. A volume fraction of 0.0 refers to water and a volume fraction of 1.0 refers to air. A volume fraction between these two numbers includes a mixture of water and air, which mainly refers to water spray.

The third row shows the skin friction coefficient distribution over the bottom surface. This coefficient refers to the shear stresses that are generated by the effective viscosity that is acting on the wall of the vessel. It is computed through:

$$C_f = \frac{\tau_w}{0.5\,\rho_w u^2} \tag{11}$$

where τ_w is the shear stress that is caused by the air-water flow.

On the dried areas of the vessel, C_f the coefficient is nearly zero, and on the washed areas, its value is non-zero. At the points where turbulence is stronger, the skin friction coefficient is expected to be larger.

The last row of the presented figures shows the hydrodynamic pressure, which is higher when the vessel impacts the free surface as it penetrates the water. This coefficient is calculated through:

$$C_p = \frac{p}{0.5\,\rho_w u^2} \tag{12}$$

As observed in Figure 13, when the vessel operates at the slowest speed, no fly-over motion occurs. This can also be seen in the Supplementary Material (LF_31). Large hydrodynamic pressure might emerge on the bow of the vessel. The skin friction coefficient is seen to be increased when the bow of the vessel comes out of the water. Its value is seen to be higher in the side bodies, where the water flow is strongly turbulent. Note that similar behavior was observed in the CFD simulations of [47]. At $t = T/2$, the crest of the wave has reached under the bow of the vessel causing noticeable hydrodynamic pressure. This results in a negative pitch motion. Then, the crest passes the transom and the wetted surface becomes smaller. The vessel is pitched down, and a negative pitch angle occurs; it is obvious in the Supplementary Material (LF_31).

Figure 14 shows the snapshots corresponding to the Froude number of 3.9 and incoming wave with $\lambda = 2L$. As was previously mentioned, the fly-over motion occurs at this speed. The occurrence of this phenomenon is obvious. The video that is presented in the Supplementary Material (LF_39) also proves that the fly-over motion occurs.

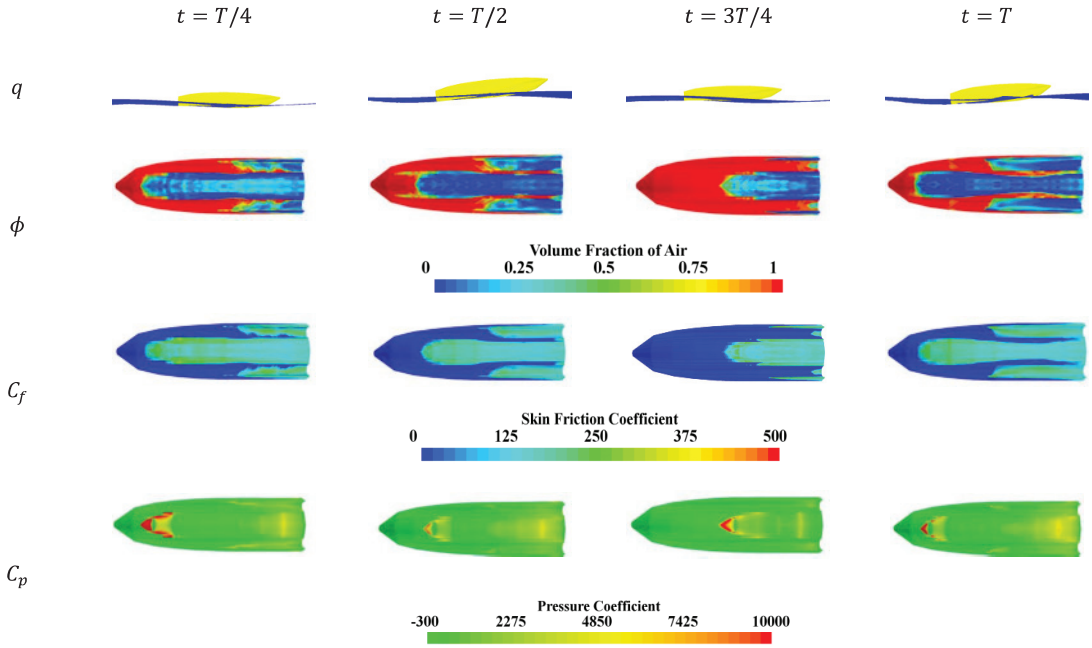


Figure 13. Snapshots of Model B motion during different stages. The first, second, third, and fourth rows, receptively, show the snapshots of the vessel's position to the water surface, volume fraction over, skin friction coefficient, and the hydrodynamic pressure coefficient. The results correspond to the wavelengths of 2L and a beam Froude number of 3.1.

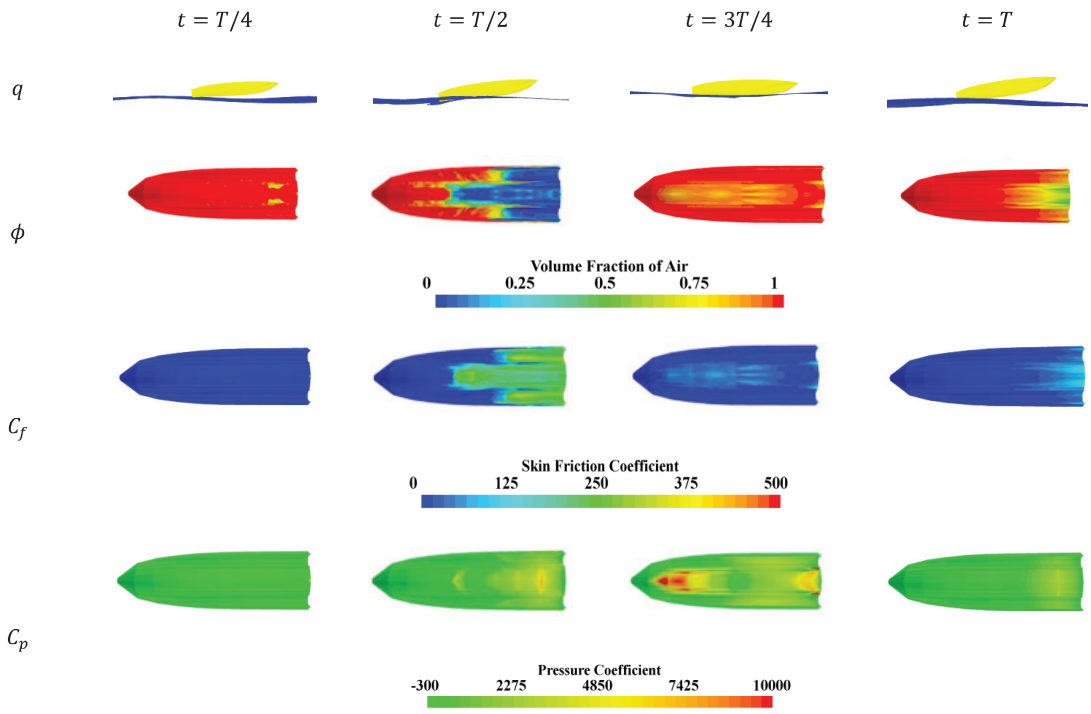


Figure 14. As in Figure 13, but for a beam Froude number of 3.9.

At the first snapshot, the first column, the vessel positions itself above the water surface. The surface is nearly dry and there is a low volume of the air-water mixture near the stern. The skin friction is observed to be zero on the whole body of the vessel, which agrees with the observations that were made in Figure 10. Interestingly, the hydrodynamic pressure on the whole body of the vessel is zero, which matches with the physics of the problem, i.e., no water flows under the body at this instant and thus the hydrodynamic pressure is zero over the entire bottom surface.

It can be seen that the vessel re-enters the water at the next stage, the second column. The water washes the bottom surface, mainly the stern of the vessel. A large hydrodynamic pressure emerges, and the skin friction coefficient becomes large on the side hulls, where the shear stresses are larger as turbulence kinematic energy is larger on the side bodies. The hydrodynamic pressure reaches a very large peak value at the point near the transom, which matches with previous observations (e.g., in [48,49]). Such a larger pressure is expected to be caused by the rigid body movement when the vessel falls (related discussions on water entry and the related high hydrodynamic pressure can be found in [50,51]. Note that the rear part of the vessel enters the water first.

At the next time step, the third column, the pitch angle of the vessel decreases, the heave position decreases, and the vessel skims on the water surface. In this condition, the hydrostatic pressure converges to zero. The skin friction coefficient is seen to be decreased at this stage. The hydrodynamic pressure becomes very large on the bow of the vessel. This large pressure prepares the vessel to exit the water.

At the final stage, the vessel jumps out of the water. Its bow is highly pitched up and the CG is high above the water surface. Only the rear area of the bottom is washed by water, and the skin friction is nearly zero over the bottom surface. A large pressure that was observed in the previous stage, the third column, has vanished.

The sampled data corresponding to the beam Froude number of 4.7 are displayed in Figure 15. The Supplementary file (LF_47) also shows the motion of the vessel as it is

exposed to water waves. Snapshots are presented with a shorter time step as Doppler effects lead to a shorter encounter period at this speed. The fly-over motion is observed to occur at this speed. It can also be seen in the video file that is presented in the Supplementary files (LF_47).

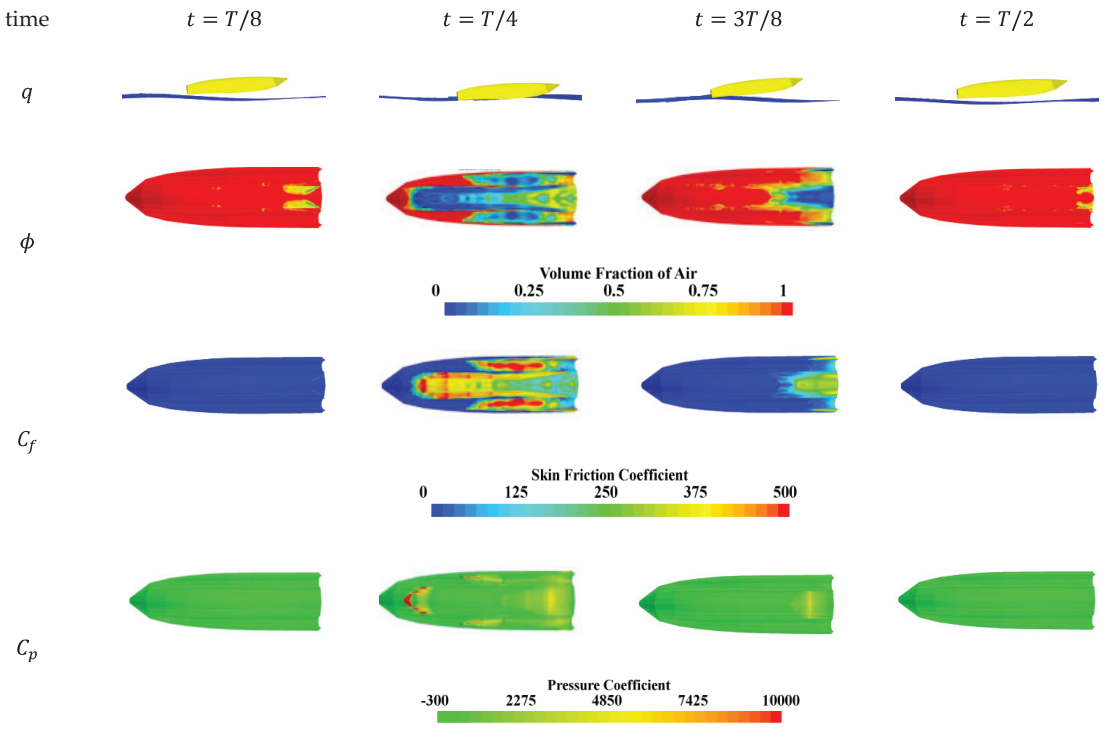


Figure 15. As in Figure 13, but for a beam Froude number of 4.7.

It can be seen that the vessel is above the water surface at the first and last time-steps, first and fourth columns. At the first time-step, the first column, the vessel is advancing above the water. The skin friction is zero on the surface of the vessel, signifying that no shear stress emerges on the body of the vessel as it is moving above the air-water interface. Similarly, the hydrodynamic pressure is zero on the whole body of the vessel.

As the vessel re-enters water, high pressure is seen to emerge near the bow of the vessel. This can be seen in the second column of Figure 15. The vessel is entering the water and its bow is washed by the water. Interestingly, the skin friction coefficient gets relatively large near the bow of the vessel and on the side hulls. Such a distribution of the skin friction coefficient over the bottom of the vessel is different from what was observed at two previous speeds. This implies that the gradient of the velocity near the bow of the vessel and on the side-walls is higher compared to the rear part of the vessel. The vessel enters the water with its bow, and the turbulence is strong there. In addition, water flow is prone to move toward the side hulls, which leads to the generation of vortices between the main hull and side bodies. Such a motion may result in strong skin friction on the side-bodies.

The large pressure emerging on the bow of the vessel, bounces the vessel back. Thus, its bow is highly pitched up, and the rear part of the body remains partially submerged. This can be seen in the third snapshot. The rear part of the body is wet, and the skin friction is non-zero around there.

Eventually, the vessel comes out of the water and a fly-over motion occurs; this can be observed in the fourth column of Figure 15. The vessel is located above the water surface. A small proportion of it is washed by the mixture of water-air, which is the water spray

that is trapped between the tunnels and the main hull. The third and fourth rows show that the skin friction and hydrodynamic pressure are zero on the whole body of the vessel.

Figure 16 demonstrates the snapshots that are related to the highest Froude number. The waves with $\lambda = 2L$ are generated, causing unsteady vertical motions for the vessel. Again, the snapshots are sampled with a time-step of $T/8$ as the speed of the vessel is relatively high. As is apparent, the fly-over movement occurs during the unsteady motion of the vessel at this speed. This can be also seen in the related Supplementary file (LF_56).

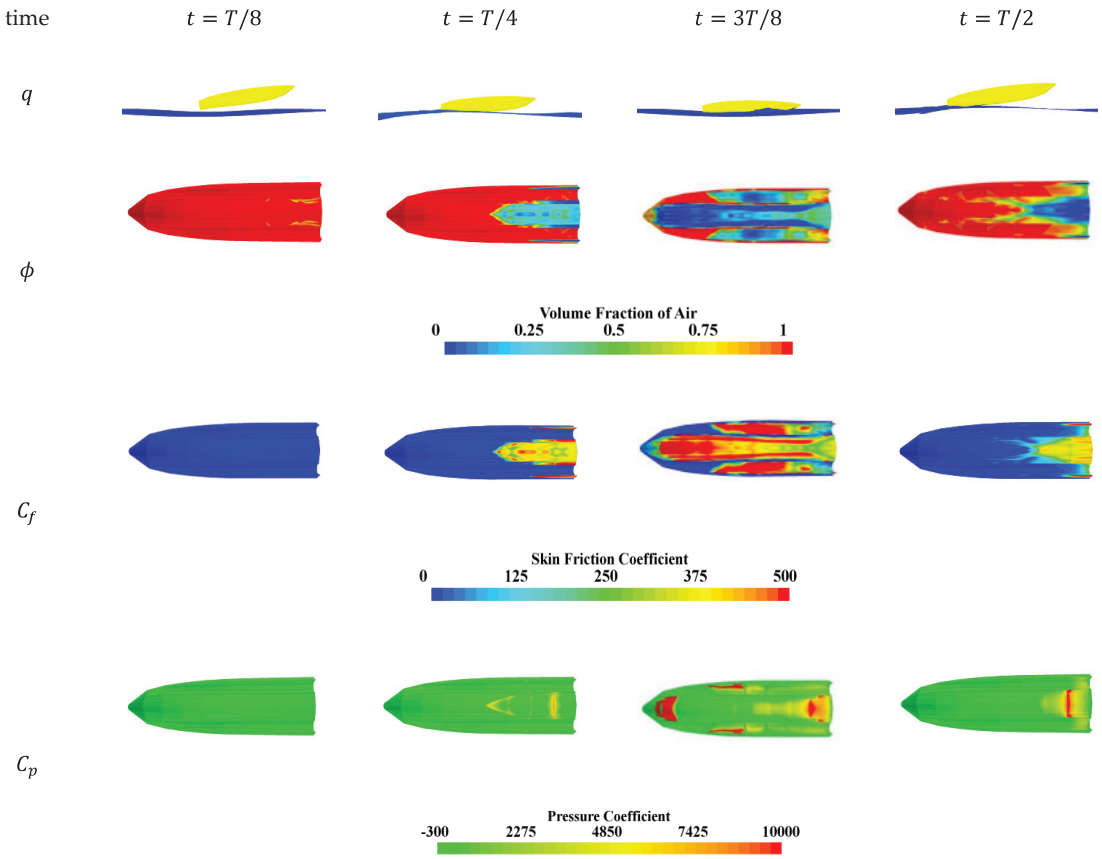


Figure 16. As in Figure 13, but for a beam Froude number of 5.6.

The first snapshot shows the vessel's movement above the water surface. Its bow is pitched up, and its stern is located above the water. Compared to the Froude number of 4.7, the pitch angle of the vessel during the fly-over motion is higher. The skin friction and hydrodynamic pressure are both zero at this stage.

The vessel then enters the water. This can be seen in the second column of Figure 16. The interesting point is that the stern of the vessel enters the water first. This is in contrast with what was observed for the previous Froude numbers. The hydrodynamic pressure is zero near the bow of the vessel, but it is non-zero near the stern. As a result, a large negative pitching moment is caused.

This phenomenon lasts over two time-steps as seen. Besides, the outer edges of the side bodies are only washed. The hydrodynamic pressure emerges on the washed area on the main body, but its value is not significant. Meanwhile, the skin friction coefficient on the washed area of the side bodies becomes very high.

First, its stern is partially washed, as can be seen in the second column of Figure 16. Clearly, only two small areas that are located near the stern of the vessel are partially washed by the water. The fall of the vessel into the water then continues for one more time-step, $t = 3T/8$. The bow of the vessel is pitched down, compared to the previous time-step, and then the vessel impacts the water surface. A high volume of spray water flows toward the surrounding free surface where large shear stresses emerge. At this time-step, an extremely high hydrodynamic pressure emerges on the bow of the vessel. Also, high hydrodynamic pressure appears on the front area of the side bodies. This leads to a fly-over motion (the last column of Figure 16), and the cycle occurs again.

It was previously mentioned that two fly-over motions occur when the vessel operates with a Froude number of 5.6 in waves that are 2L long. The evidence was observed in the presented time history for the vertical acceleration of the vessel (Figure 12). The vertical acceleration was seen to equal $-g$ over two different periods and the resistance was also seen to be zero over those periods. The snapshots that are shown in Figure 16, are presented with a time step of $T/4$. Such a time interval was not able to help us to capture the second fly-over motion properly. It was mentioned that the second fly-over motion corresponds to the second harmonic of the motion or a larger frequency. This means that the second fly-over motions last for a very short time, in comparison with the first one. Therefore, for the case of the highest speed, snapshots with a very small time interval are presented in Figure 17. Clear support for the second fly-over motion is seen in the presented snapshots. This fly-over motion is observed to occur between two time-steps, $t = 2.05T$ and $t = 2.24/T$. This supports the hypothesis that the second fly-over movement occurs in a short period of time, which is around $0.1T$.

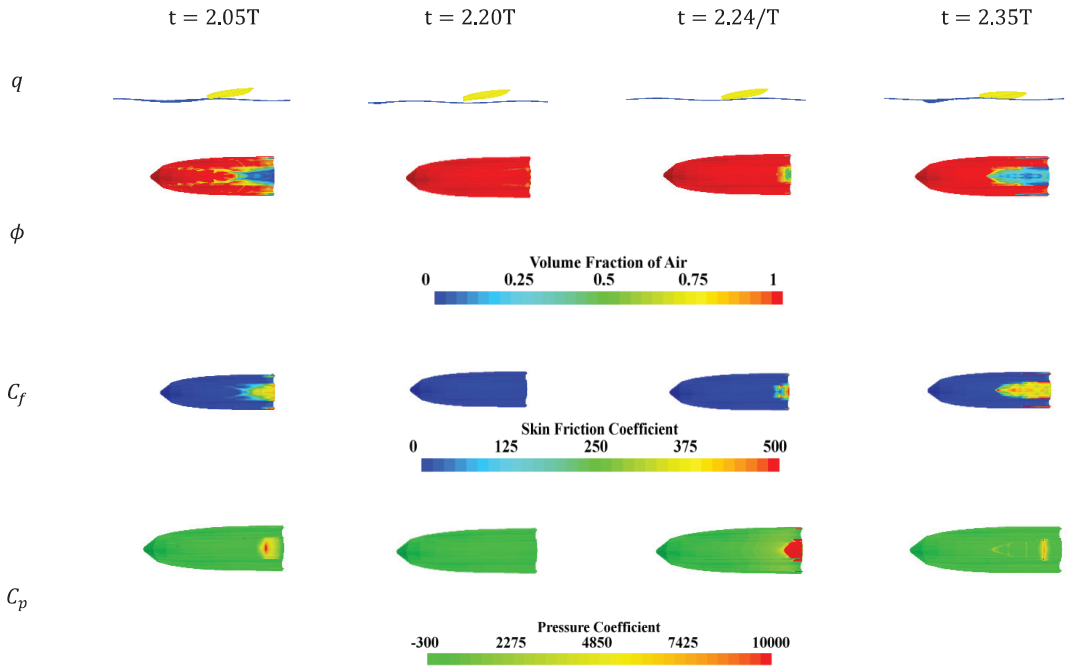


Figure 17. The second fly-over motion of Model B happens at the highest speed, corresponding with a Froude number of 5.6.

Interestingly, high pressure occurs near the transom before and after fly-over. As the vessel enters the water, its bow is pitched down and a large skin friction emerges near the transom. The pressure is non-zero on the side hull. When the vessel is pitched down, the pressure noticeably decreases. The skin friction gets larger on the main hull, and the

fluid motion around the vessel leads to larger skin friction on the side hulls compared to the main hull. Then, the vessel locates at a negative pitch angle, which is not shown in Figure 17. The snapshots that are presented in Figure 17 can fit between time-steps $T/8$ and $3T/8$ in Figure 16. This means that the presented snapshots demonstrate that a second fly-over motion occurs after the first fly-over motion, happening before the vessel reaches a negative pitch displacement.

To improve the understanding of fluid flow around the hull during the unsteady motion of the vessel, streamlines are also sampled and presented in Figure 18. The presented results correspond to a Froude number of 5.6 and waves with a wavelength of $2L$. The snapshots that are shown in Figure 18 cover the wave-induced motion of the vessel in a wave period. Streamlines of air and water flow are marked with red and blue colors. This helps to understand the flow behavior.

As is evident in Figure 18, when the vessel flies over the water surface, only airflow streamlines exist (Figure 18a,b). This again confirms that the vessel's bottom surface is dry during the fly-over motion. During the fly-over motion when the vessel moves downward, the streamlines deviate from the center-line (Figure 18b). This is more significant in the near transom region. The vessel is close to the water surface and moves forward at high speed. Hence, the bottom surface drives the airflow toward the edges of the vessel. This can be also viewed as a preparation stage for the vessel to re-enter water (pre-water entry stage).

After flying over the water surface, the vessel re-enters the water surface with a positive pitch angle (it was previously observed before). As the water enters, high-pressure areas emerge in the middle part and near transom regions (Figure 18c). This makes the fluid flow strongly turbulent and also causes the development of air vortex flow in the tunnels. The high pressure near the transom, as explained earlier, causes a large negative pitch motion. Hence, the vessel is pitched down at the next stage (Figure 18d). High pressure emerges near the bow of the vessel. Interestingly, the air vortex disperses at this stage. The vessel is pitched down and a large pressure occurs near the bow. Thus, air can flow under the vessel and the airflow vortex vanishes.

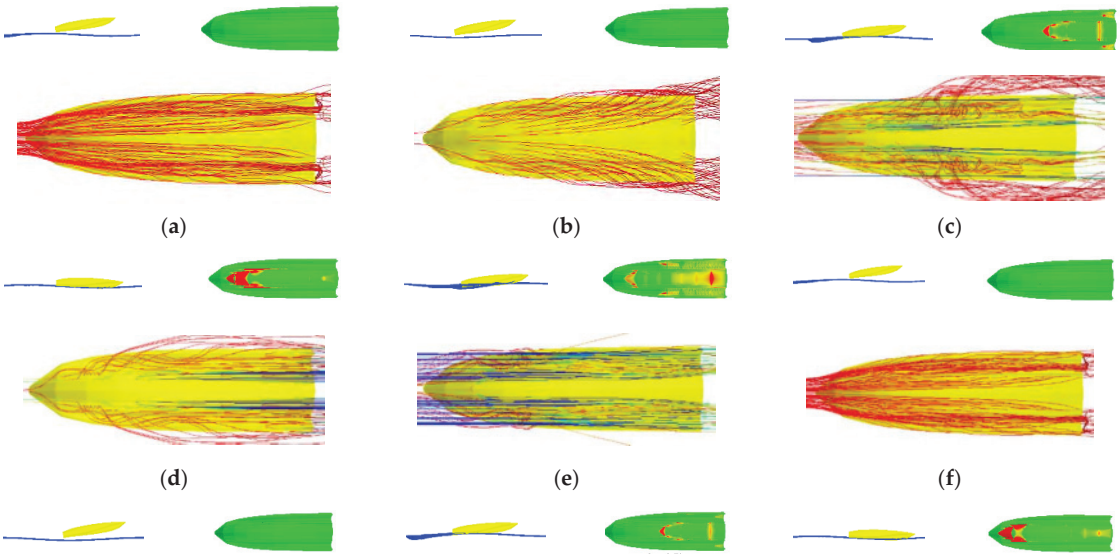


Figure 18. *Cont.*

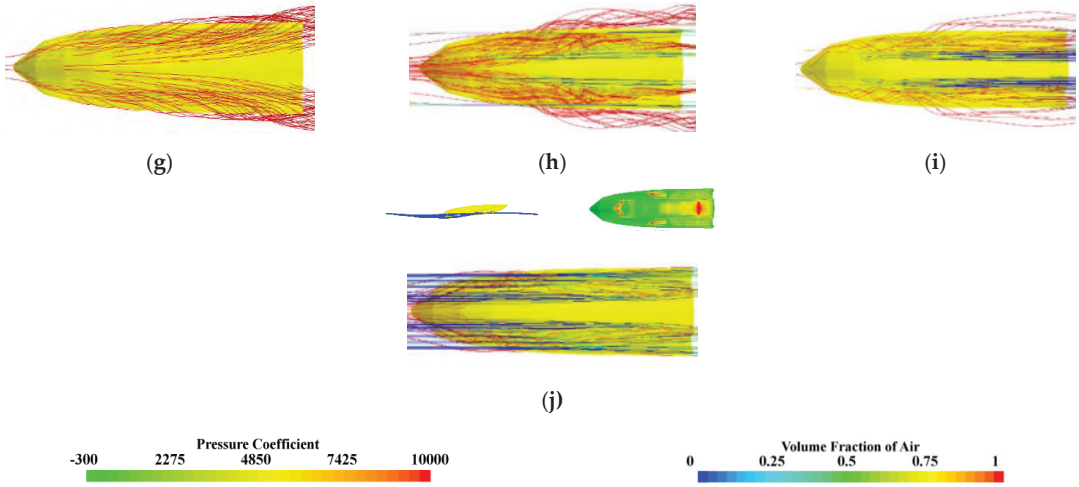


Figure 18. Snapshots of the air and water streamlines around the bottom surface of the Model B. The presented snapshots correspond to the motion of the vessel in wavelengths of 2*L* with a beam Froude number of 5.6. The panels respectively refer to the data that were sampled at (**a**) $t = T/10$, (**b**) $t = 2T/10$, (**c**) $t = 3T/10$, (**d**) $t = 4T/10$, (**e**) $t = 5T/10$, (**f**) $t = 6T/10$, (**g**) $t = 7T/10$, (**h**) $t = 8T/10$, (**i**) $t = 9T/10$, and (**j**) $t = T$. Each panel shows the position of the vessel with respect to the water (up on the left side), hydrodynamic pressure distribution over the bottom surface (up on the right side), and the streamlines (down).

When the vessel re-positions itself at a positive pitch angle, a large pressure emerges near the transom (Figure 18e). The vessel is moving upward with a relatively large acceleration at this stage. No air vortex emerges in this case. Note that the vessel experiences a water-exit stage, and the large pressure shifts toward the transom while the vessel moves upward. Thus, an air vortex is not generated.

Later, the vessel comes out of the water and flies over the water surface (Figure 18f,g). No water streamlines can be detected in this case. Also, no air vortex is observed. The vessel re-enters the water and again a large pressure near the transom and in the middle part of the body emerges (Figure 18h). This again leads to the generation of an air vortex in tunnels. The bow is then pitched down, and a large pressure occurs near the bow. The air vortex disperses at this stage (Figure 18i). This is exactly similar to what was observed before (in Figure 18d). The vessel locates at a positive pitch angle and is again ready to jump out of the water (Figure 18j).

Generally, we expect the airflow to damp the motion of the vessel. However, when the air vortex occurs, air cannot contribute to the damping of the motion. Instead, the vortex power might trigger a larger motion and increase the pitch motion. The air vortex is expected to occur when the vessel enters the water at a relatively large speed. At this time, a large pressure area emerges near the transom. When the vessel is pitched down, a large pressure might emerge near the bow of the vessel, which pushes the vessel up and might decrease the wave forces instantly.

All in all, the presented sampled data in this section showed that as the speed increases, the fly-over motion becomes more severe, i.e., the vessel is positioned at a higher level with a higher pitch angle as it flies over the air-water interface. The higher longitudinal speed of the vessel causes the bow of the vessel to be pitched down, and it slams into the water as its stern reaches water again. A very large hydrodynamic pressure emerges on the sides and bow of the vessel, leading to very large acceleration. Thus, a second fly-over motion occurs, during which the vessel is located at a lower level, compared to the previous fly-over movement. This movement confirms that the motion of the tunneled hulls becomes strongly non-linear and the energy of motion is divided between two dominant harmonics.

When fly-over motion occurs two times with different frequencies, the hydrodynamic pressure can lead to a very large drag force. Although a tunneled vessel is subjected to a significant value of the added resistance during the fly-over motion at high speeds, it has a superiority in comparison to the conventional hard chine planing vessels that have a lower vertical acceleration at the same speed (see [34]) and an overall reduction of the resistance, at least in calm-water at very high speed, as mentioned by [52]. The air flow between the tunnels cannot damp the motion of the vessel properly during the water entry stage. The air vortex is likely to be caused by large hydrodynamic pressure emerging near the transom. A stepped bottom design might distribute the hydrodynamic pressure more evenly. This might lead to modulating the motion of the vessel by decreasing the occurrence probability of the fly-over motion. Therefore, it is highly recommended to consider the dynamic response of the stepped hull design of tunneled planing craft in future studies.

6. Conclusions

Tunneled planing hulls can smoothly operate in calm-water conditions as the air flowing between the side-body and the main hull leads to a slightly larger lift coefficient. But air entrapping can influence the hull motions which becomes more important in real sea conditions. In this study, the hydrodynamic performance of the tunneled planing hulls in regular waves has been simulated using a commercial URANSE solver. The simulation results have been validated and verified by comparing against previously published experimental data.

The results showed that tunneled planing hull motions (heave and pitch) and vertical acceleration are signified by the increase in speed. Interestingly, the pitch displacement of the vessel was seen to become negative in some cases because of the fly-over motion.

During the fly-over motion, the tunneled boat was seen leaving the water and got entirely dry as it pitched up. At this stage, the vertical acceleration was found to be constant, being equal to $-g$, and drag (both hydrodynamic pressure and shear stresses) was zero. Then, as the vessel impacted water, the hydrodynamic pressure near the bow was seen to abruptly increase, inducing a very large instant drag. The shear stresses were seen to be very large in the side hulls of the vessel at this stage. This showed that the water flow becomes highly turbulent in the sidewalls, causing a large drag force over there. Moreover, when the vessel was ready to jump out of the water, the hydrodynamic pressure was seen to be very large near the transom.

For the case of the highest considered speed, two fly-over motions with different frequencies were seen. When the vessel impacts the water at this speed, the force is strong enough to direct the vessel upward again (with ~5g vertical acceleration), leading to a second fly-over motion with a shorter period and lower acceleration (~2g). The two-consecutive fly-over motions, however, were seen to modify the vertical acceleration by distributing the energy that was related to the work that was done by water waves between two harmonics.

The results of the present paper provide an in-depth understanding of the fly-over phenomenon that can be implemented in the design of very high-speed efficient small craft where safety and crew injuries are of great importance. As a recommendation for future studies, one may simulate the wave-induced motions of the tunneled hulls in more degrees of freedom in oblique and randomized waves, where waves may stimulate noticeable coupled motions.

Supplementary Materials: The following supporting information can be downloaded at: https://www.mdpi.com/article/10.3390/jmse10081038/s1. Supplementary material includes six video files. Each video file shows the simulated vertical motion of Model B advancing in water waves. There are six video files that are presented. Four of these videos show the dynamic response of the vessel from a longitudinal side view. These videos are labeled with LF_NN. Here, NN refers to the beam Froude number of the vessel. All the videos correspond to the waves having a wavelength of 2L. Two of the videos show different views of the vessel. These two videos are labeled with 3V1 and 3V2. The first video, 3V1, shows the three-dimensional, bottom, and front views of the vessel motion. All three

views demonstrate the air-water interface and the solid body of the vessel. 3V2 shows the vertical motion of the vessel from similar views. But, for the case of the bottom view, the pressure distribution over the bottom of the vessel is shown. 3V1 and 3V2 files show the simulations corresponding to the highest Froude Number.

Author Contributions: F.R.: Investigation, validation, visualization, software, writing, original draft; S.T.: Formal analysis, writing—original draft, conceptualization, methodology, visualization, editing; S.M.: Investigation, writing—review and editing, A.D.: Resources, formal analysis, writing—review and editing, conceptualization, methodology, supervision. All authors have read and agreed to the published version of the manuscript.

Funding: The APC was funded by KTH Royal Institute of Technology.

Conflicts of Interest: The authors declare that they have no known competing financial interests or personal relationships that could have appeared to influence the work reported in this paper.

Abbreviation

AVIC	Aviation Industry Corporation of China
CF	Correction Factor
CFD	Computation Fluid Dynamics
CG	Centre of Gravity
DFBI	Dynamic Fluid Body Interaction
GCI	Grid Convergence Index
HRIC	High-Resolution Interface Capturing
ITTC	International Towing Tank Conference
LSR	Least Square Root
PISO	Pressure-Implicit with Splitting of Operators
URANS	Unsteady Reynolds Averaged Navier–Stokes Equations
VOF	Volume of Fluid

Nomenclature

A_{in}	Amplitude of the wave (m)
B	Maximum Beam of the boat (m)
C_f	Frictional drag coefficient (-)
C_p	Pressure drag coefficient (-)
E	Error of obtained results against the previous data
$\mathbf{F} = \left[\boldsymbol{F}_x, \boldsymbol{F}_y, \boldsymbol{F}_z\right]$	Fluid force acting on the vessel in different directions (N)
$Fr_{\mathbf{B}} = u/(gB)^{-1}$	Beam Froude Number (-)
$\mathbf{f}$	Body force vector (N)
$\mathbf{f}_{in}$	Wave frequency (Hz)
g	Gravity acceleration (m/s^2)
I	Pitch moment of inertia (Kg-m^2)
k_{in}	Wave number (m^{-1})
k_{xx}	Second moment of inertia in x direction (m)
k_{yy}	Second moment of inertia in y direction (m)
L_{CG}	The longitudinal position of the center of gravity (CG) from transom (m)
L	Length of bout (m)
m	Mass of the boat (Kg)
$\mathbf{M} = \left[\boldsymbol{M}_\phi, \boldsymbol{M}_\theta, \boldsymbol{M}_\psi\right]$	Moment vector (N-m)
$\boldsymbol{n}$	Normal vector
p	Fluid pressure (N/m^2)
P_{G_th}	Theoretical order of accuracy
P_G	Estimated order of accuracy
$\mathbf{r}$	Distance vector
$R_{\mathbf{A}}$	Resistance in waves (N)
$R_{\mathbf{G}}$	Converges ratio

t	Time (s)
T	Normal vector of tensor
T_{in}	Wave period (s)
u	Boat speed (m/s)
U_G	Uncertainty of grids
U_{SN}	Uncertainty of numerical simulation
$\mathbf{v} = [v_x, v_y, v_z]$	Velocity vector in the fluid domain (m/s)
V_{CG}	Vertical location of center of gravity (m)
W	Weight of the boat (N)
z, $\dot{z}, \ddot{z}$	Heave displacement (m), speed (m/s), and acceleration (m/s^2)
β	Deadrise angle of the vessel (deg)
ζ	Water surface elevation (m)
θ, $\dot{\theta}$, $\ddot{\theta}$	Pitch angle (rad), velocity (rad/s), and acceleration (rad/s^2)
λ	Wavelength (m)
μ_a	Dynamic viscosity of air (Kg/m-s)
μ_m	Dynamic viscosity of the Air-Water mixture at any point (Kg/m-s)
μ_t	Dynamic turbulent viscosity (Kg/m-s)
μ_w	Dynamic viscosity of water (Kg/m-s)
ρ_a	Density of air (Kg/m^3)
ρ_m	Density of the air-water mixture at any point (Kg/m^3)
ρ_w	Density water (Kg/m^3)
σ	Stress tensor
ϕ	Volume fraction (-)
τ_w	Shear stress caused by the air-water flow (N/m^3)
ω_{in}	Wave frequency (rad/s)

Appendix A. Calm-Water Performance of Model B

The calm-water performance of Model B is presented in this Appendix A. Experimental and numerical data are both plotted and shown in Figure A1. The numerical results are obtained by using the CFD model. The water waves are set to have a height of zero. This represents a calm-water condition. The pitch angle and heave displacements of the vessel vary over time; however, they converge to steady values. The reason is that there is no exciting force, and thus the dynamic equilibrium is established in the vertical plane. This signifies that the lift force equals the weight and pitching moment that is caused by the water pressure, which is zero. Overall, the results computed through such a set-up enable us to numerically model the calm-water test of a planing vessel. The results can be compared against the experimental test. Note that these CFD runs were previously performed and presented in [53,54] For this reason, they are not presented in the main text. These results are briefly presented in this Appendix A to evaluate the accuracy of the CFD model in the computation of the calm-water operation of Model B. Discussions on the results of the calm-water condition are presented in [54].

As mentioned, the calm-water performance of Model B is presented in Figure A1. It was previously discussed that we aim to simulate the dynamic motion of this vessel in water waves since it has a lower resistance compared to another model (Model A). For the case of Model B, no seakeeping data are available, but a limited number of regular wave tests are carried out for Model A. The accuracy of the numerical model in the simulation of dynamic motion of a tunneled planing hull was previously investigated in Section 4.

Resistance of Model B is seen to be insensitive to a Froude number over the range of $1.6 < Fr_B < 2$. When increasing the Froude number, the resistance increases linearly. Then its value is not affected by the increase in the Froude number. This happens at $Fr_B > 5$. CFD data are seen to follow the experimental data, confirming that the setup is accurate enough in the computation of the resistance force acting on Model B in a calm-water operation.

Dynamic trim angle (pitch angle) is seen to decrease by the increase in the Froude number. This increase is seen to follow a linear pattern. Note that this increase is observed to occur over the range of $1.6 < Fr_B < 2.3$. Eventually, the pitch angle converges to a value between 2 and 4. Again, CFD and experimental data are seen to agree.

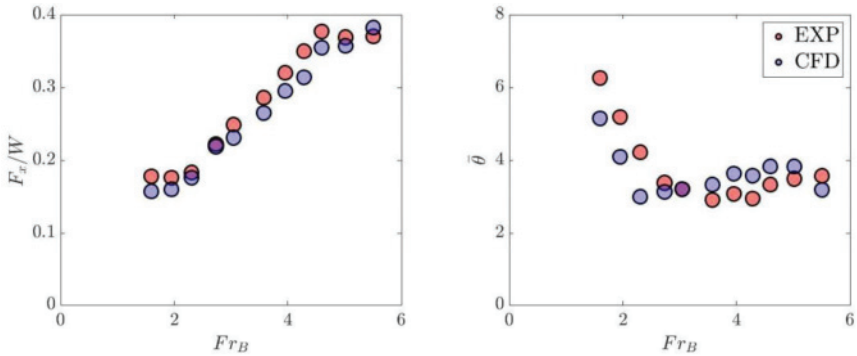


Figure A1. Resistance (**left**) and dynamic trim angle (**right**) of Model B in calm-water conditions. The CFD data and experimental measurements of [12] are presented in the Figure.

References

1. Naghdi, P.M.; Rubin, M.B. On the transition to planing of a boat. *J. Fluid Mech.* **1981**, *103*, 345–374. [CrossRef]
2. Cumberbatch, E. Two-dimensional planing at high Froude number. *J. Fluid Mech.* **1958**, *4*, 466–478. [CrossRef]
3. Ting, L.; Keller, J.B. Planing of a flat plate at high Froude number. *Phys. Fluids* **1974**, *17*, 1080–1086. [CrossRef]
4. Faltinsen, O.M. *Hydrodynamics of High-Speed Marine Vehicles*; Cambridge University Press: Cambridge, UK, 2005.
5. McCauley, J.L. Hydrodynamic Lift on Boats. *arXiv* **2018**, arXiv:1808.03313. [CrossRef]
6. Tuck, E.O. Planing surfaces. In *Numerical Solution of Integral Equations*; Springer: Boston, MA, USA, 1990; pp. 363–372.
7. Squire, H.B. The motion of a simple wedge along the water surface. *Proc. R. Soc. Lond. Ser. A Math. Phys. Sci.* **1957**, *243*, 48–64. [CrossRef]
8. Chung, Y.K.; Chun, H.H. High speed theory for the planing of a flat plate at high Froude number. *Ocean. Eng.* **2007**, *34*, 1552–1560. [CrossRef]
9. Fridsma, G. *A Systematic Study of the Rough-Water Performance of Planing Boats*; Stevens Institute of Technology Davidson Laboratory: Hoboken, NJ, USA, 1969.
10. Kim, D.J.; Kim, S.Y.; You, Y.J.; Rhee, K.P.; Kim, S.H.; Kim, Y.G. Design of high-speed planing hulls for the improvement of resistance and seakeeping performance. *Int. J. Nav. Archit. Ocean. Eng.* **2013**, *5*, 161–177. [CrossRef]
11. Savitsky, D.; Brown, P.W. Procedures for hydrodynamic evaluation of planing hulls in smooth and rough water. *Mar. Technol. SNAME News* **1976**, *13*, 381–400. [CrossRef]
12. Ma, W.; Sun, H.; Zou, J.; Yang, H. Test research on the resistance performance of high-speed trimaran planing hull. *Pol. Marit. Res.* **2013**, *20*, 45–51. [CrossRef]
13. Li, Y.; Ding, J. CFD and Experimental Analysis of Planing Trimaran Performance. In Proceedings of the 29th International Ocean and Polar Engineering Conference, OnePetro, Honolulu, HI, USA, 16–21 June 2019.
14. Jiang, Y.; Sun, H.; Zou, J.; Hu, A.; Yang, J. Analysis of tunnel hydrodynamic characteristics for planing trimaran by model tests and numerical simulations. *Ocean. Eng.* **2016**, *113*, 101–110. [CrossRef]
15. Su, G.; Shen, H.; Su, Y. Numerical Prediction of Hydrodynamic Performance of Planing Trimaran with a Wave-Piercing Bow. *J. Mar. Sci. Eng.* **2020**, *8*, 897. [CrossRef]
16. Sun, H.; Zou, J.; Sun, Z.; Lu, S. Numerical investigations on the resistance and longitudinal motion stability of a high-speed planing trimaran. *J. Mar. Sci. Eng.* **2020**, *8*, 830. [CrossRef]
17. Savitsky, D. Hydrodynamic design of planing hulls. *Mar. Technol. SNAME News* **1964**, *1*, 71–95. [CrossRef]
18. Zarnick, E.E. *A Nonlinear Mathematical Model of Motions of a Planing Boat in Regular Waves*; David Taylor Naval Ship Research and Development Center: Bethesda, MD, USA, 1978.
19. Bilandi, R.N.; Dashtimanesh, A.; Tavakoli, S. Hydrodynamic study of heeled double-stepped planing hulls using CFD and 2D+T method. *Ocean. Eng.* **2020**, *196*, 106813. [CrossRef]
20. Abrate, S. Hull slamming. *Appl. Mech. Rev.* **2011**, *64*, 35. [CrossRef]
21. Hughes, K.; Vignjevic, R.; Campbell, J.; De Vuyst, T.; Djordjevic, N.; Papagiannis, L. From aerospace to offshore: Bridging the numerical simulation gaps–Simulation advancements for fluid structure interaction problems. *Int. J. Impact Eng.* **2013**, *61*, 48–63. [CrossRef]
22. Stern, F.; Wang, Z.; Yang, J.; Sadat-Hosseini, H.; Mousaviraad, M.; Bhushan, S.; Diez, M.; Sung-Hwan, Y.; Wu, P.C.; Yeon, S.M.; et al. Recent progress in CFD for naval architecture and ocean engineering. *J. Hydrodyn.* **2015**, *27*, 1–23. [CrossRef]
23. De Marco, A.; Mancini, S.; Miranda, S.; Scognamiglio, R.; Vitiello, L. Experimental and numerical hydrodynamic analysis of a stepped planing hull. *Appl. Ocean. Res.* **2017**, *64*, 135–154. [CrossRef]
24. Sukas, O.F.; Kinaci, O.K.; Cakici, F.; Gokce, M.K. Hydrodynamic assessment of planing hulls using overset grids. *Appl. Ocean. Res.* **2017**, *65*, 35–46. [CrossRef]

25. Esfandiari, A.; Tavakoli, S.; Dashtimanesh, A. Comparison between the dynamic behavior of the non-stepped and double-stepped planing hulls in rough water: A numerical study. *J. Ship Prod. Des.* **2020**, *36*, 52–66. [CrossRef]
26. Mousaviraad, S.M.; Wang, Z.; Stern, F. URANS studies of hydrodynamic performance and slamming loads on high-speed planing hulls in calm water and waves for deep and shallow conditions. *Appl. Ocean. Res.* **2015**, *51*, 222–240. [CrossRef]
27. Judge, C.; Mousaviraad, M.; Stern, F.; Lee, E.; Fullerton, A.; Geiser, J.; Schleicher, C.; Merrill, C.; Weil, C.; Morin, J.; et al. Experiments and CFD of a high-speed deep-V planing hull—-Part I: Calm water. *Appl. Ocean. Res.* **2020**, *96*, 102060. [CrossRef]
28. Ponzini, R.; Salvadore, F.; Begovic, E.; Bertorello, C. Automatic CFD analysis of planing hulls by means of a new web-based application: Usage, experimental data comparison and opportunities. *Ocean. Eng.* **2020**, *210*, 107387. [CrossRef]
29. Casalone, P.; Dell'Edera, O.; Fenu, B.; Giorgi, G.; Sirigu, S.A.; Mattiazzo, G. Unsteady RANS CFD Simulations of Sailboat's Hull and Comparison with Full-Scale Test. *J. Mar. Sci. Eng.* **2020**, *8*, 394. [CrossRef]
30. Nimmagadda, N.V.R.; Polisetty, L.R.; Iyer, A.S.V. Simulation of air–water interface effects for high-speed planing hull. *J. Mar. Sci. Appl.* **2020**, *19*, 398–414. [CrossRef]
31. Kahramanoglu, E.; Yıldız, B.; Çakıcı, F.; Yilmaz, H. Numerical roll damping prediction of a planing hull. *Ships Offshore Struct.* **2021**, *16*, 363–372. [CrossRef]
32. Kahramanoğlu, E.; Çakıcı, F.; Doğrul, A. Numerical Prediction of the Vertical Responses of Planing Hulls in Regular Head Waves. *J. Mar. Sci. Eng.* **2020**, *8*, 455. [CrossRef]
33. Liu, L.; Wang, X.; He, R.; Zhang, Z.; Feng, D. CFD prediction of stern flap effect on Catamaran seakeeping behavior in long crest head wave. *Appl. Ocean. Res.* **2020**, *104*, 102367. [CrossRef]
34. Judge, C.; Mousaviraad, M.; Stern, F.; Lee, E.; Fullerton, A.; Geiser, J.; Schleicher, C.; Merrill, C.; Weil, C.; Morin, J.; et al. Experiments and CFD of a high-speed deep-V planing hull–part II: Slamming in waves. *Appl. Ocean. Res.* **2020**, *97*, 102059. [CrossRef]
35. Bi, X.; Zhuang, J.; Su, Y. Seakeeping Analysis of Planing Craft under Large Wave Height. *Water* **2020**, *12*, 1020. [CrossRef]
36. González, A.T.; Dunning, P.; Howard, I.; McKee, K.; Wiercigroch, M. Is Wave Energy Untapped Potential? *Int. J. Mech. Sci.* **2021**, *205*, 106544. [CrossRef]
37. Hirt, C.W.; Nichols, B.D. Volume of fluid (VOF) method for the dynamics of free boundaries. *J. Comput. Phys.* **1981**, *39*, 201–225. [CrossRef]
38. Nguyen, V.T.; Phan, T.H.; Park, W.G. Modeling and numerical simulation of ricochet and penetration of water entry bodies using an efficient free surface model. *Int. J. Mech. Sci.* **2020**, *182*, 105726. [CrossRef]
39. Srivastava, S.; Chatterjee, A. Planar oscillations of a boat in a tank. *Int. J. Mech. Sci.* **2014**, *79*, 152–161. [CrossRef]
40. Siemens, P.L.M. *STAR CCM + User's Guide Version 14.02.010*; CD-adapco: Melville, NY, USA, 2019.
41. ITTC. *ITTC Quality System Manual: Recommended Procedures and Guidelines 2017*; ITTC 7.5; ITTC: Wuxi, China, 2017.
42. Ma, W.; Sun, H.; Zou, J.; Zhuang, J. Test studies of the resistance and seakeeping performance of a trimaran planing hull. *Pol. Marit. Res.* **2015**, *1*, 22–27. [CrossRef]
43. Eça, L.; Hoekstra, M. Discretization uncertainty estimation based on a least squares version of the grid convergence index. In Proceedings of the Second Workshop on CFD Uncertainty Analysis, Lisbon, Portugal, 19–20 October 2006; Instituto Superior Técnico: Lisbon, Portugal, 2006.
44. Eça, L.; Hoekstra, M. A procedure for the estimation of the numerical uncertainty of CFD calculations based on grid refinement studies. *J. Comput. Phys.* **2014**, *262*, 104–130. [CrossRef]
45. De Luca, F.; Mancini, S.; Miranda, S.; Pensa, C. An extended verification and validation study of CFD simulations for planing hulls. *J. Ship Res.* **2016**, *60*, 101–118. [CrossRef]
46. Sun, H.; Faltinsen, O.M. Dynamic motions of planing vessels in head seas. *J. Mar. Sci. Technol.* **2011**, *16*, 168–180. [CrossRef]
47. Tavakoli, S.; Bilandi, R.N.; Mancini, S.; De Luca, F.; Dashtimanesh, A. Dynamic of a planing hull in regular waves: Comparison of experimental, numerical and mathematical methods. *Ocean. Eng.* **2020**, *217*, 107959. [CrossRef]
48. Garme, K. Improved time domain simulation of planing hulls in waves by correction of the near-transom lift. *Int. Shipbuild. Prog.* **2005**, *52*, 201–230.
49. Morabito, M.G. Empirical equations for planing hull bottom pressures. *J. Ship Res.* **2014**, *58*, 185–200. [CrossRef]
50. Jalalisendi, M.; Porfiri, M. Water entry of compliant slender bodies: Theory and experiments. *Int. J. Mech. Sci.* **2018**, *149*, 514–529. [CrossRef]
51. Javanmardi, N.; Ghadimi, P.; Tavakoli, S. Probing into the effects of cavitation on hydrodynamic characteristics of surface piercing propellers through numerical modeling of oblique water entry of a thin wedge. *Brodogr. Teor. I Praksa Brodogr. I Pomor. Teh.* **2018**, *69*, 151–168. [CrossRef]
52. Ding, J.; Jiang, J. Tunnel flow of a planing trimaran and effects on resistance. *Ocean. Eng.* **2021**, *237*, 109458. [CrossRef]
53. Roshan, F.; Dashtimanesh, A.; Tavakoli, S.; Niazmand, R.; Abyn, H. Hull–propeller interaction for planing boats: A numerical study. *Ships Offshore Struct.* **2020**, *16*, 955–967. [CrossRef]
54. Roshan, F.; Dashtimanesh, A.; Bilandi, R.N. Hydrodynamic characteristics of tunneled planing hulls in calm water. *Brodogr. Teor. I Praksa Brodogr. I Pomor. Teh.* **2020**, *71*, 19–38. [CrossRef]

Appendix 3 (Publication III)

Paper III

Roshan, F., Dashtimanesh, A., De Luca, F., Mancini, S. (2025). High-speed craft with double interceptor system in calm water: URANS Solution. 21st International Conference on Ships and Maritime Research – Messina, NAV 2025 (accepted).

21st International Conference on Ships and Maritime Research – Messina
NAV 2025

High-speed craft with double interceptor system in calm water: URANS Solution

Fatemeh Roshan [a,*], Abbas Dashtimanesh [b], Fabio De Luca [c], Simone Mancini [c]

[a] *Estonian Maritime Academy, Tallinn University of Technology, 11712 Tallinn, Estonia*

[b] *Center of Naval Architecture, Department of Engineering Mechanics, School of Engineering Science, KTH Royal Institute of Technology, 11428, Stockholm, Sweden*

[c] *Department of Industrial Engineering, University of Napoli" Federico II", 80125, Napoli, Italy.*

Abstract

Interceptor is a high-lifting device used in high-speed crafts to correct trim angle and, to some extent, reduce hull resistance. Double Interceptors System (DIS) is an unconventional configuration that involves two interceptors, one is installed on the transom and the other in the middle of the hull length. This design can lead to a higher reduction in drag and trim angle, though designing and implementing efficient DIS requires a thorough understanding of its hydrodynamic performance. This study uses the SIEMENS PLM StarCCM+ code to numerically simulate high-speed craft with and without DIS in calm water and presents the effects of DIS on hull trim angle, drag, and pressure distribution on the hull bottom. Furthermore, the effects of different interceptor heights on its efficiency have been investigated. The accuracy of the current models is examined by comparing the measured trim angle and drag against the experimental results of towing tank tests provided by De Luca and Pensa, (2012a). The obtained results revealed that using DIS causes an unwetted surface area behind the forward interceptor, consequently reducing the wetted surface area and shear drag. Moreover, a high-pressure region appears when the water flow encounters the interceptor, which can affect the pressure drag. As this high pressure does not lead to a rise in total drag, it can improve lift force distribution and longitudinal stability.

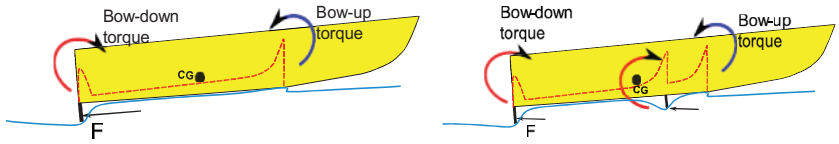
Keywords: High speed craft, Double interceptor system, Hydrodynamic performance, CFD simulation;

1. Introduction

Studies on the hydrodynamic performance of high-speed craft (HSC) are mainly focused on minimizing drag to reduce fuel emissions as well as reducing hull motions to enhance occupants' safety. Interceptor is an efficient device designed to decrease hull motion and resistance in different conditions and consequently improve safety and fuel efficiency.

Interceptor is a high-lifting device installed in the HSC transom to reduce the trim angle by generating a bow-down torque. Many studies, such as those by Brizzolara (2003), Johan et al. (2011), Song et al. (2018), and Putra and Suzuki (2024), have proven the effectiveness of using interceptors in reducing trim angle and drag in calm water. Moreover, interceptor effects on reducing heave and pitch motions in wave conditions have been demonstrated by Park et al. (2019) and Roshan et al. (2024).

Since the use of a transom interceptor system (TIS) creates a high-pressure region that causes a reduction in trim angle and drag, using a double interceptor system (DIS) that generates an additional lift force and bow-down torque could be more efficient in reducing trim angle and resistance. Figure 1 indicates a schematic of TIS and DIS performance.



(a) TIS (b) DIS

Figure 1. A schematic TIS and DIS performance.

As it has been shown in Figure 1, DIS is an unconventional interceptor configuration consisting of a transom interceptor and another interceptor located in the middle of the hull length. In addition to creating a high-pressure region in the middle of the hull length through the forward interceptor, flow separation occurring in this area can also affect the hydrodynamic performance of HSC.

Although DIS performance has been studied previously by De Luca and Pensa (2012a) and (2012b) during the numerous towing tank tests at the *Università degli Studi di Napoli "Federico II,"* certain hydrodynamic details cannot be obtained experimentally. To investigate these details, numerical simulation is an efficient method; however, it should be validated against the experimental results to ensure simulation accuracy.

This paper aims to investigate the effect of using DIS on HSC performance in calm water, specifically in terms of hull resistance and trim angle. To achieve this goal, the trim angle, pressure distribution, shear drag, and pressure drag of the bare hull, TIS model, and DIS (i3 y3 and i4 y4) models are investigated at different speeds. The current simulations are validated by comparing the obtained trim angle and drag values with the measured values presented by De Luca and Pensa (2012a) for the C0301 hull with and without DIS. The results of the simulations are then analyzed to determine the effectiveness of DIS in reducing trim and drag (shear and pressure drag) compared to the TIS. Moreover, the effect of interceptor height in DIS models is investigated.

2. Numerical setup

This study simulates a high-speed craft model C0301 with and without interceptors by using commercial software STAR-CCM+ that is based on unsteady Reynolds averaged Navier Stokes (RANS) equations which can accurately model the fluid flow around the HSC including small devices located on along the hull (e.g. transom flap, wedge, etc.). Therefore, it has been implemented by previous researchers to study interceptor performance (Ghassemi et al. 2011, Mansoori, and Fernandes 2017, and Samuel et al. 2022). The governing equations of the hydrodynamic simulations and defined settings are explained in this section.

2.1 Governing Equations

Assuming incompressible, homogeneous, and Newtonian fluid flow, the governing equations for the Reynolds Averaged Navier Stokes (RANS) are

$$\frac{\partial \rho}{\partial t} + \frac{\partial}{\partial x_i}(\rho u_i) = 0, \tag{1}$$

$$\frac{\partial (\rho u_i)}{\partial t} + \frac{\partial}{\partial x_j}\left(\rho u_i u_j\right) = -\frac{\partial P}{\partial x_i} + \frac{\partial}{\partial x_j}\left(\mu \frac{\partial u_i}{\partial x_j} - \rho \overline{\acute{u}_i \acute{u}_j}\right) + F_i\,, \qquad (i,j = 1,2,3) \tag{2}$$

that ρ is the fluid density; t is time; μ indicates fluid viscosity; u_i and u_j refer to the velocity component, and P is pressure. In addition, F_i refers to additional volume force.

In simulating a vessel operating on the water surface, ρ and μ in equations (1) and (2) should be defined on the free surface due to the air and water mixture at any point. Therefore, the volume of fluid (VOF) method is used to capture the free surface accurately.

$$\rho_m = (1-\phi)\rho_w + \phi\rho_a, \tag{3}$$

$$\mu_m = (1-\phi)\mu_w + \phi\mu_a, \tag{4}$$

where ϕ refers to volume fraction, which varies between 0 and 1, while $\phi=0$ is water and $\phi=1$ indicates pure air. Moreover, w and a subscript in equations (3) and (4) are water and air.

In the computational domain, the realizable k-ε model with wall function is used to simulate the turbulence model. Additionally, due to the symmetric hull form, a half model has been used to reduce the solving time. The hull simulations take into consideration two degrees of freedom: heave and pitch, while forward motion is assumed to be fixed and flow passes through the hull at constant speed. The boat motions are computed over the physical time using the Dynamic Fluid Body Interaction module combined with a morphing mesh strategy (DFBI Morphing), which simplifies the simulation setup and reduces computational effort (Niazmand Bilandi et al., 2024). In this approach, the hull moves during every time step under the fluid forces and moments thanks to the morphing of the cells nearby the hull. According to the ITTC 7.5-03_02-03 (2021) guidelines, a time step of 0.001s is used in current simulations.

2.2 Model Geometry

Table 1 presents the model (C0301) properties with and without the interceptors. All models have the same dimensions but differ in their interceptor configurations. This allows for a comparison of the effects of installing a transom interceptor system (TIS), a double interceptor system (DIS), and different interceptor heights in DIS models. The main characteristics of the bare hull, DIS i3 y3, and DIS i4 y3 models are defined according to De Luca and Pensa's (2012a) models, and the obtained results can be validated against their results.

Table 1. Main dimensions of different model (C0301) configurations.

Properties	Values			
	Bare hull	TIS I3 y0	DIS I3 y3	DIS I4 y3
L_{wl} (m)	2.387	2.387	2.387	2.387
B_{wl} (m)	0.6	0.6	0.6	0.6
Displacement (kg)	102.8	102.8	102.8	102.8
L/B	3.978	3.978	3.978	3.978
$L/\nabla^{1/3}$	5.09	5.09	5.09	5.09
L_{CG}/L_{wl}	0.332	0.332	0.332	0.332
Deadrise angle (deg)	20	20	20	20
Initial trim angle (deg)	3.0	3.0	3.0	3.0
Forward interceptor heigh (mm)	0	0	3	4
Forward interceptor length/L_{wl}	0	0	0.524	0.524
Transom interceptor height (mm)	0	3	3	3

2.3 Computational domain

A computational domain is defined around the hull to simulate a virtual towing tank. Figure 2 shows the dimensions of this computational domain and its respective boundary conditions. As shown in Figure 2, the inlet boundary is located 2.1 L from the transom with a velocity inlet condition. The right side of the computational domain (located on the model's centerline) is considered a symmetry plane, and the

left side (located at 2 L from the hull) is defined as a velocity inlet condition. The outlet boundary is at a distance of 4.34 L from the transom of the model with a pressure outlet condition. Additionally, the water surface is considered to be at a distance of 0.65 L from the top and 2 L from the bottom. Finally, both the top and bottom boundaries have velocity inlet conditions.

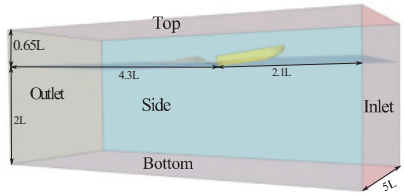


Figure 2. Computational domain dimensions and boundary conditions.

2.4 Mesh generation

The 3D volume mesh is created within the computational domain and hull surface, as seen in Figure 3. This mesh structure is defined using three mesh models: surface mesh, prism layer, and trimmer. To increase the capability of the grid resolution to capture flow details, three refinement zones with a smaller mesh size are defined around the hull and interceptors. For an accurate prediction of the interaction between the hull and the water surface, a six-layer prism mesh is created around the hull. Additionally, a region of high significance is the free surface, for which the trimmer mesh with a specific mesh size in the x, y, and z directions is employed.

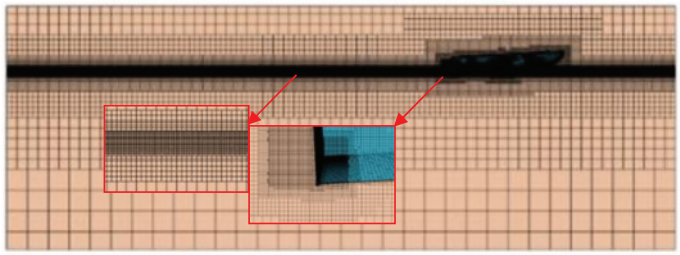
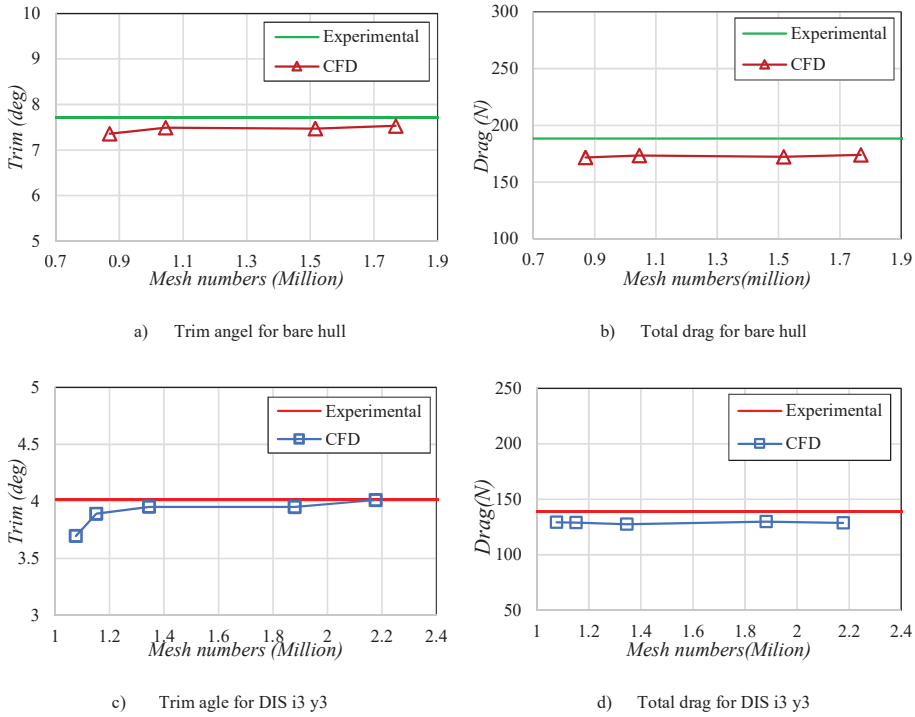


Figure 3. Mesh structure in the computational domain.

2.5 Mesh independency

Before conducting simulations for all models at different speeds, it is necessary to confirm that the results obtained are not significantly affected by the grid resolution. The most suitable mesh should be chosen, with a good level of accuracy and the shortest solution time. Figure 4 displays the results of the mesh independence study conducted for the bare hull and DIS i3 y3 models.



a) Trim angel for bare hull

b) Total drag for bare hull

c) Trim agle for DIS i3 y3

d) Total drag for DIS i3 y3

Figure 4. Mesh convergence study at Fr=2.48.

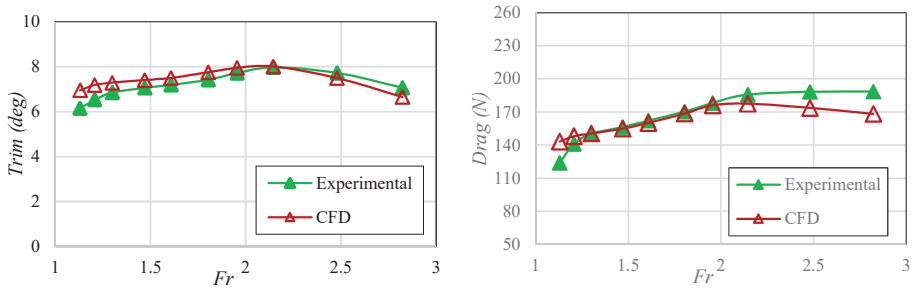
According to Figure 4(a,b), when the grid numbers go higher than 1.04M, there is no significant difference in the calculated trim angle and drag of the bare hull. Moreover, the results found with this mesh number at Froude 2.84 are in good agreement with the experimental results, with a trim error of -2.97% and a drag error of -7.76%. Therefore, this mesh number is selected to be used for bare-hull simulations at other speeds.

As discussed in Section 2.4, by considering the smaller cells around the interceptor, the mesh number for models with interceptors is higher than the bare hull in order to accurately predict the fluid flow around the interceptors. As shown in Figure 4(d), the total drag for all considered mesh numbers is almost equal; however, there is a significant error in the trim angle for mesh numbers lower than 1.3 M (see Figure 4(c)). Therefore, mesh number 1.3 M with a trim error of -1.5% and a drag error of -8.32% is selected for hulls that contain DIS at other speeds.

2.6 Validation

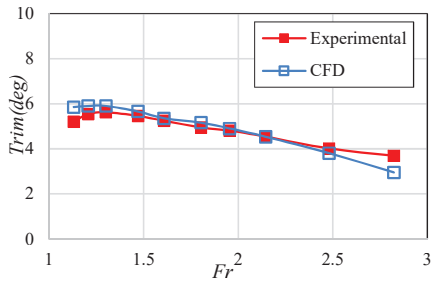
Figure 5 presents a comparison between the numerical results and the experimental trim angle and drag measured by De Luca and Pensa (2012a). This comparison is essential to ensuring the accuracy of current simulations in predicting the trim angle and drag. According to Figure 5, numerical simulations overpredict the trim angle for the bare hull, DIS i3 y3, and DIS i4 y3 models at low speeds. However, for higher Froude numbers, predicted trim angles are lower than the experimental results. In addition, Figure 5 shows that the calculated drag for hull models containing DIS is lower than the measured drag during towing tank tests.

A similar trend is also demonstrated for the bare hull at high Froude numbers, though current simulations overestimate the drag at lower speeds.

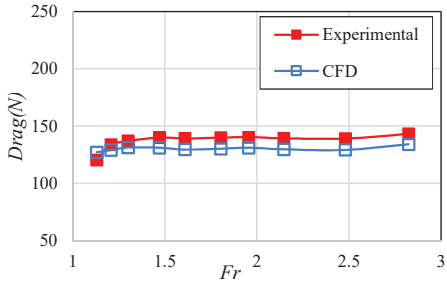


a) Trim angel for bare hull

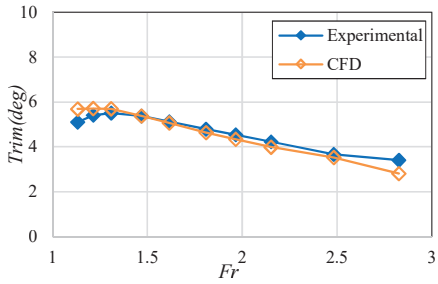
b) Drag for bare hull



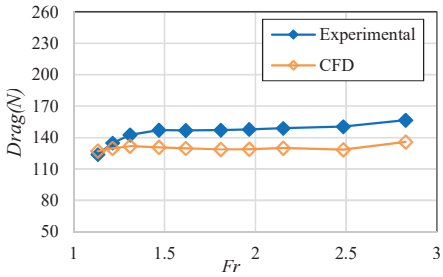
c) Trim angle for DIS i3 y3



d) Drag for DIS I y3



e) Trim angle for DIS i4 y3



f) Drag for DIS i4 y3

Figure 5. A comparison between the obtained trim angle and Drag against the experimental results.

Table 2 indicates the root mean square (RMS) errors in predicting the trim angle and drag of the bare hull, DIS i3 y3, and DIS i4 y3 models. Based on the calculated RMS numerical model, it is reliable for predicting the hydrodynamics of high-speed craft with and without the interceptor.

Table 2. RMS error for present simulations in predicting trim angle and drag.

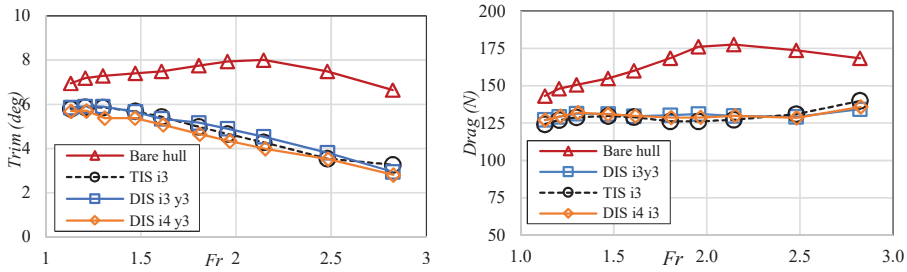
RMS Errors	Bare hull	Model i3 y3	Model i4 y3
RMS error for trim angle	6.6%	8.3	7.4%
RMS error for drag	6.8%	6.1	11%

3. Results

3.1 Interceptor effect in reducing trim angle

Figure 6 shows the effects of different interceptor configurations on trim angle and drag. The trim angles of the bare hull, TIS, and DIS have been compared and indicate a significant reduction in trim angle with the use of an interceptor. However, there is not a notable difference in the trim angle between the TIS model and DIS. Thus, it can be concluded that the primary reason for trim reduction is the transom interceptor, while the addition of a forward interceptor has little impact on trim angle. Additionally, increasing the height of the transom interceptor has been shown to improve its performance in reducing trim, though the difference is not significant. It is worth noting that, as mentioned by Mansoori et al. (2017), the interceptor should be lower than the thickness of the boundary layer.

Figure 6 (b) indicates a significant reduction in total drag by using both TIS and DIS, though the difference between TIS and DIS and also the DIS i3 y3 and DIS i4 y3 models is negligible.



a) Trim angle b) Drag

Figure 6. DIS influence in hull trim angle and drag in different Froud numbers.

3.2 Interceptor effect in pressure distribution

The effects of installing interceptors on reducing trim angle can be explained by the high-pressure region generated on the hull bottom at the interceptor position. Figs. 7 and 8 show the pressure coefficient over the considered models calculated using equation (5).

$$C_p = \frac{p}{0.5\rho_w v^2} \tag{5}$$

that p is fluid pressure and v is hull speed.

According to Figure 7, the installation a transom interceptor (TIS i3) leads to move forward the stagnation point compared to the bare hull, resulting in a trim reduction. Then, by adding the forward interceptor DIS i3 y3 model, the high-pressure region at the stagnation point moves backward compared to the model with a TIS i3. This highlights the advantage of transom interceptor's in reducing trim compared to the DIS i3 y3 model. Additionally, when comparing the DIS i3 y3 and i4 y3 models, the stagnation point moves forward with an increase in interceptor height.

In hull models that include the DIS, when the water flow passes through the forward interceptor, it separates from the hull bottom and reattaches after detachment. This creates a high-pressure region in the middle of the hull. When comparing the DIS i3 y3 and i4 y3 models in Figs. 7 and 8, it is evident that the high-pressure region generated at forward interceptor is similar for both models. However, the negative pressure behind the interceptor for the DIS i3 y3 model is significantly higher than the i4 y4 model. This may be due to the higher trim angle in the DIS i3 y3 model (see Figure 6), which can result in better ventilation.

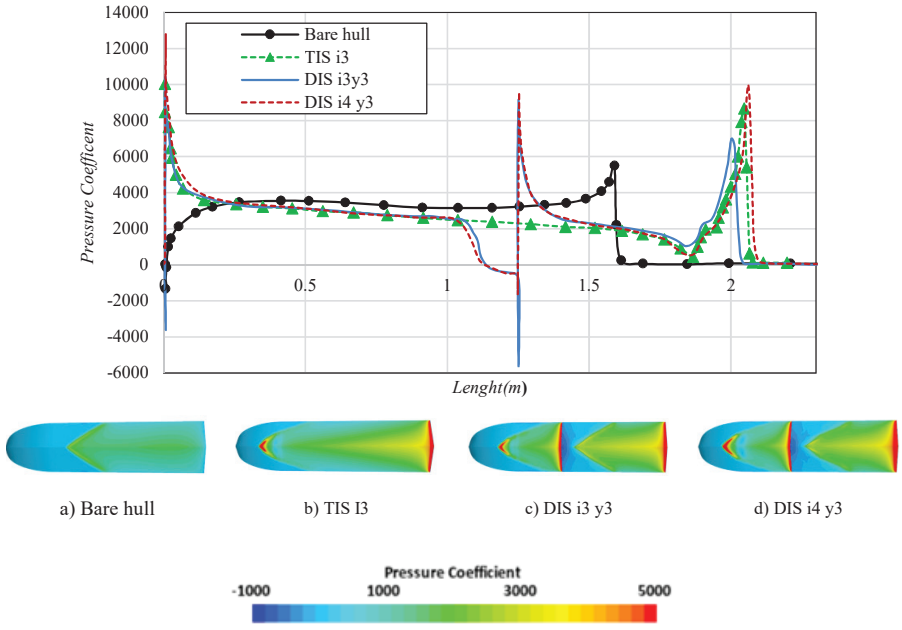


Figure 7. Pressure distribution in the center line at Fr = 2.15.

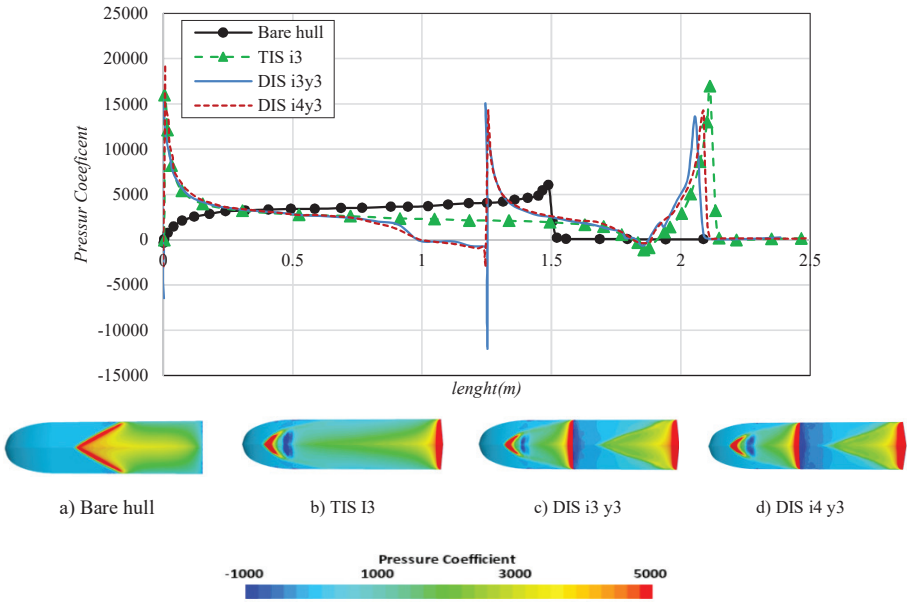


Figure 8. Pressure distribution in the centerline at Fr = 2.8.

3.3 Interceptor effect in drag

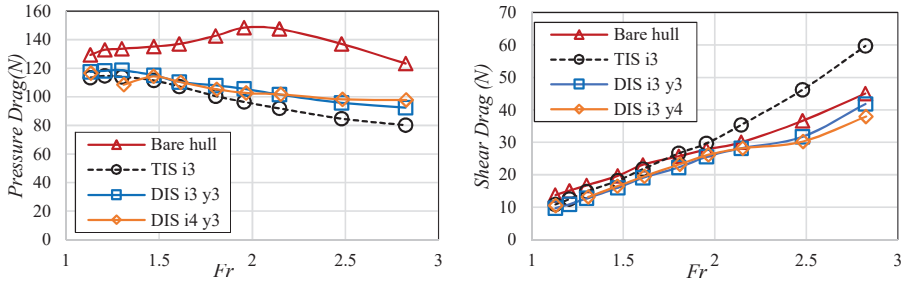
As shown in Figs. 7 and 8, there is a high-pressure peak on the bare hull at the stagnation point. Adding each interceptor is associated with generating another peak pressure at the interceptor position. Therefore, it is expected that installing interceptors can affect the pressure drag. Furthermore, reducing the trim

angle using the interceptor increases the wetted surface area and, consequently, the frictional drag. However, previous studies indicated a reduction in the total hull drag by using interceptors (De Luca and Pensa 2013; Seok et al. 2020). This section investigates the interceptor effects on hull pressure and shear drag to understand the main reason for the drag reduction demonstrated by De Luca and Pensa (2013). Figure 9 shows the pressure and shear drag of the bare hull, TIS, and DIS models.

Pressure drag depends on hull speed and trim angle, though any discontinuity in the flow path can affect it. Therefore, the pressure drag for each model has the same trend as its trim angle. In addition, adding both TIS and DIS reduces the pressure drag compared to the bare hull as a result of the trim angle reduction. According to Figure 9(a), using TIS i3 reduces pressure drag from 12.3% to 38.3% compared to the bare hull. This reduction is in the range of 9.2% to 31.1% and 9.9% to 31.0% for the DIS i3 y3 and DIS i4 y3 models, respectively. As the trim angle between TIS i3 and DIS i3 y3 models is almost the same, the higher pressure drag obtained in model DIS i3 y3 compared to TIS i3 can be explained due to the forward interceptor discontinuity in the flow path.

Figure 9(a) also shows a lower pressure drag for the TIS i3 model compared to the DIS at Fr = 2.8, while the DIS has a lower trim angle (as shown in Figure 6). In addition to the effect of the number of discontinuities, it might be related to entering the bow section into the water. Thus, correcting the trim has positive effects until the bow sections enter the water. This leads to an overcorrection that becomes negative for the hull performance and increases the pressure drag.

Shear drag is a function of wetted surface area and hull speed. Therefore, shear drag increases as the Froude number increases in all considered models. As shown in Figure 9(b), the shear drag of model TIS i3 is significantly higher than that of other models at high Froude numbers, but there is no significant difference at lower speeds. A comparison between the bare hull and TIS model shows a 21.4% reduction in shear drag at Fr = 1.13, while there is a 32.6% increase at Fr = 2.8. Additionally, using DIS reduces shear drag compared to the bare hull at all speeds considered. The HSC with DIS i3 y3 shows a shear drag reduction in the range of 6.0% to 29.8%, while the range is 5.9% to 23.47% when using DIS i4 y3, based on hull speed. This reduction in shear drag in DIS models (i3 y3 and i4 y4) is due to the ventilation length created behind the forward interceptor in the DIS i3 y3 and DIS i3 y4 models, which reduces the wetted surface area and consequently shear drag. Figure 10 illustrates the wake profile behind the forward interceptor at different speeds. In Figure 10, the red color illustrates the air flow generated behind the interceptor, and the blue region represents water.



(a) pressure drag (b) shear drag

Figure 9. DIS effect in pressure and shear drag.

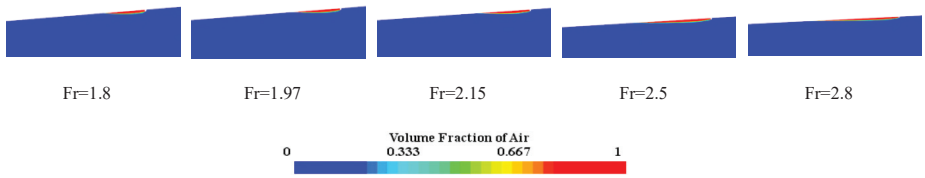


Figure 10. Forward interceptor ventilation in HSC with DIS at various Froude numbers.

4. Conclusion

This study investigates the effect of DIS performance in calm water compared to the bare hull and TIS. The hydrodynamic behaviors of an HSC with and without interceptors have been predicted numerically using RANS simulation with the VOF model and morphing mesh methods. The numerical simulations were validated against experimental trim angles and drag measured by De Luca and Pensa (2012a). The obtained results demonstrate a significant reduction in the trim angle and drag of the HSC by employing DIS or TIS. While DIS did not show significant improvement over TIS in reducing trim angle, it was able to significantly decrease drag by creating a ventilated length behind the forward interceptor. It is worth noting that the position and height of the interceptor can impact its performance and may improve the efficiency of the DIS. Therefore, further studies should investigate the effect of forward interceptor height and position.

Abbreviation

CFD	Computation Fluid Dynamics
DFBI	Dynamic Fluid Body Interaction
DIS	Double interceptor system
Fr_{∇}	volumetric Froud number
HSC	high speed craft
i	After interceptor height
ITTC	International Towing Tank Conference
RANS	Reynolds averaged Navier Stokes
RMS	Root mean square
TIS	Transom Interceptor system
VOF	Volume of Fluid
y	Forward interceptor height

References

Brizzolara, S. 2003, October. Hydrodynamic analysis of interceptors with CFD methods. In Proceedings of the 7th International Conference on Fast Sea Transportation, Fast (p. 49).

De Luca, F., & Pensa, C. 2012a. Unconventional interceptors in still water and in regular waves: Experimental study on resistance reduction and dynamic instability. In 17th International Conference on Ships and Shipping Research (NAV), Naples 17-19 October.

De Luca, F., & Pensa, C. 2012b. Experimental investigation on conventional and unconventional interceptors. Trans. Int. J. Small Craft Tech, 154, 65-72.

Ghassemi, H., Mansouri, M., & Zaferanlouei, S. 2011. Interceptor hydrodynamic analysis for handling trim control problems in the high-speed crafts. Proceedings of the Institution of Mechanical Engineers, Part C: Journal of Mechanical Engineering Science, 225(11), 2597-2618.

ITTC 7.5-03-02-03. 2021. Recommended Procedures and Guidelines: Practical Guidelines for Ship CFD.

John, S., Kareem Khan, M. D., Praveen, P. C., Manu, K., & Panigrahi, P. K. 2011. Hydrodynamic performance enhancement using stern wedges, stern flaps and interceptors. Naval Science & Technological Laboratory, India.

Mansoori, M., & Fernandes, A. C. 2017. Interceptor and trim tab combination to prevent interceptor's unfit effects. Ocean engineering, 134, 140-156.

Mansoori, M., Fernandes, A. C., & Ghassemi, H. 2017. Interceptor design for optimum trim control and minimum resistance of planing boats. Applied Ocean Research, 69, 100-115, doi:10.1016/j.apor.2017.10.006.

Niazmand Bilandi, R., Mancini, S., Dashtimanesh, A., & Tavakoli, S. 2024. A revisited verification and validation analysis for URANS simulation of planing hulls in calm water. Ocean Engineering, 293, 116589, doi:10.1016/j.oceaneng.2023.116589.

Park, J. Y., Choi, H., Lee, J., Choi, H., Woo, J., Kim, S., ... & Kim, N. 2019. An experimental study on vertical motion control of a high-speed planing vessel using a controllable interceptor in waves. Ocean Engineering, 83, 173, 841-850, doi:10.1016/j.oceaneng.2019.01.019.

Putra, A. M. F., & Suzuki, H. 2024. Experimental and numerical study on the high-speed ship hydrodynamics influenced by an interceptor with varied angle of attack. International Journal of Naval Architecture and Ocean Engineering, 16, 100566.

Roshan, F., Dashtimanesh, A., & Kujala, P. 2024. Safety Improvements for High-Speed Planing Craft Occupants: A Systematic Review. Journal of Marine Science and Engineering, 12(5), 845, doi:10.3390/jmse12050845.

Samuel, S., Mursid, O., Yulianti, S., Kiryanto, K., & Iqbal, M. 2022. Evaluation of interceptor design to reduce drag on planing hull. Brodogradnja: Teorija i praksa brodogradnje i pomorske tehnike, 73(3), 93-110, doi:10.21278/brod73306.

Seok, W., Park, S. Y., & Rhee, S. H. 2020. An experimental study on the stern bottom pressure distribution of a high-speed planing vessel with and without interceptors. International Journal of Naval Architecture and Ocean Engineering, 12, 691-698, doi:10.1016/j.ijnaoe.2020.08.003.

Song, K. W., Guo, C. Y., Gong, J., Li, P., & Wang, L. Z. 2018. Influence of interceptors, stern flaps, and their combinations on the hydrodynamic performance of a deep-vee ship. Ocean Engineering, 2018, 170, 306-320, doi:10.1016/j.oceaneng.10.048.

Appendix 4 (Publication IV)

Paper IV

Roshan, F., Niazmand Bilandi. R., De Luca, F., Mancini, S., Kõrgesaar, M., (2026). Numerical Investigation of Transom and Double Interceptor Systems on a High-Speed Planing Craft in Regular Waves with Experimental Validation. Ocean Engineering, 367, p. 128197. https://doi.org/10.1016/j.oceaneng.2026.128197.

Ocean Engineering 367 (2026) 128197

Contents lists available at ScienceDirect

Ocean Engineering

journal homepage: www.elsevier.com/locate/oceaneng

Research paper

Numerical investigation of transom and double interceptor systems on a high-speed planing craft in regular waves with experimental validation

Fatemeh Roshan [a,*], Rasul Niazmand Bilandi [b], Fabio de Luca [c], Simone Mancini [b,c], Mihkel Kõrgesaar [a]

[a] Kuressaare College, School of Engineering, Tallinn University of Technology, Tallinna 19, Kuressaare, 93811, Estonia
[b] Hydrodynamics & Aerodynamics, Simulation, Ports & Training, FORCE Technology, Hjortekærsvej 99, Kgs. Lyngby, 2800, Denmark
[c] Department of Industrial Engineering, Università degli Studi di Napoli Federico II, Via Claudio 21, Naples, 80125, Italy

ARTICLE INFO

Keywords:
High speed planing craft
Regular waves
Interceptor system
CFD
Occupant safety
Fly-over

ABSTRACT

High-speed planing craft (HSPC) operating in waves can experience severe vertical motions and impact accelerations, potentially affecting operational performance and occupant safety. This study investigates the effects of a transom interceptor system (TIS) and a double interceptor system (DIS) on the seakeeping performance of an HSPC in regular head waves at a constant beam Froude number of $Fr_B = 3.0$. A CFD model was validated against towing tank measurements of heave, pitch, and vertical acceleration for three configurations: the bare hull, TIS-equipped hull, and DIS-equipped hull. The validated model was then applied to a range of regular wave conditions with different wavelengths and wave steepnesses. HSPC responses were evaluated using Response amplitude operators (RAOs), pressure distribution, and hull-motion characteristics to identify the hydrodynamic mechanisms governing interceptor performance. While both systems have limited influence under mild and moderate waves, their differences become more significant under severe conditions. The TIS maintains a more favorable pressure distribution, reducing fly-over severity and water re-entry impact acceleration. Within the investigated wave conditions, the TIS reduced peak vertical acceleration by up to 28.9% compared with the bare hull. In contrast, the DIS produces longer airborne phases and higher impact acceleration.

1. Introduction

High-speed planing craft (HSPC) are widely used in military, rescue, patrol, and transportation operations because of their ability to operate at high speeds. However, when operating in rough sea conditions, they are subjected to severe impact shocks and vertical accelerations caused by wave encounters. These impacts can degrade hydrodynamic performance, reduce operational capability, and compromise occupant safety. Operators often reduce speed to limit impact accelerations and safety risks, but this can conflict with mission requirements where high speed is essential. Therefore, practical methods for reducing impact loads and severe accelerations are required to improve the safe operating envelope of HSPC in rough seas.

Occupant safety is one of the primary concerns in HSPC operation. Several studies have shown that onboard vertical accelerations may exceed the limits recommended by international standards for human exposure to whole-body vibration and repeated shock, including ISO 2631-1, 1997, ISO 2631–5, 2004, EU Directive 2002/44/EC, 2002, and British Standards Institution 6841(BS), 1987. Some of these studies include Folsø (2004), Allen et al. (2008), and Garme et al. (2011). Furthermore, Myers et al. (2012), Lo Martire et al. (2017) and de Alwis and Garme (2021) confirmed the high potential for human injury onboard high-speed craft. Therefore, reducing HSPC accelerations remains a key objective for improving occupant safety and operational performance.

In addition to speed reduction, motion reduction devices can be implemented to reduce hull motions and accelerations and consequently improve occupant safety. Among these devices, interceptor systems have received particular attention. Based on a systematic review of previous studies, Roshan et al. (2024) identified interceptors as an effective device for reducing hull acceleration and improving occupant safety onboard HSPC.

A transom interceptor system (TIS) is a vertical flap installed on the hull transom. There are numerous studies that confirmed the effectiveness of interceptors in improving the hydrodynamic performance of HSPC, including reductions in resistance, trim, and sinkage (Seo et al.,

* Corresponding author.
E-mail address: fatemeh.roshan@taltech.ee (F. Roshan).

https://doi.org/10.1016/j.oceaneng.2026.128197
Received 20 July 2026; Received in revised form 28 August 2026; Accepted 12 September 2026
Available online 17 September 2026
0029-8018/© 2026 Published by Elsevier Ltd.

2013; Avci and Barlas, 2019; Sahin et al., 2023). As indicated by Brizzolara and Villa (2009), Roshan et al. (2025a), and Putra et al. (2026), a TIS generates a high-pressure region near the transom. This pressure increases the lift force near the transom (Putra and Suzuki, 2024) and shifts the center of pressure (Mansoori and Fernandes, 2015), directly affect the hull trim angle.

Reducing hull trim angles using transom interceptors has been demonstrated in several studies, including Ghassemi et al. (2011) and Suneela et al. (2020). However, Seok et al. (2020) showed that an interceptor with small height can adversely affect HSPC performance by increasing the trim angle, whereas an appropriate height can reduce trim. Samuel et al., 2022aandSamuel et al., 2022b showed that a properly designed interceptor can reduce hull sinkage by 17% and trim angle by 8.48% for a planing hull in calm water. Nevertheless, calm water results do not fully represent interceptor behaviours in wave conditions.

As the influence of interceptors on hull pressure distribution, lift force, and trim has been well established in calm water conditions, their potential effectiveness is also expected to extend to wave conditions. In regular waves, Jangam and Sahoo (2021) showed that interceptors can reduce heave motion by 16-18% at a Froude number of 1.78. Similarly, Şahin et al. (2022) demonstrated reductions of 30% in heave, 25% in pitch, and 6% in resistance for a planing hull operating in regular waves with a wavelength of 1.5L at $Fr_B = 1.373$. Although the TIS has shown favorable performance in regular waves, some researchers have proposed the Double Interceptor System (DIS) to further improve the dynamic performance of HSPC.

A DIS consists of a transom interceptor and an additional interceptor located further forward along the hull bottom. The use of this system can generate two high-pressure regions, one near the transom and another in the forward interceptor. These pressure regions produce two bow-down trimming moments that reduce excessive trim angle (De Luca and Pensa, 2012a, 2012b); the same experiments, however, showed that while the DIS reduces resistance, it can increase hull motions and accelerations in regular waves. In addition, a properly ventilated DIS may create an air cavity behind the forward interceptor that can significantly affect hull resistance, as shown by Sorrentino et al. (2025) and Deng et al. (2022).

The effectiveness of both TIS and DIS in reducing hull motions and accelerations in irregular waves was investigated and compared by Roshan et al. (2025b). They compared the heave, pitch, and vertical acceleration for the bare hull, the TIS-equipped hull, and the DIS-equipped hull using towing tank experiments. Additionally, the potential of TIS and DIS to improve occupants' safety was also evaluated by comparing the RMS and VDV of vertical accelerations with the limits recommended by ISO 2631-1 and EU Directive 2002/44/EC for health and comfort assessment. The results indicated that the TIS can efficiently reduce the likelihood of health risks and discomfort in planing mode. However, the DIS amplified some acceleration peaks and may therefore increase occupant-safety risks.

Although previous studies have demonstrated the effects of TIS on HSPC motions and accelerations in irregular waves (Roshan et al., 2025b), statistical parameters such as one-third significant acceleration, RMS, and VDV may not fully capture infrequent but severe acceleration peaks that occur under critical, near-resonant wave conditions. These extreme accelerations may have a disproportionate effect on occupant safety and hull stability despite having a limited contribution to the overall statistical response and may therefore be overlooked in purely statistical analyses.

One of the most severe accelerations in HSPC operation is associated with the fly-over phenomenon. Fly-over may occur when a high-speed craft operates in waves with wavelengths approximately 1.5-4 times the hull length (Fridsma, 1969; Kim et al., 2013; Tavakoli et al., 2026). Under these conditions, the hull may separate from the free surface near a wave crest and subsequently re-enter the water with a high impact acceleration, posing considerable risks for both hull stability and occupant safety. Roshan et al. (2022) showed that reducing hull speed can decrease the likelihood of fly-over events. In addition, previous studies have shown that actively controlled interceptor systems can improve hull responses, particularly near resonance. Park et al. (2019) reported reductions of 33.4% in heave and 41.3% in pitch near the resonant frequency of the hull (wavelength 3.5L), compared with reductions of 20.7% and 21.1%, respectively, for a fixed TIS. They also reported a 32.4% reduction in pitch RMS and a 12.1% reduction in heave RMS when active interceptors were used in irregular waves. Similarly, Karimi et al. (2015) demonstrated that controllable TIS can effectively reduce hull heave and pitch motions, especially near the resonant frequency. However, the effectiveness of TIS and DIS in mitigating fly-over phenomenon and the associated impact accelerations remains unclear. Further investigation is therefore required to evaluate the effects of TIS and DIS on heave, pitch, vertical acceleration, and fly-over behavior under critical wave conditions.

The present study aims to investigate and compare the performance of transom and double interceptor systems on an HSPC operating in regular waves. Attention is given to identifying critical wavelengths, reducing impact accelerations, and the fly-over phenomena. For this aim, a CFD model is first validated against towing-tank measurements for one regular wave condition. The validated model is then applied to analyse heave, pitch, and vertical acceleration over a range of wave conditions at $Fr_B = 3.0$. The resulting CFD data are used to identify critical wavelengths and to evaluate the effectiveness of the TIS and DIS in reducing impact acceleration and fly-over probability. These results provide a detailed comparison of TIS and DIS performance for improving the seakeeping and dynamic behaviour of HSPC.

2. Methodology

This study employs a CFD model to simulate a high-speed planing craft operating in regular waves at $Fr_B = 3.0$. The analysis focuses on the ability of the TIS and DIS to reduce hull motions and vertical accelerations. For this purpose, model C5 from the Naples systematic series (NSS) was selected and analyzed with and without interceptor systems over a range of regular waves.

2.1. Hull model

This study investigates the dynamic response of a hard-chine high speed planing craft (model C5) from the NSS in regular wave conditions. The principal geometric characteristics of the model are listed in Table 1, and the hull geometry is shown in Fig. 1.

The mass properties of the model, including the centre of gravity and radii of gyration, were determined experimentally prior to the towing tank tests, following the procedure reported by Roshan et al. (2025b).

To examine the effect of interceptor systems on hull motions and vertical accelerations, two interceptor configurations were defined and implemented on the hull bottom in both experimental and numerical analyses, as shown in Fig. 2.

Table 1
Principal particulars of the NSS C5 model.

Parameter	Value model C5
LOA	2.611 m
L_{wl}	2.400 m
B_{wl}	0.41 m
LCG	0.945 m
VCG	0.205 m
SF	15
Displacement	37.4 Kg
K_{xx}	0.164
K_{yy}	0.6
Bt	13.2
B0.5	22.3 (deg)
B0.75	38.5 (deg)
Fr_B	3.0

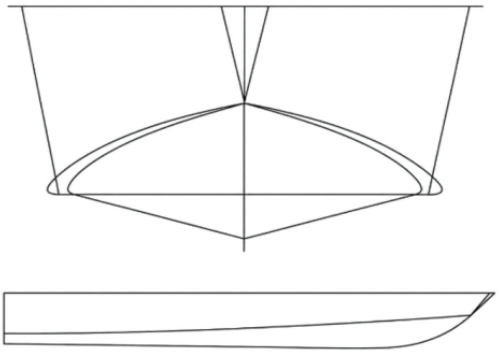


Fig. 1. Geometry of the NSS C5 hull model.

The first configuration is a Transom Interceptor System (TIS) installed at the hull transom, with a height of 2 mm and a length equal to $0.25B_{WL}$. The second configuration is a Double Interceptor System (DIS), which combines the same TIS with an additional interceptor of the same height (2 mm) and a length equal to B_{WL}, located 0.8 m forward of the transom.

The interceptor dimensions were fixed according to the experimental test configuration and were not optimized within the present study. The selected height of 2 mm corresponds to $i/L_{WL} = 0.83\times10-3$. This value is consistent with the lower range of nondimensional interceptor depths experimentally investigated by De Luca and Pensa (2012), who demonstrated that interceptor depth strongly influences lift generation, trim correction, and resistance and that excessive interceptor dimensions may lead to over-correction at high speeds. Previous studies have also shown that interceptor performance depends on blade height, span, and longitudinal arrangement (De Luca and Pensa, 2012; Şahin et al., 2022). Accordingly, the quantitative findings of the present study are specific to the investigated TIS and DIS geometries; different interceptor dimensions or positions may alter both the magnitude of the response and the relative effectiveness of the two configurations.

The effectiveness of the interceptor systems was evaluated by comparing the heave and pitch motions, vertical accelerations, and fly-over behavior of the bare hull with those of the hulls equipped with the TIS and DIS.

2.2. Experimental setup

Experimental investigations were carried out at the Department of Industrial Engineering (DII), Università degli Studi di Napoli "Federico II." The towing tank has overall dimensions of 136 m × 9 m x 4.5 m, and the maximum towing carriage speed is 10 m/s. Fig. 3 presents the experimental towing-tank arrangement used for the regular-wave tests. The generated wave field was first inspected without the model to confirm the formation of a clear and repeatable regular-wave pattern along the tank, as shown in Fig. 3(a). The model was subsequently installed beneath the towing carriage and tested under the prescribed regular-wave conditions, as illustrated in Fig. 3(b). This arrangement enabled the hydrodynamic response of the model to be measured under controlled and repeatable wave conditions.

The experiments were conducted in a single regular head wave generated by the tank wavemaker. A wave amplitude of 0.03 m and a period of 1.51 s were used for all test conditions. During the tests, model C5 was free to move in heave and pitch, while surge was restrained by the towing carriage, which maintained a constant speed of 6 m/s ($Fr_B = 3.0$).

Hull motions and accelerations were measured using two triaxial accelerometers (Crossbow CXL04GP3-R-AL) with an input range of ±4 g, a noise level of 10 mg RMS, a bandwidth of DC-100 Hz, and a sensitivity of 500 ± 15 mV/g. The accelerometers were installed at the center of gravity (CG) and at a longitudinal position $0.5L_{WL}$ forward of the CG. A Qualisys motion capture system was used to measure heave and pitch, while wave elevation was monitored using capacitive wave probes installed inside the towing tank.

All measured signals were sampled at 500 Hz. A Butterworth band-pass filter with cutoff frequencies between 0.05 and 20 Hz was applied to remove measurement noise and low-frequency disturbances. To ensure repeatability, each test condition was repeated several times under identical operating conditions.

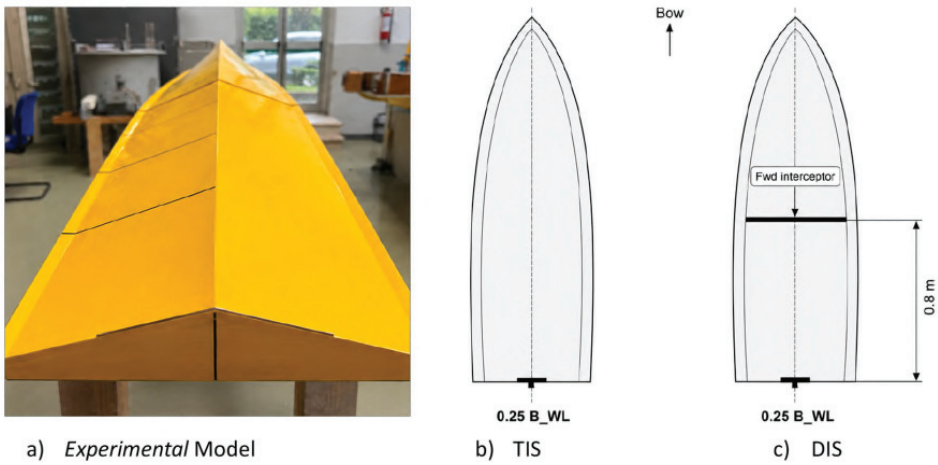


Fig. 2. Interceptor arrangements on the hull bottom: a) experimental DIS installation showing the transom interceptor and the full-beam forward interceptor positioned 0.8 m ahead of the transom; b) TIS configuration; and c) DIS configuration. The initial experimental transom-interceptor span was 0.5 B_{WL}. After a pronounced bow-down response and increased resistance were observed, the span was reduced to 0.25 B_{WL} for the configurations reported in this study. The interceptor height (h) was 2 mm.



Fig. 3. Experimental investigation in the towing tank: a) generated regular-wave field; b) model test under regular-wave conditions.

2.3. Numerical setup

The simulations were performed using STAR-CCM+ (v2506, 20.04.007). The computational framework extends the numerical setup published in the authors' previous studies (Roshan et al., 2022; Bilandi et al., 2024a, 2025, Bilandi et al., 2024b).

The hull motions were simulated using the Dynamic Fluid Body Interaction (DFBI) morphing-mesh approach available in STAR-CCM+. In this setup, the hull was allowed to move freely in heave and pitch, while surge was restrained to reproduce the towing-tank condition. At each time step, the hydrodynamic forces and moments acting on the hull were integrated and used to update the rigid-body position. The mesh deformation was handled using a radial-basis-function-based morphing approach. In this method, the displacement of the moving hull boundary is propagated smoothly into the surrounding volume mesh while the far-field boundaries of the morphing region remain fixed. The mesh connectivity is therefore preserved during the DFBI heave and pitch motion, and the computational grid follows the rigid-body displacement without remeshing. RBF-based mesh morphing has been widely used for continuous mesh deformation because it transfers prescribed boundary displacements to the internal mesh nodes while retaining the original mesh topology (Biancolini et al., 2020).

A three-dimensional computational domain was defined to reproduce the towing-tank environment. To reduce computational cost, the longitudinal symmetry plane of the hull was used, and only half of the domain was simulated. A schematic of the computational domain and boundary conditions is shown in Fig. 4.

As shown in Fig. 4, the computational domain had dimensions of 17L x 2.5L x 6L. The free surface was located 2L below the top boundary. A velocity inlet boundary condition was applied at the inlet, while the outlet was defined as a pressure outlet. The top and bottom boundaries were also velocity inlets, and side boundaries were symmetry planes.

Regular head waves were generated using the fifth-order Stokes wave formulation implemented in STAR-CCM+, based on the nonlinear wave theory of Fenton (1985). To reduce numerical reflections from the computational boundaries, wave-forcing zones were applied adjacent to the inlet, outlet, and outer lateral boundary. A forcing-zone length of 3 m was adopted. Within these regions, the numerical solution is

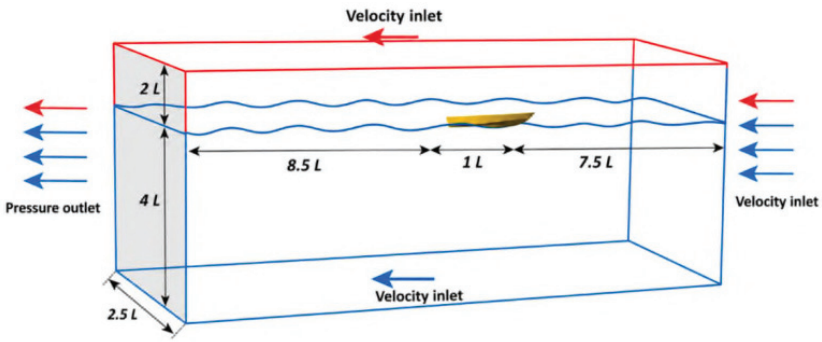


Fig. 4. Computational domain and boundary conditions.

progressively driven toward the prescribed analytical wave solution, which allows outgoing disturbances to be damped while maintaining the target incident wave conditions in the computational domain.

The computational domain was discretized using the Trimmer meshing model, with local volumetric refinement applied around the hull, free surface, and near-field wake, where comparatively large gradients of velocity, pressure, and volume fraction were expected. Particular attention was given to the spatial resolution of the generated waves. The cell size within the free-surface refinement region was adjusted according to the wavelength and wave height of each simulated condition, providing approximately 80 cells per wavelength and 20 cells per wave height. This wave-dependent refinement strategy provides sufficient spatial resolution of the free-surface profile and associated wave kinematics without imposing the same fine resolution throughout the entire numerical tank.

The governing equations were solved using the Finite Volume Method (FVM). The hull surface was discretized using a surface remesher, and a trimmer mesh was applied in the free-surface region to improve the resolution of the air-water interface. In addition, six prism layers with a total thickness of 0.002 m were generated around the hull surface to improve the prediction of the near-wall flow. The mesh structure of the computational domain is shown in Fig. 5.

2.3.1. Governing equations

The present study assumes incompressible flow for both water and air. The flow is governed by the Unsteady Reynolds-Averaged Navier-Stokes (URANS) equations. The continuity and momentum equations are therefore given by

$$\frac{\partial \overline{U}_i}{\partial x_i} = 0, \tag{1}$$

$$\frac{\partial \overline{U}_i}{\partial t} + \overline{U}_j \frac{\partial \overline{U}_i}{\partial x_j} = -\frac{1}{\rho}\frac{\partial \overline{p}}{\partial x_i} + \nu \frac{\partial^2 \overline{U}_i}{\partial x_j{}^2} + g - \frac{\partial \overline{u_i u_j}}{\partial x_j} \tag{2}$$

where $\overline{U}_i$ is the Reynolds-averaged velocity component in the *i-th* direction, $\overline{p}$ averaged pressure, ρ is the fluid density, ν is the kinematic viscosity, and g is the gravitational acceleration. The term $\overline{u_i u_j}$ v represents the Reynolds stress tensor.

To accurately capture the free surface, the Volume of Fluid (VOF) method is implemented. For two phase, immiscible, and non-reacting flow (air and water in free surface), the mixture properties are expressed as:

$$\rho_m = (1-\alpha)\rho_w + \alpha\rho_a \tag{3}$$

$$\nu_m = (1-\alpha)\nu_w + \alpha\nu_a \tag{4}$$

where w and a refer to water and air, respectively, and α denotes the volume fraction of air, where $\alpha = 1$ represents pure air and $\alpha = 0$ represents pure water. The free surface is reconstructed based on the distribution of the volume fraction field. The k-Omega SST turbulence model was used to simulate turbulence effects, combining the near-wall accuracy of the k-Omega formulation with the freestream robustness of the k-ε model.

The simulations consider two degrees of freedom in heave and pitch motions. Therefore, the hull motions are modelled by solving the rigid-

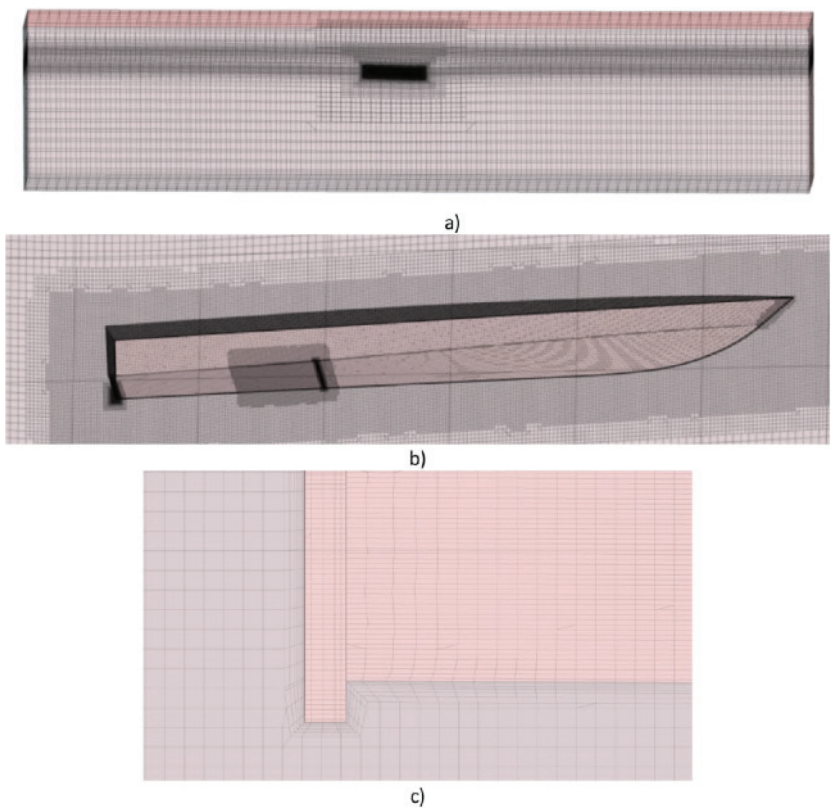


Fig. 5. Mesh structure: a) computational domain, b) mesh around the hull, and c) prism layers around model C5 with DIS.

body dynamic equation using a Dynamic Fluid Body Interaction (DFBI) morphing approach. The heave motion and pitch rotation of the hull are governed by Newton's second law as:

$$\sum F_z = m\frac{d^2z}{dt^2} \tag{5}$$

$$\sum M_{yy} = I_{yy}\frac{d^2\theta}{dt^2} \tag{6}$$

Where m is the hull mass, z is the vertical displacement (heave), θ is the pitch angle, and I_{yy} is the pitch moment of inertia. Furthermore, $\sum F_z$ and $\sum M_{yy}$ represent the total dynamic forces in the vertical direction, and moments acting on the hull, respectively.

In the DFBI morphing-mesh approach, the hull motion is solved in a fully coupled manner with the flow field. The hydrodynamic forces and moments obtained from the pressure and shear-stress distributions are used to update the heave displacement and pitch rotation of the hull. The computational grid is then deformed smoothly to follow the computed rigid-body motion, allowing the hull boundary and the free surface to remain accurately resolved without remeshing. This coupling is performed at each time step, so the instantaneous hull response directly reflects the unsteady wave loading.

The motion of the hull is fully coupled with the flow solver in a two-way interaction, ensuring that hydrodynamic forces and hull responses were solved simultaneously at each time step (0.002 s).

Fig. 6 presents the y + distributions for the bare Hull and the TIS- and DIS-equipped hulls using the selected meshes and a time step of 0.002 s. The corresponding average y + values were approximately 31.6, 0.95, and 2.42, respectively. Six prism layers were employed for all configurations; however, the near-wall mesh settings differed. For the Bare Hull, a total prism-layer thickness of 0.0075 m and a stretching factor of 1.3 were used, whereas for the TIS- and DIS-equipped hulls the total prism-layer thickness was 0.001 m with a stretching factor of 1.5. The finer near-wall resolution for the interceptor-equipped configurations was adopted to resolve the flow around the 2-mm-high interceptor surfaces and edges. Since these prism-layer settings were applied to the complete hull-wall boundary, the lower y + values also extend to regions upstream of the forward interceptor.

The same All y + Wall Treatment was employed for all configurations. This treatment provides a continuous formulation across low and high y + regimes and therefore does not require the wall-adjacent cells to lie exclusively within either the y+ <1 and most likely y+ <30 range. Consequently, the differences in y + shown in Fig. 6 reflect the different near-wall mesh resolutions adopted for the Bare Hull and interceptor-equipped configurations rather than differences in the wall-treatment formulation.

The regular wave conditions simulated in this study are summarized in Table 2. All simulations were performed at a constant speed of 6 m/s, corresponding to $Fr_B = 3.0$, in a range of wavelengths and steepness values to identify critical wave conditions and evaluate the effects of the interceptor systems on hull motions and vertical accelerations. Wave steepness, defined as ε = kA (wave number times wave amplitude), of ε = 0.07 and ε = 0.10 were applied over the full wavelength range. A higher steepness of ε = 0.12 was then simulated for the critical wave conditions identified from the ε = 0.07 and ε = 0.10 cases, where significant increases in motions and accelerations were observed. These critical conditions correspond to the largest heave, pitch, and vertical acceleration responses and were therefore used to further investigate the effects of the TIS and DIS on fly-over behavior.

Table 2
Wave properties for model C5.

λ/L	λ	k (rad/m)	$T\sqrt{g/B}$	H/B		
				ε = 0.07	ε = 0.1	ε = 0.12
0.69	1.67	3.76	5.04	-	0.12	-
1	2.4	2.62	5.61	0.0546	0.17	-
1.5	3.6	1.75	6.87	0.0804	0.26	-
2	4.8	1.31	7.93	0.1072	0.35	0.417
3	7.2	0.87	9.71	0.1608	0.52	0.275
4	9.6	0.65	11.21	0.214	0.69	0.367
6	14.4	0.44	13.73	0.321	1.04	-

2.3.2. Grid verification and numerical uncertainty

A formal grid-verification study was performed for the bare-hull validation condition with a wave amplitude of 0.03 m and a period of 1.51 s. Five systematically refined meshes, M1–M5, containing approximately 1.47, 2.24, 3.41, 5.18, and 7.87 million cells, respectively, were considered. The response amplitudes of pitch, heave, and CG vertical acceleration were used as the quantities of interest. The corresponding experimental amplitudes were 1.06°, 13.92 mm, and 3.51 m/s^2, respectively. The mean pitch and heave results are provided separately in Appendix A.

The numerical uncertainty due to spatial discretization was quantified following the ITTC Recommended Procedure 7.5-03-01-01 (ITTC, 2024a,b) using the least-squares grid-refinement approach of Eça and Hoekstra (2014). Since the meshes are three-dimensional, the relative grid spacing was defined from the cell count as

$$r_i = \left(\frac{N_f}{N_i}\right)^{1/3} \tag{7}$$

where N_f and N_i denote the cell counts of the finest and i-th meshes, respectively. The successive meshes correspond to an approximately constant cell-count refinement ratio of 1.52, equivalent to a characteristic grid-spacing refinement ratio of approximately 1.15. The grid-dependent solution was represented in the least-squares form

$$\varphi_i = \varphi_0 + \alpha r_i^p \tag{8}$$

where φ_0 is the extrapolated solution, α is a fitting coefficient, and p is the observed order of grid convergence. The scatter of the grid solutions was characterized by

$$\Delta\varphi = \frac{\varphi_{max} - \varphi_{min}}{n_g - 1} \tag{9}$$

where n_g is the number of grids. The fitted apparent orders were 5.70, 3.29, and 3.11 for pitch, heave, and vertical acceleration amplitudes, respectively. These values are greater than the nominal second-order range and are associated with the flattening of the response on the finer meshes; they are therefore not interpreted as evidence of higher-order numerical accuracy. Following the ITTC procedure, fixed first- and second-order error estimators were examined, and the second order

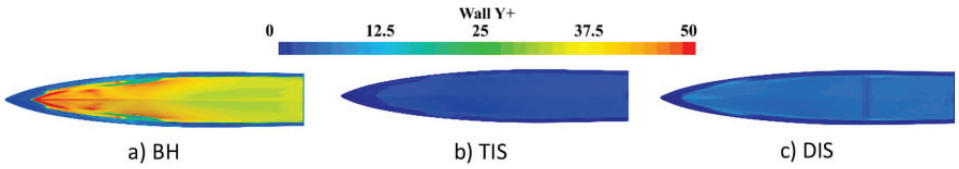


Fig. 6. y + distribution for three hull configurations at FrB = 3.0.

least-squares representation provided the lowest standard deviation for all three response quantities. A conservative safety factor of $F_S = 3$ was consequently applied.

For the present cases, where the standard deviation of the fit satisfies $\sigma < \Delta\varphi$, the numerical uncertainty on grid i was evaluated as

$$U_\varphi(\varphi_i) = F_S\,|\varepsilon_\varphi(\varphi_i)| + \sigma + |\varphi_i - \varphi_{fit,i}| \tag{10}$$

where $\varepsilon_\varphi(\varphi_i)$ is the estimated spatial-discretization error and $\varphi_{fit,i}$ is the corresponding fitted solution.

The resulting grid-verification results are summarized in Table 3, while Fig. 7(a) shows the evolution of the response amplitudes normalized by the corresponding experimental values and Fig. 7(b) presents the estimated numerical uncertainties. For the selected M3 mesh, the numerical uncertainties are 12.84% for pitch amplitude, 14.03% for heave amplitude, and 16.36% for vertical-acceleration amplitude. Further refinement to M5 reduces these uncertainties to 7.83%, 8.18%, and 9.54%, respectively.

The M3 predictions differ from the experimental amplitudes by −2.83% for pitch, −18.61% for heave, and −28.21% for vertical acceleration. The pitch discrepancy is therefore smaller than the estimated spatial-discretization uncertainty, whereas the heave and acceleration discrepancies remain larger than their corresponding grid uncertainties. Moreover, refinement from M3 to M5 changes the heave amplitude only from 11.33 to 11.47 mm and the vertical-acceleration amplitude from 2.52 to 2.56 m/s^2, compared with experimental values of 13.92 mm and 3.51 m/s^2. This indicates that spatial discretization alone does not account for the remaining underprediction of these responses.

Considering the observed response plateau, the formal numerical-uncertainty assessment, and the substantial increase in computational cost associated with M4 and M5, mesh M3, containing 3,406,185 cells, was retained for the subsequent bare-hull simulations.

The same formal ITTC/Eça-Hoekstra grid-verification procedure was also applied to the TIS- and DIS-equipped configurations, with the complete results provided in Appendix A. For the selected M3 meshes, containing 3,688,620 cells for TIS and 4,981,298 cells for DIS, the numerical uncertainties in pitch, heave, and vertical-acceleration amplitudes are 14.34%, 13.22%, and 18.68% for TIS, and 22.10%, 18.46%, and 21.78% for DIS, respectively. The five-grid data exhibit the same response-plateau behavior observed for the Bare Hull; therefore, the fixed second-order least-squares estimator with the conservative safety factor $F_S = 3$ was retained. These meshes were used for the subsequent TIS and DIS simulations.

2.4. Data representation and post-Processing of hull responses

The effects of the TIS and DIS on the dynamic response of the HSPC were investigated using both numerical and experimental approaches. Initially, a validation case under a regular wave condition (wave amplitude of 0.03 m and a period of 1.51 s) was performed at a Froude number of $Fr_B = 3.0$ for all three hull configurations, including the bare hull, the TIS-equipped hull, and the DIS-equipped hull. Subsequently, the validated numerical model was extended to a systematic range of regular wave conditions, as listed in Table 2. Each simulation was performed for a total physical time exceeding 8 s, to ensure that initial transient effects are fully dissipated. Only the statistically stationary portion of the response, corresponding to at least five steady wave cycles, was post-processed.

The comparison between experimental and CFD results, as well as dynamics performance of three hull configurations, was performed in term of Response Amplitude Operator (RAO) for heave, pitch, and vertical accelerations. For this purpose, the time history of heave and pitch motions were first processed by subtracting their mean values to ensure that the oscillations are centered around the zero.

The high-frequency noise in the experimental acceleration signals occurs because of measurement-induced structural vibrations. Therefore, a Butterworth low-pass filter was applied to the measured acceleration signals using a sampling frequency of 500 Hz and a cut-off frequency of 20 Hz. This procedure removed high-frequency noise while preserving the dominant hydrodynamic response. A comparison between the recorded and filtered acceleration signals is shown in Fig. 8.

To extract the heave, pitch, and vertical acceleration, the time series was divided into individual wave cycles using consecutive zero-crossing points. Within each cycle, the local maximum and minimum values were identified. The representative positive and negative amplitudes were then calculated as the average maxima and minima over all cycles. The motion amplitude is then defined as

$$A = \frac{\overline{X_{max}} - \overline{X_{min}}}{2} \tag{11}$$

This procedure provides a robust estimate of the periodic response amplitude while reducing sensitivity to cycle-to-cycle variations.

3. Validation

3.1. Trim angle and resistance in calm water

The calm-water performance of the Bare Hull, TIS, and DIS configurations was first assessed by comparing the numerical predictions with the experimental measurements. Fig. 9 presents the comparison in terms of (a) dynamic trim angle and (b) total resistance. Overall, the CFD model reproduces the experimentally observed trends for all three configurations.

The measured resistance values are 69.78 N, 69.08 N, and 56.63 N for the Bare Hull, TIS, and DIS, respectively, compared with the corresponding CFD predictions of 74.92 N, 74.30 N, and 61.06 N. The CFD results therefore overpredict the measured resistance by approximately 7.37%, 7.55%, and 7.82%, respectively. Despite this systematic offset, the relative effect of the interceptor configurations is reproduced accurately. Relative to the Bare Hull, the TIS produces only a small resistance reduction of approximately 1.0% experimentally and 0.83% numerically. In contrast, the DIS reduces the resistance by approximately 18.84% experimentally and 18.50% numerically.

The corresponding experimental trim angles are 2.65°, 1.00°, and 3.17° for the Bare Hull, TIS, and DIS, respectively, while the CFD predictions are 2.40°, 0.883°, and 2.82°. Thus, the numerical model also reproduces the characteristic strong trim reduction produced by the TIS and the higher running trim associated with the DIS. The substantial resistance reduction obtained with the DIS is consistent with its

Table 3
Grid-refinement results and estimated numerical uncertainties for the bare-hull response amplitudes according to the ITTC/Eça–Hoekstra verification procedure. The relative grid spacing is defined as $r_i = (N_f/N_i)^{1/3}$. M3 denotes the mesh selected for the subsequent systematic simulations.

Mesh	Cells	r_i	Pitch		Heave		Acceleration	
			Amplitude (°)	Uφ (%)	Amplitude (mm)	Uφ (%)	Amplitude (m/s^2)	Uφ (%)
M1	1,474,284	1.748	0.99	23.05	10.90	24.74	2.41	29.27
M2	2,240,911	1.520	1.02	17.18	11.12	18.40	2.47	21.57
M3	**3,406,185**	**1.322**	**1.03**	**12.84**	**11.33**	**14.03**	**2.52**	**16.36**
M4	5,177,401	1.150	1.04	9.82	11.43	10.48	2.55	12.29
M5	7,869,650	1.000	1.04	7.83	11.47	8.18	2.56	9.54

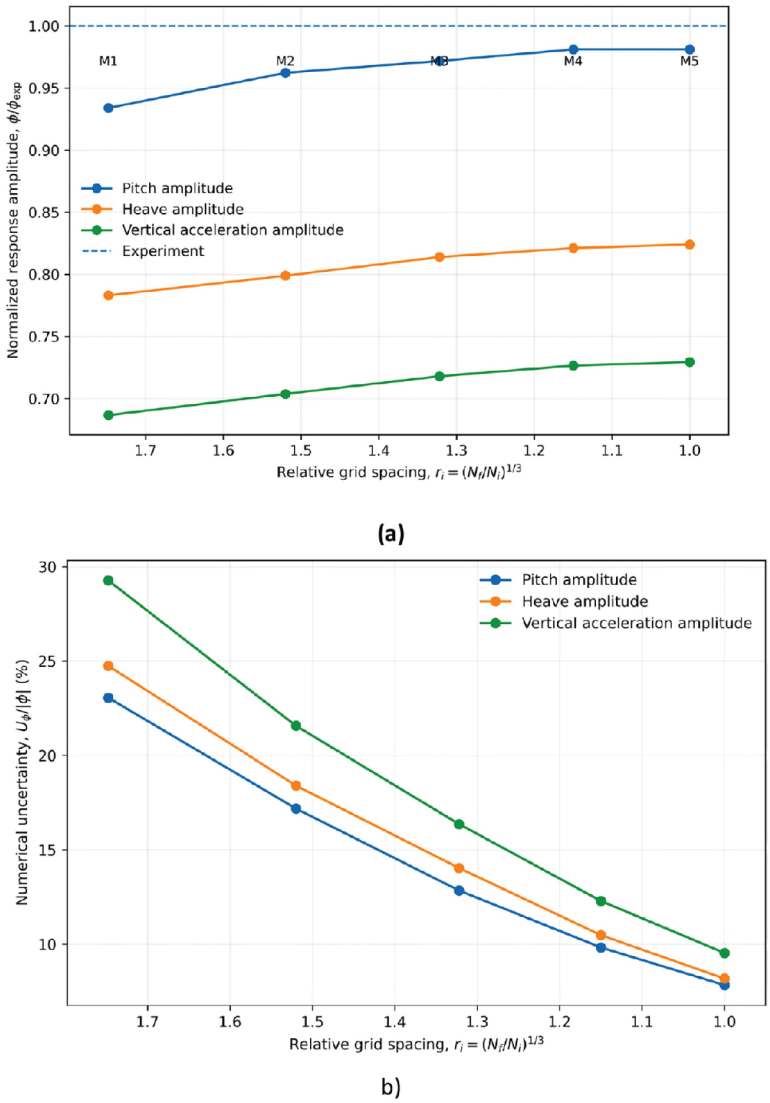


Fig. 7. Grid-verification results for the bare-hull validation condition: a) response amplitudes normalized by the corresponding experimental values as functions of the relative grid spacing $r_i = (N_f/N_i)^{1/3}$; and b) numerical uncertainties estimated according to the ITTC/Eça–Hoekstra grid-refinement procedure.

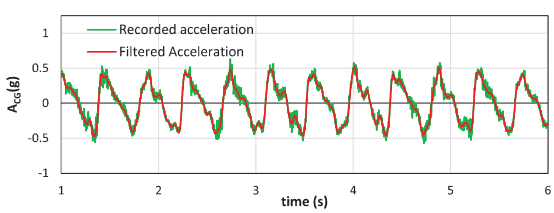


Fig. 8. Recorded and filtered experimental acceleration signals in regular waves at $Fr_B = 3.0$.

characteristic hydrodynamic mechanism, whereby the forward interceptor modifies the pressure distribution and wetted surface and can promote the formation of a ventilated region downstream of the forward blade (De Luca and Pensa, 2012; Sorrentino et al., 2025).

These calm-water results highlight an important trade-off between the two interceptor arrangements. The DIS provides a substantial resistance benefit, whereas the subsequent regular-wave analysis shows that its influence on heave, pitch, vertical acceleration, and re-entry severity is more dependent on the encountered wave condition. Conversely, the TIS provides only a limited resistance reduction in calm water but yields a more consistent reduction of some of the severe dynamic responses investigated in waves. The relative performance of TIS and DIS should therefore be assessed by considering both resistance and seakeeping characteristics.

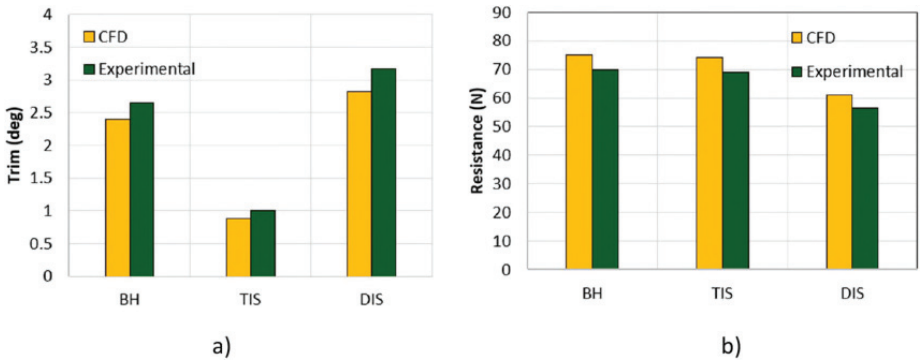


Fig. 9. Comparison of experimental and CFD results for the bare Hull (BH), TIS, and DIS configurations in calm water at $Fr_B = 3.0$: a) dynamic trim angle and b) total resistance.

3.2. Numerical waves vs theoretical waves

Fig. 10 presents the incident wave-elevation histories for the Bare Hull, TIS, and DIS simulations together with the corresponding fifth-order Stokes solution (Fenton, 1985) under the validation condition. The numerical wave histories closely reproduce the theoretical waveform in both amplitude and phase and are nearly coincident for the three hull configurations. The maximum absolute differences relative to the bare Hull wave are 0.307 mm for TIS and 0.676 mm for DIS, corresponding to approximately 0.51% and 1.13% of the prescribed wave height (H = 60) mm, respectively. These small differences confirm that the three hull configurations are subjected to essentially equivalent incident-wave conditions. Therefore, differences in the subsequent hull responses can primarily be associated with the hydrodynamic influence of the interceptor configurations rather than differences in the imposed wave field.

3.3. Heave, pitch, and acceleration responses in regular waves

A validation study is conducted to assess the accuracy of the numerical models by comparing the CFD predictions with experimentally measured heave, pitch, and vertical acceleration. The comparison included the bare hull, the TIS-equipped hull, and the DIS-equipped hull under regular waves with an amplitude of 0.03 m, a frequency of 0.66 Hz, and a wavelength of 3.585 m.

Fig. 11 compares the experimental measurements and numerical predictions of pitch, heave, and CG vertical acceleration for the bare hull. Similar comparisons for the TIS- and DIS-equipped hulls are shown in Figs. 12 and 13, respectively.

To assess the possible influence of the mesh-motion strategy on the predicted dynamic response, the same validation condition was additionally simulated using an overset-mesh approach. Figs. 11–13 therefore compare the experimental measurements with both the overset- and

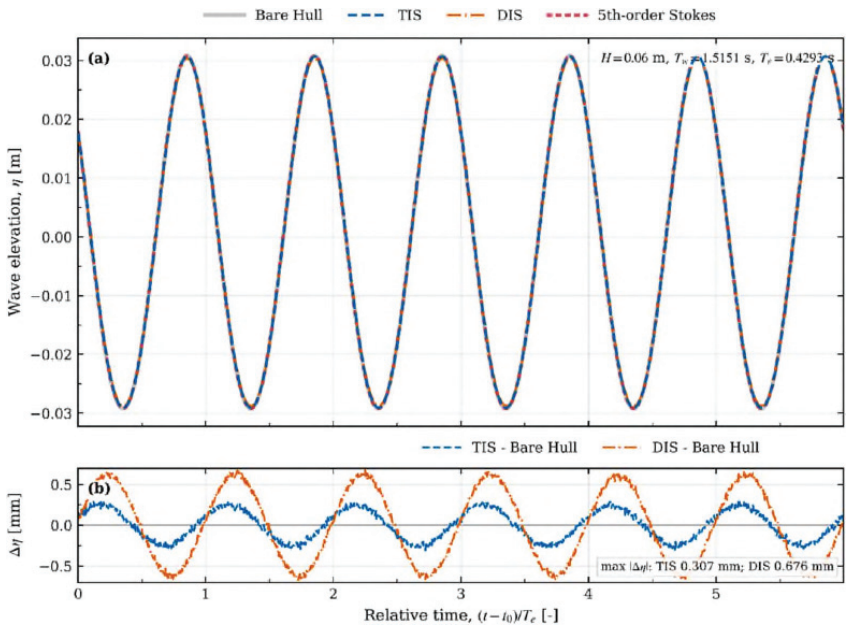


Fig. 10. Incident wave-elevation verification for the validation condition. (a) Comparison of the numerical wave-elevation histories for the bare-hull, TIS, and DIS configurations with the fifth-order Stokes solution; (b) instantaneous wave-elevation differences of the TIS and DIS cases relative to the bare-hull case. The maximum absolute differences are 0.307 mm for TIS and 0.676 mm for DIS. m, s, and s.

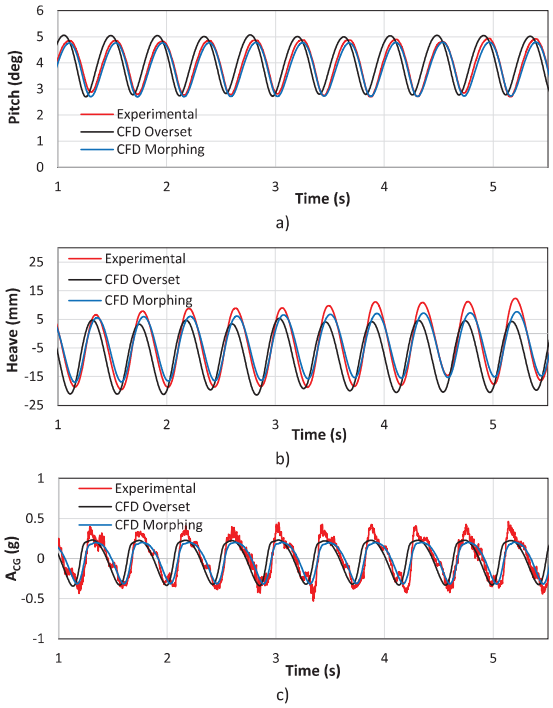


Fig. 11. Experimental and CFD time histories of a) pitch, b) heave, and c) vertical acceleration for the bare hull in regular waves.

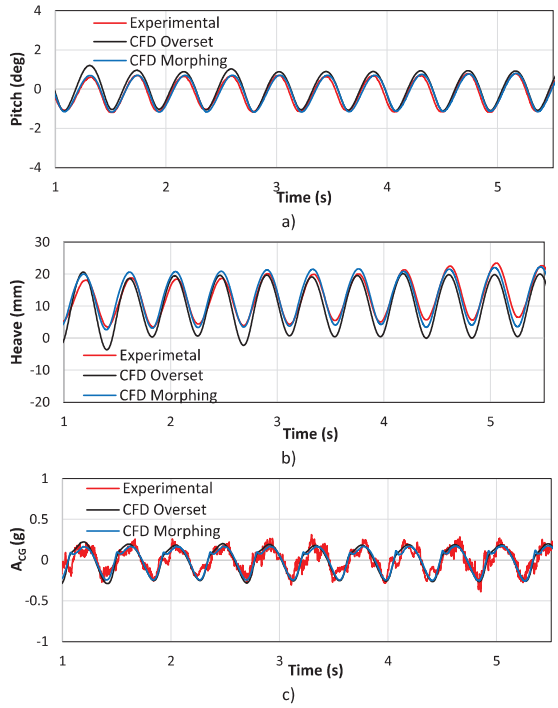


Fig. 12. Experimental and CFD time histories of a) pitch, b) heave, and c) vertical acceleration for the TIS-equipped hull in regular waves.

morphing-mesh CFD predictions, while the corresponding response-amplitude operators (RAOs) and relative errors are summarized in Table 4.

Figs. 11–13 show that the numerical model agrees well with the experimental data in both the amplitude and phase of heave and pitch motions for all configurations. The periodic response of the hull in regular waves is reproduced accurately by the CFD model, although a slight underprediction of heave amplitude is observed.

For vertical acceleration, the numerical model correctly predicts the dominant oscillatory behavior and response frequency, as shown in Figs. 11(c), 12(c) and 13(c). However, discrepancies are observed in the peak values. These differences are mainly attributed to the highly nonlinear character of vertical acceleration in high-speed planing craft, which is strongly affected by local flow separation, wave-impact forces, spray generation, and transient pressure fluctuations that are difficult to fully capture in CFD. In addition, the experimental acceleration signals include high-frequency noise and local vibration effects that are not completely reproduced by the numerical model. For the vertical acceleration, the comparison should be interpreted with particular care because the experimental signal contains high-frequency fluctuations superimposed on the main rigid-body response. These fluctuations are mainly associated with measurement noise, local structural vibration, and short-duration impact events during water re-entry. As a result, the exact instantaneous peak values are more difficult to compare directly than the heave and pitch motions. Nevertheless, the CFD results reproduce the dominant oscillation frequency and the main acceleration trend, which makes them suitable for assessing the relative response of the bare hull, TIS-equipped hull, and DIS-equipped hull.

Table 4 quantifies the comparison between the experimental RAOs and the two CFD mesh-motion approaches. Overall, the overset and morphing simulations provide comparable predictions of the global heave, pitch, and CG vertical-acceleration responses and reproduce the same principal trends relative to the experiments. For the Bare Hull, the overset and morphing approaches predict heave RAOs of 0.41 and 0.38, respectively, compared with the experimental value of 0.46, while the corresponding pitch RAOs are 0.39 and 0.36 compared with 0.37 experimentally. Similar consistency between the two numerical approaches is observed for the TIS and DIS configurations. In particular, for DIS the vertical-acceleration RAOs are 0.207 and 0.211 for the overset and morphing approaches, respectively, compared with the experimental value of 0.39. The persistence of a similar discrepancy with both mesh-motion strategies indicates that the remaining difference, particularly for the DIS acceleration response, is unlikely to originate primarily from the morphing treatment. Instead, it is more plausibly associated with the broader difficulty of resolving the strongly nonlinear, short-duration hydrodynamic response during high-speed wave interaction, together with the experimental high-frequency content discussed above. Since the morphing approach reproduces the principal global responses with accuracy comparable to the overset approach while requiring fewer computational cells and lower computational effort, it was retained for the systematic simulations presented in the remainder of this study.

Fig. 14 presents the frequency-domain comparison of the experimental measurements with the CFD-Overset and CFD-Morphing predictions for heave, pitch, and CG vertical acceleration. One-sided FFT amplitude spectra were calculated from the normalized response signals, with frequency presented relative to the encounter frequency, (f/fe). In addition, least-squares Fourier fitting was applied at $f/fe = 1$, 2, and 3 to quantify the fundamental, second-, and third-harmonic amplitudes independently at the prescribed harmonic frequencies. Frequency-domain analysis and higher-harmonic decomposition are particularly relevant for high-speed planing craft, for which nonlinear wave–hull interaction, intermittent variations of the wetted surface, and re-entry behavior can generate significant higher-harmonic response

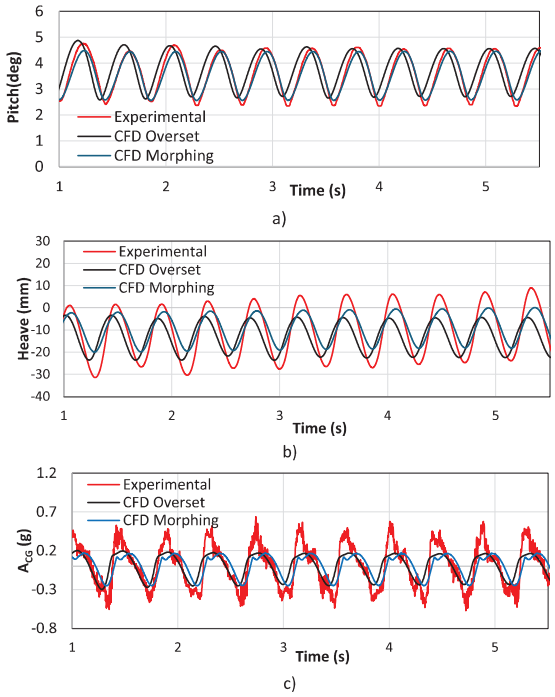


Fig. 13. Experimental and CFD time histories of a) pitch, b) heave, and c) vertical acceleration for the DIS-equipped hull in regular waves.

components (Tavakoli et al., 2026).

For all three hull configurations, both numerical approaches reproduce the dominant response at the encounter frequency and the principal higher-harmonic components observed experimentally. The agreement in the dominant frequency content is particularly clear for heave and pitch. For CG vertical acceleration, the experimental spectra exhibit greater broadband and higher-frequency content between the principal harmonic peaks, consistent with the high-frequency fluctuations observed in the measured acceleration time histories. Nevertheless, the CFD results reproduce the dominant spectral frequencies and the main harmonic structure of the experimental response. The frequency-domain comparison therefore provides additional evidence that the numerical model captures the principal wave-induced response characteristics, despite the larger discrepancies observed in the absolute acceleration amplitudes.

Because the acceleration and impact-related responses of high-speed planing craft can be sensitive to temporal resolution, a time-step sensitivity study was performed for the DIS validation condition using the morphing-mesh setup. Three systematically refined fixed time steps, $\Delta t = 0.004$, 0.002, and 0.001s, were considered, corresponding to a refinement ratio of two.

The time-step selection was also assessed against the ITTC Practical Guidelines for Ship CFD Applications. For simulations employing one- or two-equation turbulence models, ITTC recommends $\Delta t < 0.01L/U$ (ITTC, 2024a,b). For the present model, with (L = 2.4) m and (U = 6) m/s, this reference value is 0.004 s. The selected $\Delta t = 0.002$s is therefore a factor of two smaller than the ITTC reference value. A second-order temporal discretization scheme was employed in all simulations, consistent with the unsteady nature of the wave-induced hull response. ITTC notes that first-order accurate schemes in time should only be used when a steady-state solution is sought.

As shown in Table 5, reducing the time step from 0.002 to 0.001 s produces relatively small changes in the principal response quantities. Taking the finest solution as the reference, the differences obtained with $\Delta t = 0.002$s are approximately 3.3% for heave RAO, 5.7% for pitch RAO, and 1.9% for CG-acceleration RAO. In contrast, the corresponding differences for $\Delta t = 0.004$s are approximately 10.0%, 10.0%, and 3.3%, respectively. The reduction in sensitivity between the medium and fine time steps indicates that the principal global responses become less sensitive to further temporal refinement below 0.002 s.

This behavior is also consistent with previous CFD investigations of planing craft. Bi et al. (2020), for example, compared time steps of 0.001 and 0.002 s and reported nearly identical numerical results, selecting 0.002 s as an appropriate compromise between accuracy and computational cost.

4. Results and discussion

To provide further insight into the hydrodynamic effects of the TIS and DIS, the hydrodynamic responses of the HSPC are compared for the bare hull (BH), the TIS-equipped hull, and the DIS-equipped hull at a constant beam Froude number of $Fr_B = 3.0$ under the regular wave conditions listed in Table 2. This section is organized into four parts. First, the RAOs of heave, pitch, and vertical acceleration are analyzed. Next, the hydrodynamic mechanisms responsible for the observed responses are discussed using pressure distribution, wetted surface, and hull motion characteristics. Finally, the influence of the TIS and DIS on fly-over phenomenon is evaluated because of its direct relevance to occupant safety.

A final quantitative analysis compares cycle-ensemble peak vertical force and the corresponding CG acceleration during representative re-entry conditions.

4.1. RAO responses

4.1.1. Heave response

Fig. 15 presents the heave RAOs of the bare hull (BH), the TIS-equipped hull, and the DIS-equipped hull in regular waves with wave steepnesses of $\varepsilon = 0.07$, 0.10, and 0.12. For all three configurations, the heave RAO generally increases with wavelength, reaches a maximum at

Table 4
RAO validation for heave, pitch, and vertical acceleration.

Hull	Response	RAO Definition	Exp RAO	CFD Overset		CFD Morphing	
				RAO	Error (%)	RAO	Error (%)
Bare hull	Heave	z/A	0.46	0.41	−10.87	0.38	−18.61
	Pitch	θ/ε	0.37	0.39	5.38	0.36	−2.34
	Acceleration	A_{CG}/g	0.36	0.28	−22.42	0.26	−28.71
Hull with TIS	Heave	z/A	0.25	0.33	32.02	0.30	18.27
	Pitch	θ/ε	0.32	0.35	8.73	0.33	2.33
	Acceleration	A_{CG}/g	0.18	0.22	22.52	0.21	17.40
Hull with DIS	Heave	z/A	0.54	0.31	−43.52	0.29	−45.86
	Pitch	θ/ε	0.38	0.33	−13.01	0.33	−14.34
	Acceleration	A_{CG}/g	0.39	0.207	−50.89	0.211	−46.15

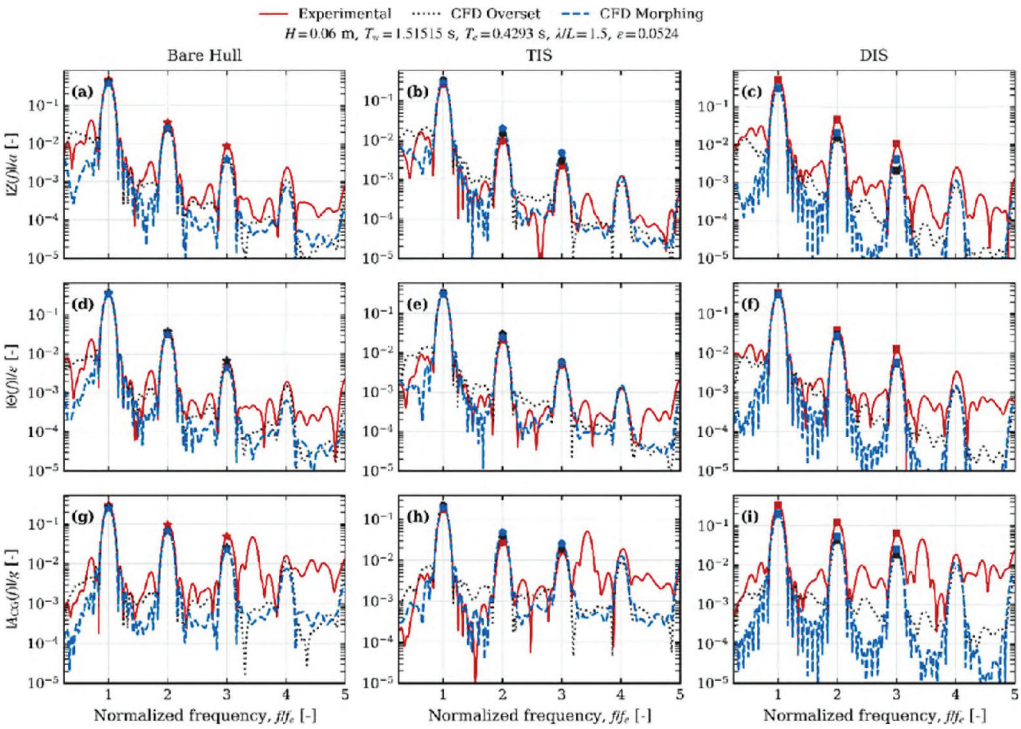


Fig. 14. Experimental and numerical one-sided FFT amplitude spectra of the normalized (a–c) heave, (d–f) pitch, and (g–i) CG vertical-acceleration responses for the Bare Hull, TIS, and DIS configurations, respectively, under the validation condition H = 0.06 m, Tw = 1.51515 s, Te = 0.4293 s, $\lambda/L = 1.5$, and $\varepsilon = 0.0524$. The red solid, black dotted, and blue dashed curves denote the experimental, CFD-Overset, and CFD-Morphing results, respectively. Frequency is normalized by the encounter frequency, *fe*. The superimposed symbols indicate the harmonic amplitudes obtained from least-squares Fourier fitting at $f/fe = 1,2$, and 3, corresponding to the fundamental, second-, and third-harmonic components. Stars, circles, and squares denote the Bare Hull, TIS, and DIS configurations, respectively. (For interpretation of the references to colour in this figure legend, the reader is referred to the Web version of this article.)

Table 5
Time-step sensitivity of the DIS configuration under the validation wave condition.

Δt (s)	Heave RAO	Difference from 0.001 s	Pitch RAO	Difference from 0.001 s	CG Acc. RAO	Difference from 0.001 s
0.004	0.270	10.0%	0.315	10.0%	0.208	3.26%
0.002	0.290	3.33%	0.330	5.71%	0.211	1.86%
0.001	0.300	—	0.350	—	0.215	—

approximately $\lambda/L = 3$, and then gradually decreases as wavelength increases further. An exception is observed for the bare hull at $\varepsilon = 0.12$ (Fig. 15(c)), where the response deviates from this general trend. The peak response occurs consistently at $\lambda/L = 3$ for all configurations and wave steepnesses, indicating that the interceptor systems do not significantly shift the critical wavelength for heave. This wavelength represents the critical wave condition for the heave response of the investigated craft.

As shown in Fig. 15(a), for $\varepsilon = 0.07$, the TIS reduces the heave RAO by approximately 3.0% at the critical wavelength ($\lambda/L = 3$) compared with the bare hull, whereas the DIS response remains close to that of the bare hull. For $\varepsilon = 0.10$, both interceptor configurations produce heave responses very close to the bare hull response over the investigated wavelength range, indicating that the interceptor systems have only a limited influence under these conditions. Fig. 15 also shows that, except near the critical wavelength ($\lambda/L \approx 3$), only minor differences occur among the three hull configurations for $\varepsilon = 0.07$ and $\varepsilon = 0.10$.

For the highest wave steepness ($\varepsilon = 0.12$), a different trend is observed, and the influence of the interceptor systems becomes more pronounced. At the shortest investigated wavelength ($\lambda/L = 2$), the bare hull indicates a pronounced nonlinear response (as shown in Fig. 16), whereas the response is smoother for λ/L = 3-4. As wavelength increases to $\lambda/L = 3$ and 4, the heave response of the TIS-equipped hull increases significantly, while the DIS response remains close to the bare-hull response. This indicates that the TIS causes a noticeable increase in heave RAO under this severe wave condition.

The influence of the interceptor systems on heave response depends strongly on wave steepness. Only minor differences are observed under low and moderate wave conditions ($\varepsilon = 0.07$ and $\varepsilon = 0.10$), whereas larger deviations appear under the steepest wave condition, particularly near the critical wavelength for the TIS-equipped hull.

4.1.2. Pitch response

Fig. 17 presents the pitch RAOs of the bare hull, the TIS-equipped hull, and the DIS-equipped hull for the regular-wave conditions listed in Table 2. Similar to the heave response, the pitch RAO generally increases with wavelength, reaches a peak, and then gradually decreases toward approximately 1.0 at longer wavelengths. For the lowest wave steepness ($\varepsilon = 0.07$), the maximum pitch response occurs at $\lambda/L = 3$. As wave steepness increases to $\varepsilon = 0.10$ and 0.12, the critical wavelength shifts to $\lambda/L = 4$ for all three hull configurations. This indicates that

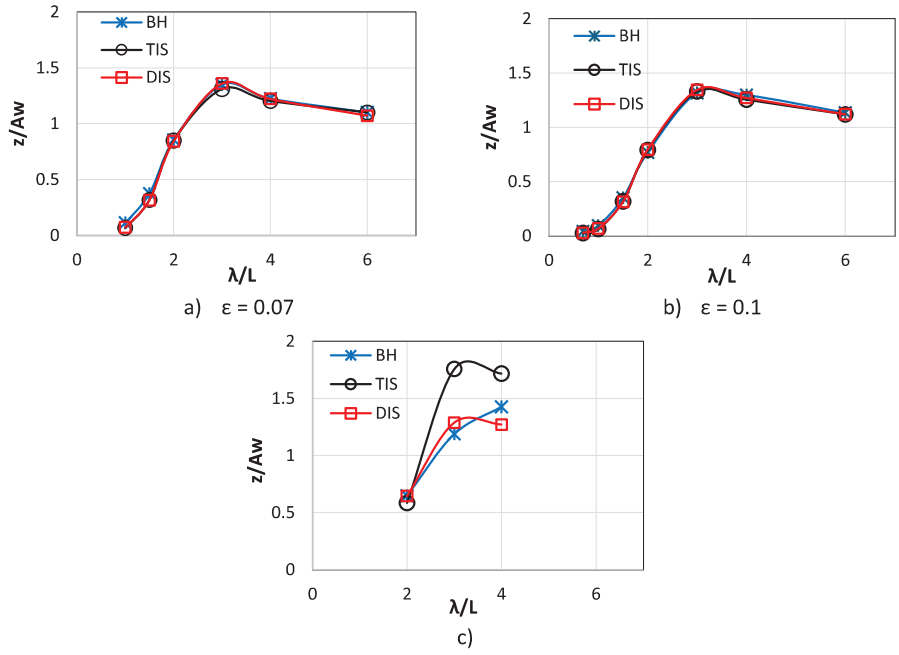


Fig. 15. Heave RAOs of the bare hull (BH), TIS-equipped hull, and DIS-equipped hull under regular-wave conditions with wave steepnesses of a) $\varepsilon = 0.07$, b) $\varepsilon = 0.10$, and c) $\varepsilon = 0.12$ at $Fr_B = 3.0$.

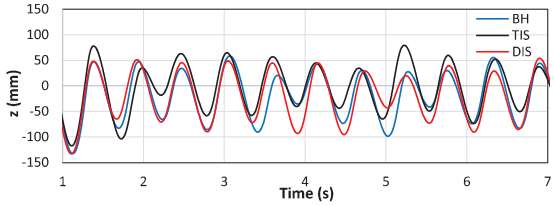


Fig. 16. Time history of heave motion for the bare hull, TIS-equipped hull, and DIS-equipped hull at $\varepsilon = 0.12$ and $\lambda/L = 2$, $Fr_B = 3.0$.

although the interceptor systems do not shift the critical wavelength, increasing wave steepness does shift the wavelength at which the maximum pitch response occurs.

As shown in Fig. 17(a), for $\varepsilon = 0.07$, the TIS reduces the pitch RAO by approximately 3.3% compared with the bare hull at $\lambda/L = 3$, whereas the DIS increases the pitch RAO by approximately 5.12% under the same condition. For $\varepsilon = 0.10$, the pitch RAOs of the TIS- and DIS-equipped hulls remain close to each other and are both slightly higher than that of the bare hull. For $\varepsilon = 0.12$, the highest pitch RAO at $\lambda/L = 3$ is observed for the DIS-equipped hull, followed by the TIS-equipped hull and the bare hull. The response at $\varepsilon = 0.12$ and $\lambda/L = 2$ is also nonlinear, consistent with the heave response shown in Fig. 16.

Overall, Fig. 17 indicates that the TIS provides a slight reduction in pitch RAO at $\varepsilon = 0.07$, whereas both interceptor configurations generally increase the pitch response under steeper wave conditions, particularly near the critical wavelength range. Away from the critical wavelength region, both TIS and DIS have only a limited influence on pitch response.

4.1.3. Acceleration response

Fig. 18 presents the vertical acceleration RAOs for the three hull configurations under the regular-wave conditions listed in Table 2. For all three hull configurations, the acceleration RAO generally increases with wavelength, reaches its maximum at approximately $\lambda/L = 3$, and then reduces as wavelength increases further. Similar to the heave response, the critical wavelength associated with the maximum vertical acceleration remains nearly constant for the investigated wave steepnesses and hull configurations. This indicates that the TIS and DIS do not significantly alter the wavelength corresponding to the peak acceleration response.

Fig. 18(a) shows that, at $\varepsilon = 0.07$, only negligible differences occur among the three hull configurations over the investigated wavelength range. At the critical wavelength ($\lambda/L = 3$), both interceptor systems produce acceleration responses close to that of the bare hull, suggesting that their influence on vertical acceleration is limited under low steepness conditions.

As wave steepness increases to $\varepsilon = 0.10$, the effect of the interceptor systems becomes more evident. At $\lambda/L = 3$, the TIS and DIS reduce the peak vertical acceleration by approximately 15% and 5.6%, respectively, compared with the bare hull. For the steepest wave condition ($\varepsilon = 0.12$) at $\lambda/L = 4$, this trend becomes more pronounced, with the TIS producing a vertical acceleration RAO 28.9% lower than that of the bare hull. The DIS also reduces acceleration compared with the bare hull in this condition; however, it increases the acceleration RAO by 10.5% at $\lambda/L = 3$.

Overall, the results show that the effectiveness of the interceptor systems in reducing vertical acceleration increases with wave steepness. Their influence is negligible under lower wave steepness, but both interceptor configurations reduce acceleration in steeper waves, with the TIS providing the largest improvement. Because vertical acceleration is directly related to occupant comfort and wave-impact severity, these results indicate that the TIS offers the smoothest dynamic

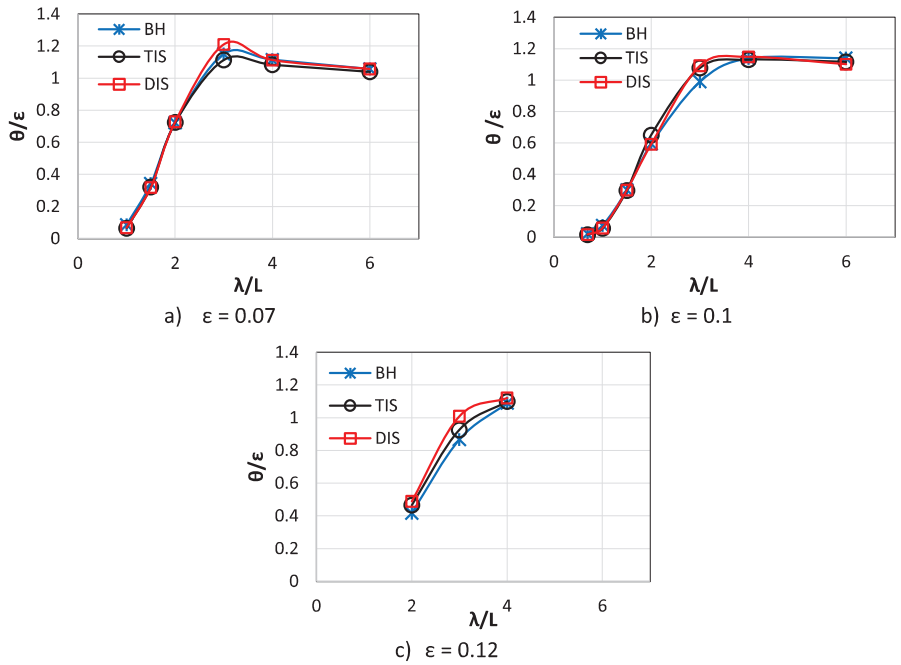


Fig. 17. Pitch RAOs of the bare hull (BH), TIS-equipped hull, and DIS-equipped hull under regular wave conditions with wave steepnesses of a) $\varepsilon = 0.07$, b) $\varepsilon = 0.10$, and c) $\varepsilon = 0.12$ at $Fr_B = 3.0$.

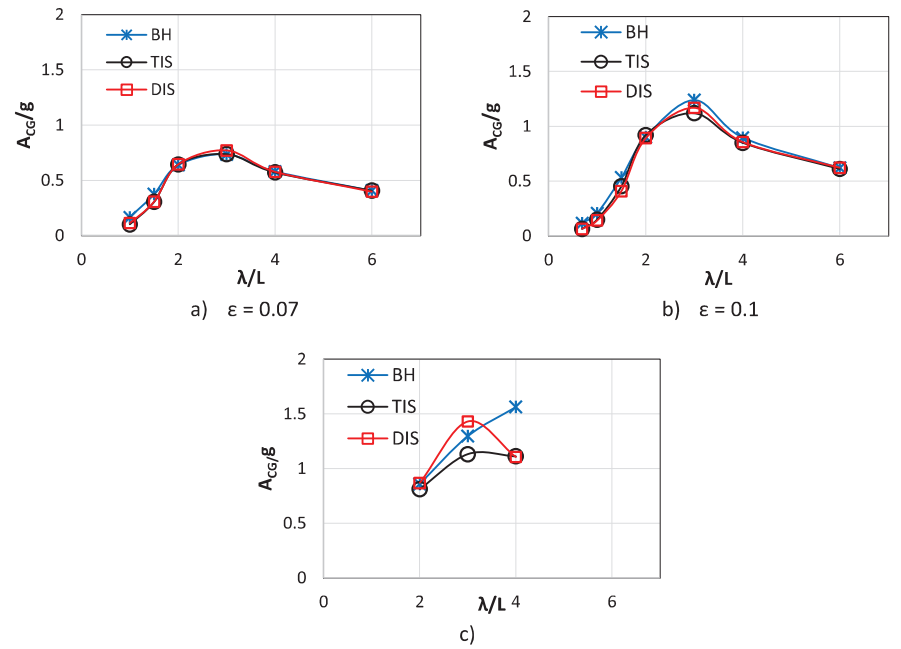


Fig. 18. Acceleration RAOs of the bare hull (BH), TIS-equipped hull (TIS), and DIS-equipped hull (DIS) under regular wave conditions with wave steepnesses of a) $\varepsilon = 0.07$, b) $\varepsilon = 0.10$, and c) $\varepsilon = 0.12$ at $Fr_B = 3.0$.

performance among the investigated configurations under severe wave conditions.

4.2. Hydrodynamic characteristics

To provide the influence of the TIS and DIS on hull dynamics in regular waves, the heave motion envelopes of the three hull configurations are presented in Figs. 19–21. These figures show both the oscillation amplitude and the mean heave relative to the corresponding obtained sinkage in calm water measured experimentally. For all investigated wave steepnesses, heave amplitude generally increases with wavelength, while only minor differences are observed among the configurations. In contrast, the mean heave position differs substantially, which is not evident from the heave RAOs alone.

As shown in Figs. 19–21, the smallest calm water sinkage is obtained for the TIS-equipped hull, followed by the bare hull and the DIS-equipped hull, respectively. The TIS-equipped hull generally oscillates around a positive mean heave position, except at $\lambda/L = 3$ and 4 for $\varepsilon = 0.12$. In contrast, both the bare hull and the DIS-equipped hull oscillate around negative mean heave positions for almost all investigated wave conditions.

Comparison with the dashed red line further shows that the mean heave position of the TIS-equipped hull remains close to the experimentally measured calm-water sinkage, whereas the bare hull and the DIS-equipped hull oscillate around positions noticeably lower than their corresponding calm-water sinkage.

To present both mean pitch and oscillation amplitude, Figs. 22–24 show the pitch motion envelopes of the three hull configurations under the investigated regular wave conditions. The calm water trim angle for each hull is indicated by the dashed red line. Similar to the heave response, the smallest calm-water trim angle is obtained for the TIS-equipped hull, followed by the bare hull and the DIS-equipped hull.

For $\varepsilon = 0.07$ and $\varepsilon = 0.12$ (Figs. 22 and 24), the pitch oscillation amplitude generally increases with wavelength and reaches a maximum at approximately $\lambda/L = 3$, after which it gradually decreases. In contrast, for $\varepsilon = 0.10$ (Fig. 23), the pitch amplitude continues to increase up to $\lambda/L = 4$, consistent with the pitch RAOs discussed earlier.

Although there is no significant difference in pitch amplitudes of the three hull configurations, there are noticeable differences in mean pitch. The TIS-equipped hull oscillates around a mean pitch value close to zero and below the calm water trim angle for $\varepsilon = 0.07$ and 0.10, whereas the bare hull oscillates around a higher mean pitch angle. The DIS-equipped hull exhibits less uniform behavior, with its mean pitch varying more significantly among the investigated wave conditions. The TIS-equipped hull also shows a more consistent mean pitch over the investigated wavelength range, whereas larger variations are observed for the bare hull and the DIS-equipped hull.

An important feature observed in Figs. 22–24 is the occurrence of negative instantaneous pitch angles during part of the oscillation cycle, particularly at the larger wavelengths. This indicates that the bow rotates below the initial trim attitude as the hull passes through portions of the wave profile. The presence of these negative pitch angles demonstrates that the vessel response is not simply a symmetric oscillation about its calm-water trim angle but is influenced by the transient hydrodynamic loading associated with the encounter between the hull and the incident wave. This effect becomes more pronounced as the wave-induced pitching motion increases.

Fig. 25 shows the instantaneous positions of the bare hull, the TIS-equipped hull, and the DIS-equipped hull while propagating in a regular wave with $\varepsilon = 0.10$ and $\lambda/L = 4$. The corresponding pressure distributions for the same wave condition are presented in Fig. 26. The same time instants are shown for all three hull configurations, allowing a direct comparison of hull position and pressure distribution during one wave encounter. These results provide a physical explanation for the differences in heave, pitch, and vertical acceleration responses discussed in the previous sections.

As shown in Fig. 25, the three hull configurations interact differently with the incident wave despite being subjected to identical wave conditions. These differences are reflected in the pressure distributions shown in Fig. 26.

The interceptor systems modify the pressure distribution on the hull bottom throughout the wave cycle, producing lift distributions that differ from those of the bare hull. The TIS generates a more favorable pressure distribution that helps maintain hydrodynamic support during wave propagation, whereas the pressure beneath the DIS-equipped hull changes more rapidly.

The relatively localized low-pressure region immediately downstream of the forward interceptor is associated with the local flow separation induced by the blade. The magnitude and extent of this region depend on the interceptor geometry and operating condition, including the interceptor height, local immersion, hull attitude, and instantaneous wave phase (Şahin et al., 2022). In addition, the pronounced low-pressure area visible in Fig. 26 should not be interpreted as representing the full extent of the separated or ventilated flow downstream of the interceptor. Previous investigations of double-interceptor systems have shown that the low-pressure region behind the forward interceptor and the associated ventilation can modify the pressure distribution, wetted surface, and running attitude of the hull (De Luca and Pensa, 2012; Sorrentino et al., 2025). This interpretation is also supported by the calm-water results of the present model: at $Fr_B = 3.0$ (V = 6 m/s), the DIS-equipped hull showed approximately 18% lower resistance than both the bare hull and the TIS-equipped hull, confirming that the

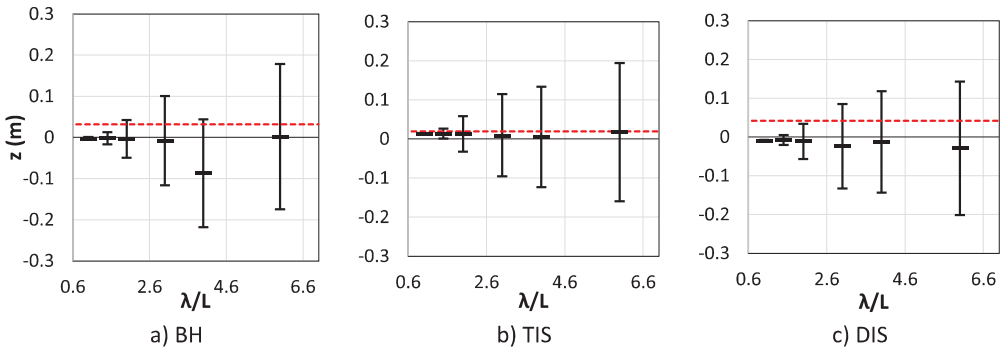


Fig. 19. Heave motion responses for $\varepsilon = 0.07$ on three hull configurations. The dashed red line indicates the experimentally measured calm water sinkage. (For interpretation of the references to colour in this figure legend, the reader is referred to the Web version of this article.)

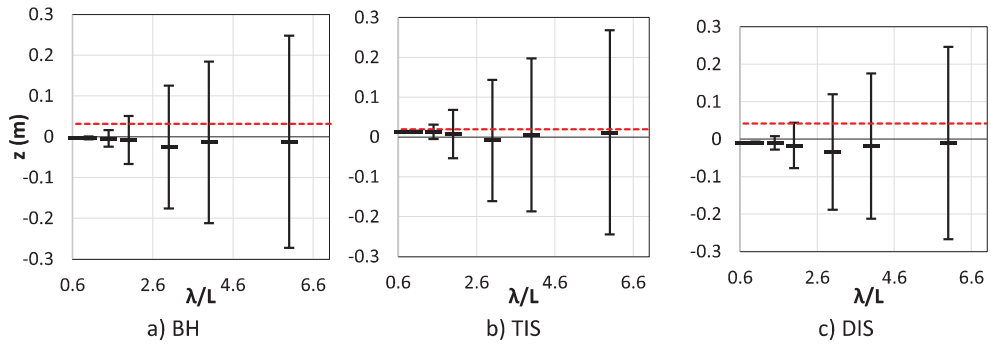


Fig. 20. Heave motion responses for $\varepsilon = 0.10$ on three hull configurations. The dashed red line indicates the experimentally measured calm water sinkage. (For interpretation of the references to colour in this figure legend, the reader is referred to the Web version of this article.)

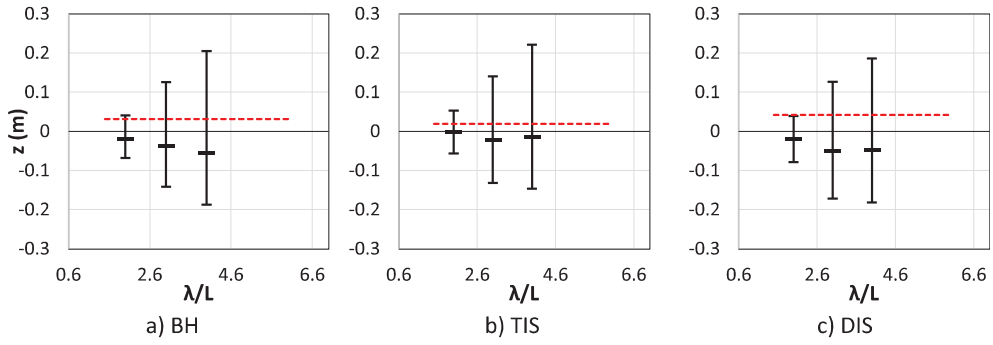


Fig. 21. Heave motion responses for $\varepsilon = 0.12$ on three hull configurations. The dashed red line indicates the experimentally measured calm water sinkage. (For interpretation of the references to colour in this figure legend, the reader is referred to the Web version of this article.)

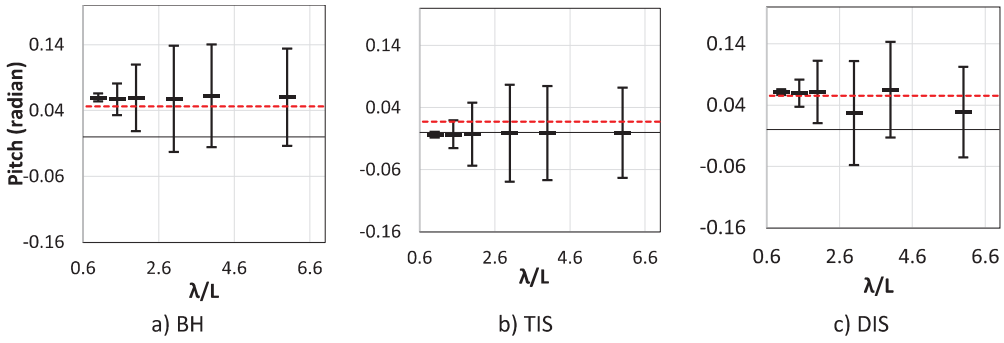


Fig. 22. Pitch motion responses for $\varepsilon = 0.07$ on three hull configurations. The dashed red line indicates the experimentally measured calm water trim angle. (For interpretation of the references to colour in this figure legend, the reader is referred to the Web version of this article.)

forward interceptor has a substantial overall hydrodynamic influence despite the relatively localized low-pressure region visible at the particular instant shown in Fig. 26.

Overall, the combined analysis of hull position and pressure distribution shows that the interceptor systems influence the vessel response not only by changing motion amplitudes but also by modifying the hydrodynamic interaction between the hull and the free surface. Maintaining hydrodynamic support through a more favorable pressure distribution is expected to reduce the likelihood of complete hull separation from the water surface. This mechanism provides the basis for the fly-over analysis presented in the following section. These pressure fields are used here only to explain the mechanism qualitatively, from four-time instants per condition; vertical force, trim moment, and center of pressure were not computed by integrating pressure over the wetted surface, so the mechanism proposed below is illustrative rather than quantitatively established.

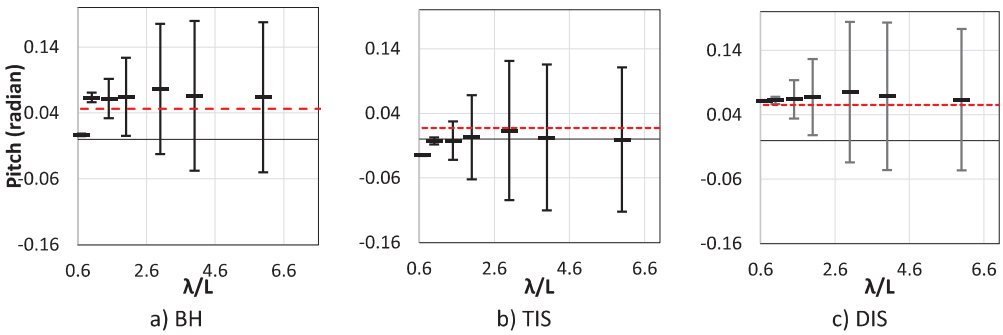


Fig. 23. Pitch motion responses for $\varepsilon = 0.10$ on three hull configurations. The dashed red line indicates the experimentally measured calm water trim angle. (For interpretation of the references to colour in this figure legend, the reader is referred to the Web version of this article.)

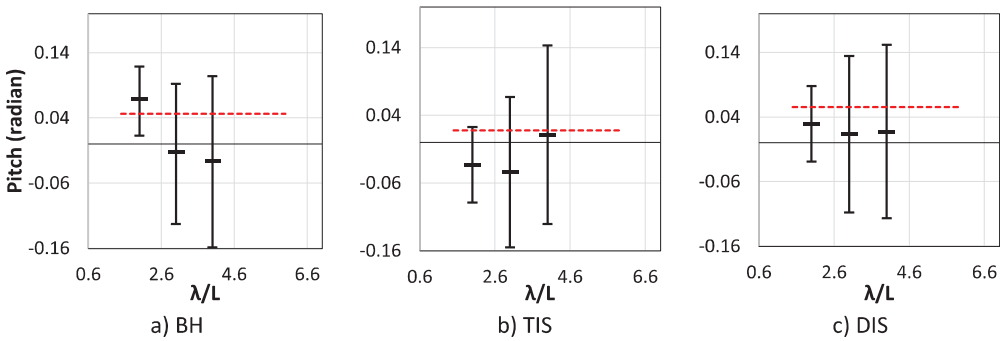


Fig. 24. Pitch motion responses for $\varepsilon = 0.12$ on three hull configurations. The dashed red line indicates the experimentally measured calm water trim angle. (For interpretation of the references to colour in this figure legend, the reader is referred to the Web version of this article.)

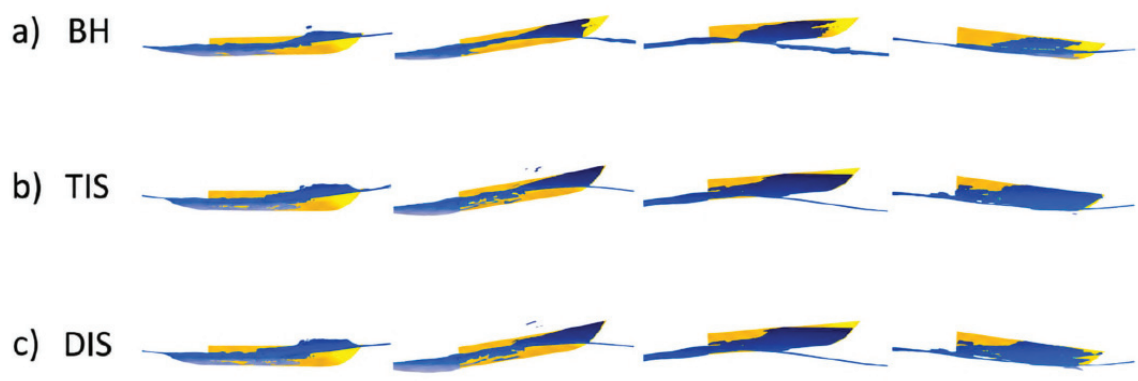


Fig. 25. Positions of hull configurations in a regular wave with $\varepsilon = 0.10$ and $\lambda/L = 4$.

4.3. fly-over phenomenon

Based on the RAO analysis in Section 4.1, the most severe vessel responses occur near the critical wavelengths $\lambda/L = 3$ and $\lambda/L = 4$, where the largest heave, pitch, and vertical acceleration responses are observed. These wave conditions are therefore the most likely to induce hull separation from the free surface and subsequent slamming during re-entry. Since both phenomena are directly associated with the occupants' safety, the fly-over behavior of the three hull configurations is compared in detail under the considered regular-wave conditions.

In the present study, fly-over is defined as the period during which the hull completely loses hydrodynamic contact with the water surface while passing over a wave crest. During this interval, the hydrodynamic pressure acting on the hull bottom approaches zero and the vessel motion is governed primarily by gravity and inertia. Consequently, the measured vertical acceleration approaches $-g$, corresponding to a near

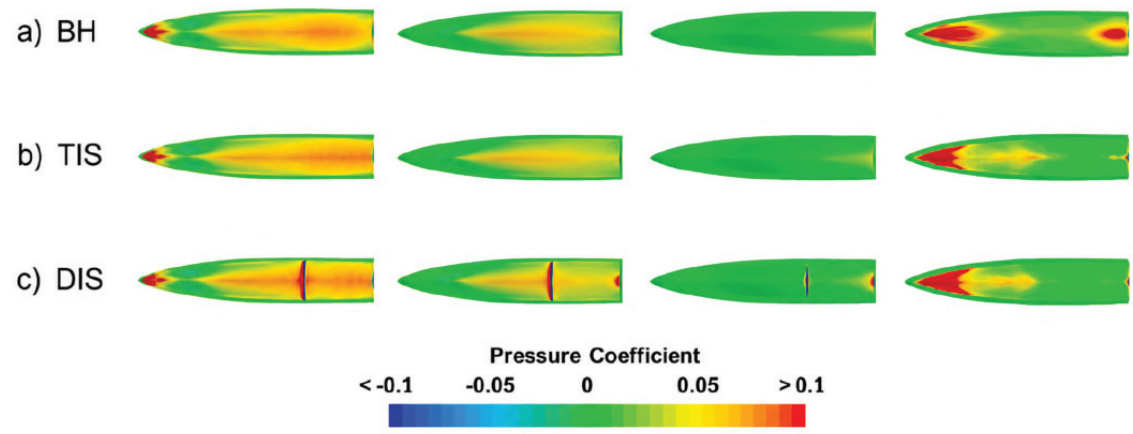


Fig. 26. Pressure distributions for hull configurations in a regular wave with $\varepsilon = 0.10$ and $\lambda/L = 4$.

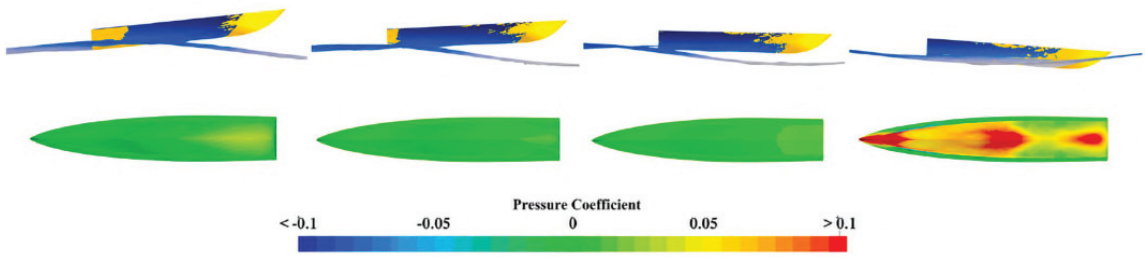


Fig. 27. Fly-over phenomenon for the bare hull under the critical wave condition $\varepsilon = 0.12$ and $\lambda/L = 3$.

free-fall condition. The fly-over phase begins at the instant of hull-water separation and ends when the hull re-establishes contact with the free surface during re-entry.

Fig. 27 shows a typical fly-over phenomenon for the bare hull under the critical wave condition of $\varepsilon = 0.12$ and $\lambda/L = 3$. The corresponding snapshots of hull position and pressure distribution demonstrate the physical evolution of the fly-over phenomenon. As the hull rises over the wave crest, the hydrodynamic pressure on the hull bottom reduces. At complete separation, the pressure acting on the hull bottom nearly disappears, confirming the loss of hydrodynamic support. During subsequent re-entry, hydrodynamic pressure rapidly recovers, which generates the impact force responsible for the large positive acceleration peaks.

These observations indicate that the fly-over phenomenon is governed by the progressive reduction of hydrodynamic support rather than by the hull motion alone. Therefore, the evolution of pressure distribution provides the physical mechanism responsible for the acceleration response discussed in the previous sections.

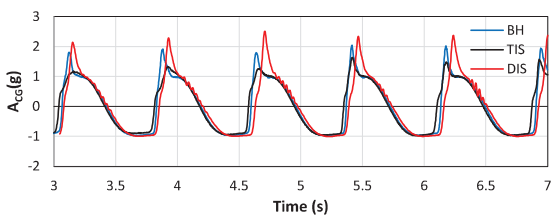


Fig. 28. Time history of vertical acceleration for the hull configurations under $\varepsilon = 0.12$ and $\lambda/L = 3$.

A comparison between time history of vertical acceleration of the bare hull, the TIS-equipped hull, and the DIS-equipped hull are presented in Fig. 28 for the critical wave condition $\varepsilon = 0.12$ and $\lambda/L = 3$. For all three configurations, the acceleration decreases toward -g, indicating hull separation and re-entry to the water surface. After re-entry, a sharp positive acceleration peak is generated by the slamming impact.

Although fly-over occurs for all investigated configurations, noticeable differences are observed in both impact acceleration magnitude and airborne duration. Airborne duration is defined as the time interval between hull separation from the water surface and re-entry, during which the vertical acceleration approaches -g.

As shown in Fig. 28, the TIS-equipped hull has the shortest airborne duration and the lowest impact acceleration, indicating that the interceptor improved hydrodynamic support and moderated the slam impact compared with the bare hull. In contrast, the DIS-equipped hull remains near the free-fall condition (vertical acceleration close to -g) for a longer period and experiences larger impact accelerations after water re-entry, indicating a more severe fly-over compared to the bare hull.

4.4. Quantitative vertical loading during re-entry

To further quantify the re-entry behavior identified from the motion, acceleration, and free-surface results, the vertical hydrodynamic force was examined for five representative conditions covering the critical response range: $(\varepsilon, \lambda/L) = (0.07, 3)$, $(0.10, 3)$, $(0.10, 4)$, $(0.12, 3)$, and

Table 6
Cycle-ensemble mean peak full-craft vertical force and peak absolute vertical acceleration at the centre of gravity for the selected re-entry conditions. Values following ± denote the standard deviation over the N retained cycles. Δ is the change in mean peak vertical force relative to the Bare Hull at the same wave condition.

ε	λ/L	Configuration	$F_{z,max}/W$	Δ (%)	$\lvert a_z\rvert_{max}/g$
0.07	3	Bare Hull	1.653 ± 0.017	ref.	0.649 ± 0.016
		TIS	1.656 ± 0.012	+0.2	0.651 ± 0.012
		DIS	1.901 ± 0.061	+15.0	0.712 ± 0.023
0.10	3	Bare Hull	2.538 ± 0.032	ref.	1.518 ± 0.031
		TIS	2.545 ± 0.085	+0.3	1.531 ± 0.084
		DIS	2.530 ± 0.107	−0.3	1.519 ± 0.107
0.10	4	Bare Hull	1.850 ± 0.020	ref.	0.838 ± 0.017
		TIS	1.800 ± 0.026	−2.7	0.797 ± 0.026
		DIS	1.807 ± 0.020	−2.3	0.803 ± 0.019
0.12	3	Bare Hull	2.971 ± 0.133	ref.	1.916 ± 0.103
		TIS	2.573 ± 0.082	−13.4	1.556 ± 0.075
		DIS	4.978 ± 0.314	+67.6	2.313 ± 0.151
0.12	4	Bare Hull	8.440 ± 0.582	ref.	2.657 ± 0.224
		TIS	2.981 ± 0.347	−64.7	1.263 ± 0.150
		DIS	3.199 ± 0.037	−62.1	1.099 ± 0.130

(0.12, 4). Only the established cyclic part of each simulation was considered, thereby excluding the initial transient response. Analysis of repeated steady impact cycles, rather than isolated instantaneous peaks, is particularly relevant for planing craft because re-entry loads may exhibit appreciable cycle-to-cycle variability even under nominally regular-wave conditions (Camilleri et al., 2018; Judge et al., 2020).

For each retained steady cycle, the maximum normalized force was determined. The value used for comparison is the cycle-ensemble mean,

$$\left\langle \frac{F_z}{W} \right\rangle_{max} = \frac{1}{N} \sum_{i=1}^{N} \left(\frac{F_z}{W} \right)_{max,i}, \tag{12}$$

where N is the number of analyzed steady cycles, F_z is full-craft vertical hydrodynamic force, and $W = mg$, in which m denotes the displacement mass and g the gravitational acceleration. In order to compare the temporal development of the impact between configurations, individual cycles were aligned on the instant of maximum vertical force, $t_{Fz,max}$, and time was normalized by the encounter period, T_e, giving the phase variable $(t - t_{Fz,max})/T_e$. This representation removes the dependence on absolute simulation time and permits a direct comparison of the Bare Hull, TIS and DIS re-entry pulses. The resulting cycle-averaged peak vertical forces and corresponding peak CG accelerations are summarized in Table 6, while Fig. 29 provides the comparison of the mean peak vertical force across the selected wave conditions.

Fig. 29 summarizes the mean peak vertical force over the selected wave conditions. For the lower and moderate wave conditions, the differences among the configurations are comparatively small. As shown in Table 6, at $\varepsilon = 0.07$ and $\lambda/L = 3$, the mean peak values are $1.653W$, $1.656W$, and $1.901W$ for the Bare Hull, TIS, and DIS, respectively. At $\varepsilon = 0.10$ and $\lambda/L = 3$, all three configurations produce approximately the same peak load (2.530-$2.545W$). Likewise, at $\varepsilon = 0.10$ and $\lambda/L = 4$, the peak loads remain within the relatively narrow range 1.800-$1.850W$.

A considerably stronger configuration dependence is observed for $\varepsilon = 0.12$. At $\lambda/L = 3$, the Bare Hull reaches $2.971W$, while TIS reduces the peak to $2.573W$, corresponding to a reduction of approximately 13.4%. In contrast, DIS produces a pronounced re-entry peak of $4.978W$, approximately 67.6% above the Bare Hull value. The corresponding peak CG accelerations reported in Table 6 are $1.916g$, $1.556g$, and $2.313g$ for the Bare Hull, TIS, and DIS, respectively. The consistent force and acceleration trends confirm the more severe re-entry of DIS for this condition.

At $\varepsilon = 0.12$ and $\lambda/L = 4$, the loading mechanism changes markedly. The Bare Hull experiences a narrow and intense vertical-force peak of $8.440W$. TIS and DIS reduce the peak to $2.981W$ and $3.199W$, corresponding to reductions of approximately 64.7% and 62.1%, respectively. The same behavior is evident in the CG acceleration, which decreases from $2.657g$ for the Bare Hull to $1.263g$ for TIS and $1.099g$ for DIS. The phase-aligned force histories in Fig. 30 show that the interceptor-equipped configurations substantially modify the magnitude and temporal development of the re-entry load.

The strong dependence of the response on wavelength and interceptor configuration is consistent with the highly nonlinear nature of planing-hull operation in waves. Previous experimental and numerical investigations have shown that slamming and re-entry loads are strongly influenced by instantaneous hull attitude, wetted-surface evolution, wave encounter characteristics, and intermittent emergence and re-entry of the hull (Judge et al., 2020; Tavakoli et al., 2026). In particular, Tavakoli et al. (2026) showed that intermediate-wave conditions can involve airborne motion followed by slamming, while variations in the instantaneous wetted surface contribute significantly to the nonlinear response of planing hulls. The present results therefore indicate that interceptor effectiveness cannot be characterized by a single wave condition: TIS reduces the severe re-entry peak at both

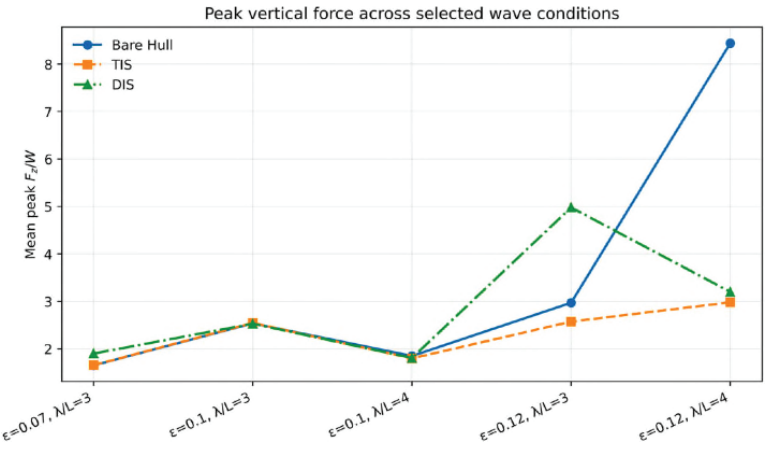


Fig. 29. Cycle-ensemble mean peak vertical force, $Fz,max/W$, for the bare Hull, TIS, and DIS configurations at the selected wave conditions. The vertical force corresponds to the full craft; the STAR-CCM + half-domain force was multiplied by two before normalization by vessel weight.

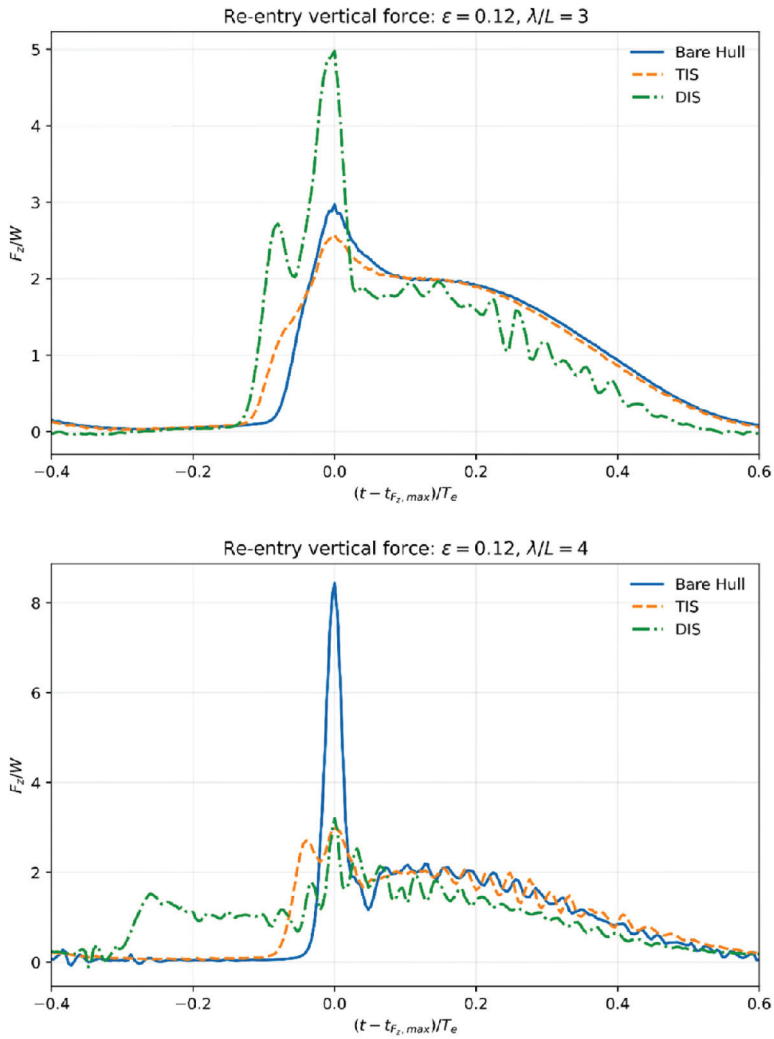


Fig. 30. Phase-aligned full-craft vertical-force histories during re-entry for the Bare Hull, TIS, and DIS configurations at $\varepsilon = 0.12$: (a) $\lambda/L = 3$ and (b) $\lambda/L = 4$. Time is referenced to the instant of maximum vertical force and normalized by the encounter period, T_e. Only the established cyclic portion of each simulation is included.

investigated conditions, whereas the DIS response is considerably more condition dependent.

5. Conclusion

The effects of a transom interceptor system (TIS) and a double interceptor system (DIS) on the dynamic response of a high-speed planing craft (HSPC) operating in regular waves were investigated using combined experimental and numerical approaches. The numerical model was validated against towing tank measurements of heave, pitch, and vertical acceleration and was then applied to a systematic range of regular wave conditions.

The results showed that the critical heave response consistently occurred around $\lambda/L \approx 3$, whereas the maximum pitch response occurred around $\lambda/L \approx 3$-4, depending on wave steepness. The interceptor systems did not significantly shift the critical wavelengths associated with the maximum heave and pitch responses. Under wave steepnesses $\varepsilon = 0.07$ and $\varepsilon = 0.10$, both interceptor configurations produced only minor changes in RAOs compared with the bare hull.

Differences between the interceptor configurations became more pronounced at higher wave steepness conditions. The TIS generally maintained hull motions close to those of the bare hull while producing more favorable mean motion characteristics. In contrast, the DIS tended to increase pitch response and showed less favorable dynamic behavior under the investigated severe wave conditions.

The analyses of hull position and pressure distribution clarified the physical mechanisms responsible for these differences. The TIS maintained a more continuous pressure distribution on the hull bottom, preserving hydrodynamic support over a larger portion of the wave encounter. However, the DIS-equipped hull experienced an earlier loss of hydrodynamic support.

The fly-over analysis further demonstrated that all three configurations experienced hull separation under severe wave conditions, however the severity of this phenomenon differed considerably. The TIS reduced airborne duration and the subsequent impact acceleration during water re-entry, whereas the DIS produced the longest airborne

interval and the highest impact severity, which may adversely affect occupant safety. These findings indicate that the TIS is the most effective of the configurations investigated for improving seakeeping performance and reducing the safety risks associated with fly-over events.

The quantitative re-entry analysis confirms that interceptor effectiveness is strongly wave-condition dependent. At $\varepsilon = 0.12$ and $\lambda/L = 3$, TIS reduced the cycle-ensemble mean peak vertical force by 13.4%, whereas DIS increased it by 67.6% relative to the Bare Hull. At $\varepsilon = 0.12$ and $\lambda/L = 4$, TIS and DIS reduced the mean peak force by 64.7% and 62.1%, respectively.

5.1. Limitations and future work

This study was limited to one TIS configuration, and one DIS configuration. Interceptor height, blade length, and longitudinal position were not varied, although these parameters significantly affect hydrodynamic performance. The analysis was also conducted at a single beam Froude number ($Fr_B = 3.0$); therefore, the influence of operating speed was not addressed. Moreover, the wave analysis was limited to a selected set of regular head wave conditions. These conditions were selected to provide a systematic comparison of the hydrodynamic responses of the bare hull, TIS, and DIS configurations, rather than to represent the full operational envelope of high-speed planing craft. Therefore, the results should be interpreted as configuration-specific insights under the investigated operating and wave conditions, and the observed trends should not be directly generalized to other wave directions, wave characteristics, or operating conditions without further verification. Nevertheless, the systematic regular-wave analysis provides a useful basis for identifying critical wavelength ranges, comparing the relative performance of the investigated configurations, and selecting relevant conditions for subsequent studies under more realistic operational environments.

Future studies should evaluate a broader range of interceptor geometries, hull speeds, and wave conditions to determine whether the trends observed here remain valid under more realistic operating conditions.

CRediT authorship contribution statement

Fatemeh Roshan: Writing – original draft, Visualization, Validation, Software, Methodology, Investigation, Formal analysis, Data curation, Conceptualization. **Rasul Niazmand Bilandi:** Writing – review & editing, Validation, Software, Investigation, Data curation, Conceptualization. **Fabio de Luca:** Writing – review & editing, Resources, Conceptualization. **Simone Mancini:** Writing – review & editing, Supervision, Conceptualization. **Mihkel Kõrgesaar:** Writing – review & editing, Supervision, Formal analysis.

Declaration of competing interest

The authors declare that they have no known competing financial interests or personal relationships that could have appeared to influence the work reported in this paper.

Appendix A. Detailed Grid-Verification Results

The mesh-series data in Appendix A were re-evaluated using the same formal ITTC/Eça-Hoekstra procedure described in Section 2.3.2. Numerical uncertainty was quantified for the response amplitudes and for the available mean pitch and heave values. All fitted apparent orders were greater than two and are associated with the plateauing response on the finer grids rather than with higher-order numerical accuracy. The fixed second-order least-squares estimator provided the smallest standard deviation, and the conservative safety factor $F_S = 3$ was used. The M3 row is shaded because M3 is the production mesh selected for each configuration.

A.1 Bare Hull

For the selected M3 mesh, the numerical uncertainties in pitch amplitude, heave amplitude, and vertical-acceleration amplitude are 12.84%, 14.03%, and 16.36%, respectively. The original CFD-to-experiment errors from Appendix A are retained in the tables, while the formal numerical-uncertainty estimate is added for each grid.

Table A1
Formal grid-verification results for pitch motion of the Bare Hull. Experimental values: pitch amplitude = 1.06 deg; mean pitch = 3.92 deg.

Mesh	Cells	r_i	CFD amp.	Uφ amp. (%)	Reported error amp. (%)	CFD mean	Uφ mean (%)	Reported error mean (%)
M1	1,474,284	1.748	0.99	23.05	−6.60	3.48	26.01	−11.22
M2	2,240,911	1.520	1.02	17.18	−4.25	3.56	19.19	−9.18
M3	3,406,185	1.322	1.03	12.84	−2.83	3.63	14.77	−7.40
M4	5,177,401	1.150	1.04	9.82	−2.36	3.66	10.99	−6.63
M5	7,869,650	1.000	1.04	7.83	−2.17	3.67	8.69	−6.38

Table A2
Formal grid-verification results for heave motion of the Bare Hull. Experimental values: heave amplitude = 13.92 mm; mean heave = −2.33 mm.

Mesh	Cells	r_i	CFD amp.	Uφ amp. (%)	Reported error amp. (%)	CFD mean	Uφ mean (%)	Reported error mean (%)
M1	1,474,284	1.748	10.90	24.74	−21.70	−3.18	34.75	36.48
M2	2,240,911	1.520	11.12	18.40	−20.11	−3.08	27.08	32.19
M3	3,406,185	1.322	11.33	14.03	−18.61	−2.99	22.09	28.33
M4	5,177,401	1.150	11.43	10.48	−17.89	−2.96	16.59	27.04
M5	7,869,650	1.000	11.47	8.18	−17.60	−2.95	13.36	26.61

Table A3
Formal grid-verification results for vertical acceleration of the Bare Hull. Experimental amplitude = 3.51 m/s^2.

Mesh	Cells	r_i	CFD amplitude	Uφ (%)	Reported error (%)
M1	1,474,284	1.748	2.41	29.27	−31.38
M2	2,240,911	1.520	2.47	21.57	−29.67
M3	3,406,185	1.322	2.52	16.36	−28.21
M4	5,177,401	1.150	2.55	12.29	−27.45
M5	7,869,650	1.000	2.56	9.54	−27.16

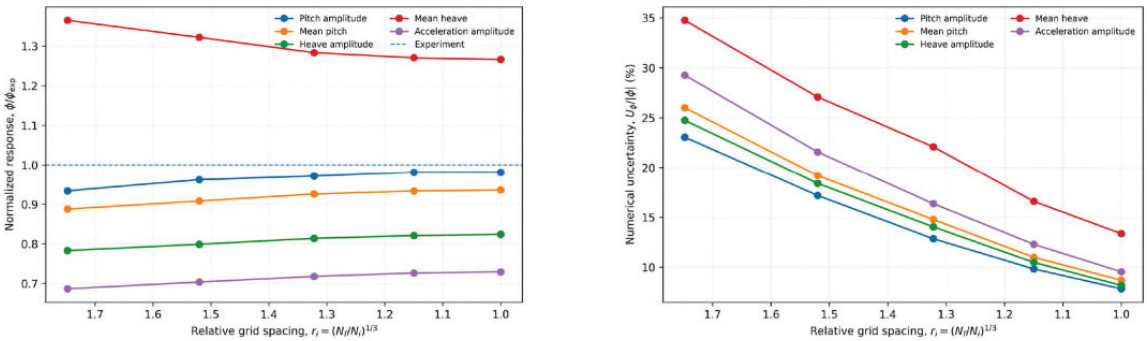


Fig. A1. Formal grid-verification results for the Bare Hull: (a) numerical responses normalized by the corresponding experimental values; (b) estimated numerical uncertainty as a function of relative grid spacing, $r_i = (N_f/N_i)^{1/3}$.

A.2 TIS

For the selected M3 mesh, the numerical uncertainties in pitch amplitude, heave amplitude, and vertical-acceleration amplitude are 14.34%, 13.22%, and 18.68%, respectively. The original CFD-to-experiment errors from Appendix A are retained in the tables, while the formal numerical-uncertainty estimate is added for each grid.

Table A4
Formal grid-verification results for pitch motion of the TIS. Experimental values: pitch amplitude = 0.92 deg; mean pitch = −0.17 deg.

Mesh	Cells	r_i	CFD amp.	Uφ amp. (%)	Reported error amp. (%)	CFD mean	Uφ mean (%)	Reported error mean (%)
M1	1,596,529	1.748	0.98	22.74	5.98	−0.24	57.29	38.24
M2	2,426,724	1.520	0.96	17.48	3.80	−0.22	47.65	29.41
M3	3,688,620	1.322	0.94	14.34	2.17	−0.21	39.96	23.53
M4	5,606,702	1.150	0.94	10.77	1.74	−0.21	28.82	21.76
M5	8,522,188	1.000	0.93	8.18	1.52	−0.21	24.31	21.18

Table A5
Formal grid-verification results for heave motion of the TIS. Experimental values: heave amplitude = 7.51 mm; mean heave = 14.30 mm.

Mesh	Cells	r_i	CFD amp.	Uφ amp. (%)	Reported error amp. (%)	CFD mean	Uφ mean (%)	Reported error mean (%)
M1	1,596,529	1.748	9.25	21.28	23.17	13.20	17.70	−7.69
M2	2,426,724	1.520	9.02	16.55	20.11	13.45	13.22	−5.94
M3	3,688,620	1.322	8.88	13.22	18.24	13.62	10.26	−4.76
M4	5,606,702	1.150	8.84	9.80	17.71	13.67	7.54	−4.41
M5	8,522,188	1.000	8.82	7.94	17.44	13.69	6.15	−4.27

Table A6
Formal grid-verification results for vertical acceleration of the TIS. Experimental amplitude = 1.75 m/s^2.

Mesh	Cells	r_i	CFD amplitude	Uφ (%)	Reported error (%)
M1	1,596,529	1.748	2.18	29.14	24.84
M2	2,426,724	1.520	2.11	22.90	20.55
M3	3,688,620	1.322	2.06	18.68	17.98
M4	5,606,702	1.150	2.05	13.78	17.51
M5	8,522,188	1.000	2.05	11.44	17.28

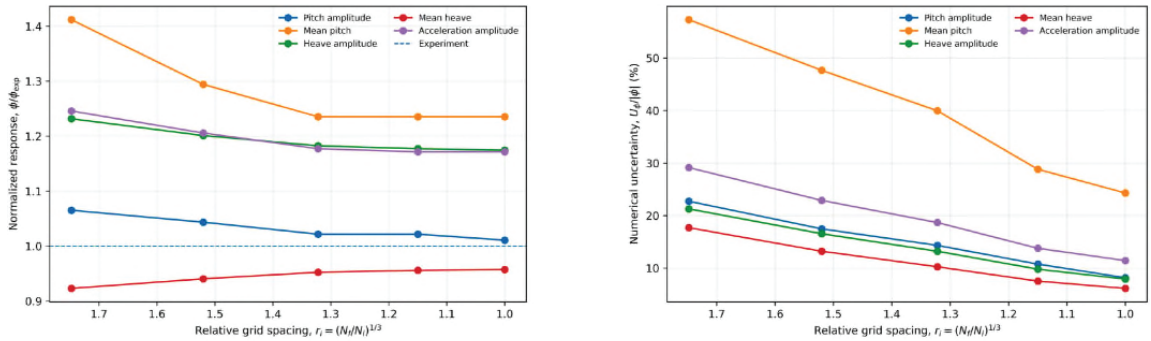


Fig. A2. Formal grid-verification results for the TIS: (a) numerical responses normalized by the corresponding experimental values; (b) estimated numerical uncertainty as a function of relative grid spacing, $r_i = (N_f/N_i)^{1/3}$.

A.3 DIS

For the selected M3 mesh, the numerical uncertainties in pitch amplitude, heave amplitude, and vertical-acceleration amplitude are 22.10%, 18.46%, and 21.78%, respectively. The original CFD-to-experiment errors from Appendix A are retained in the tables, while the formal numerical-uncertainty estimate is added for each grid.

Table A7
Formal grid-verification results for pitch motion of the DIS. Experimental values: pitch amplitude = 1.10 deg; mean pitch = 3.62 deg.

Mesh	Cells	r_i	CFD amp.	Uφ amp. (%)	Reported error amp. (%)	CFD mean	Uφ mean (%)	Reported error mean (%)
M1	2,156,033	1.748	0.88	39.22	−20.00	3.18	31.61	−12.15
M2	3,277,170	1.520	0.91	28.67	−17.27	3.27	23.20	−9.67
M3	4,981,298	1.322	0.94	22.10	−14.55	3.35	17.86	−7.46
M4	7,571,573	1.150	0.95	16.38	−13.91	3.38	13.21	−6.63
M5	11,508,791	1.000	0.95	13.19	−13.64	3.39	10.51	−6.35

Table A8
Formal grid-verification results for heave motion of the DIS. Experimental values: heave amplitude = 16.30 mm; mean heave = −9.53 mm.

Mesh	Cells	r_i	CFD amp.	Uφ amp. (%)	Reported error amp. (%)	CFD mean	Uφ mean (%)	Reported error mean (%)
M1	2,156,033	1.748	8.35	32.64	−48.77	−7.80	27.19	−18.15
M2	3,277,170	1.520	8.60	23.93	−47.24	−8.00	20.02	−16.05
M3	4,981,298	1.322	8.82	18.46	−45.89	−8.18	15.63	−14.17
M4	7,571,573	1.150	8.89	13.58	−45.46	−8.22	11.42	−13.75
M5	11,508,791	1.000	8.92	10.86	−45.28	−8.24	9.26	−13.54

Table A9
Formal grid-verification results for vertical acceleration of the DIS. Experimental amplitude = 3.86 m/s^2.

Mesh	Cells	r_i	CFD amplitude	Uφ (%)	Reported error (%)
M1	2,156,033	1.748	1.95	38.98	−49.51
M2	3,277,170	1.520	2.02	28.44	−47.70
M3	4,981,298	1.322	2.08	21.78	−46.15
M4	7,571,573	1.150	2.10	15.98	−45.63
M5	11,508,791	1.000	2.11	12.74	−45.50

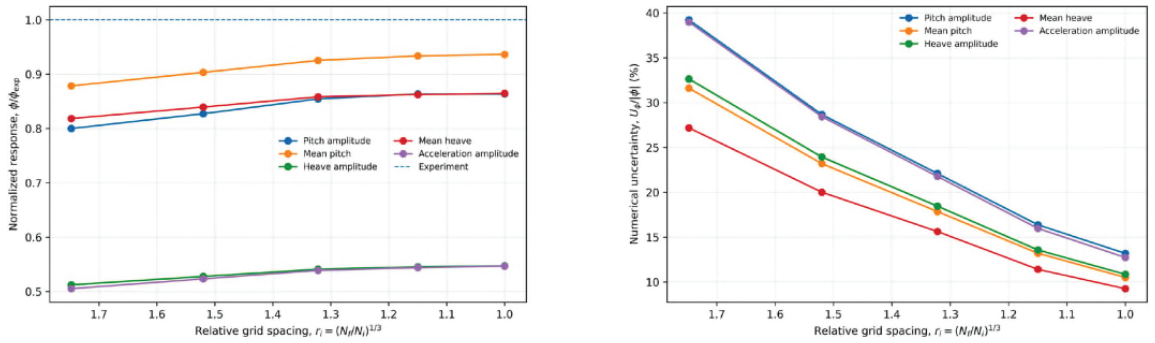


Fig. A3. Formal grid-verification results for the DIS: (a) numerical responses normalized by the corresponding experimental values; (b) estimated numerical uncertainty as a function of relative grid spacing, $r_i = (N_f/N_i)^{1/3}$.

References

Allen, D.P., Taunton, D.J., Allen, R., 2008. A study of shock impacts and vibration dose values onboard highspeed marine craft. Transact. Royal Instit.Naval Archit. Part: Int. J. Marit. Eng. 150 (A3), A3.

Avci, A.G., Barlas, B., 2019. An experimental investigation of interceptors for a high speed hull. Int. J. Nav. Archit. Ocean Eng. 11 (1), 256–273. https://doi.org/10.1016/j.ijnaoe.2018.05.001.

Bi, X., Zhuang, J., Su, Y., 2020. Seakeeping analysis of planing craft under large wave height. Water 12 (4), 1020. https://doi.org/10.3390/w12041020.

Biancolini, M.E., Chiappa, A., Cella, U., Costa, E., Groth, C., Porziani, S., 2020. Radial basis functions mesh morphing: a comparison between the bi-harmonic spline and the Wendland C2 radial function. In: Computational Science - ICCS 2020 (Lecture Notes in Computer Science, 12142. Springer, pp. 294–308. https://doi.org/10.1007/978-3-030-50433-5_23.

Bilandi, R.N., Dashtimanesh, A., Tavakoli, S., Mancini, S., 2025. Performance prediction of planing catamarans using mathematical and CFD models. In: Technology and Science for the Ships of the Future: Proceedings of the 21st International Conference on Ships and Maritime Research (NAV 2025), Messina, Italy, 18-20 June 2025, EC1Y 1SP. SAGE Publications, London, pp. 408–417. https://doi.org/10.3233/PMST250048. 1 Oliver's Yard, 55 City Road.

Bilandi, R.N., Mancini, S., Dashtimanesh, A., Tavakoli, S., 2024a. A revisited verification and validation analysis for URANS simulation of planing hulls in calm water. Ocean Eng. 293, 116589. https://doi.org/10.1016/j.oceaneng.2023.116589.

Bilandi, R.N., Tavakoli, S., Mancini, S., Dashtimanesh, A., 2024b. Dynamic motion analysis of stepless and stepped planing hulls in random waves: a CFD model perspective. Appl. Ocean Res. 149, 104046. https://doi.org/10.1016/j.apor.2024.104046.

British Standards Institution 6841(BS), 1987. Measurement and Evaluation of Human Exposure to Whole-Body Mechanical Vibration. BSI, London, UK, p. 6841.

Brizzolara, S., Villa, D., 2009. A systematic CFD analysis of flaps/interceptors hydrodynamic performance. In: Proceedings 10th International Conference on Fast Sea Transportation (FAST 2009). Athens.

Camilleri, J., Taunton, D.J., Temarel, P., 2018. Full-scale measurements of slamming loads and responses on high-speed planing craft in waves. J. Fluid Struct. 81, 201–229. https://doi.org/10.1016/j.jfluidstructs.2018.05.006.

de Alwis, M.P., Garme, K., 2021. Effect of occupational exposure to shock and vibration on health in high-performance marine craft occupants. Proc. IME M J. Eng. Marit. Environ. 235 (2), 394–409. https://doi.org/10.1177/1475090220981188.

De Luca, F., Pensa, C., 2012. Experimental investigation on conventional and unconventional interceptors. Trans. RINA Part B Int. J. Small Craft. Tech 153, B65–B72.

De Luca, F., Pensa, C., 2012a. Unconventional interceptors in still water and in regular waves: experimental study on resistance reduction and dynamic instability. In: 17th International Conference on Ships and Shipping Research (NAV). Naples 17-19 October.

Deng, R., Zhang, Z., Luo, F., Sun, P., Wu, T., 2022. Investigation on the lift force induced by the interceptor and its affecting factors: experimental study with captive model. J. Mar. Sci. Eng. 10 (2), 211. https://doi.org/10.3390/jmse10020211.

Eça, L., Hoekstra, M., 2014. A procedure for the estimation of the numerical uncertainty of CFD calculations based on grid refinement studies. J. Comput. Phys. 262, 104–130. https://doi.org/10.1016/j.jcp.2014.01.006.

EU Directive 2002/44/EC, 2002. Directive 2002/44/EC of the European Parliament and of the Council of 25th June 2002 on the Minimum Health and Safety Requirements Regarding the Exposure of Workers to the Risks Arising from Physical Agents (Vibration).

Fenton, J.D., 1985. A fifth-order Stokes theory for steady waves. J. Waterw. Port, Coast. Ocean Eng. 111 (2), 216–234. https://doi.org/10.1061/(ASCE)0733-950X(1985)111:2(216).

Folsø, R., 2004. Comfort Monitoring of High-Speed Passenger Ferries. Technical University of Denmark. PhD Thesis.

Fridsma, G., 1969. A Systematic Study of the Rough-Water Performance of Planing Boats. Davidson Laboratory, Stevens Institute of Technology, Hoboken, NJ, USA.

Garme, K., Burström, L., Kuttenkeuler, J., 2011. Measures of vibration exposure for a high-speed craft crew. Proc. IME M J. Eng. Marit. Environ. 225 (4), 338–349. https://doi.org/10.1177/1475090211418747.

Ghassemi, H., Mansouri, M., Zaferanlouei, S., 2011. Interceptor hydrodynamic analysis for handling trim control problems in the high-speed crafts. Proc. IME C J. Mech. Eng. Sci. 225 (11), 2597–2618.

International Towing Tank Conference (ITTC), 2024. Practical Guidelines for Ship CFD Applications. ITTC Recommended Procedures and Guidelines. No. 7.5-03-02-03, Revision 02, Effective Date 2024.

ISO 2631–5, 2004. Shock–Evaluation of Human Exposure to Whole Body Vibration–Part 5: Method for Evaluation of Vibration Containing Multiple Shocks. ISO, Geneva, Switzerland. https://www.iso.org/standard/7612.html.

ISO 2631-1, 1997. Mechanical Vibration and shock—Evaluation of Human Exposure to whole-body vibration—Part 1: General Requirements. International Organization for Standardization, ISO, 2631-1. https://www.iso.org/standard/7612.html.

ITTC, 2024. Uncertainty analysis in CFD verification and validation, methodology and procedures. Recomm. Proced. Guidel. 7.5-03-01-01, Revision 05, 15pp.

Jangam, S., Sahoo, P., 2021. Numerical investigation of interceptor effect on seakeeping behaviour of planing hull advancing in regular head waves. Brodogradnja 72, 73–92. https://doi.org/10.21278/brod72205.

Judge, C., Mousaviraad, M., Stern, F., Lee, E., Fullerton, A., Geiser, J., Schleicher, C., Merrill, C., Weil, C., Morin, J., Jiang, M., Ikeda, C., 2020. Experiments and CFD of a high-speed deep-V planing hull – part II: slamming in waves. Appl. Ocean Res. 97, 102059. https://doi.org/10.1016/j.apor.2020.102059.

Karimi, M.H., Seif, M.S., Abbaspoor, M., 2015. A study on vertical motions of high-speed planing boats with automatically controlled stern interceptors in calm water and head waves. Ships Offshore Struct. 10 (3), 335–348. https://doi.org/10.1080/17445302.2013.867647.

Kim, D.J., Kim, S.Y., You, Y.J., Rhee, K.P., Kim, S.H., Kim, Y.G., 2013. Design of high-speed planning hulls for the improvement of resistance and seakeeping performance. Int. J. Nav. Archit. Ocean Eng. 5 (1), 161–177. https://doi.org/10.2478/IJNAOE-2013-0124.

Lo Martire, R., de Alwis, M.P., Äng, B.O., Garme, K., 2017. Construction of a web-based questionnaire for longitudinal investigation of work exposure, musculoskeletal pain and performance impairments in high-performance marine craft populations. BMJ Open 7 (7), e016006. https://doi.org/10.1136/bmjopen-2017-016006.

Mansoori, M., Fernandes, A.C., 2015. Hydrodynamics of the interceptor on a 2-D flat plate by CFD and experiments. J. Hydrodyn. Ser. B 27 (6), 919–933. https://doi.org/10.1016/S1001-6058(15)60555-8.

Myers, S.D., Dobbins, T.D., King, S., Hall, B., Holmes, S.R., Gunston, T., Dyson, R., 2012. Effectiveness of suspension seats in maintaining performance following military high-speed boat transits. Hum. Factors 54 (2), 264–276. https://doi.org/10.1177/0018720811436201.

Park, J.Y., Choi, H., Lee, J., Choi, H., Woo, J., Kim, S., et al., 2019. An experimental study on vertical motion control of a high-speed planing vessel using a controllable interceptor in waves. Ocean Eng. 173, 841–850. https://doi.org/10.1016/j.oceaneng.2019.01.019.

Putra, A.M.F., Rahadi, C.W.K., Muryadin, M., Prasetyo, D.F., Noor, F.M., Setiyobudi, N., et al., 2026. Hydrodynamic evaluation of interceptor configuration on a high-speed ship with tunnel propeller for resistance reduction. J. ETA Marit. Sci. https://doi.org/10.4274/jems.2026.45556.

Putra, A.M.F., Suzuki, H., 2024. Experimental and numerical study on the high-speed ship hydrodynamics influenced by an interceptor with varied angle of attack. Int. J. Nav. Archit. Ocean Eng. 16, 100566. https://doi.org/10.1016/j.ijnaoe.2023.100566.

Roshan, F., Bilandi, R.N., De Luca, F., Mancini, S., Kujala, P., Dashtimanesh, A., 2025b. High speed planing craft dynamics in irregular waves: safety improvement using interceptor systems. Appl. Ocean Res. 161, 104692. https://doi.org/10.1016/j.apor.2025.104692.

Roshan, F., Dashtimanesh, A., De Luca, F., Mancini, S., 2025a. High-speed craft with double interceptor system in calm water: URANS solution. Progr. Mar. Sci. Technol. https://doi.org/10.3233/PMST250047.

Roshan, F., Dashtimanesh, A., Kujala, P., 2024. Safety improvements for high-speed planing craft occupants: a systematic review. J. Mar. Sci. Eng. 12 (5), 845. https://doi.org/10.3390/jmse12050845.

Roshan, F., Tavakoli, S., Mancini, S., Dashtimanesh, A., 2022. Dynamic of tunneled planing hulls in waves. J. Mar. Sci. Eng. 10 (8), 1038. https://doi.org/10.3390/jmse10081038.

Şahin, O.S., Kahramanoglu, E., Cakici, F., 2022. Numerical evaluation on the effects of interceptor layout and blade heights for a prismatic planing hull. Appl. Ocean Res. 127, 103302. https://doi.org/10.1016/j.apor.2022.103302.

Sahin, O.S., Kahramanoglu, E., Cakici, F., Pesman, E., 2023. Control of dynamic trim for planing vessels with interceptors in terms of comfort and minimum drag. Brodogradnja: Int. J. Naval Archit. Ocean Eng. Res. Develop. 74 (1), 1–17. https://doi.org/10.21278/brod74101.

Samuel, S., Mursid, O., Yulianti, S., Kiryanto, K., Iqbal, M., 2022a. Evaluation of interceptor design to reduce drag on planing hull. Brodogradnja: Int. J. Naval Archit. Ocean Eng. Res. Develop. 73 (3), 93–110. https://doi.org/10.21278/brod73306.

Samuel, S., Yulianti, S., Manik, P., Fathuddiin, A., 2022b. A study of interceptor performance for deep-v planing hull. In: IOP Conference Series: Earth and Environmental Science, 1081. IOP Publishing, 012004. https://doi.org/10.1088/1755-1315/1081/1/012004. No. 1.

Seo, K.C., Gopakumar, N., Atlar, M., 2013. Experimental investigation of dynamic trim control devices in fast speed vessel. J. Navig. Port Res. 37 (2), 137–142.

Seok, W., Park, S.Y., Rhee, S.H., 2020. An experimental study on the stern bottom pressure distribution of a high-speed planing vessel with and without interceptors. Int. J. Nav. Archit. Ocean Eng. 12, 691–698. https://doi.org/10.1016/j.ijnaoe.2020.08.003.

Sorrentino, V., Pigazzini, R., De Luca, F., Mancini, S., Pensa, C., 2025. Experimental and numerical investigation of air lubrication on a planing hull with double interceptor system. Ocean Eng. 319, 120135. https://doi.org/10.1016/j.oceaneng.2024.120135.

Suneela, J., Krishnankutty, P., Anantha Subramanian, V., 2020. Numerical investigation on the hydrodynamic performance of high-speed planing hull with transom interceptor. Ships Offshore Struct. 15 (Suppl. 1), S134–S142. https://doi.org/10.1080/17445302.2020.1738134.

Tavakoli, S., Bilandi, R.N., Roshan, F., Singh, M., Mancini, S., 2026. Planing hull dynamics in water waves: physical insights from nonlinear strip theory models and fully nonlinear computational fluid dynamics simulations. Phys. Fluids 38 (2). https://doi.org/10.1063/5.0311446.

Appendix 5 (Publication V)

Paper V

Roshan, F., Niazmand Bilandi, R., De Luca, F., Mancini, S., Kujalaa, P., Dashtimanesh, A., (2025). High Speed Planing Craft Dynamics in Irregular waves: Safety Improvement using Interceptor Systems. Applied Ocean Research. https://doi.org/10.1016/j.apor.2025.104692.

Applied Ocean Research 161 (2025) 104692

Contents lists available at ScienceDirect

Applied Ocean Research

journal homepage: www.elsevier.com/locate/apor

High speed planing craft dynamics in irregular waves: Safety improvement using interceptor systems

Fatemeh Roshan [a,*], Rasul Niazmand Bilandi [a,b], Fabio De Luca [c], Simone Mancini [c], Pentti Kujala [a], Abbas Dashtimanesh [d]

[a] Estonian Maritime Academy, Tallinn University of Technology, Tallinn, Estonia
[b] Department of Aero and Hydrodynamics, Force Technology, Kgs. Lyngby, Denmark
[c] Department of Industrial Engineering, University of Naples "Federico II," Naples, Italy
[d] Engineering Mechanics Department, School of Engineering Science, KTH Royal Institute of Technology, 100 44 Stockholm, Sweden

ARTICLE INFO

Keywords:
High speed planing craft
Irregular head waves
Human safety
Interceptor
Double interceptor system

ABSTRACT

This study investigates the potential for improving the dynamic performance and human safety of High-Speed Planing Craft (HSPC) in irregular head waves through the implementation of a Transom Interceptor System (TIS) and a Double Interceptor System (DIS). Experimental tests measure hull resistance, heave and pitch motions, and vertical accelerations in semi-planing, transient, and planing modes. The recorded data for the bare hull, the hull equipped with TIS in transient mode, and the hull equipped with TIS and DIS in planing mode are compared to evaluate the interceptor performance in improving the dynamics of HSPC. Additionally, the crew safety exposed to vertical acceleration is evaluated according to the ISO 2631–1 (1997), ISO 2631–5 (2004), and EU Directive 2002/44/EC (2002). The results indicate that TIS effectively enhances dynamic performance in transient and planing modes as well as human safety and comfort by reducing moderate vertical acceleration. However, in transient mode, TIS may amplify impact shocks, increasing the possibility of adverse health effects. Moreover, the DIS increases hull motions, vertical acceleration, and the potential for health and comfort risks in planing mode. These findings emphasize the potential of TIS in enhancing HSPC dynamics and safety, while it is crucial to optimize interceptor configurations based on operational speeds.

1. Introduction

High-speed planing craft (HSPC) are commonly used in various maritime missions that demand high-speed operations, such as patrol, racing, and search and rescue. However, the performance of HSPC in rough waters is significantly influenced by the hull's dynamic behavior and crew's safety.

Operating at high speeds in rough waters exposes HSPCs to severe hull motions and harsh accelerations, as demonstrated by Roshan et al. (2022) and Niazmand Bilandi et al. (2024). These conditions can lead to increased structural stress, compromised hull stability and control, and safety risks for crews exposed to such accelerations. The effect of vertical accelerations on human health and comfort aboard high-speed craft has been analyzed by Allen et al. (2008), Dobbins et al., (2008), Garme et al. (2011), and Taunton et al. (2011), indicating a high possibility of safety risks for onboard crews.

While reducing hull speed on rough water can effectively minimize hull motions and accelerations and consequently reduce the probability of adverse health risks for the crews, it contradicts the primary purpose of HSPCs, particularly in time-critical missions such as rescue operations. As a result, improving HSPC performance necessitates the implementation of shock/vibration mitigation devices to reduce the transfer of hull accelerations to the human body, as well as motion reduction devices to prevent severe accelerations in rough seas (Roshan et al., 2024).

Although both strategies improve human safety onboard the HSPC, motion reduction devices offer additional advantages. These devices not only reduce the risk of adverse health effects caused by hull accelerations but also improve hull stability and control (Lau et al., 2024; Niazmand Bilandi, 2024). These are useful to reduce the likelihood of critical events such as loss of stability, impaired maneuverability, or even hull capsizing under challenging wave conditions by minimizing excessive motions. This improvement underscores the importance of implementing advanced motion-control devices to ensure both safety and dynamic performance.

* Corresponding author.
E-mail address: fatemeh.roshan@taltech.ee (F. Roshan).

https://doi.org/10.1016/j.apor.2025.104692
Received 12 February 2025; Received in revised form 27 May 2025; Accepted 30 June 2025
Available online 7 July 2025
0141-1187/© 2025 The Author(s). Published by Elsevier Ltd. This is an open access article under the CC BY license (http://creativecommons.org/licenses/by/4.0/).

Nomenclature and observations

A_{iz} i^{th}	peak of acceleration between two zero crossings
$a_{1/n}$	Mean of 1/n highest height of vertical acceleration
$a_w(t)$	Frequency-weighted acceleration signals (ms^{-2})
B_{WL}	Maximum moulded breadth at water line (m)
F_p	Peak frequency
Fr_B	Beam Froude number
g	Acceleration of gravity (ms-2)
CG	Centre of Gravity
$H_{1/n}$	Mean of 1/n highest height of heave motion
H_s	Significant wave height (m)
K	Wave number (m^{-1}), ω^2/g
K_{xx}	Roll radius of gyration (m)
K_{yy}	Pitch radius of gyration (m)
L_{CG}	Longitudinal center of gravity (m)
L_{OA}	Overall length of the hull
L_{WL}	Length of waterline (m)
m	Applied mas (kg)
R_w	Total resistance of model in waves (kg)
S	Wave steepness (radian), $K.H_s/2$.
T	Measurement time (s)
t_d	Duration of the daily exposure
T_p	Peak period (s)
V_{CG}	Vertical center of gravity (m)
x	Distance from the center screw (m)
β_T	Deadrise angle at the transom (deg)
$\beta_{0.5}$	Deadrise angle at 0.5 L_{WL} (deg)
$\beta_{0.75}$	Deadrise angle at 0.75 L_{WL} (deg)
γ	Overshoot Parameter
Δ	Displacement (buoyant) force (kg)
θ	Pitch or trim angle (deg)
$\theta_{1/n}$	Mean of 1/n highest height of pitch motion (deg)
λ	Wavelength (m)
ω	Angular Frequency ($radians^{-1}$), $\omega = 2\pi F_p$
CF	Crest Factor
DII	Dipartimento di Ingegneria Industriale
DIS	Double Interceptor System
HSPC	High Speed Planing Craft
ISO	International Standard Organization
NSS	Naples Systematic Series
PSD	Power Spectral Density
RMS	Root Mean Square of weighted frequency acceleration (ms^{-2})
SF	Scale Factor
TIS	Transom Interceptor System
VDV	Vibration Doze Value (ms^{-2})
WBV	Whole Body Vibration

There are numerous documents indicating that using a Transom Interceptor System (TIS) can efficiently reduce hull resistance and trim angle in calm water, such as John et al., (2011), Day and Cooper (2011), Karimi et al. (2013), and Seok et al. (2020). Furthermore, Najafi et al. (2015), Karimi et al. (2015), and Suneela and Sahoo (2021) highlighted the effectiveness of TIS in reducing vertical motions and accelerations in regular waves. However, despite these valuable insights, most existing research focuses on calm water or regular wave conditions, which do not fully represent the complex and random nature of real sea states. Therefore, the TIS performance in irregular wave conditions remains relatively limited, particularly regarding its influence on human safety.

Assessment of human safety affected by HSPC acceleration requires statistical analysis under irregular waves due to their random characteristics, as regular wave tests lack this complexity and cannot be statistically analyzed in accordance with safety standards (ISO 2631 or EU Directives). However, there is a significant knowledge gap concerning the effects of TIS in irregular wave conditions, which are critical for human safety assessments.

In addition to the conventional transom interceptor, De Luca and Pensa (2011) introduced an unconventional interceptor configuration consisting of a TIS and an additional interceptor located in the middle of hull length. This Double Interceptor System (DIS) is an innovative configuration designed to generate an extra lift force at the forward interceptor position, potentially leading to more reduction in hull motions. Furthermore, DIS can generate an air cavity behind the forward interceptor, which contributes to a reduction in hull shear resistance. The performance of DIS in calm water and regular waves has been presented in De Luca and Pensa (2012). They observed the possibility of increasing hull motions and accelerations when using DIS in regular waves, though it is efficient in resistance reduction. However, the dynamic performance of a hull equipped with DIS in irregular waves remains unexplored, highlighting a gap that must be addressed for a comprehensive understanding of DIS behavior.

Although interceptors are designed to reduce hull motions and resistance, their performance can significantly vary depending on the hull's operational speeds. For instance, Tsai and Hwang, (2004), Mansoori and Fernandes (2017), and Suneela et al. (2020) demonstrate the possibility of negative trim angles (bow down) in planing mode when an improperly designed interceptor is employed. However, these studies also highlight that such an interceptor can be effective in correcting trim angle and reducing hull resistance at lower speeds. This variability underscores the importance of designing interceptors that are optimized for the intended operational speed range for the hull. An interceptor optimized for lower speeds might become unsuitable at higher speeds, potentially leading to stability issues and compromising overall performance.

In addition to the importance of selecting an appropriately designed interceptor for an HSPC to minimize hull motions and resistance at operational speeds, it is also crucial to consider the impact of interceptors on motion accelerations. This aspect directly affects human safety onboard the HSPCs, as severe accelerations can cause discomfort, fatigue, and impaired the crew performance and their ability to carry out duties, and adverse health effects. Therefore, designing an appropriate interceptor must prioritize both dynamic efficiency and reducing vertical acceleration to enhance human safety.

This study aims to investigate the potential for improving the dynamic behaviors of HSPCs and crews' safety in irregular head seas by employing different configurations of interceptors tailored to operational speeds. To achieve this, the objectives include:

- Improving HSPC seakeeping and the crew's safety onboard in transient mode using TIS.
- Improving HSPC seakeeping and the crew's safety onboard in planing mode using TIS and DIS.

By addressing these objectives, this study seeks to provide valuable insights into the potential for improving both the dynamic performance of HSPCs and human safety under realistic sea conditions by employing an interceptor system.

For this purpose, a high-speed planing hull, model C5, is tested in a towing tank under three different irregular wave conditions at various speeds, representing semi-planing, transient, and planing modes. Subsequently, different interceptor configurations are installed on the hull, and the tests are repeated for the hull equipped with interceptors. The obtained results for the dynamic behaviors and human safety of the hull equipped with interceptors are compared to those of the bare hull. This

comparative analysis aimed to evaluate the efficiency of each interceptor configuration in improving the seakeeping performance and human safety of an HSPC.

The remaining part of this study is structured as follows: after the introduction, Section 2 presents the experimental procedure for measuring hull motions and accelerations in irregular waves, model characteristics, and the properties of considered wave conditions. Section 3 discusses the measures used for evaluating human safety based on current safety standards for humans exposed to WBVs and shocks. In Section 4, the results are presented, which include the data representation method (Section 4.1) and an investigation of the dynamic behaviors of the bare hull, the hull with TIS in transient mode, and the hull with TIS and DIS in planing mode (Section 4.2). Additionally, Section 4.3 predicts the possibility of adverse health effects and discomfort for the bare hull, examines safety improvements using TIS in transient mode, and explores safety improvement in planing mode using TIS and DIS. Finally, discussion and conclusions are provided in Sections 5 and 6, respectively.

2. Experimental procedures

The towing tank tests for this study is carried out at the Department of Industrial Engineering (DII) of the Università degli Studi di Napoli "Federico II". The towing tank facility has a length of 136.0 m, a width of 9.0 m, and a depth of 4.5 m. The carriage has a maximum speed of 10.0 ms^{-1}. For this study, tests are performed at speeds of 2.5, 3.5, 4.5, and 6.0 ms^{-1}, corresponding to the beam Froude numbers of 1.2, 1.7, 2.2, and 3.0. These Froude numbers are chosen to represent semi-planing, transient, and planing modes for an HSPC.

A hard-chine hull model from the Naples Systematic Series (NSS), as published in De Luca and Pensa (2019), are tested with and without the interceptor system. Fig. 1 shows the hull model C5 from NSS, and the details of model geometry are provided in Table 1.

During the experiments, two interceptors are added to the hull: a transom interceptor with a height of 2 mm and a length of either 0.5 B_{WL} or 0.25B_{WL} (as explained in Section 4, Results), and a forward interceptor with a height of 2 mm and a length equal to the full B_{WL}, located 0.8 m forward of the transom.

The vertical and longitudinal positions of the model's center of gravity were determined using an inertial balance equipped with a longitudinal weight rack (As shown in Fig. 2). After weighing the bare hull with all instrumentation installed, the model was placed on the balance, and its L_{CG} was found by translating it along the platform until a horizontal equilibrium was achieved, at which point the pivot point of the balance coincided with the L_{CG}. The V_{CG} was then determined by applying a known mass m at a known distance x from the central axis of

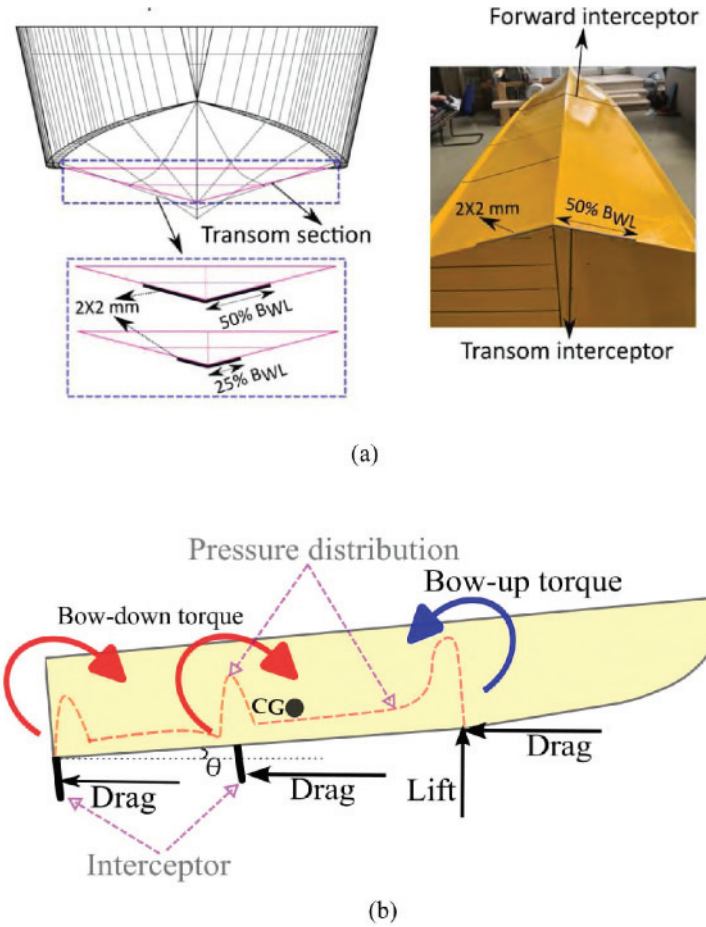


Fig. 1. HSPC hull (model C5 of NSS) and b) A schematic of hull with DIS.

Table 1
Hull characteristics for model C5.

Parameter	Value
L_{OA} (m)	2.611
L_{WL} (m)	2.400
B_{WL} (m)	0.41
L_{CG} (m)	0.945
V_{CG} (m)	0.205
SF	15
Δ (kg)	37.4
Kxx/B_{WL}	0.4
Kyy/L_{wl}	0.25
β_T (deg)	13.2
$\beta_{0.5}$ (deg)	22.3
$\beta_{0.75}$ (deg)	38.5

the weight rack and measuring the resulting trim angle θ. Using multiple combinations of m and x, the V_{CG} was calculated from the relation.

$$V_{CG} = \frac{mx\cot(\theta)}{m+M} \quad (1)$$

where M is the hull mass. To determine the radii of gyration, the hull was suspended at the pivot point and subjected to free oscillations in both roll and pitch. The resulting motions were recorded using accelerometers, from which natural frequencies and oscillation angles were extracted. These measurements were used to calculate the radii of gyration in roll (K_{xx}) and pitch (K_{YY}).

The natural periods of oscillation were recorded using a stopwatch and repeated five times to ensure consistency. The average values were then used to calculate the radii of gyration using the standard pendulum formula. The total mass of the model was measured using an electronic scale with 0.01 kg accuracy. All mass properties were determined before towing tests and remained unchanged throughout the experiments.

During the towing tank test, two triaxial accelerometers are used to record the hull acceleration at CG and at 0.5 L_{WL} forward from the CG. These accelerometers are Cross Bow CXL04GP3-R-AL, with an input range (g) of ±4, noise (mgrms) of 10, and bandwidth (Hz) of DC-100, with a sensitivity (mV/g) of 500 ± 15. Additionally, hull resistance is measured by an HBM load cell (PW115AH 20 kg, accuracy Class III), suitable for applications requiring reliable accuracy.

The dynamic performance of hull model C5 is tested by allowing free heave and pitch motions while the model is restrained in the surge direction by the towing carriage. Furthermore, a Qualisys Motion Capture System is used to measure hull motions in wave conditions. This is a high-precision optical tracking system that is widely used in engineering applications.

The model's dynamic behavior is studied in three different irregular head waves from the JONSWAP spectrum, as presented in Table 2. The produced wave profile with towing tank wave makers is verified by employing two ACAMINA AWP-24–2 Wave Height Gauges sensors (a capacitive probe that is used for measuring wave height in the towing tank) fixed on the towing tank and four Baumer UNDK 30U6103 sensors (an ultrasonic proximity sensor designed to measure distances with high precision and reliability) fixed on the carriage are employed.

To ensure a reliable comparison between the results for the bare hull and the hull equipped with the interceptor system, it is crucial to analyze the hull behavior in the same wave spectra. Therefore, recorded wave heights by capacitive probes are measured and compared with theoretical spectra to verify the generated wave spectrum. Fig. 3 shows the comparison of generated wave spectra with theoretical JONSWAP spectra.

Furthermore, the recorded data are sampled at a frequency of 500 Hz and filtered with a Butterworth bandpass filter of 0.05–20 Hz. To analyze the recorded data for unsteady phenomena, a large number of tests are required to ensure the reliability of the statistical approaches. Therefore, several tests (15 or more) are carried out to reach a sufficient number of wave encounters (about 200). In this regard, 256 (2^8) Fourier components are used. The repetition period is 250 s, a single random seed is generated to build the wave profile in the time domain, and the start time of wave generation is shifted from run to run.

3. International standards for evaluating acceleration exposure

For a high-speed planing craft operating in rough water, hull acceleration can affect human safety. Exposure to this acceleration may cause adverse health effects, discomfort, and motion sickness for the occupants.

There are various standards and regulations that investigate the safety of humans exposed to WBV and shocks in a vibrated environment.

Table 2
Characteristics of considered irregular head waves.

Wave condition	Spectrum	H_s (m)	$H_{s\text{-}full\text{-}scaled}$ (m)	γ	T_p (s)	$T_{p\text{-}full\text{-}scaled}$ (s)	F_p(Hz)
1	JONSWAP	0.075	1.125	3.3	1.52	5.89	0.66
2	JONSWAP	0.060	0.9	3.3	1.356	5.25	0.737
3	JONSWAP	0.045	0.675	3.3	1.176	4.55	0.850



Fig. 2. Determining the CG position and radii of gyration for model C5.

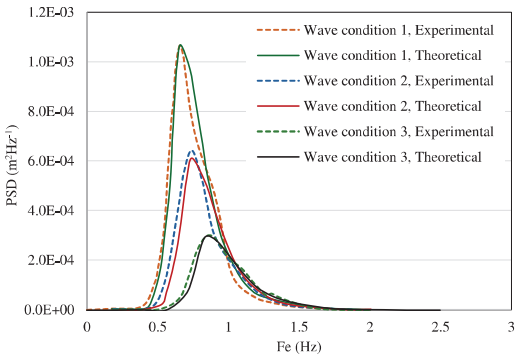


Fig. 3. Generated wave spectra and theoretical JONSWAP wave spectra.

This study uses ISO 2631-1, (1997); ISO 2631-5, (2004), , and Directive 2002/44/EC, (2002) to assess the health and comfort risks onboard the HSPC in different wave conditions and speeds. Additionally, the effectiveness of using an interceptor system in improving the safety of HSPC crews is examined using these standards.

For this purpose, vertical accelerations measured in the CG and bow during the towing tests are used to calculate the root mean square (RMS) and vibration dose value (VDV). These parameters are recognized by the standards as measures for assessing the effects of WBV and shock exposure on human health and comfort as

$$RMS = \left\{ \frac{1}{T} \int_0^T a_w^2(t)dt \right\}^{1/2} \tag{2}$$

$$VDV = \left\{ \int_0^T [a_w(t)]^4 dt \right\}^{\frac{1}{4}} \tag{3}$$

where *RMS* represents the root mean square of frequency-weighted acceleration, $a_w(t)$ is the frequency-weighted acceleration signal, and T is the measurement time for acceleration exposure, which is computed based on Eq. (4) for the full-scale boat.

$$T = T_{\text{model}}\, SF^{0.5} \tag{4}$$

Frequency-weighted accelerations are calculated by transferring recorded acceleration to the frequency domain and multiplying the data by the weighting transfer function recommended by ISO 2631-1, (1997). Afterward, the frequency-weighted accelerations are transformed back to the time domain. Fig. 5 shows a sample of frequency-weighted acceleration compared to the unweighted signals in wave condition 1 at $Fr_B = 2.2$. In this Figure, the real-time duration of the experiment is 207.18 s, which has been scaled to 802.41 s for the full-scale hull using Eq. (4).

ISO 2631-1, (1997) considers the RMS value as a key parameter to predict human discomfort due to WBVs and shocks. According to this standard, an RMS value below 0.315 ms^{-2} is considered to represent a "not uncomfortable" level, while values between 0.315 and 0.63 ms^{-2} are associated with "a little discomfort". As the RMS increases, the likelihood of discomfort rises. Specifically, RMS values between 0.5 and 1 ms^{-2} indicate "fairly uncomfortable," values between 0.8 and 1.6 ms^{-2} suggest "uncomfortable," and values between 1.25 and 2.5 ms^{-2} denote a "very uncomfortable" condition. Additionally, ISO 2631-1, (1997) defines an RMS value above 2 ms^{-2} as indicating an "extremely uncomfortable" condition. Fig. 4

The RMS value is also used by ISO 2631-1, (1997) to assess the possibility of adverse health effects as a result of accelerations. However, predicting the probability of health risks in EU Directive 2002/44/EC, (2002) estimates considers the VDV value. This study follows the EU Directive 2002/44/EC, (2002) guidance for evaluating the effects of HSPC acceleration on human health since VDV is the fourth power of accelerations and is more sensitive to the acceleration peak. For a high-speed planing craft operating in rough water, impact shocks could be so harsh with a serious effect on human health, while RMS value might underestimate the effects of these shocks.

EU Directive 2002/44/EC, (2002) considers VDV_{8h} to predict the possibility of adverse health effects during the 8-hour work shift. VDV_{8h} are computed as:

$$VDV(8h) = VDV.\left[\frac{t_d}{T}\right]^{1/4} \tag{5}$$

where t_d is the duration of the daily exposure, which is 8 h here. Directive 2002/44/EC, (2002) introduces 9.1 $ms^{-1.75}$< VDV_{8h} as the action value that requires reducing WBVs and shocks to avoid health problems. Additionally, there is a high probability of health negative effects that requires immediate action to prevent health risks if VDV_{8h} becomes higher than the limit value (21.0 $ms^{-1.75}$ < VDV_{8h}).

According to ISO 2631-5, (2004), long-term whole-body multiple shocks can lead to adverse health effects, particularly affecting the lower lumbar spine and connected nervous system. The relationship between the input vertical shock and the peak acceleration response in the spine is described by Eq. (6) for an 8-hour daily work shift.

$$S_{ed} = \left[(m_k D_{zd})^6\right]^{1/6} \tag{6}$$

where, m_z=*0.032* MPa/ms^{-2} is defined by ISO 2631-5, (2004), and D_{zd} is computed as,

$$D_{zd} = D_z\left[\frac{t_d}{T}\right]^{1/6} \tag{7}$$

D_z in Eq. (6) is the average daily dose in the vertical direction defined as

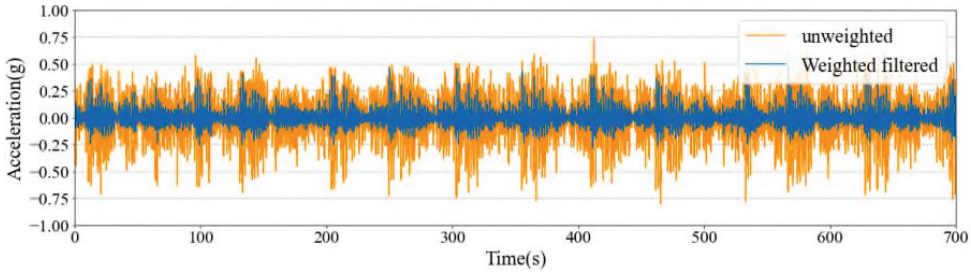


Fig. 4. Weighted filtered acceleration and unweighted acceleration of bare hull at $Fr_B = 2.2$.

$$D_z = \left[\sum_i A_{iz}^6\right]^{1/6} \quad (8)$$

where A_{iz} is the i^{th} peak of the response acceleration between two zero crossings. It should be noted that counting peak accelerations in vertical direction only contains positive peaks.

According to ISO 2631-5, (2004), $S_{ed} < 0.5$ MPa indicates a low probability of adverse health effects, whereas 0.8 MPa $< S_{ed}$ indicates a high probability of negative health effects. These values are considered for 220 workdays during a year, for a person who started being exposed at the age of 20 to 65 years.

By considering these standards, a comparison of the RMS, VDV_{8h}, and S_{ed} values for the bare hull and the hull equipped with an interceptor system can be used to examine the effectiveness of the interceptor system in improving human safety onboard an HSPC.

4. Results

The following subsections first examine the dynamic characteristics of the bare hull, the effects of a transom interceptor system (TIS) in transient mode, and the effects of the TIS and double interceptor system (DIS), individually, in planing mode. These analyses provide insights into resistance, heave and pitch motions, and vertical acceleration at the CG and bow. Subsequently, human safety factors are assessed based on ISO 2631-1, (1997); ISO 2631-5, (2004) and EU Directive 2002/44/EC, (2002), with a focus on the potential for reducing adverse health risks and discomfort achieved through the TIS in transient mode, TIS in planing mode, and DIS in planing mode.

There are three different configurations suggested for the interceptor system in this study. The first recommended configuration for the transient mode ($1.7 < Fr_B < 2.2$) consists of a transom interceptor with a height of 2 mm and a length of $0.5B_{WL}$. A comparison between the results for the bare hull and the hull equipped with this TIS demonstrates the effectiveness of using the TIS to improve the dynamic performance of HSPC and human safety in transient mode.

In planing mode ($Fr_B = 3$), a double interceptor system (DIS) is implemented on the hull bottom. This system consists of a transom interceptor and another interceptor located at the middle of the hull length. Both interceptors are designed with a height of 2 mm, and an initial length of $0.5B_{WL}$ for the transom interceptor, and a length of B_{WL} for the forward interceptor. However, due to the overcorrection of the trim angle that prevented proper ventilation of the forward interceptor at $Fr_B = 3$, the length of the transom interceptor is reduced to $0.25B_{WL}$. Therefore, the results presented for the DIS in planing mode refer to hull performance in wave condition 1, with a transom interceptor height of 2 mm and a length of $0.25B_{WL}$, and a forward interceptor with a length of B_{WL} and height of 2 mm, located 0.8 m from the transom.

Afterwards, the forward interceptor is removed, and the tests are repeated for a hull with a transom interceptor, with a length of $0.25B_{WL}$ and a height of 2 mm at $Fr_B = 3$ in wave condition 1. A comparison of the obtained results for the bare hull, the hull with DIS, and the hull with TIS examines the efficiency of suggested configurations in improving the dynamic performance of HSPC and human safety in planing mode.

4.1. Data representation

Although the generated wave spectra for testing the bare hull are the same as for the hull equipped with an interceptor system, the time history of wave elevation may differ. Therefore, the efficiency of the interceptor system is analyzed through statistical distribution.

A sample of recorded heave, pitch, and vertical acceleration at the CG and bow in wave condition 1 at $Fr_B = 2.2$ is presented in Fig. A1 in appendix A. The analysis of the interceptor system's effect on the dynamic behavior of HSPC is conducted by comparing statistics of significant heave, pitch, and acceleration heights, as well as their 1/3, 1/10, and 1/100 values. The mean values and associated uncertainties for the presented results are provided in Appendix B.

Significant heave motions, which correspond to the 1/3 highest values in the recorded time history, are calculated by identifying the maximum or minimum points between two zero-crossing points. The heave motion height value is calculated by subtracting consecutive maximum and minimum values. Subsequently, the 1/10, and 1/100 of the highest heave motion heights are determined. A similar process is applied for hull acceleration at the CG and bow, as well as for pitch motions.

It is worth noting that since recorded pitch motions are always positive (bow-up) with no zero-crossing point, the pitch data are shifted downward by the mean pitch values to calculate the significant height of pitch motion.

4.2. Dynamic behavior in irregular waves

4.2.1. Bare hull

Fig. 5 indicates the average total resistance of the bare hull in wave conditions 1, 2, and 3 at different Froude numbers. This figure shows that an increase in hull speed leads to a noticeable rise in hull resistance, while the wave conditions have no significant effect. The negligible effects of wave characteristics on hull resistance at each Froude number can be attributed to the similar wave steepness ($S = 0.065$) maintained for the three wave conditions.

Although the effect of wave height on hull resistance is negligible, it can substantially influence hull motions and human safety. Therefore, it is essential to analyze the effects of sea conditions on hull motions and consequently human safety at varying operational speeds.

A statistical analysis is conducted on random wave conditions 1, 2, and 3 to evaluate dynamic hull performance across various waves and speeds. Fig. 6 presents the non-dimensional $H_{1/3}$, $H_{1/10}$, and $H_{1/100}$ significant heave motions in different sea conditions at various speeds. As shown in Fig. 6, in semi-planing and transient modes ($Fr_B = 1.2$ to 2.2), heave motion in wave conditions 1 and 2 decreases with increased hull speed. However, when entering the planing mode ($Fr_B = 3$), heave motion increases. Additionally, the comparison of heave motion in different waves shows higher motions in wave conditions 1, 2, and 3, respectively, due to the higher wave heights.

Fig. 6 also indicates that, for wave condition 1, $H_{1/10}$ at $Fr_B = 1.2$ and $H_{1/100}$ at $Fr_B = 1.2$, 1.7, and 3 exceed the Hs, indicating higher vertical motions compared to the free surface elevation. In contrast, for wave conditions 2 and 3, $H_{1/3}$, $H_{1/10}$, and $H_{1/100}$ are all below Hs across all speeds.

Fig. 7 shows significant pitch motions in wave conditions 1, 2, and 3 at different speeds. As depicted in Fig. 7, the pitch motion decreases with increasing hull speed in semi-planing and transient modes; however, it increases when the speed reaches the planing mode ($Fr_B = 3$), similar to the observation for heave motion. Furthermore, the pitch angle

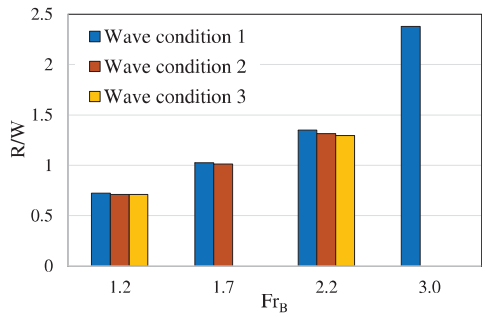


Fig. 5. Nondimensional total resistance in wave conditions 1, 2, and 3 at different Froude numbers.

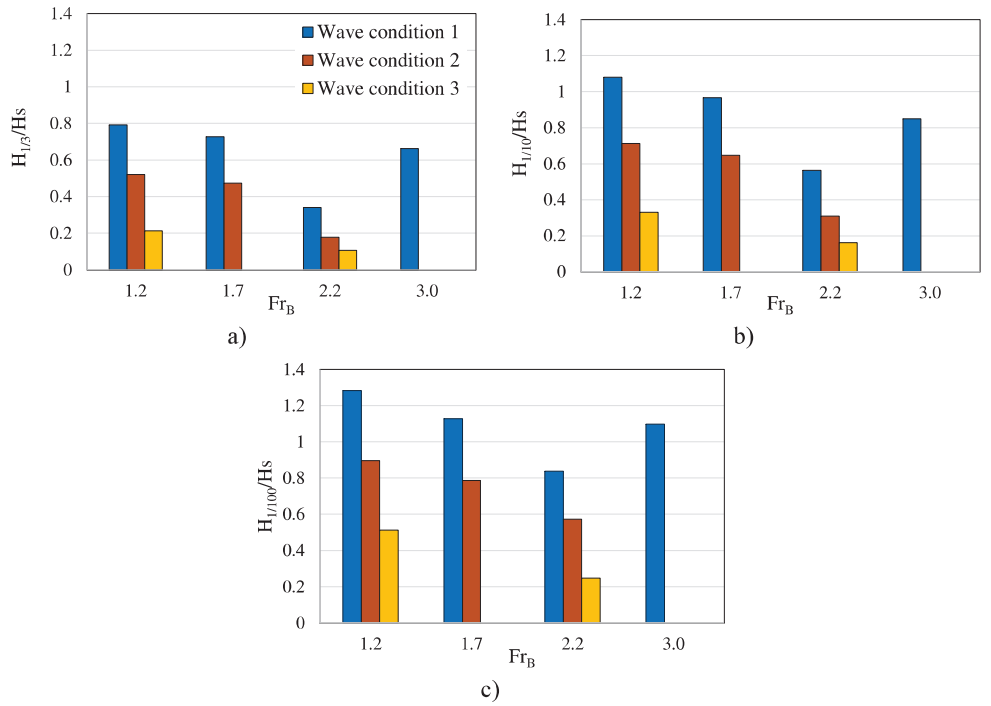


Fig. 6. Significant heave motions for the bare hull in wave conditions 1, 2, and 3 at different Froude numbers: a) $H_{1/3}$, b) $H_{1/10}$, and c) $H_{1/100}$.

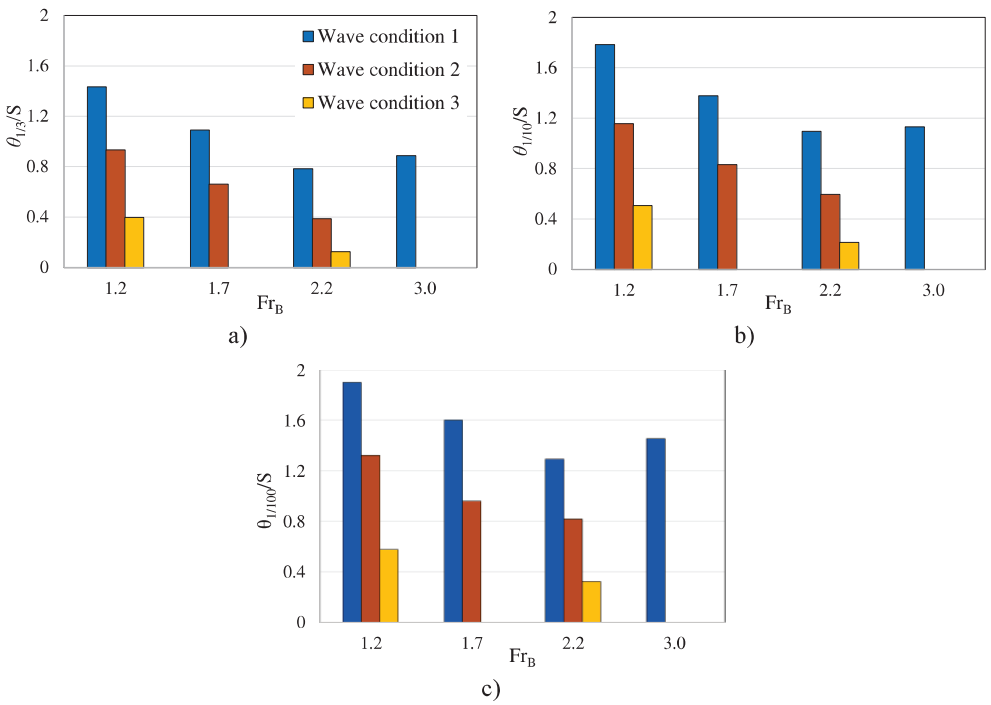


Fig. 7. Significant pitch angles for the bare hull in wave conditions 1, 2, and 3 at different Froude numbers: a) $\theta_{1/3}$, b) $\theta_{1/10}$, and c) $\theta_{1/100}$.

decreases with a reduction in wave height at all examined speeds.

Although undesired hull motion in wave conditions is an important parameter that can affect the HSPC performance, vertical motion acceleration also needs to be considered. Severe vertical impact shocks caused by slam impact could be significant and surpass 20 g (ABCD Group, 2008), with serious effects on crews' safety. Therefore, evaluating and minimizing hull accelerations is crucial to improve HSPC performance and crews' safety. Fig. 8 indicates the significant vertical accelerations on HSPC measured at the bow and CG.

According to Fig. 8, operational speed has a nonlinear effect on vertical accelerations. Comparing vertical acceleration in different wave conditions with a constant steepness indicates that higher accelerations are related to wave conditions 1, 2, and 3, respectively, with higher H_s. Furthermore, a comparison of vertical acceleration and heave motion in Figs. 6 and 8 reveals no similar trend. For instance, in wave condition 1, $a_{1/100}$ at Fr = 1.7 is significantly higher than $Fr_B = 1.2$, while it has a lower heave motion, as shown in Fig. 6.

According to Fig. 8, the considered hull experiences severe vertical accelerations at $Fr_B = 3$, exceeding gravitational acceleration. These high accelerations are likely caused by slam impacts, posing significant risks to the hull stability, crew safety, and structural stress. Therefore, minimizing hull motions and accelerations in wave conditions is crucial. The implementation of an interceptor system offers a promising solution to reduce these effects, improving dynamic performance and ensuring higher safety for the crew.

In the subsequent section, the effects of the TIS interceptor $0.5B_{WL}$ on dynamic hull performance in irregular waves at transient mode are analyzed in comparison to the bare hull. To manage the time-consuming nature of irregular wave testing, the evaluation focuses on two wave conditions (wave conditions 1 and 2).

4.2.2. TIS effect on dynamic performance in irregular waves at transient mode

This section analyzes the effects of installing a TIS with a $0.5B_{WL}$ length on the dynamic performance, compared to the bare hull. Fig. 9 shows a comparison between the total resistance of the bare hull and the hull equipped with TIS in wave conditions 1 and 2 during transient mode. According to Fig. 9, the TIS effectively reduces hull resistance. In wave condition 1, hull resistance is reduced by 4.7 % and 4.9 % at $Fr_B = 1.7$ and 2.2, respectively. A similar trend is observed in wave condition

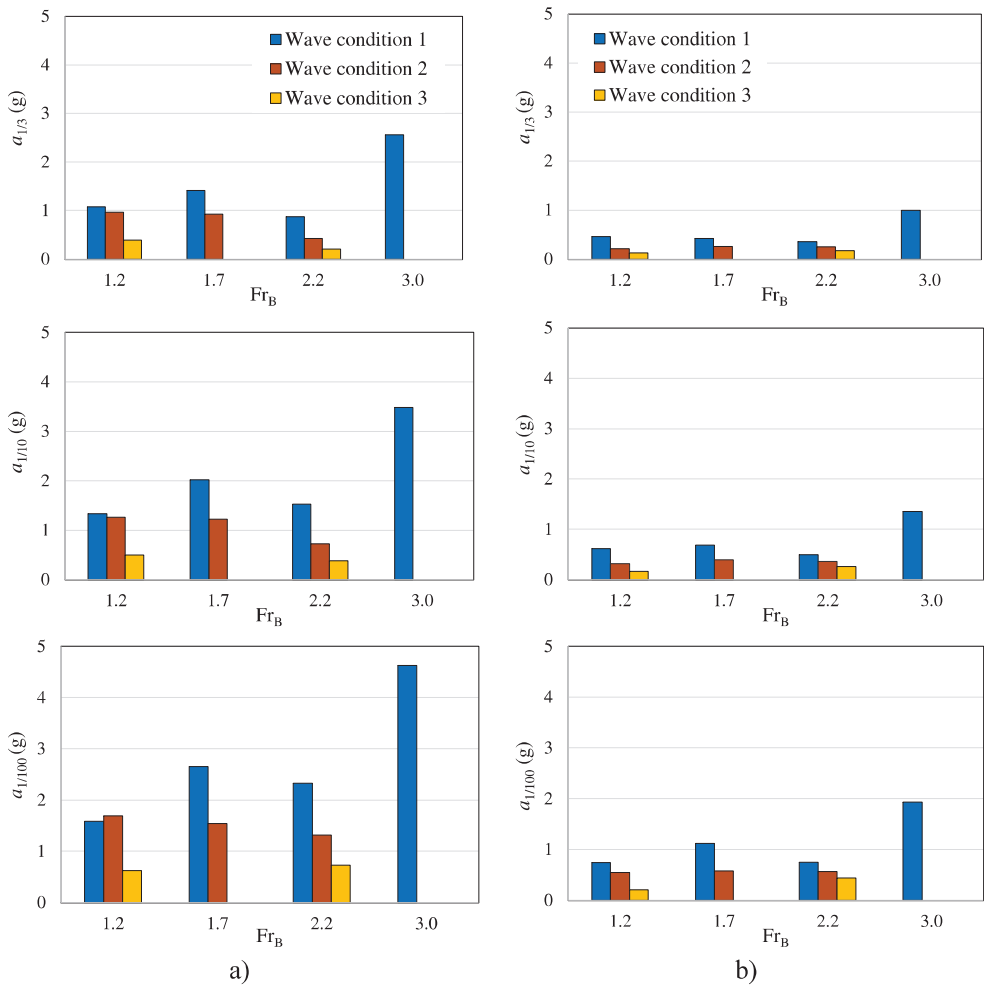


Fig. 8. Non-dimensional significant vertical accelerations for the bare hull in wave conditions 1, 2, and 3 at different Froude numbers: a) $a_{1/3}$, $a_{1/10}$, and $a_{1/100}$ at the bow, and b) $a_{1/3}$, $a_{1/10}$, and $a_{1/100}$ at CG.

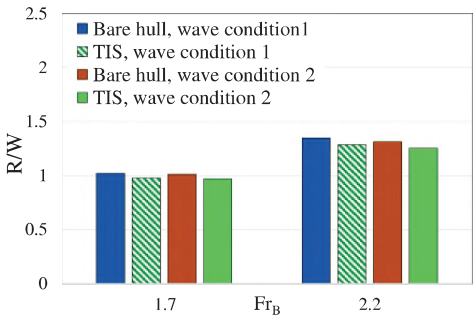


Fig. 9. Hull resistance with and without the TIS ($0.5B_{WL}$) in transient mode for wave conditions 1 and 2.

2, demonstrating the effectiveness of the TIS in transient conditions (detailed results are provided in Appendix C, Table C1).

Fig. 10 provides a statistical analysis of the TIS effect on significant heave motions ($H_{1/3}$, $H_{1/10}$, and $H_{1/100}$) in wave conditions 1 and 2 during transient mode (Fr_B = 1.7 and 2.2). The time history of heave motion at Fr_B = 2.2 under wave conditions 1 and 2, both with and without the TIS are provided in Fig. A2 in Appendix A.

According to Fig. 10, the TIS effectively reduces heave motions in both wave conditions 1 and 2 demonstrating greater efficiency at lower Froude numbers. For instance, $H_{1/3}$ in wave condition 1 at Fr_B = 1.7 is reduced by 59.7 % compared to the bare hull, whereas, at Fr_B = 2.2, the reduction is 13.9 %. Furthermore, reductions at Fr_B = 1.7 in $H_{1/10}$ and $H_{1/100}$ for wave condition 1 are 47.1 % and 27.6 %, respectively. It is evident that the TIS is most effective in reducing moderate heave motions ($H_{1/3}$) compared to extreme values ($H_{1/10}$ and $H_{1/100}$). For detailed information on the percentage of the heave reduction, refer to Table C1 in Appendix C.

As highlighted in previous studies, such as Putra and Suzuki (2024) and John et al., (2011), the implementation of TIS has been shown to effectively reduce the hull trim angle in calm water. This, in turn, influences the pitch motion in wave conditions, as demonstrated by De Luca and Pensa (2014) and Najafi et al. (2015). The time histories of pitch motion at Fr_B = 2.2 under wave conditions 1 and 2 for both the bare hull and hull equipped with TIS are presented in Fig. A3 in Appendix A. As expected, adding TIS causes the hull to rotate around a lower trim angle (reducing the oscillation point for pitch motion), while its effect on reducing pitch amplitude is comparatively limited.

Fig. 11 shows a comparison of $\theta_{1/3}$, $\theta_{1/10}$, and $\theta_{1/100}$ between the bare hull and hull equipped with TIS in transient mode across wave conditions 1 and 2. Further details are provided in Appendix B. Similar to the TIS effect on heave motions, the system is most effective in reducing moderate pitch angles; however, it can amplify higher pitch angles in certain cases. For instance, as shown in Fig. 11, the TIS increases $\theta_{1/100}$ by 7.4 % compared to the bare hull at Fr_B = 1.7 in wave condition 1, while reducing $\theta_{1/3}$ and $\theta_{1/10}$ by 21.4 % and 6.7 %, respectively. A similar trend is observed in wave condition 2, where the TIS achieves the greatest reduction in $\theta_{1/3}$ compared to the $\theta_{1/100}$. Notably, $\theta_{1/100}$ does not increase at this Froude number in wave condition 2, as its value is lower than that in wave condition 1. Detailed reductions for other conditions are available in Table C1 in Appendix C.

In conclusion, the most extreme pitch motions ($\theta_{1/100}$ highest values) provide insight into the most severe events affecting the TIS-equipped hull. Except at Fr_B = 1.7 in wave condition 1, where $\theta_{1/100}$ increases slightly compared to the bare hull, the TIS effectively reduces extreme pitch motions under other conditions. This indicates that the TIS generally improves performance by decreasing the moderate pitch motion occurrences while increasing the severe shocks in rough seas is

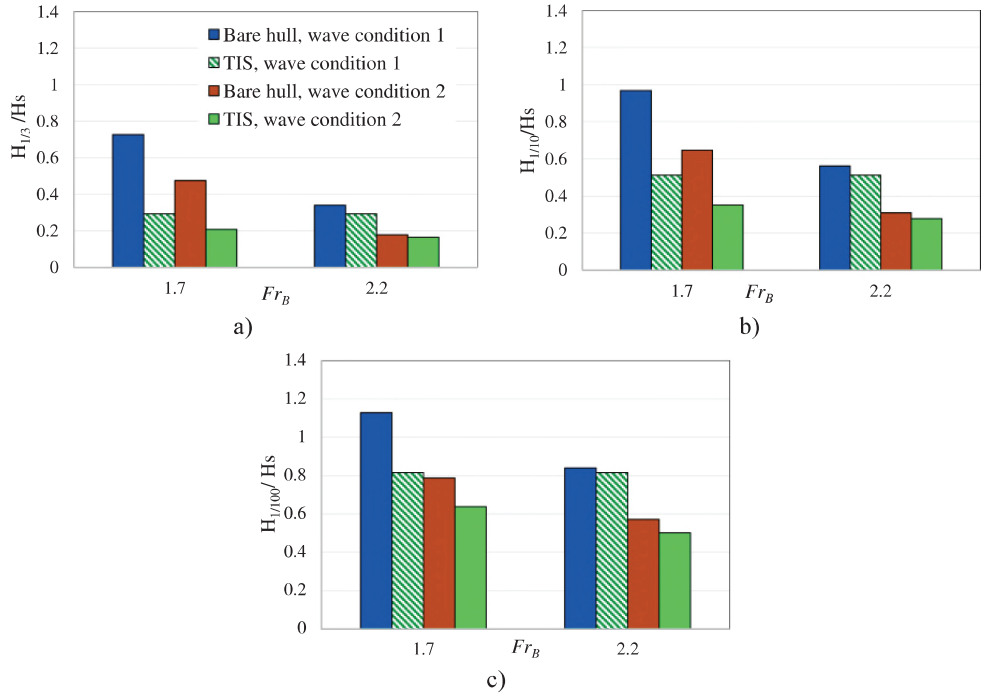


Fig. 10. Non-dimensional significant heave motions for the bare hull and TIS ($0.5B_{WL}$) in transient mode across wave conditions 1 and 2: a) $H_{1/3}$, b) $H_{1/10}$, and c) $H_{1/100}$.

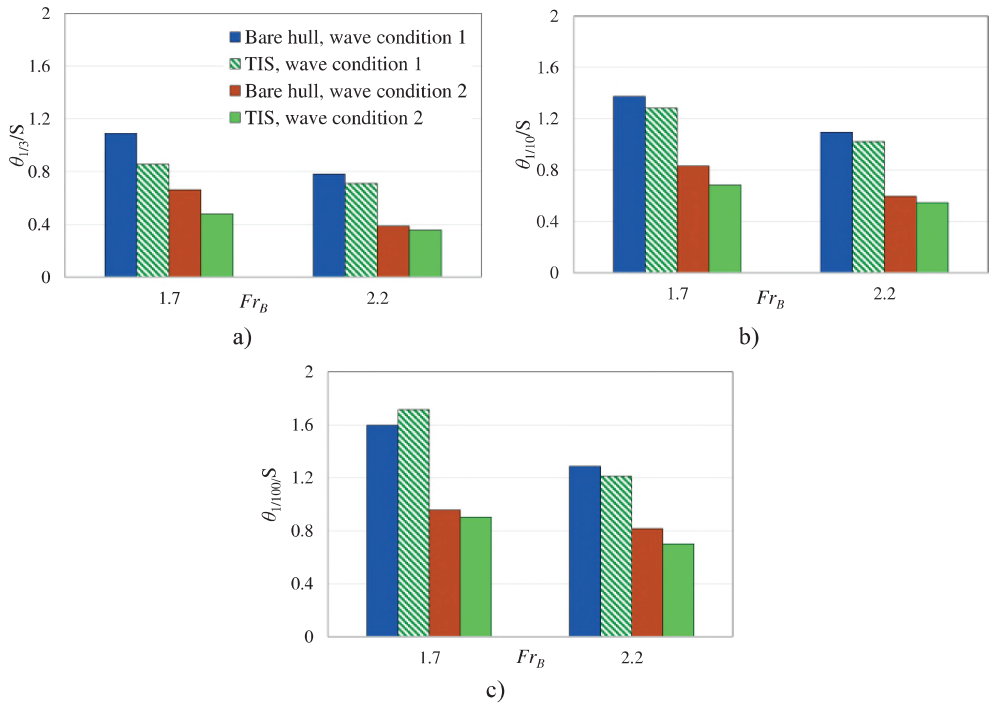


Fig. 11. Non-dimensional significant pitch angle for the bare hull and TIS ($0.5B_{WL}$) in transient mode across wave conditions 1 and 2: a) $\theta_{1/3}$, b) $\theta_{1/10}$, and c) $\theta_{1/100}$.

probable.

Appendix A Fig. A4 presents the time history of vertical acceleration at CG in wave conditions 1 and 2 at $Fr_B = 2.2$ for the bare hull and hull equipped with TIS. Furthermore, a statistical analysis of TIS effect on vertical acceleration at the bow and CG is shown in Fig. 12, with additional details in Appendix B.

As shown in Fig. 12(a), significant bow acceleration in $Fr_B = 1.7$ for the hull equipped with TIS is significantly lower than the bare hull in both sea conditions. Similarly, the TIS reduces bow acceleration in wave 2 at $Fr_B = 2.2$ compared to the bare hull. Nevertheless, in wave 1 at $Fr_B = 2.2$, the $a_{1/100}$ value of bow acceleration, there is an increase from 2.3 g for the bare hull to 2.9 g for the hull with the TIS, posing an increment of potential safety risks to occupants.

Additionally, as Fig. 12(b) shows, the TIS effectively decreases vertical accelerations at CG for wave conditions 1 and 2 at $Fr_B = 1.7$, and for wave 2 at $Fr_B = 2.2$. However, in wave 1 at $Fr_B = 2.2$, TIS leads to an increase in CG acceleration. For instance, the significant CG acceleration $a_{1/10}$ increases by 1.9 % compared to the bare hull. This observation highlights reducing the effectiveness of the TIS at higher speeds in rough water and its potential to amplify motions and accelerations under this condition. Further details can be found in Appendix B and Table C1 in Appendix C.

These findings underscore the need to explore alternative interceptor configurations for improving its performance in planing mode that has higher Froude numbers. To address this, the efficiency of the TIS in improving the dynamic performance of an HSPC in planing mode is compared with DIS performance to identify the most efficient configuration. Based on prior studies (De Luca and Pensa, 2012), it is anticipated that the DIS might demonstrate greater efficiency in reducing hull resistance. In addition, generating an extra lift force by the forward interceptor potentially influences the hull motions and acceleration.

However, experimental tests conducted in calm water revealed that adding a forward interceptor to the current TIS configuration causes an overcorrecting trim angle at $Fr_B = 3$, which prevents proper ventilation of the forward interceptor. Therefore, for investigating TIS and DIS performances in planing mode, the transom interceptor is reduced to $0.25B_{WL}$ to reduce generated bow-down torque by the transom interceptor and avoid overcorrecting trim angle.

4.2.3. TIS and DIS effect on dynamic performance in irregular waves at planing mode

As the results in transient mode demonstrated a decrease in the efficiency of the Transom Interceptor System (TIS) with $0.5B_{WL}$ at higher speeds, two alternative interceptor configurations are tested in planing mode to identify the most effective solution: a TIS with $0.25B_{WL}$, and a Double Interceptor System (DIS), consisting of an interceptor with $0.25B_{WL}$ at the transom and a forward interceptor with the length of 100 % B_{WL} located at 0.8 L_{WL} from the transom. Fig. 13 compares the hull resistance for the bare hull, hull with DIS, and hull with TIS in wave condition 1.

As shown in Fig. 13, the use of DIS results in a 4.6 % increase in hull resistance compared to the bare hull, while the TIS leads to a more significant 23 % increase. The smaller increase in total resistance observed with the DIS is attributed to the forward interceptor's ventilation, which reduces the wetted surface area. Based on these results, neither the DIS nor the TIS configuration reduces hull resistance in planing mode. In the following sections, the effects of these configurations on heave, pitch, and vertical acceleration will be analyzed.

Figs. A5 and A6 in Appendix A, present the effects of TIS and DIS on the time histories of heave and pitch motions in transient mode. Obtained results show that the pitch motion of the hull equipped with TIS oscillates around a lower mean angle compared to the bare hull. However, DIS behaves differently, increasing the trim angle around which the hull rotates.

Fig. 14 presents significant heave and pitch motions for the bare hull, the hull with DIS, and hull with TIS in planing mode. Further details can

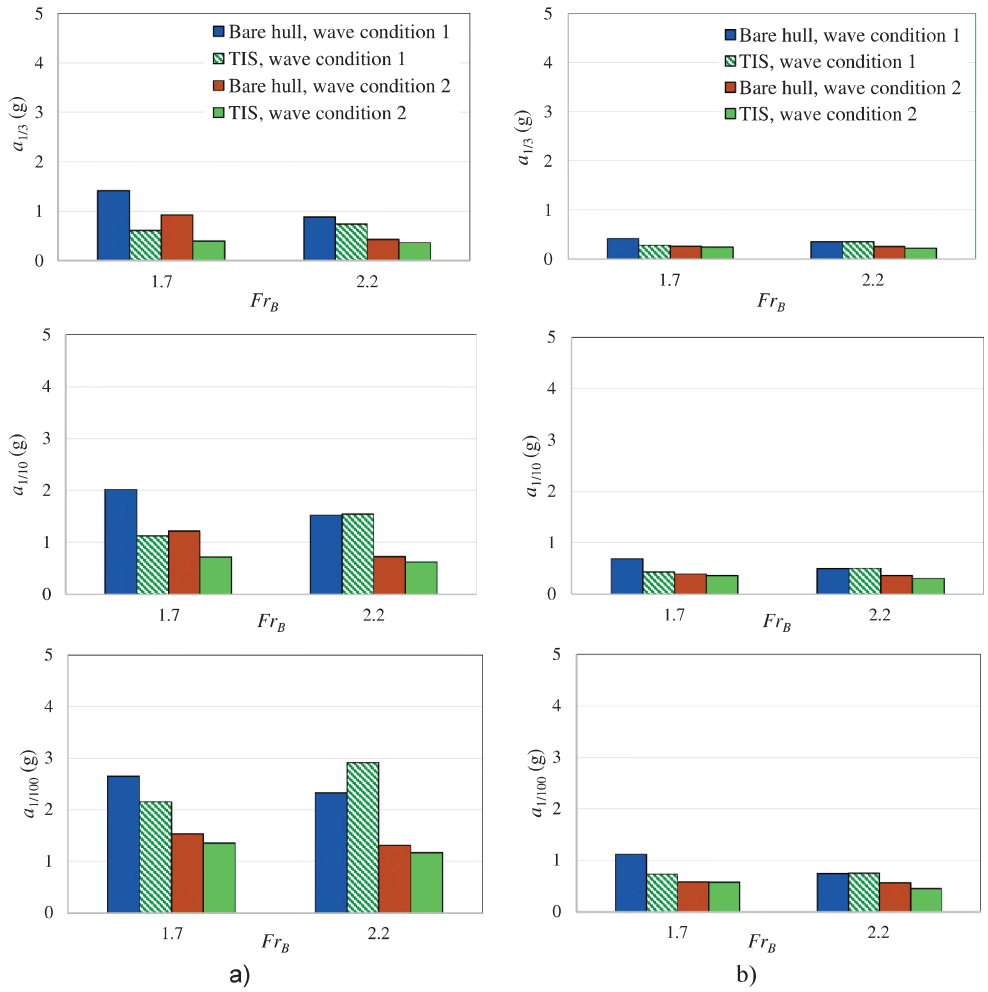


Fig. 12. Non-dimensional significant vertical accelerations for the bare hull and hull equipped with TIS ($0.5B_{WL}$) in transient mode across wave conditions 1 and 2, a) $a_{1/3}$, $a_{1/10}$, and $a_{1/100}$ at the bow, and (b) $a_{1/3}$, $a_{1/10}$, and $a_{1/100}$ at CG.

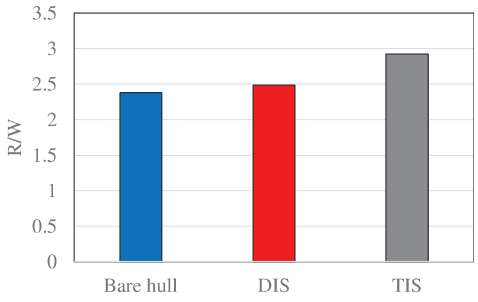


Fig. 13. TIS and DIS effects on hull resistance in wave condition 1 at $Fr_B = 3$.

be found in Appendix B. As shown in Fig. 14, the DIS reduces pitch motions compared to the bare hull, though it leads to an increase in heave motions. In contrast, the TIS effectively reduces both heave and pitch motions when compared to the bare hull. Additionally, a comparison of TIS and DIS performance in reducing pitch motion demonstrates the superiority of TIS. This suggests that the TIS provides a more balanced improvement in dynamic motions. Additional details on the motion reductions can be found in Table C3 in Appendix C. recorded vertical accelerations during the towing tank tests demonstrate that TIS efficiently reduces vertical acceleration at the CG, while DIS has no significant effect. The time history of vertical acceleration for bare hull and hull equipped with TIS and DIS in planing mode is presented Fig. A7 in Appendix A.

Fig. 15 presents significant vertical acceleration at the CG and bow for the bare hull, hull with TIS, and hull with DIS in wave condition 1. Similar to the observed hull motions, the TIS effectively reduces vertical acceleration at both the bow and the CG. In contrast, the DIS amplifies vertical acceleration at both locations. For instance, at the CG, the $a_{1/3}$ acceleration decreases by 45.5 % compared to the bare hull when the TIS is applied, highlighting its significant effect on reducing vertical accelerations. However, when the DIS is used, the $a_{1/3}$ acceleration increases by 12 % compared to the bare hull. This trend is observed at both the CG and bow, with the DIS configuration consistently resulting in higher accelerations. The percentage changes in vertical acceleration for both

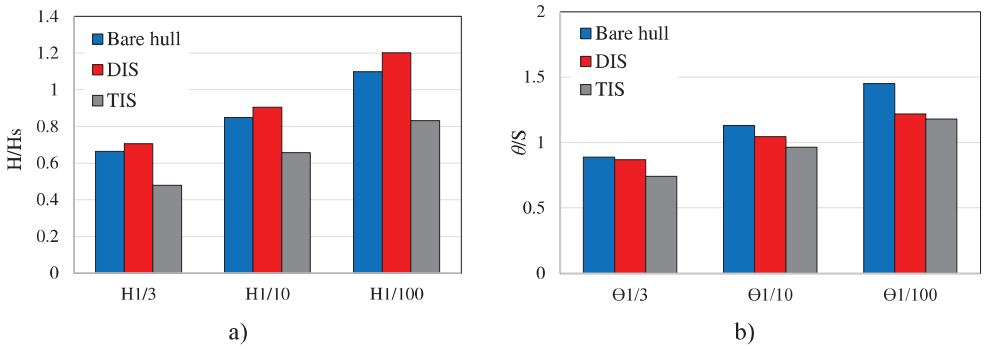


Fig. 14. TIS and DIS performance in reducing a) heave and b) pitch motions in wave condition 1 at Fr_B=3.

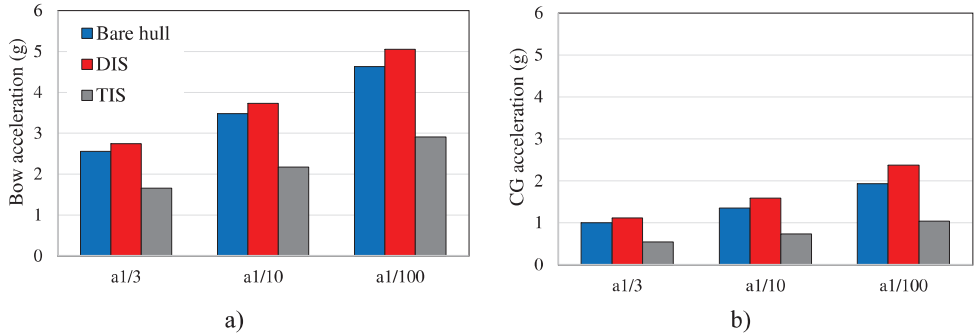


Fig. 15. TIS and DIS performance in reducing hull vertical acceleration at Fr_B = 3 in a) Bow and b) CG.

the DIS and TIS configurations are summarized in Table C3 in Appendix C, providing further insights into the performance of each interceptor system.

The next section evaluates the human safety onboard HSPCs across the considered irregular head wave conditions (wave details are presented in Table 2) at various speeds, regarding ISO 2631-1, (1997); ISO 2631-5, (2004), and EU Directive 2002/44/EC, (2002). These standards provide guidance for assessing the effects of whole-body vibrations (WBV) and shocks on human safety. Therefore, we will apply them to investigate the effects of using different interceptor configurations on improving human safety onboard the HSPC.

4.3. Human safety onboard the HSPCs

Ensuring human safety onboard HSPCs is a critical concern, particularly during high-speed operations, as it directly impacts the vessel's operational capabilities. Consequently, investigating the effects of hull accelerations on human health and comfort across various modes and sea conditions is essential.

4.3.1. Bare hull

To evaluate the effects of hull accelerations on human comfort, Fig. 16 presents the full-scaled RMS of weighted vertical acceleration at CG and bow for the bare hull across different wave conditions and speeds. According to Fig. 16(a), the RMS decreases as the wave height is

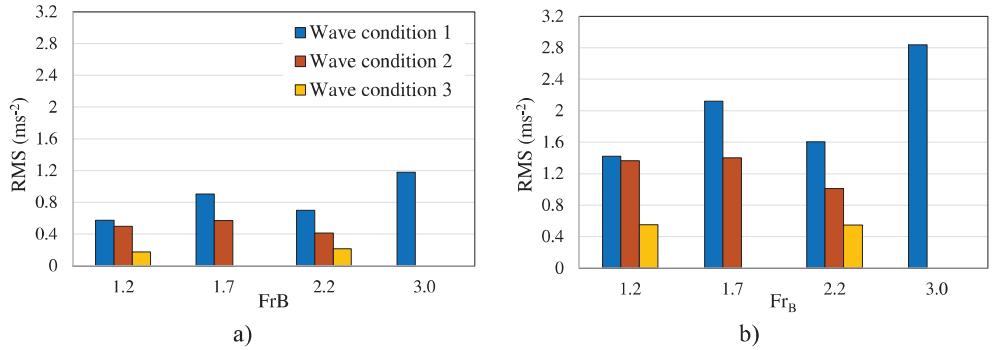


Fig. 16. Weighted RMS acceleration of the bare hull in a) CG and b) bow in wave conditions 1, 2, and 3 at different Froude numbers.

reduced. Consequently, the highest RMS is observed in wave conditions 1, 2, and 3, respectively, at each Froude number.

In wave condition 1, RMS at CG ranges from 0.57 to 1.18 ms^{-2}, while at the bow, it falls between 1.42 and 2.84 ms^{-2}, as evident from Fig. 16. These RMS values at the CG indicate "fairly uncomfortable" to "uncomfortable" conditions for the human, while the values at the bow correspond to "uncomfortable" to "very uncomfortable" conditions, according to [ISO 2631-1, (1997). Furthermore, results obtained in wave conditions 2 and 3 show lower RMS values, demonstrating no serious effects on human comfort at CG. However, RMS at the bow in wave condition 2 could still result in an "uncomfortable" condition, as per ISO 2631-1, (1997). Since HSPCs must be capable of operating in various sea conditions, reducing the vertical acceleration of this hull is essential to improving human comfort, particularly in rough waters.

Although human comfort is an important parameter for HSPCs crews, the risks to human health are even more critical and must also be considered. According to Directive 2002/44/EC, (2002), in the case of high vertical shocks in a vibrated environment, VDV_{8h} can be used to estimate the potential for adverse health effects resulting from WBVs and shocks. Fig. 17 presents full-scaled VDV_{8h} values for the HSPC at CG and bow across different wave conditions and speeds. According to EU Directive 2002/44/EC, (2002), a VDV_{8h} higher than 9.1 $ms^{-1.75}$ indicates an action value for potential health risks, while $VDV_{8h} > 21$ $ms^{-1.75}$ indicates a limit value for adverse health effects.

Fig. 17(a) shows that VDV_{8h} at the CG is significantly lower than the bow. However, under wave condition 1 conditions, it is still higher than the action value at all considered Froude numbers, and it even exceeds the limit value at $Fr_B = 3$ (planing mode). Similarly, VDV_{8h} in wave condition 2 surpasses the action value at $Fr_B = 1.2$ and 1.7, while wave condition 3 exhibits a lower VDV_{8h}, which may indicate a lower probability of health risks due to the lower acceleration intensity.

As shown in Fig. 17(b), VDV_{8h} at the bow exceeds the limit value recommended by EU Directive 2002/44/EC, (2002) in both wave conditions 1 and 2 across all Froude numbers. Additionally, VDV_{8h} in wave condition 3 exceeds the action level at two considered Froude numbers. Although an 8-hour work shift is uncommon for an HSPC, these results demonstrate a significant risk of adverse health effects for crews onboard this HSPC during 8 h of work, especially in planing mode. Therefore, there is a pressing need for safety improvement to reduce the possibility of adverse health risks.

In addition to the possibility of adverse human health risks during HSPCs missions, the long-term negative health effects of vibration exposure can be evaluated using the S_{ed} factor, as recommended by ISO 2631-5, (2004). According to ISO 2631-5, (2004), for a crew aged 20 to 65 years working 220 days a year, $S_{ed} > 0.8$ MPa indicates a high probability of health risks, while $S_{ed} < 0.5$ MPa indicates a low risk. Figs. 18 and 19 present full-scaled $S_{ed,1h}$ and $S_{ed,8h}$ values for daily work onboard this HSPC, considering CG and bow accelerations.

Fig. 18 shows that $S_{ed\text{-}1h}$ and $S_{ed\text{-}8h}$ values are both below the risk threshold in semi-planing and transient mode in wave conditions 1, 2, and 3. However, in planing mode ($Fr_B = 3$), $S_{ed\text{-}1h}$ reaches 0.67 MPa, and $S_{ed\text{-}8h}$ rises to 0.94 MPa, demonstrating a high probability of adverse health effects and underscoring the urgent need to reduce vertical accelerations.

Fig. 19 shows that both $S_{ed\text{-}1h}$ and $S_{ed\text{-}8h}$ values in the bow are below 0.5 MPa at Froude numbers 1.2 and 1.7 across three wave conditions, which is generally considered a low risk for adverse health effects according to ISO 2631-5, (2004). However, at Fr = 2.2, $S_{ed\text{-}1h}$ reaches 1.34 MPa in wave condition 1, indicating high probability of health risks and 0.59 MPa in wave condition 2, indicating probable health risks. Furthermore, at $Fr_B = 3.0$, $S_{ed\text{-}1h}$ increases significantly upon entering the planing regime, reaching 2.45 MPa in wave condition 1, which predicts a high likelihood of long-term negative health effects.

Given that S_{ed} values increase with increasing acceleration exposure time (as seen when comparing $S_{ed\text{-}1h}$ and $S_{ed\text{-}8h}$ in Figs. 18 and 19), reducing exposure duration or implementing acceleration reduction devices becomes essential at higher speeds to reduce human health risks.

The assessment of adverse health effects and discomfort due to hull accelerations highlights the critical need for effective acceleration reduction strategies, particularly in demanding operational scenarios such as high-speed operation in rough sea conditions. For this aim, the TIS has shown promise in reducing accelerations, as observed results in Section 4.2 indicate. To better understand the interceptor's potential for enhancing crew safety, the following section investigates the TIS's impact on safety improvement during transient mode operations, where hull performance is particularly sensitive to wave interactions and speed variations.

4.3.2. TIS effect on safety improvement in transient mode

The effects of the TIS on vertical acceleration in transient mode operations have direct implications for human safety onboard HSPCs. To evaluate the TIS's effect on human comfort, a comparison of the full-scaled weighted RMS acceleration of the hull with and without the TIS is presented in Fig. 20 for both the CG and bow.

As shown in Fig. 20, the TIS significantly reduces RMS acceleration at both the CG and bow in transient mode. Specifically, RMS acceleration at the CG decreases by 40.1 % and 36.8 % in wave conditions 1 and 2, respectively, compared to the bare hull at a Froude number of 1.7. Similarly, RMS acceleration at the bow reduces by 43.2 % and 43.9 % relative to the bare hull under the same conditions.

At a higher Froude number of 2.2, the TIS continues to provide a reduction in RMS acceleration, albeit less pronounced. RMS at the CG decreases by 9.6 % and 9.5 %, while RMS at the bow reduces by 11.6 % and 11.3 % in wave conditions 1 and 2, respectively. These results demonstrate that the TIS successfully enhances crew comfort onboard HSPCs during transient mode. However, its effects are notably more

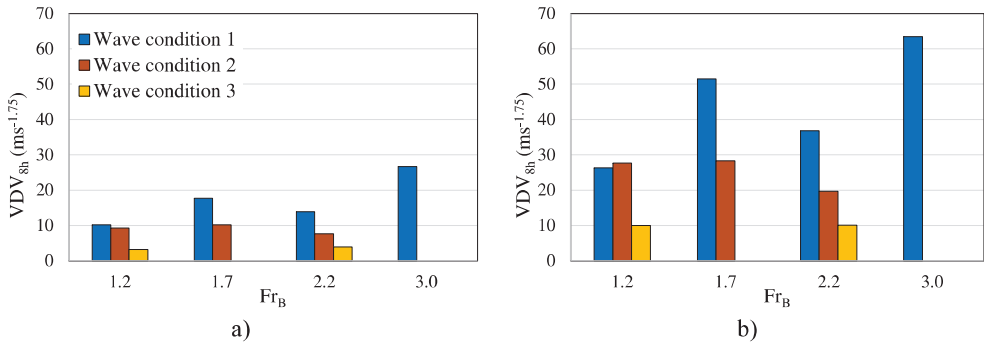


Fig. 17. VDV_{8h} for weighted acceleration in a) CG and b) bow in wave conditions 1, 2, and 3 at different Froude numbers.

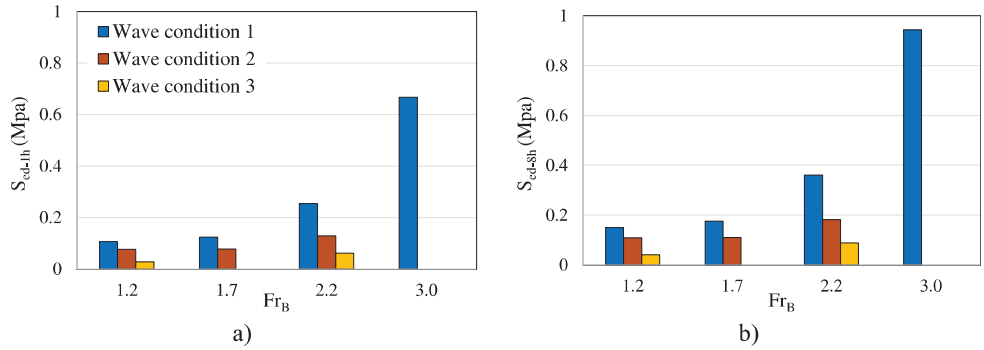


Fig. 18. a) $S_{ed\text{-}1\ h}$, and b) $S_{ed\text{-}8\ h}$ values of weighted accelerations in CG in wave conditions 1, 2, and 3 at different Froude numbers.

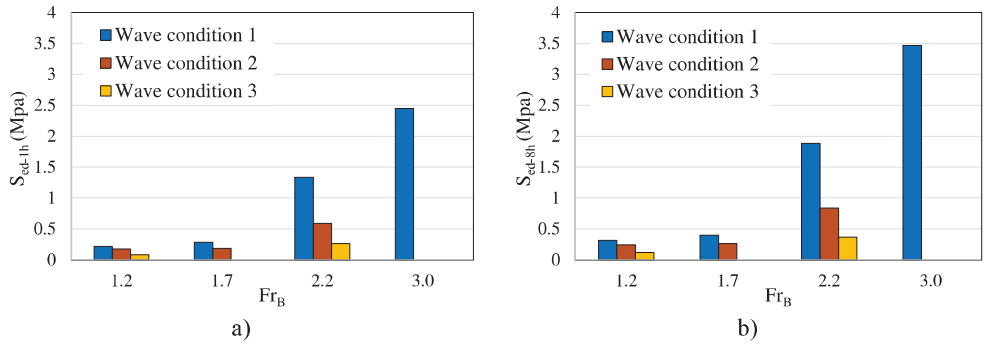


Fig. 19. a) $S_{ed\text{-}1\ h}$, and b) $S_{ed\text{-}8\ h}$ values of weighted accelerations at bow in wave conditions 1, 2, and 3 at different Froude numbers.

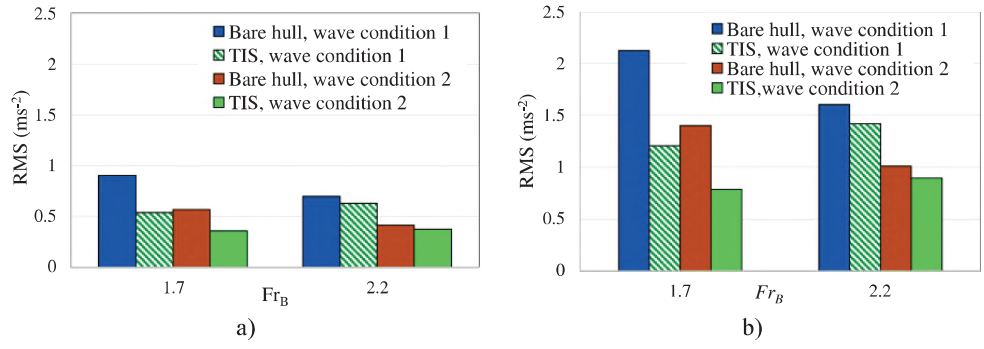


Fig. 20. Weighted RMS acceleration in a) CG and b) bow of the bare hull and hull with a TIS ($0.5B_{WL}$) in transient mode across wave conditions 1 and 2.

substantial at lower speeds, where the influence of the TIS is most effective.

Fig. 21 presents the full-scaled VDV_{8h} value at the CG and bow for the hull with and without the TIS in wave conditions 1 and 2 during the transient mode. The results indicate a significant reduction in VDV_{8h} at both CG and bow when TIS is employed. For instance, at $Fr_B = 1.7$, the VDV_{8h} at the CG and bow decreases by 38.2 % and 45.1 %, respectively, compared to the bare hull under wave condition 1. Similarly, for wave condition 2, the reductions are 36.0 % at the CG and 42.2 % at the bow. These results highlight the TIS's notable capability in improving on-board crews' safety, especially at lower speeds.

Although the TIS effectively reduces VDV_{8h} values at both the CG and bow in wave conditions 1 and 2, its efficiency reduces at higher speeds. For instance, at $Fr_B = 2.2$, the percentage reductions are smaller compared to those observed at $Fr_B = 1.7$, as illustrated in Fig. 21. This trend suggests that the TIS's efficiency in reducing vertical shocks decreases as the vessel transitions into higher speed regimes, likely due to reduced flow control effectiveness at the transom.

Further details, including the precise percentage reductions of VDV_{8h} values, are provided in Appendix C, Table C2. These insights emphasize the importance of optimizing TIS design for varying speed ranges to maximize its safety benefits.

Figs. 22 and 23 show the full-scaled $S_{ed\text{-}1h}$ and $S_{ed\text{-}8h}$ values at the CG and bow for both the bare hull and hull equipped with a TIS in wave

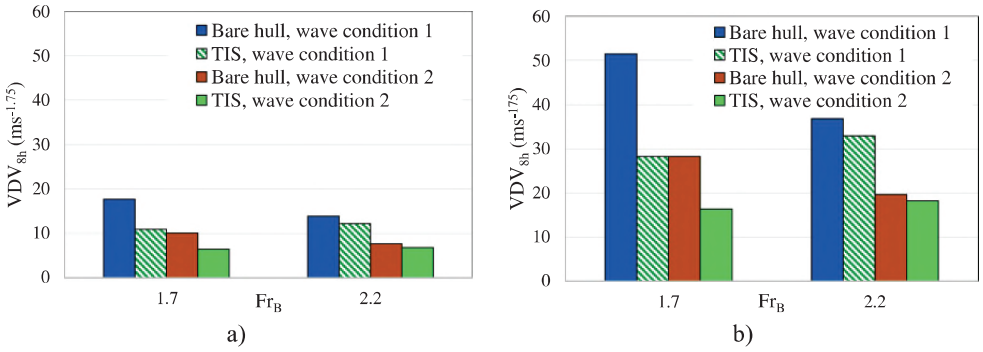


Fig. 21. VDV_{8h} in a) CG and b) bow of the bare hull and hull with a TIS ($0.5B_{WL}$) in transient mode across wave conditions 1 and 2.

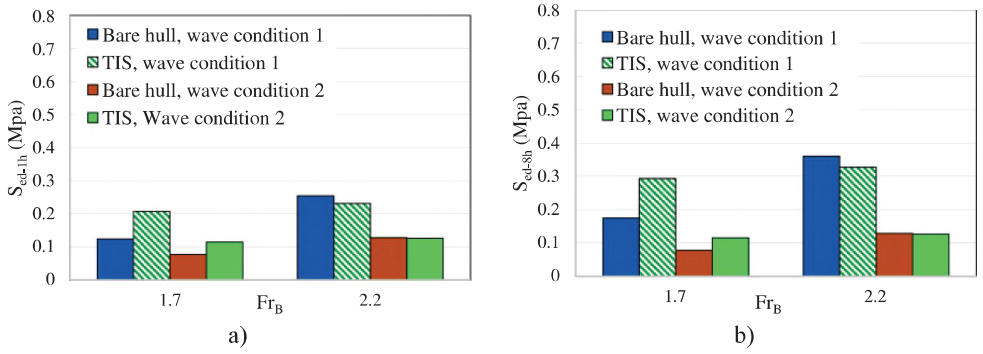


Fig. 22. a). $S_{ed\text{-}1h}$, and b) $S_{ed\text{-}8h}$ in CG for the bare hull and hull with a TIS ($0.5B_{WL}$) in transient mode across wave conditions1 and 2.

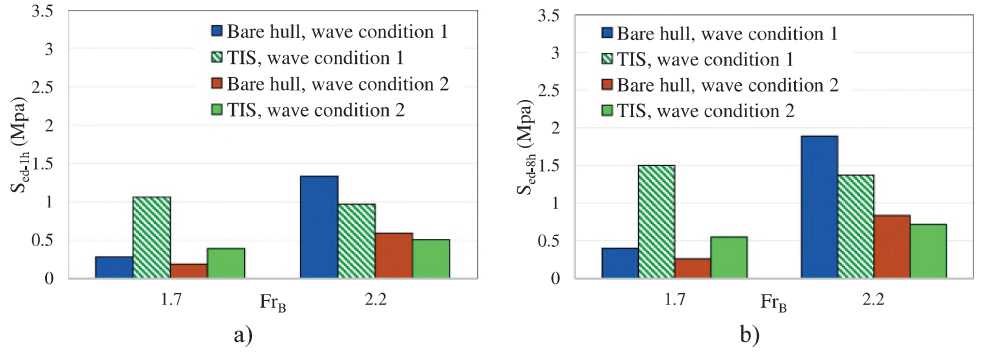


Fig. 23. a). $S_{ed\text{-}1h}$, and b) $S_{ed\text{-}8h}$ in bow for the bare hull and hull with a TIS ($0.5B_{WL}$) in transient mode across wave conditions 1 and 2.

conditions 1 and 2 during the HSPC operation in transient mode. While Figs. 20 and 21 indicated that TIS is more efficient in reducing RMS and VDV_{8h} at lower speeds, it amplifies acceleration effects on the human spine at lower Froude numbers, as evidenced in Figs. 22 and 23.

According to Fig. 22, at $Fr_B = 1.7$, the use of the TIS increases S_{ed} at the CG by 67.2 % and 47.9 % in wave conditions 1 and 2, respectively, compared to the bare hull. Despite this increase, the S_{ed} value for a hull equipped with a TIS at $Fr_B = 1.7$ remains below 0.5 MPa, which ISO 2631-5, (2004) categorizes as having a low probability of long-term health risks. In contrast, at $Fr_B = 2.2$, the S_{ed} at the CG decreases by 9.1 % and 1.6 % in wave conditions 1 and 2, respectively, when the TIS is implemented, highlighting its effectiveness at higher speeds.

Fig. 23 shows the TIS's influence on S_{ed} values at the bow. According to Fig. 23, at $Fr_B = 1.7$, S_{ed} at the bow increases significantly, by 275.7 % and 110.0 % in wave conditions 1 and 2, respectively, compared to the bare hull. This substantial increase causes $S_{ed\text{-}8\ h}$ in wave condition 1 to exceed 0.8 MPa, signifying a high probability of adverse long-term health effects for a human stationed near the bow. Conversely, at $Fr_B = 2.2$, the TIS effectively reduces S_{ed} at the bow by 27.2 % and 14.2 % in wave conditions 1 and 2, respectively.

As a conclusion on the effects of the TIS on human safety at $Fr_B = 1.7$, it effectively reduces WBVs and moderate shocks onboard the HSPC, as

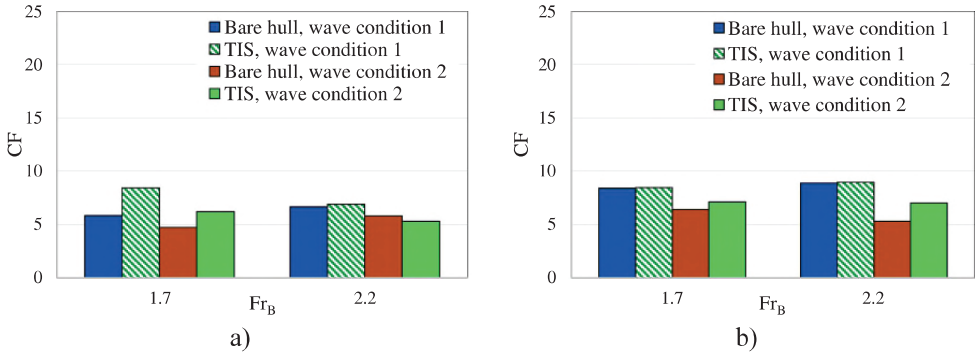


Fig. 24. CF for bare hull and hull with TIS ($0.5B_{WL}$) in a) CG and b) bow in transient mode across wave conditions 1 and 2.

indicated by RMS and VDV_{8h} reduction. However, the TIS may also allow or amplify occasional high acceleration peaks, resulting in an increase in the S_{ed} value. Since S_{ed} is calculated based on the sixth power of weighted acceleration (Eq. (5)), it is highly sensitive to peak acceleration compared to RMS and VDV_{8h}. To further investigate the effect of the TIS on acceleration peak, the full-scaled Crest Factor (CF) for the bare hull and the hull equipped with a TIS is compared in Fig. 24, considering both CG and bow accelerations.

The CF is a nondimensional value defined as the ratio of the maximum weighted acceleration peak to the RMS value. As expected, Fig. 24 shows that TIS amplifies the CF at $Fr_B = 1.7$ in wave conditions 1 and 2, due to an increase in the maximum acceleration peak. This increase in CF correlates with the rise in S_{ed}, even as reductions in RMS and VDV_{8h} indicate decreased WBVs and moderate shocks. In contrast, at $Fr_B = 2.2$, the TIS leads to reductions in CF, S_{ed}, VDV, and RMS across both wave conditions 1 and 2, indicating an overall improvement in human safety at higher speeds.

Up to this point, the analysis is focused on the performance and safety improvement by a TIS with a length of $0.5B_{WL}$ during transient mode operations. This configuration is selected to optimize vertical acceleration reduction at transient mode while ensuring acceptable dynamic performance.

In the next section, the focus shifts to planing mode, where the TIS length are adjusted to $0.25B_{WL}$ to accommodate higher speeds. Additionally, the effects of both the TIS and the DIS are investigated to evaluate their impact on safety improvements and human comfort in this operational regime.

4.3.3. TIS and DIS effect on safety improvement in planing mode

This section investigates the effects of the Transom interceptor system (TIS) with a length of $0.25B_{WL}$ and the DIS on human health and comfort during planing mode operations. As discussed earlier, the TIS length is reduced from $0.5B_{WL}$ to $0.25B_{WL}$ to better accommodate the higher speeds characteristic of planing conditions. The analysis focuses on assessing the effectiveness of these configurations in improving human safety and enhancing crew comfort during high-speed operations.

Considering the effects of the TIS and DIS on vertical acceleration in planing mode, these systems can also affect the WBV and shocks, which directly affect human safety on board HSPCs. Therefore, a comparison of full-scaled RMS and VDV_{8h} values for the bare hull and hulls equipped with TIS and DIS is presented in Fig. 25, focusing on CG and bow accelerations in wave condition 1 at $Fr_B = 3$.

As shown in Fig. 25, the DIS results in a 6.4 % and 8.7 % increase in RMS and VDV_{8h} of weighed CG accelerations, respectively, compared to the bare hull. Similarly, there is a 0.3 % and 4.7 % increase in RMS and VDV_{8h} for weighted bow acceleration. Although these increases in RMS and VDV are not substantial, it can be concluded that the DIS is not efficient in improving human safety onboard HSPCs in planing mode. In fact, it may even increase the probability of adverse health effects and discomfort in planing mode.

Fig. 25 also indicates that RMS and VDV_{8h} for the hull equipped with TIS are significantly lower than the bare hull. The percentage reductions in RMS and VDV for both CG and bow accelerations are presented in Table C3 in Appendix C. These results suggest that the use of TIS can improve safety by reducing the risks of human comfort and adverse health effects in planing mode. Tables B1, B2, B3.

The effects of using TIS and DIS on long-term negative health effects in planing mode are investigated by comparing the full-scaled S_{ed} values for the bare hull, the hull equipped with TIS, and the hull equipped with DIS, as shown in Fig. 26. According to Fig. 26, the use of DIS increases S_{ed} by 18.8 % in the CG compared to the bare hull, while its effect on the S_{ed} of the bow is negligible. Moreover, TIS successfully reduces S_{ed} at both CG and bow by 60.6 % and 51.1 %, respectively, highlighting TIS's effectiveness in improving human safety onboard HSPCs.

Fig. 27 shows a comparison of the effect of TIS and DIS on the full-scaled CF of weighted CG and bow accelerations in wave condition 1 at $Fr_B = 3$. As shown in Fig. 27, the use of DIS results in a 12.0 % and 6.6 % increase in CF for the CG and bow, respectively, compared to the bare hull. In contrast, TIS increases the CF in the bow by 3.0 %, while it efficiently reduces CF in the CG by 37.1 %.

5. Discussion

This study investigated the effects of Transom Interceptor Systems (TIS) and Double Interceptor Systems (DIS) on the dynamic performance and crew's safety onboard a High-Speed Planing Craft in rough water under varying operational regimes. A bare hull was used as a benchmark to highlight the improvements achieved through these systems. The findings provided a comprehensive evaluation of wave-induced motions, hull accelerations, and human safety risks, focusing on weighted root-mean-square (RMS), vibration dose value (VDV), and spine dose value (S_{ed}) indices as defined by ISO 2631-1, (1997); ISO 2631-5, (2004), and EU Directive 2002/44/EC, (2002) standards.

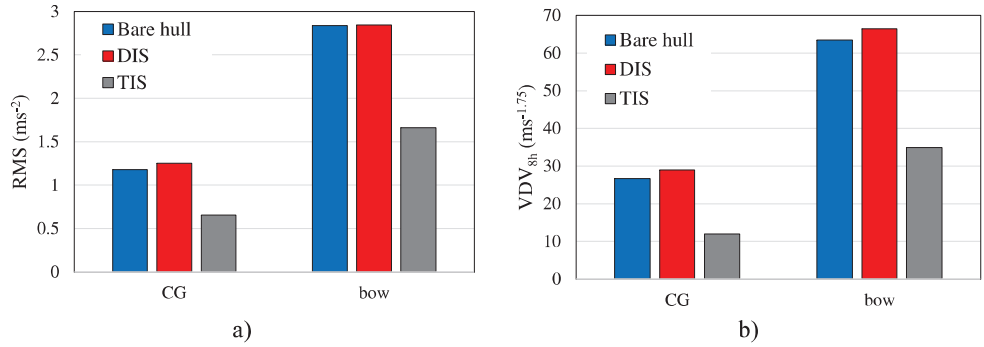


Fig. 25. TIS and DIS effects in a) RMS and b) VDV_{8h} of weighted CG and bow acceleration in wave condition 1 at Fr_B= 3.

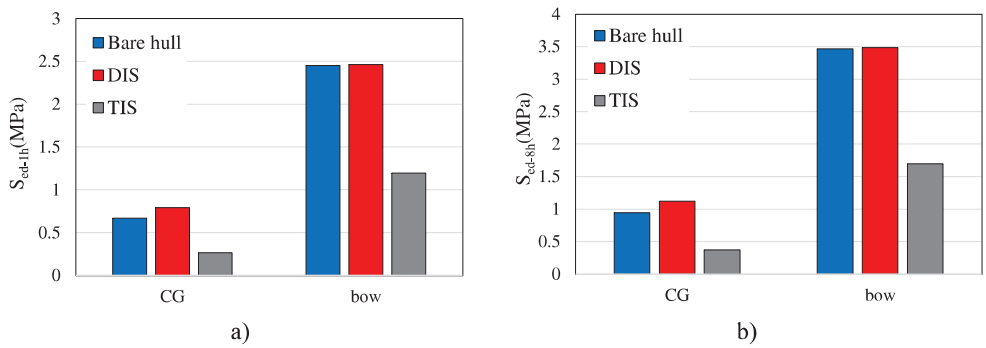


Fig. 26. TIS and DIS effects in a) $S_{ed\text{-}1h}$ and b) $S_{ed\text{-}8h}$ in wave condition 1 and Fr_B=3.

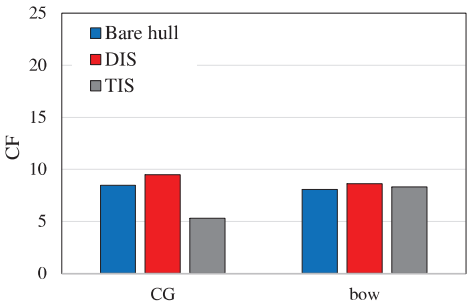


Fig. 27. TIS and DIS effects in crest factor in wave condition 1 at Fr_B = 3.

The results show that TIS, particularly when optimized for specific speed regimes, significantly improves dynamic performance and crew safety. In transient mode, a TIS length of $0.5B_{WL}$ was shown to be effective in reducing hull resistance, heave, and pitch motions, as well as moderate accelerations. Consequently, reducing vertical accelerations resulted in a decrease in RMS and VDV_{8h} values, reducing potential human health and comfort risks. However, it occasionally increased S_{ed} values due to sensitivity to peak accelerations.

In planing mode, reducing the TIS length to $0.25B_{WL}$ provided substantial advantages by reducing hull heave and pitch motions, vertical acceleration, RMS, VDV8h, and S_{ed} values across CG and bow accelerations. This observation highlights the TIS efficacy in improving the dynamic performance of an HSPC and enhancing human safety at higher speeds. However, it should be noted that implementing TIS in planing mode leads to an increase in total resistance.

Conversely, the DIS showed limited efficiency in improving dynamic performance and human safety while offering some dynamic benefits in reducing pitch motion. In planing mode, DIS slightly increased hull resistance, heave motion, vertical acceleration, RMS, and VDV_{8h} values at both CG and bow, along with S_{ed} values in the CG region. These findings suggest that employing DIS to improve dynamic and human safety in planing mode requires further refinements.

Current results align with the results of Park et al., (2019) which highlighted the effects of TIS on HSPC dynamics under irregular wave conditions. Additionally, the performance of DIS has been previously examined in regular wave by De Luca and Pensa (2011), who indicated a potential increase in hull motions. We specifically focused on the effect of TIS and DIS on human safety by analyzing their influence on hull motions and accelerations in irregular wave conditions.

This study is limited to three irregular head waves and four Froude numbers, which may not fully represent the range of operational environments encountered by HSPCs. Furthermore, the analysis considers only three degrees of freedom, neglecting other motions that could affect hull responses and human safety. Addressing these limitations in future research will enhance the generalizability of the findings.

6. Conclusion

This study analyzed the effects of using TIS and DIS on the dynamics of HSPC and their role in improving human safety by reducing accelerations. Towing tank tests are conducted at the Università degli Studi di Napoli "Federico II" providing high-fidelity data that captured the nuances of hull performance in semi-planing, transient, and planing modes. The experiments utilized advanced equipment, including triaxial accelerometers for measuring hull accelerations and motion capture systems for tracking hull responses in wave conditions. These facilities ensure accurate and reliable data to support the analysis.

The findings indicate that in both transient and planing modes, the TIS can efficiently reduce hull motions and accelerations and consequently enhance human safety. However, the measured data for DIS performance in planing mode showed higher motions and accelerations compared to the bare hull.

These results provide a new insight into the efficiency of interceptor systems in enhancing human safety, which can consider in designing and implementation of effective interceptor system. However, the scope of this study is limited to HSPC dynamics under the three degrees of freedom (surge, heave, and pitch) in three irregular head wave conditions at different speeds, along with specific interceptor system configurations. Future research could investigate the effects of interceptor on lateral motions and accelerations, considering waves from other directions and hull with unrestricted sideways motions. Furthermore, a more detailed analysis of fluid flow around the hull could be achieved by simulating HSPC with advanced computational methods.

CRediT authorship contribution statement

Fatemeh Roshan: Writing – original draft, Resources, Formal analysis, Data curation, Methodology, Conceptualization, Visualization, Investigation. **Rasul Niazmand Bilandi:** Investigation, Writing – review & editing, Formal analysis, Validation, Conceptualization, Resources, Data curation. **Fabio De Luca:** Writing – review & editing, Formal analysis, Resources, Data curation. **Simone Mancini:** Supervision, Formal analysis, Writing – review & editing, Data curation. **Pentti Kujala:** Writing – review & editing, Supervision. **Abbas Dashtimanesh:** Writing – review & editing, Supervision, Formal analysis.

Declaration of competing interest

The authors declare that they have no known competing financial interests or personal relationships that could have appeared to influence the work reported in this paper.

Acknowledgments

This study was supported by the Research Project PRIN_2022PNRR_P2022Y3PBY_001 "MADELEINE", CUP J53D23001980006, and projects funded under the National Recovery and Resilience Plan (NRRP), Mission 4 Component C2 Investment 1.1 by the European Union—NextGenerationEU.

Appendix A

Para

Appendix B

To minimize aliasing errors and identify any identify any unintended sources of error from the acquisition system, a high sampling rate is applied using the oversampling technique. As a result, a standard rate of 500 Hz—ten times the network frequency—is selected. In the benchmark study of the NSS series, De Luca and Pensa (2017) previously applied ITTC 7.5–02–02–02 to evaluate the total measurement uncertainty during towing tank tests of the NSS hull series. Their reported total uncertainties in resistance measurement are ±0.01 N, ±0.05° on trim, ±0.001 m/s on speed, and±0.01 kg on weights. Additionally, interceptor height is measured with an uncertainty of 0.02 mm. The uncertainties related to the weights for model C5 can be found in De Luca and Pensa (2017).

The mean value of significant hull motions and accelerations and the uncertainty of the mean value are calculated in accordance with ITTC 7.5–02–01–01, using following equations:

$$\overline{q} = \frac{1}{N}\sum_{t=0}^{T} q(t) \tag{B1}$$

N is the number of data points in the top *1/n* portion (e.g., 1/3, 1/10, or 1/100), T is the measurement time, and *q(t)* represents a time series of a uniformly sampled quantity (e.g., heave, pitch, or acceleration) that top 1/n subset, and $\overline{q}$ is the mean value of the quantity. Furthermore, the standard deviation of q is calculated by:

$$S = \sqrt{\frac{1}{N-1}\sum_{t=0}^{T}(q(t)-\overline{q})^2} \tag{B2}$$

Then the standard uncertainty is estimated as:

$$u(\overline{q}) = \frac{S}{\sqrt{N}} \tag{B3}$$

To consider a 95 % confidence interval, the following equation is used:

$$\overline{q} \pm 1.96.u(\overline{q}) \tag{B4}$$

Table B1
Obtained results and uncertainty for the bare hull.

Wave. No	Fr_B	Heave/Hs			*Pitch/S*			CG acceleration (g)			Bow acceleration (g)		
		$H_{1/3}$	$H_{1/10}$	$H_{1/100}$	$\theta_{1/3}$	$\theta_{1/10}$	$\theta_{1/100}$	$A_{1/3}$	$A_{1/10}$	$A_{1/00}$	$A_{1/3}$	$A_{1/10}$	$A_{1/00}$
1	1.2	0.79 ±0.04	1.08 ±0.04	1.28 ±0.03	1.43 ±0.06	1.78 ±0.03	1.90 ±0.01	0.47±0.02	0.62 ±0.03	0.74±0.04	1.08 ±0.04	1.34 ±0.05	1.59 ±0.03
1	1.7	0.73 ±0.04	0.97 ±0.03	1.13 ±0.01	1.09 ±0.05	1.38 ±0.05	1.60 ±0.01	0.42±0.03	0.69 ±0.04	1.12±0.05	1.41 ±0.09	2.02 ±0.13	2.65 ±0.06
1	2.2	0.34 ±0.02	0.56 ±0.02	0.84 ±0.02	0.78 ±0.03	1.10 ±0.02	1.29 ±0.05	0.36 ±0.004	0.49 ±0.01	0.75±0.03	0.88 ±0.04	1.53 ±0.06	2.33 ±0.10
1	3.0	0.66 ±0.03	0.85 ±0.05	1.10 ±0.01	0.89 ±0.04	1.13 ±0.05	1.45 ±0.10	1.00±0.04	1.35 ±0.07	1.93±0.10	2.56 ±0.12	3.48 ±0.15	4.63 ±0.18
2	1.2	0.52 ±0.02	0.71 ±0.03	0.90 ±0.02	0.93 ±0.03	1.16 ±0.04	1.32 ±0.01	0.21±0.01	0.32 ±0.01	0.54±0.04	0.97 ±0.04	1.26 ±0.06	1.69 ±0.06
2	1.7	0.44 ±0.02	0.60 ±0.02	0.73 ±0.01	0.66 ±0.02	0.83 ±0.02	0.96 ±0.02	0.26±0.01	0.39 ±0.01	0.58±0.03	0.92 ±0.04	1.22 ±0.05	1.54 ±0.10
2	2.2	0.16 ±0.01	0.29 ±0.01	0.53 ±0.02	0.39 ±0.02	0.60 ±0.03	0.82 ±0.03	0.25 ±0.003	0.36 ±0.01	0.57±0.02	0.42 ±0.02	0.73 ±0.04	1.32 ±0.12
3	1.2	0.21 ±0.01	0.33 ±0.01	0.51 ±0.02	0.40 ±0.01	0.51 ±0.01	0.57 ±0.01	0.13±0.00	0.16 ±0.01	0.21 ±0.004	0.39 ±0.01	0.50 ±0.02	0.63 ±0.03
3	2.2	0.11 ±0.00	0.16 ±0.00	0.25 ±0.01	0.13 ±0.01	0.21 ±0.01	0.32 ±0.01	0.17±0.00	0.26 ±0.00	0.44±0.02	0.21 ±0.01	0.38 ±0.02	0.73 ±0.04

Table B2
Obtained results and uncertainty for the hull with TIS.

Wave. No	Fr_B	Heave/Hs			*Pitch/S*			CG acceleration (g)			Bow acceleration (g)		
		$H_{1/3}$	$H_{1/10}$	$H_{1/100}$	$\theta_{1/3}$	$\theta_{1/10}$	$\theta_{1/100}$	$A_{1/3}$	$A_{1/10}$	$A_{1/00}$	$A_{1/3}$	$A_{1/10}$	$A_{1/00}$
1.0	1.7	0.33 ±0.02	0.58 ±0.03	0.97 ±0.06	0.86 ±0.05	1.28 ±0.07	1.72 ±0.07	0.26 ±0.01	0.41 ±0.01	0.71 ±0.04	0.60 ±0.04	1.10 ±0.09	2.25 ±0.19
1.0	2.2	0.29 ±0.02	0.51 ±0.03	0.82 ±0.02	0.71 ±0.03	1.02 ±0.03	1.21 ±0.03	0.36 ±0.00	0.50 ±0.01	0.75 ±0.02	0.74 ±0.06	1.54 ±0.10	2.95 ±0.10
1.0	3.0	0.48 ±0.03	0.66 ±0.04	0.83 ±0.01	0.74 ±0.03	0.96 ±0.05	1.18 ±0.04	0.54 ±0.02	0.74 ±0.04	1.04 ±0.08	1.65 ±0.07	2.17 ±0.10	2.91 ±0.57
2.0	1.7	0.19 ±0.01	0.32 ±0.01	0.59 ±0.04	0.48 ±0.02	0.68 ±0.02	0.90 ±0.01	0.24 ±0.00	0.36 ±0.01	0.58 ±0.02	0.39 ±0.02	0.72 ±0.04	1.36 ±0.05
2.0	2.2	0.15 ±0.01	0.26 ±0.01	0.46 ±0.02	0.36 ±0.02	0.55 ±0.02	0.72 ±0.02	0.22 ±0.00	0.31 ±0.00	0.45 ±0.01	0.36 ±0.01	0.63 ±0.03	1.17 ±0.08

Table B3
Obtained results and uncertainty for the hull with DIS.

Wave. No	Fr_B	Heave/Hs			*Pitch/S*			CG acceleration (g)			Bow acceleration (g)		
		$H_{1/3}$	$H_{1/10}$	$H_{1/100}$	$\theta_{1/3}$	$\theta_{1/10}$	$\theta_{1/100}$	$A_{1/3}$	$A_{1/10}$	$A_{1/00}$	$A_{1/3}$	$A_{1/10}$	$A_{1/00}$
1.0	3.0	0.70 ±0.03	0.91 ±0.05	1.20 ±0.00	0.87 ±0.03	1.05 ±0.04	1.25 ±0.04	1.12 ±0.06	1.59 ±0.09	2.37 ±0.23	2.74 ±0.14	3.73 ±0.18	5.06 ±0.22

Appendix C

Table C1
A summary of TIS $0.5B_{WL}$ effect in dynamic performance of an HSPC in waves 1 and 2 at transient mode ($Fr_B = 1.7$ and 2.2).

Wave number	Fr_B	Resistance reduction	Heave reduction			Pitch reduction			Acceleration reduction in CG			Acceleration reduction in bow		
			$H_{1/3}$	$H_{1/10}$	$H_{1/100}$	$\theta_{1/3}$	$\theta_{1/10}$	$\theta_{1/100}$	$A_{1/3}$	$A_{1/10}$	$A_{1/100}$	$A_{1/3}$	$A_{1/10}$	$A_{1/100}$
1	1.7	4.7 %	21.4 %	6.7 %	7.4 %	21.4 %	6.7 %	−7.4 %	33.0 %	38.0 %	34.2 %	56.9 %	44.5 %	18.8 %
1	2.2	4.9 %	9.1 %	6.7 %	5.8 %	9.1 %	6.7 %	5.8 %	−0.9 %	−1.9 %	−0.3 %	16.3 %	−1.4 %	−25.3 %
2	1.7	4.2 %	56.4 %	45.6 %	19.0 %	27.7 %	18.0 %	5.6 %	6.1 %	9.1 %	0.7 %	57.4 %	40.9 %	11.8 %
2	2.2	4.7 %	7.2 %	10.3 %	12.2 %	7.6 %	8.3 %	14.1 %	12.4 %	14.5 %	19.7 %	15.2 %	13.7 %	11.1 %

*Negative value means increasing the parameter.

Table C2
A summary of TIS $0.5B_{WL}$ effect in human safety onboard a HSPC in waves 1 and 2 at transient mode ($Fr_B = 1.7$ and 2.2).

Wave number	Fr_B	CF reduction		RMS reduction		VDV reduction		S_{ed} reduction	
		CG	bow	CG	bow	CG	bow	CG	bow
1	1.7	−44.1 %	−0.5 %	40.1 %	43.2 %	38.2	45.1 %	−67.2 %	−275.7 %
1	2.2	−3.5 %	0.8 %	9.6 %	11.6 %	12.1	10.6 %	9.1 %	27.3 %
2	1.7	−31.1 %	−11.1 %	36.8 %	43.9 %	36.0	42.2 %	−47.9 %	−110.0 %
2	2.2	8.32 %	−32.6 %	9.5 %	11.3 %	11.4	7.3 %	1.6 %	14.2 %

*Negative value means increasing the parameter.

Table C3
A summary of TIS $0.25B_{WL}$ and DIS effects on dynamic performance and human safety onboard an HSPC in wave 1 at planing mode ($Fr_B = 3$).

Parameters		TIS	DIS
Resistance	–	23.0 %	−4.6 %
Heave reduction	$H_{1/3}$	27.9 %	−6.2 %
	$H_{1/10}$	22.6 %	−6.6 %
	$H_{1/100}$	24.2 %	−9.5 %
Pitch reduction	$\theta_{1/3}$	16.7 %	2.0 %
	$\theta_{1/10}$	14.9 %	7.6 %
	$\theta_{1/100}$	18.6 %	15.9 %
Acceleration reduction in CG	$A_{1/3}$	45.5 %	−12.0 %
	$A_{1/10}$	45.4 %	−17.2 %
	$A_{1/100}$	46.3 %	−22.6 %
Acceleration reduction in Bow	$A_{1/3}$	35.3 %	−7.2 %
	$A_{1/10}$	37.7 %	−7.1 %
	$A_{1/100}$	37.1 %	−9.2 %
CF reduction	CG	37.1 %	−12.0 %
	Bow	−3.0 %	−6.6 %
RMS reduction	CG	44.4 %	6.4 %
	Bow	41.5 %	0.3 %
VDV reduction	CG	55.3 %	−8.7 %
	Bow	44.9 %	−4.7 %
S_{ed} reduction	CG	60.5 %	−18.8 %
	Bow	51.1 %	−0.6 %

*Negative value means increasing the parameter.

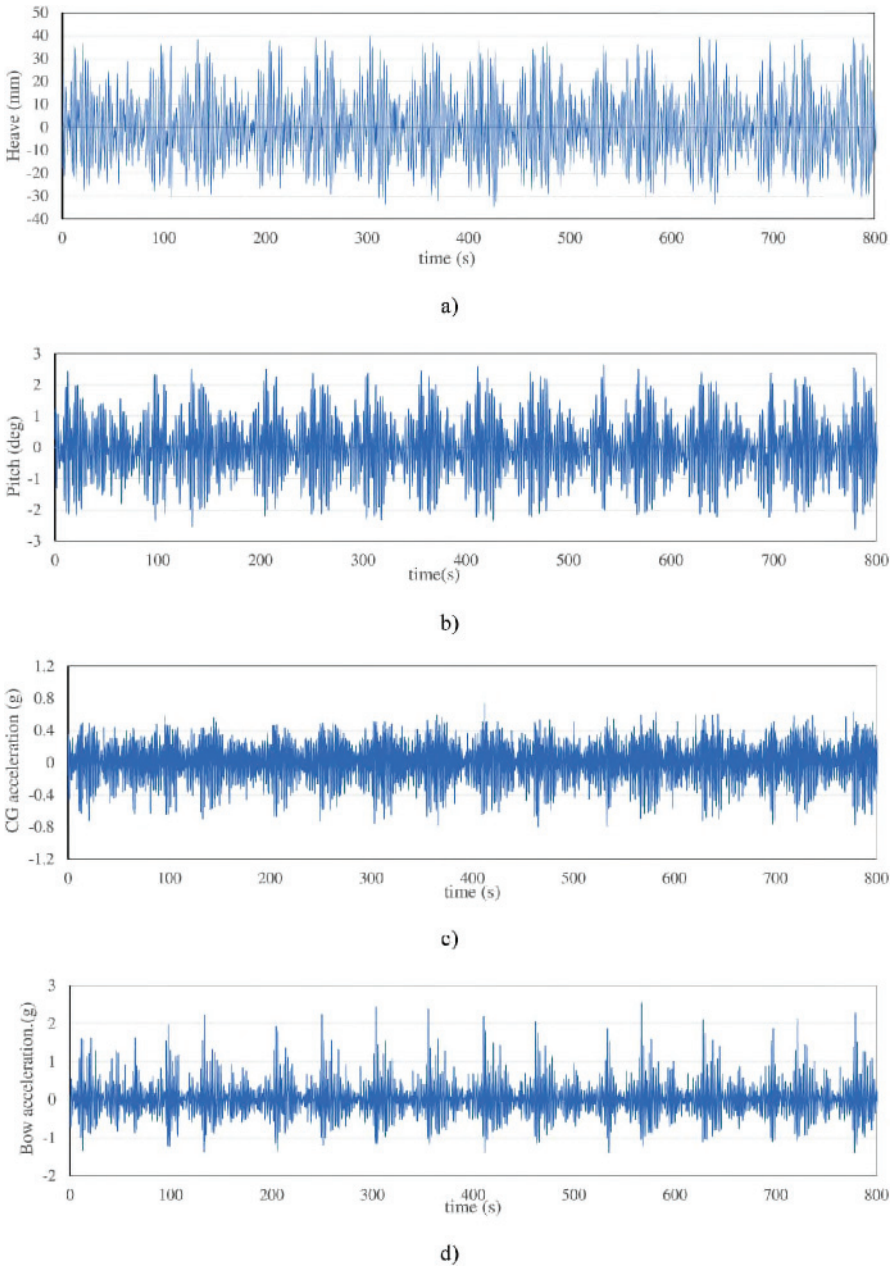


Fig. A1. A time history of recorded a) heave, b) pitch, and vertical acceleration in c) CG and d) bow in wave condition 1 at $Fr_B = 2.2$.

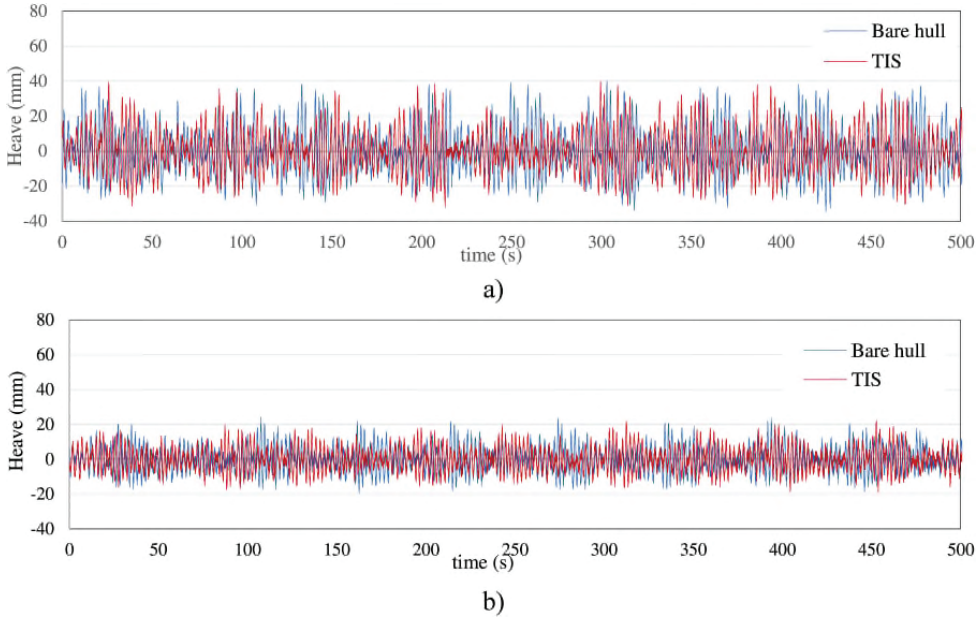


Fig. A2. Time history of heave motions for the bare hull and hull equipped with TIS in a) wave condition 1 and b) wave condition 2 at Fr_B=2.2.

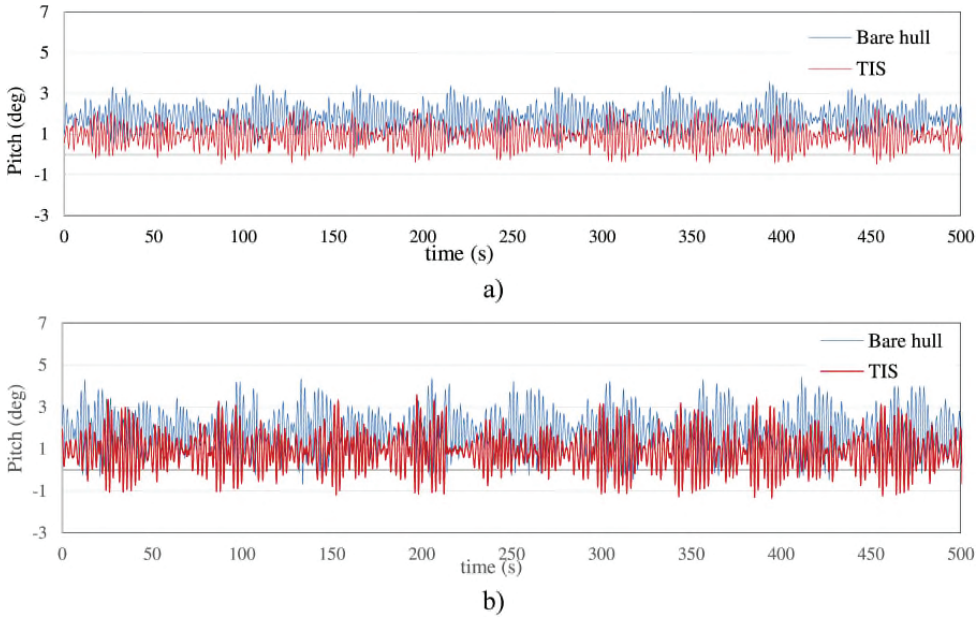


Fig. A3. Time history of pitch motion for the bare hull and hull equipped with TIS in a) wave condition 1 and b) wave condition 2 at Fr_B=2.2.

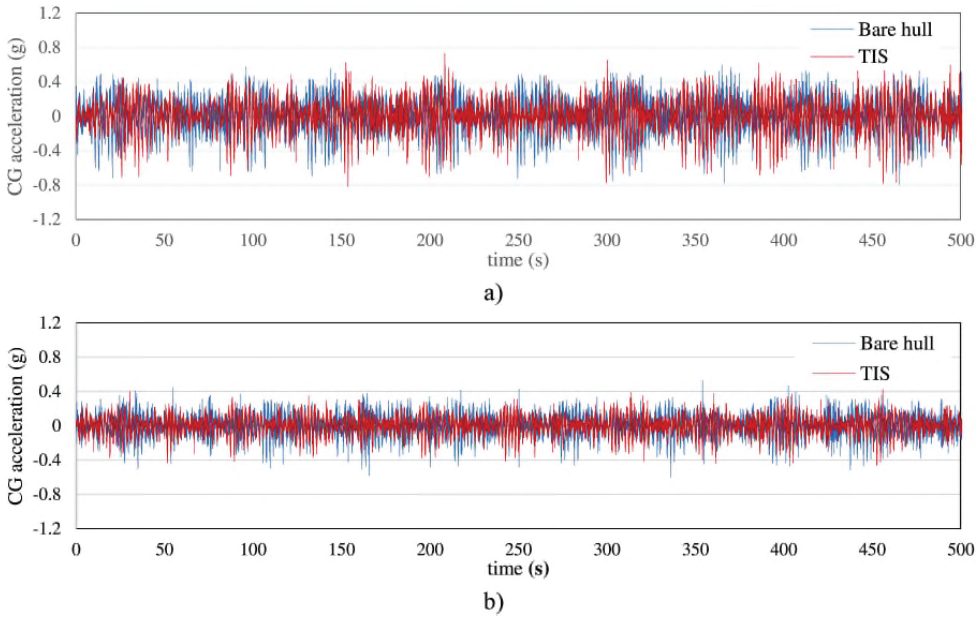


Fig. A4. Time history of the CG acceleration for the bare hull and hull equipped with TIS in a) wave condition 1 and b) wave condition 2, at Fr_B=2.2.

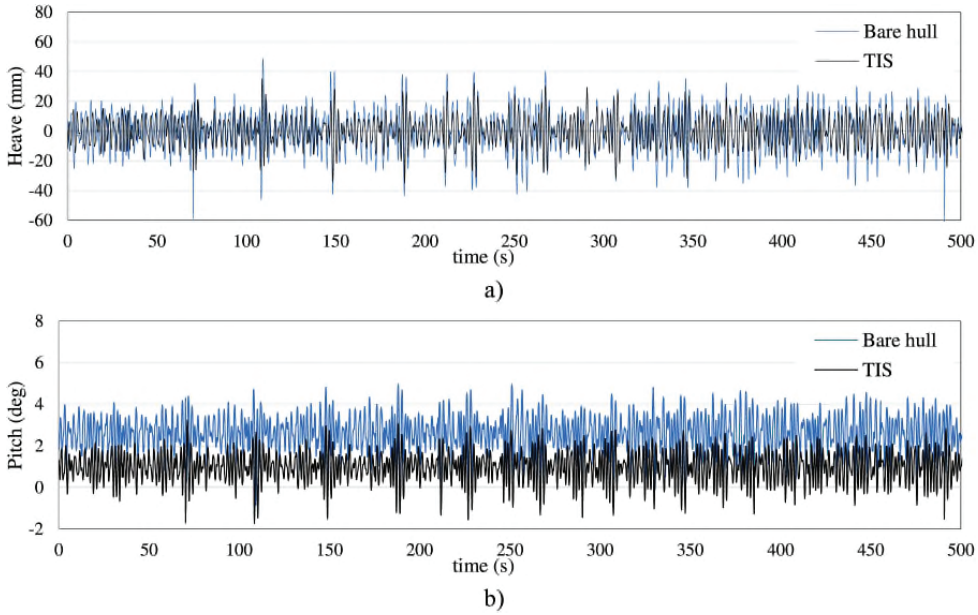


Fig. A5. TIS effect on a) heave and b) pitch motions in transient mode at Fr_B = 3.

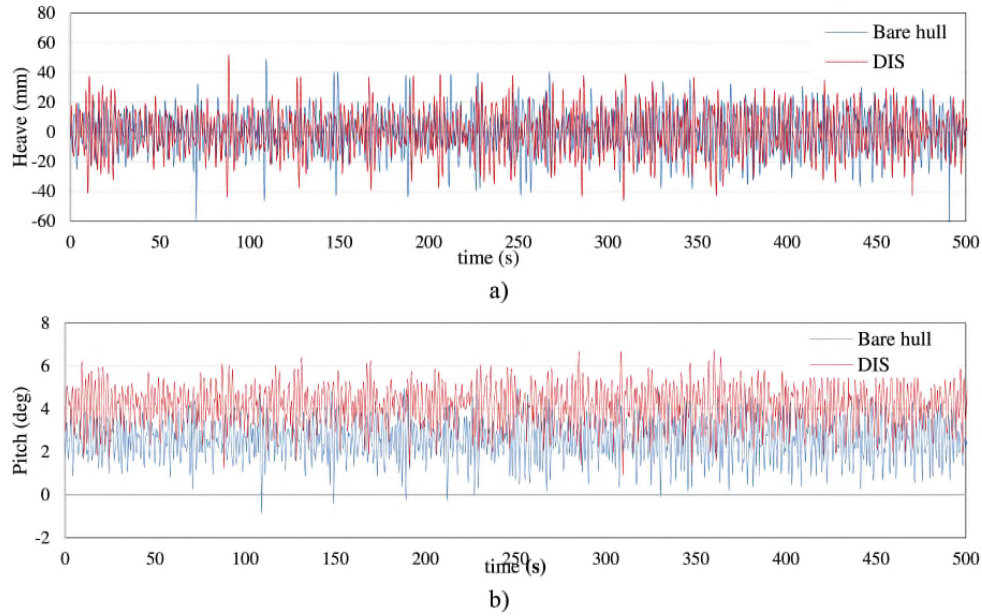


Fig. A6. DIS effect on a) heave and b) pitch motions in transient mode at $Fr_B = 3$.

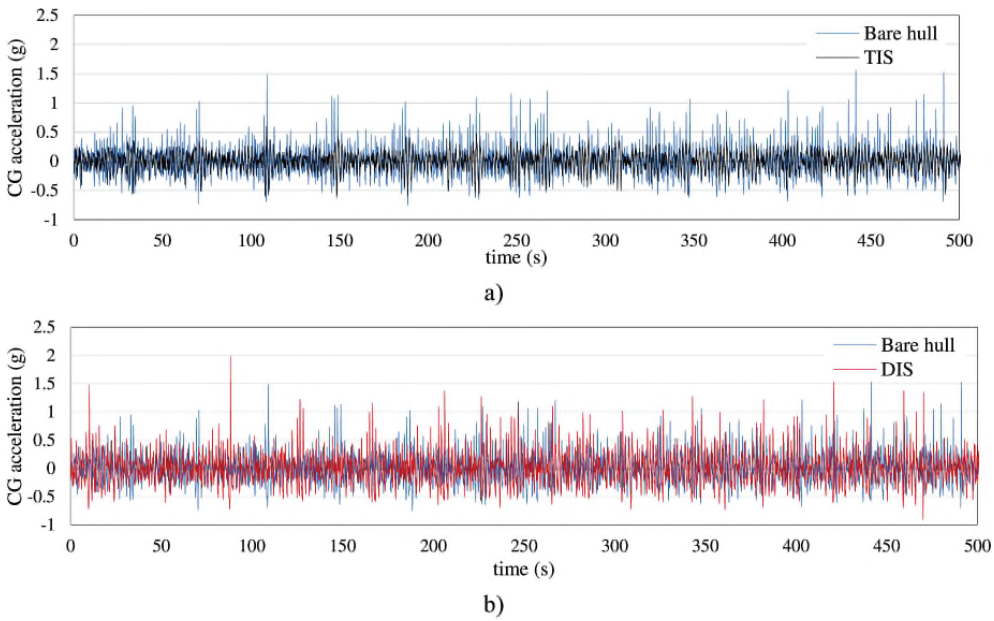


Fig. A7. Time history of CG acceleration in wave at $Fr_B = 3$ for a) bare hull and hull with TIS, and b) bare hull and hull with DIS.

References

ABCD Group. (2008). High Speed Craft Human Factors Engineering and Design Guide (ABCD TR-08-01 V1.0). Available online: https://www.ullmandynamics.com/wp-content/uploads/2011/02/hsc-human-factors-design-guide_2mg.pdf (accessed on 24 February 2022).

Allen, D.P., Taunton, D.J., Allen, R., 2008. A study of shock impacts and vibration dose values onboard highspeed marine craft. Trans. R. Inst. Naval Arch. Part A 150 (A3). Article A3.

Day, A.H., Cooper, C., 2011. An experimental study of interceptors for drag reduction on high-performance sailing yachts. Ocean Eng. 38 (8), 983–994. https://doi.org/10.1016/j.oceaneng.2011.03.006.

De Luca, F., Pensa, C., 2011. Experimental data on Interceptor's effectiveness. ITA. https://www.iris.unina.it/handle/11588/401517.
De Luca, F., Pensa, C., 2012. Experimental investigation on conventional and unconventional interceptors. Trans. R. Inst. Naval Arch. Part B 154, B65–B72. https://doi.org/10.3940/rina.ijsct.2012.b2.129.
De Luca, F., & Pensa, C. (2014). The prediction of the interceptor performances based on towing tank test data: ship-model correlation and hull form influence. 1, 231–238.
De Luca, F., Pensa, C., 2019. The Naples Systematic series – second part: irregular waves, seakeeping in head sea. Ocean Eng. 194, 106620. https://doi.org/10.1016/j.oceaneng.2019.106620.
De Luca, F., Pensa, C., 2017. The Naples warped hard chine hulls systematic series. Ocean Eng. 139, 205–236. https://doi.org/10.1016/j.oceaneng.2017.04.038.
Directive 2002/44/EC. (2002). Directive 2002/44/EC of the European Parliament and of the Council of 25thJune 2002on the Minimum Health and Safety Requirements Regarding the Exposure of Workers to the Risks Arising from Physical Agents (vibration).
Dobbins, T., Myers, S., Dyson, R., Withey, W., Gunston, T., & King, S., 2008. *High speed craft motion analysis: impact count index (ICI)*. 72. https://doi.org/10.3940/rina.surv.2009.09.
Garme, K., Burström, L., Kuttenkeuler, J., 2011. Measures of vibration exposure for a high-speed craft crew. *Proc. Inst. Mech. Eng.*, Part M 225 (4), 338–349. https://doi.org/10.1177/1475090211418747.
ISO 2631-1. (1997). *Mechanical vibration and shock—Evaluation of human exposure to whole-body vibration—Part 1: general requirements*. Int. Organ. Standardization, ISO, 2631-1. https://www.iso.org/standard/7612.html.
ISO 2631–5. (2004). *Shock–Evaluation of Human Exposure to Whole Body Vibration–Part 5: Method for Evaluation of Vibration Containing Multiple Shocks*. ISO: Geneva, Switzerland. https://www.iso.org/standard/7612.html.
John, S., Khan, M., Praveen, P., Korulla, M., & Panigrahi, P., 2011. Hydrodynamic performance enhancement using stern wedges, stern flaps and interceptors. Naval Science & Technological Laboratory, India.
Karimi, M.H., Seif, M.S., Abbaspoor, M., 2013. An experimental study of interceptor's effectiveness on hydrodynamic performance of high-speed planing crafts. Polish Maritime Res. 20 (2), 21–29. https://doi.org/10.2478/pomr-2013-0013.
Karimi, M.H., Seif, M.S., Abbaspoor, M., 2015. A study on vertical motions of high-speed planing boats with automatically controlled stern interceptors in calm water and head waves. Ships Offshore Struct. https://www.tandfonline.com/doi/full/10.1080/17445302.2013.867647.
Lau, C.-Y., Ali-Lavroff, J., Dashtimanesh, A., Holloway, D.S., Mehr, J.A., 2024. High-speed catamaran response with ride control system in regular waves by forcing function method in CFD. Ocean Eng. 297, 117111. https://doi.org/10.1016/j.oceaneng.2024.117111.
Mansoori, M., Fernandes, A.C., 2017. Interceptor and trim tab combination to prevent interceptor's unfit effects. Ocean Eng. 134, 140–156. https://doi.org/10.1016/j.oceaneng.2017.02.024.
Najafi, A., Alimirzazadeh, S., Seif, M.S., 2015. RANS simulation of interceptor effect on hydrodynamic coefficients of longitudinal equations of motion of planing catamarans. J. Braz. Soc. Mech. Sci. Eng. 37 (4), 1257–1275. https://doi.org/10.1007/s40430-014-0256-6.
Niazmand Bilandi, R., Tavakoli, S., Mancini, S., Dashtimanesh, A., 2024. Dynamic motion analysis of stepless and stepped planing hulls in random waves: a CFD model perspective. Appl. Ocean Res. 149, 104046. https://doi.org/10.1016/j.apor.2024.104046.
Park, J.Y., Choi, H., Lee, J., Choi, H., Woo, J., Kim, S., Kim, D.J., Kim, Kim, N., 2019. An experimental study on vertical motion control of a high-speed planing vessel using a controllable interceptor in waves. Ocean Eng. 173, 841–850. https://doi.org/10.1016/j.oceaneng.2019.01.019.
Putra, A.M.F., Suzuki, H., 2024. Experimental and numerical study on the high-speed ship hydrodynamics influenced by an interceptor with varied angle of attack. Int. J. Naval Arch. Ocean Eng. 16, 100566. https://doi.org/10.1016/j.ijnaoe.2023.100566.
Roshan, F., Dashtimanesh, A., Kujala, P., 2024. Safety improvements for high-speed planing craft occupants: a systematic review. J. Mar. Sci. Eng. 12 (5), 5. https://doi.org/10.3390/jmse12050845. Article.
Roshan, F., Tavakoli, S., Mancini, S., Dashtimanesh, A., 2022. Dynamic of tunneled planing hulls in waves. J. Mar. Sci. Eng. 10 (8), 8. https://doi.org/10.3390/jmse10081038. Article.
Seok, W., Park, S.Y., Rhee, S.H., 2020. An experimental study on the stern bottom pressure distribution of a high-speed planing vessel with and without interceptors. Int. J. Naval Arch. Ocean Eng. 12, 691–698. https://doi.org/10.1016/j.ijnaoe.2020.08.003.
Suneela, J., Krishnankutty, P., Subramanian, V.A., 2020. Numerical investigation on the hydrodynamic performance of high-speed planing hull with transom interceptor. Ships Offshore Struct. https://www.tandfonline.com/doi/full/10.1080/17445302.2020.1738134.
Suneela, J., Sahoo, P., 2021. Numerical investigation of interceptor effect on seakeeping behaviour of planing hull advancing in regular head waves. Brodogradnja 72 (2), 73–92. https://doi.org/10.21278/brod72205.
Taunton, D.J., Hudson, D.A., Shenoi, R.A., 2011. Characteristics of a series of high speed hard chine planing hulls - part II: performance in waves. Int. J. Small Craft Technol. 153, B1–B22. https://doi.org/10.3940/rina.ijsct.2011.b1.97.
Niazmand Bilandi, R. (2024). *Efficient high-speed small craft: performance in calm water and waves* [PhD degree, Tallinn University of Technology]. https://doi.org/10.23658/taltech.71/2024.
Tsai, F.J., Hwang, J.L., 2004. Study on the compound effects of interceptor with stern flap for two fast monohulls. In: IEEE Xplore Conference: MTTS/IEEE Techno-Ocean'04, Oceans'04, Taiwan, vol. 2. pp. 1023–1028 Nov. 9–12., doi:10.1109/OCEANS.2004.1405650.

Appendix 6 (Publication VI)

Paper VI

Roshan, F., Garme, K., & Dashtimanesh, A. (2026). Acceleration effects in the horizontal plane on the safety assessment aboard a high-speed craft. *Proceedings of the Institution of Mechanical Engineers, Part M: Journal of Engineering for the Maritime Environment*, 14750902261440461. https://doi.org/10.1177/14750902261440461.

Check for updates

Original research article

Institution of MECHANICAL ENGINEERS
Journal of ENGINEERING FOR THE MARITIME ENVIRONMENT

Proc IMechE Part M:
J Engineering for the Maritime Environment
1–17
© IMechE 2026
Article reuse guidelines:
sagepub.com/journals-permissions
DOI: 10.1177/14750902261440461
journals.sagepub.com/home/pim
Sage

Acceleration effects in the horizontal plane on the safety assessment aboard a high-speed craft

Fatemeh Roshan[1], Karl Garme[2] and Abbas Dashtimanesh[2]

Abstract

Current knowledge regarding the assessment of forward and sideways accelerations on human safety onboard the high-speed craft (HSC) remains limited, and most conventional shock mitigation seats for these vessels are designed primarily to mitigate vertical accelerations. This study analyzes recorded accelerations onboard a high-speed craft (HSC) in multiple directions to evaluate the effects of forward, sideways, and vertical accelerations on human health and comfort in accordance with ISO 2631-1:1997. To address the shortcomings of conventional seat systems, this research proposes a shock mitigation seat model that incorporates both forward and vertical suspension systems. A mathematical model is developed to predict the seat's ability to reduce multidirectional acceleration exposure, with an emphasis on vertical acceleration—the direction with the highest intensity—and the forward direction, which is often overlooked in existing designs. The results demonstrate that combining forward and vertical suspension systems in seat design can significantly reduce health and comfort risks associated with accelerations in these directions. This study provides a foundation for future innovations in HSC seat design and encourages the integration of forward suspension systems to enhance occupant safety and comfort.

Keywords

high speed planing craft, multi-directional acceleration exposure, safety assessment, shock mitigation seat, human health and comfort

Received: 3 May 2025; accepted: 21 March 2026

Introduction

Whole-body vibration (WBV) refers to a range of mechanical vibrations transmitted to the human body and causes adverse health effects, including lower back pain, and musculoskeletal disorders. During high-speed craft (HSC) operations in rough waters at high speeds, occupants experience intense shocks and continuous vibrations, posing health and comfort risks.[1–4] Therefore, identifying and minimizing harmful vibrations and shocks is essential to enhance the safety of HSC crews.

Previous studies have investigated vibration and shock effects based on direction, magnitude, and frequency.[5–7] Griffin[7] found that forward shocks can exert pressure on the spinal cord; sideways shocks can impinge on nerve fibers, potentially leading to back pain and sciatica; and vertical vibrations can cause a visual illusion known as the elevator illusion. Hence, ISO 2631-1:1997[8] considers different multiplying factors based on directions to amplify the vibration and shock magnitude in forward and sideways directions, while in most conditions, the highest vibration and shock magnitude is still related to the vertical direction.

In HSCs, WBVs and shocks derive from multidirectional hull acceleration. The acceleration peak values in each direction, primarily caused by slam impacts, are the main source of human injuries. However, the lower acceleration magnitude and repeated continuous vibrations affect human comfort and can lead to adverse health effects. Therefore, reducing peak acceleration minimize human injuries, while reducing the vibrations can improve human comfort. Since vertical impact shocks usually dominate, with the possibility of

[1]Kuressaare College, Tallinn University of Technology, Estonia
[2]Department of Engineering Mechanics, School of Engineering Science, KTH Royal Institute of Technology, Stockholm, Sweden

Corresponding author:
Fatemeh Roshan, Kuressaare College, Tallinn University of Technology, Estonia.
Email: fatemeh.roshan@taltech.ee

exceeding $20g$,[9] safety strategies often focus on vertical acceleration, neglecting other directions.

However, a self-report analysis conducted by Ullman et al.[10] revealed that 49% (889 out of 1827) of crew injuries result from impacts containing sideways forces, 18% (333 out of 1827) from forward impacts, 12% (218 out of 1827) from vertical impacts, and 14% (262 of 1827) from seat bottoming out. Comparatively, the least frequent injuries, at 0.5% (6 of 1827) are attributed to capsizing. These reported injuries could be caused by acceleration exposure or sudden harsh impacts, especially being thrown from the seat, which is preventable with seat belts.

In an HSC, being thrown from the seat is particularly likely during forward and sideways impact occasions and can be prevented using a seat belt and cupped seats. In contrast, during the vertical impacts, the seated human is pushed down into the seat, and spinal contraction can be mitigated using a seat vertical suspension system. Similarly, forward and sideways suspension systems can improve human comfort and reduce long-term negative health risks caused by acceleration exposed in these directions. However, these systems are not effective in preventing humans from being thrown from their seats.

Given that lower back pain is one of the most frequently reported human injuries,[11,12] which can be affected by forward and sideways accelerations, it is important to analyze the recorded data of acceleration in different directions onboard an HSC and evaluate their effects on safety risk quantitatively, using the current safety standards.

In the case of high acceleration exceeding the allowable ranges recommended by standards, motion reduction devices (e.g. trim tab, interceptor, etc.) and shock mitigation seats can be employed to mitigate the vibrations and shocks.[13,14] The effectiveness of shock mitigation seats in mitigating vertical accelerations has been confirmed by many researchers[15–22] through sea trial tests, drop tower tests, and mathematical models. However, no HSC seat model fully addresses forward acceleration, and previous studies mostly focus on vertical acceleration, limiting comprehensive safety assessment.

This study investigates the safety of HSC occupants exposed to multidirectional acceleration, focusing on human health and comfort risk. It evaluates vertical, forward, and sideways accelerations in accordance with the current safety standards. Moreover, a mathematical model of a shock mitigation seat incorporating both vertical and forward suspension systems is developed and analyzed. The objective is to quantify the potential improvements in occupant safety and ride comfort achieved by integrating a forward suspension element—an enhancement to conventional vertically suspended seat designs.

To achieve these objectives, acceleration data recorded by Garme et al.[23] during 12 sea trial tests of HSC operations are used. The data series serves as the basis for assessment metrics such as Crest Factor (CF), Root Mean Square (RMS), and Vibration Dose Value (VDV). The analysis encompasses evaluating the effects of an HSC acceleration on human health and comfort considering vertical, forward, or sideways directions as well as multidirectional acceleration. Moreover, a mathematical model is developed with both vertical and forward suspension systems to predict shock mitigation seat performance. The vertical spring and damper system is validated with the measured vertical acceleration on the seat during the 12 sea tests. The forward suspension system, which contains a horizontal spring and damper is evaluated by forward accelerations. In addition, the performance of a shock mitigation seat with both forward and vertical suspension systems is investigated.

Methods

This study is carried out in two phases. The first phase aims to evaluate the effects of forward, sideways, and vertical accelerations on HSC crews. The second phase introduces a shock mitigation seat model with forward and vertical suspension systems and analyzes its efficiency.

Acceleration evaluations in different directions

The measurement data are acquired from an HSC of the Swedish Coastguard, which features an 11 m length and operates at 50 knots. Ten-minute sea trials are conducted under 12 test runs.[23] Three accelerometers measure accelerations as shown in Figure 1: two measure vertical acceleration along the deck, and one measures acceleration on the seat cushion in all three directions. Although the acceleration signals were originally collected by Garme et al.,[23] all results presented in this study are based on our own processing and analysis to include forward and sideways accelerations in addition to vertical component.

Vertical acceleration at the seat base is calculated using the accelerations recorded by accelerometers 1 and 2,

$$a_{z,base} = a_1 + \frac{a_2 - a_1}{5.42}.X \tag{1}$$

where a_1 and a_2 are vertical accelerations recorded by accelerometers 1 and 2, and X is the distance of the desired point along the hull from the accelerometer 1. Therefore, vertical acceleration on the seat base is calculated with $X = 1.39$ m.

The acceleration signals from all accelerometers are sampled at 800 Hz and low-pass filtered at 200 Hz. This process is essential to minimize structural vibrations from the collected data. As an example, the recorded signals and the weighted-frequency-filtered vertical acceleration on the seat during test run 1 are shown in Figure 2.

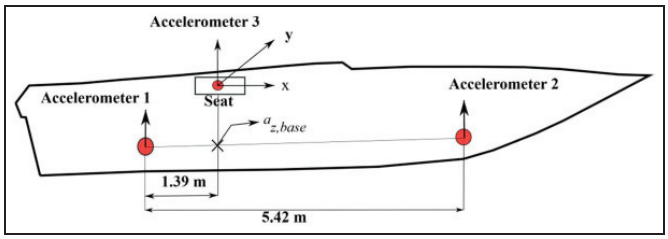


Figure 1. Location of each accelerometer on the hull.

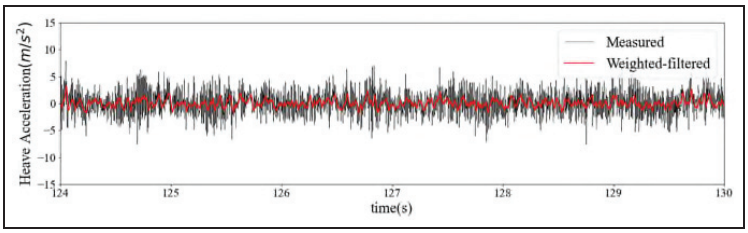


Figure 2. Measured and weighted filtered signals of vertical acceleration in test run 1.

The frequency-weighting is a meticulous process. Firstly, the collected signals are transformed into the frequency domain. Here, they are multiplied by the weighting transfer functions outlined in Annex A of ISO 2631-1:1997,[8] a recognized standard. These functions are employed individually for each direction—forward, sideways, and vertical. Subsequently, the transformed signals are transformed back into the time domain, resulting in the frequency-weighted acceleration time series.

The safety evaluation in this study aligns with ISO 2631-1:1997[8] and EU Directive 2002/44/EC[24] by assessing the potential for adverse health effects and discomfort for humans. The evaluation methods are based on two key metrics: the root-mean-square (RMS) of acceleration and the Vibration Dose Value (VDV) computed as,

$$a_w = \left\{ \frac{1}{T} \int_0^T a_w^2(t)\, dt \right\}^{1/2} \tag{2}$$

$$VDV = \left\{ \int_0^T [a_w(t)]^4\, dt \right\}^{\frac{1}{4}} \tag{3}$$

where $a_w(t)$ is the frequency-weighted acceleration and T is the time period of measurement. To analyze the effect of multidirectional acceleration on human health and comfort, the vector sums of a_w and VDV are computed as follows:

$$a_v = (k_x^2.a_{wx}^2 + k_y^2.a_{wy}^2 + k_z^2.a_{wz}^2)^{\frac{1}{2}} \tag{4}$$

$$VDV_{xyz} = (k_x^4.VDV_x^4 + k_y^4.VDV_y^4 + k_z^4.VDV_z^4)^{1/4} \tag{5}$$

with $k_x = k_y = 1.4$ and $k_z = 1$.[8] To evaluate the effect of acceleration on human health, ISO 2631-1:1997[8] and EU Directive 2002/44/EC[24] use the daily acceleration exposure over an 8-h period that can be calculated as:

$$a_{w,e} = \left[\frac{\sum a_{wi}^2.T_i}{\sum T_i} \right]^{\frac{1}{2}} \tag{6}$$

$$VDV(8h) = VDV.\left[\frac{8}{T} \right]^{1/4} \tag{7}$$

In equation (6), a_{wi} is the RMS of the weighted acceleration during the exposure time T_i. For calculating RMS_{8h}, it is assumed that the human is exposed to acceleration during the measurement time and rests during the remaining time with $a_{wi} = 0$. However, VDV_{8h} is calculated by assuming the same acceleration exposure during the 8-h workday.

According to ISO 2631-1:1997,[8] for an occupant with a potential health risk, the caution zone threshold stands RMS_{8h} ranges between 0.45 and 0.9 m/s^2. In situations involving high potential health risks, the threshold elevates to 0.9 m/s^2 (see ISO 2631-1:1997,[8] Annex B). Moreover, EU Directive 2002/44/EC[24] defines the action and limit values of 9.1 $m/s^{1.75}$ and 21.0 $m/s^{1.75}$, respectively, for VDV_{8h} to avoid the risk to human health. However, since 8-h work for HSCs rarely occurs, it is illustrative to present the time to exceed VDV $>$ 21 $m/s^{1.75}$, which is calculated as,[25]

$$Time\ to\ limit = \frac{VDV\ limit^4.T}{Measured\ VDV^4} \tag{8}$$

It is important to note that the RMS value may not adequately capture the influence of shock, when CF > 9 (CF = maximum weighted acceleration/RMS).[8] In this case, VDV or Maximum Transient Vibration Value (MTVV) have been recommended, as they are more sensitive to acceleration peaks. MTVV can be calculated as,

$$MTVV = max[a_w(t_0)] \tag{9}$$

where $a_w(t_0)$ is determined as,

$$a_w(t_0) = \left\{ \frac{1}{\tau} \int_{t_0-\tau}^{t_0} [a_w(t)]^2 \, dt \right\}^{\frac{1}{2}}, \tau = 1(s) \tag{10}$$

Despite the health risks, human comfort can be assessed using the RMS value. As per ISO 2631-1:1997,[8] the RMS falls within the range of 0.8 to 1.6 m/s^2, signifying an "Uncomfortable" condition for the occupants and RMS > 2 m/s^2, indicates "Extremely uncomfortable." However, it should be considered that RMS is unreliable for CF > 9, as acceleration peaks significantly affect comfort.

Mathematical model for shock mitigation seats

When acceleration onboard HSCs reveals a potential health risk and discomfort, acceleration reduction is essential. This study develops a mathematical model to study the shock mitigation seat performance, incorporating vertical and forward suspension systems. Sideways suspension is not included, as its effect on total VDV is negligible compared to vertical and forward accelerations.

The vertical damping and stiffness coefficients are chosen to match the seat in the Coast Guard craft, presented by Olausson and Garme.[18] The predicted vertical acceleration on the seat cushion resulting from the seat base acceleration, calculated by equation (1) is compared with the recorded acceleration on the seat cushion to validate seat model.

As the referenced seat does not have any horizontal suspension system to mitigate forward and sideways acceleration, and we lack measurement data at the seat base in those directions, it is simply assumed that the measured forward and sideways acceleration on the seat cushion are equal to the seat base. Furthermore, real forward suspension parameters for other HSC seats are not publicly available, and it is not possible to calculate the corresponding spring stiffness and damper coefficient for the forward direction. Accordingly, the forward suspension system is chosen with the same spring and damper characteristics as the seat in Stein and Múčka,[26] which was employed for a loader driving the bucket into a heap of soil, a situation involving harsh forward accelerations. These characteristics are considered representative of this type of application, allowing us to estimate the potential to mitigate forward accelerations onboard the HSC.

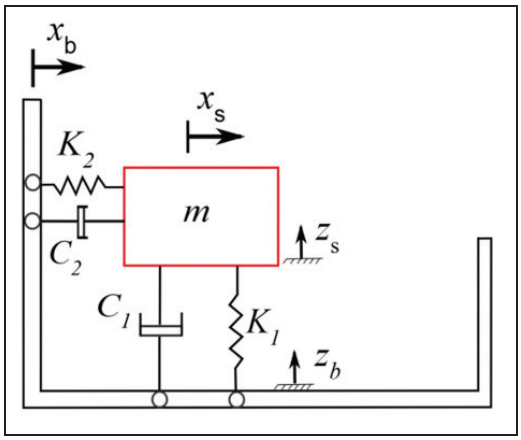


Figure 3. A schematic of the seat model and free body diagram.

Table 1. Seat model characteristics.

Parameter	Value
Mass, m	107.5 (kg)
Spring stiffness coefficient, K_1	Nonlinear, see Figure 4(a))
Spring stiffness coefficient, K_2	Nonlinear, see Figure 4(b))
Damping coefficient, C_1	2200 Ns/m
Damping coefficient, C_2	1564.88 Ns/m
Seat motion	Vertical + forward

A sketch of the seat model with forward and vertical suspension systems is shown in Figure 3, and input data is provided in Table 1.

The seat model mass is a summation of seat mass (38.0 kg), the mass of seated human thighs, and the human upper body (see Table 1). For a seated human with a total mass of 85 kg, the upper body has 72.3% of the total weight (61.4 kg), and the thighs have 9.5% (8.1 kg).[18] Therefore, m = 107.5 kg in the seat modeling. Nonlinear spring stiffness in vertical and forward directions models seat cushion characteristics, as shown in Figure 4.

The vertical damping coefficient C_1 in Table 1 matches the seat in the Olausson and Garme[18] experiment, and the horizontal damping coefficient C_2 is a linearized coefficient calculated for the nonlinear damper in Stein and Múčka.[26]

For a mass, spring, and damper system, the seat response to the seat base acceleration is derived from the equation of motion,

$$ma + F_s + F_d = F \tag{11}$$

where m is mass in kg, F_s is the total spring forces regarding to the displacement in N, F_d is the total

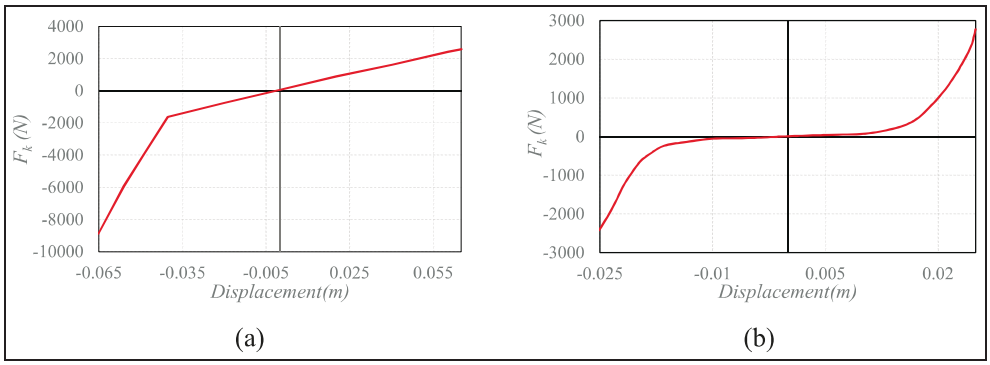


Figure 4. Nonlinear Spring characteristics in (a) vertical[18] and (b) forward directions.[26]

damper forces regarding to the velocity in N, and F is excitation force in N. Therefore, the equations of motion for the seat model with forward and vertical motions are expressed as,

$$m\ddot{x}_r + K_2.x_r + C_2.\dot{x}_r = -m\ddot{x}_b \quad (12)$$

$$m\ddot{z}_r + K_1.z_r + C_1\dot{z}_r = -m\ddot{z}_b \quad (13)$$

where $\ddot{x}_r$ and $\ddot{z}_r$ are the relative forward and vertical accelerations between the seat cushion and the seat base, and $\ddot{x}_b$ and $\ddot{z}_b$ are the seat base accelerations in corresponding directions. Furthermore, K_1 and K_2 are the spring stiffness coefficients (from Figure 4), and C_1 and C_2 are damping coefficient (Table 1). The x_r, and z_r are seat relative displacements, and $\dot{x}_r$ and $\dot{z}_r$ are relative forward and vertical velocities.

Thus, the absolute forward and vertical acceleration on the seat cushion can be calculated by

$$\ddot{x}_r = \ddot{x}_s - \ddot{x}_b \quad (14)$$

$$\ddot{z}_r = \ddot{z}_s - \ddot{z}_b \quad (15)$$

where $\ddot{x}_s$ and $\ddot{z}_s$ refer to the seat accelerations in x and z axes

Equations (12) and (13) are uncoupled and solved separately as a second-order equation by using a fourth-order Runge-Kutta scheme (see Burden and Faires[27]), with initial conditions,

$$\dot{z}_r(0) = 0, \dot{x}_r(0) = 0, z_r(0) = 0, x_r(0) = 0 \quad (16)$$

Results and discussions

The effects of forward, vertical, and sideways accelerations on human safety and comfort are analyzed in accordance with ISO 2631-1:1997[8] and EU Directive 2002/44/EC[24] to identify critical directions contributing to human safety risks. The results highlight the importance of forward acceleration, which is often overlooked in previous studies and conventional seat designs for HSC. To address this, the current study proposes using a shock mitigation seat with both forward and vertical suspension systems onboard the HSC to minimize health and comfort risks associated with acceleration in these directions. The effectiveness of this seat model is predicted by developing a mathematical model capable of simulating its performance under multidirectional acceleration conditions.

Analyzing acceleration in different directions

This section evaluates the effects of vertical, forward, and sideways accelerations as well as multidirectional acceleration on human health and comfort.

Evaluating vertical, forward, and sideways accelerations. The recorded data from 12 sea tests on the HSC seat base and seat cushion serve as the basis for assessing the effect of acceleration in various directions of HSC occupants. A sample weighted acceleration at the seat base for test run 3 is shown in Figure 5, where upward vertical shocks produce short-delayed negative forward accelerations, followed by the opposite sequence.

The CF and RMS values for all test runs are shown in Figure 6. The vertical CF values exceed the threshold of 9.0 in all runs, as depicted in Figure 6(a). According to ISO 2631-1:1997,[8] when CF $>$ 9.0, supplementary methods (VDV and MTVV) are recommended for acceleration evaluation. In contrast, the CF values for both forward and sideways accelerations remain below 9.0; consequently, RMS evaluation is sufficient in these directions.

According to Figure 6(b), RMS values range from 1.4 to 2.2 m/s^2 for forward, 0.53 to 1.4 m/s^2 for sideways, and 1.8 to 3.0 m/s^2 for vertical directions. These values correspond, respectively, to "Uncomfortable" to "Extremely Uncomfortable," "A little uncomfortable" to "Very Uncomfortable," and "Very Uncomfortable" to "Extremely Uncomfortable" conditions in these directions. Since forward and sideways accelerations

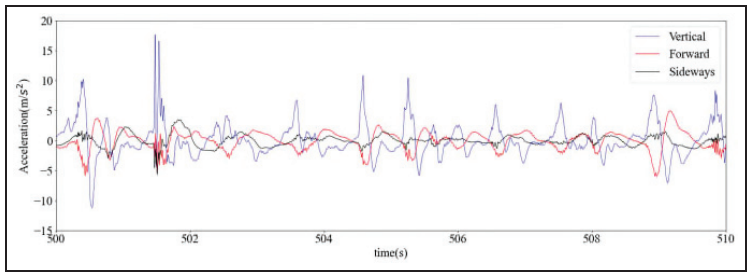


Figure 5. Sample of weighted acceleration data in different directions in test run 3.

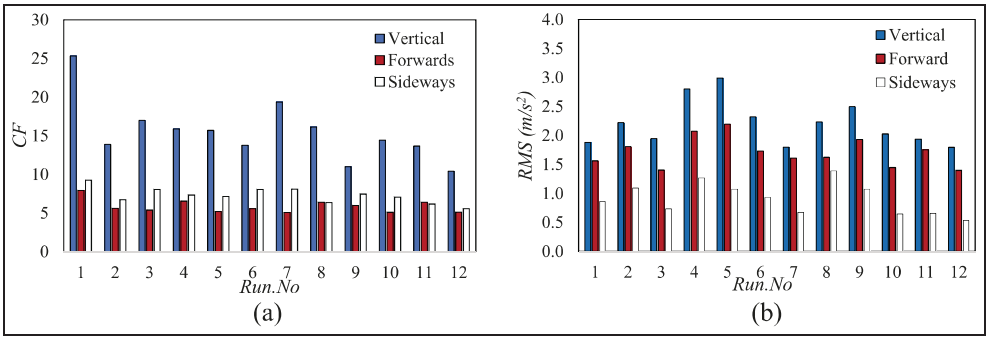


Figure 6. (a) Crest factor and (b) RMS for forward, sideways, and vertical accelerations on the seat base.

exceed 25% of the vertical RMS, they should not be neglected in comfort evaluation in accordance with ISO 2631-1:1997[8] recommendation, and acceleration mitigation in all directions is essential.

As mentioned, current standards use RMS_{8h} to evaluate the risks of adverse effects caused by acceleration on human health. Therefore, RMS_{8h} for weighted acceleration values over an 8-h duration aboard the HSC (equation (6)) is presented in Figure 7. According to ISO 2631-1:1997,[8] $RMS_{8h} > 0.43\,m/s^2$ indicates potential risk, while $RMS_{8h} > 0.9\,m/s^2$ suggests likelihood of health risk. As Figure 7 indicates, forward and sideways RMS_{8h} remain below $0.43\,m/s^2$ in all tests, while vertical RMS_{8h} exceeds this threshold only in runs 4 and 5. Thus, RMS_{8h} alone suggests low health risk in current measurement time (around 10 min), while longer exposure time would raise the risk. Moreover, since $CF > 9$ for vertical acceleration in most cases, analyzing VDV and MTVV measures is also required.

The MTVV and VDV_{8h} for acceleration in different directions are presented in Figure 8. MTVV values in Figure 8(a) are considerably higher than RMS presented in Figure 6(a), confirming the severe impact shocks on the seat. Furthermore, analyzing VDV_{8h} values reveals ranges of 37.92 to $78.5\,m/s^{1.75}$ in vertical, 25.6 to $40.5\,m/s^{1.75}$ in forward, and 9.8 to $26.5\,m/s^{1.75}$ in sideways directions, that all exceeding the EU Directive 2002/44/EC[24] limit value ($21\,m/s^{1.75}$) in several runs.

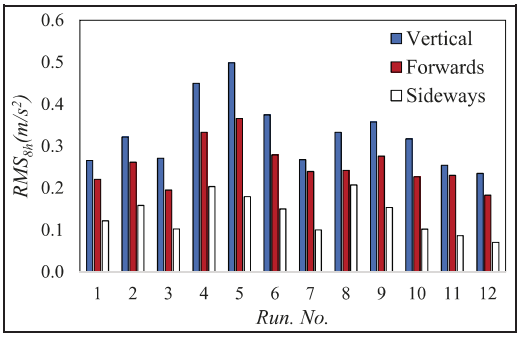


Figure 7. Daily RMS for forward, sideways, and vertical accelerations on the seat base.

These findings indicate that vertical accelerations pose the highest risk; however, forward and sideways also contribute significantly.

While the elevated VDV_{8h} for different directions of acceleration, surpassing the limit value set by Directive 2002/44/EC[24] (see Figure 8(b)), it is important to acknowledge that an 8-h work period is atypical for HSC operations.[23] Therefore, the time required to surpass the VDV threshold of $21.0\,m/s^{1.75}$ for forward and vertical accelerations is shown in Figure 9. The forward

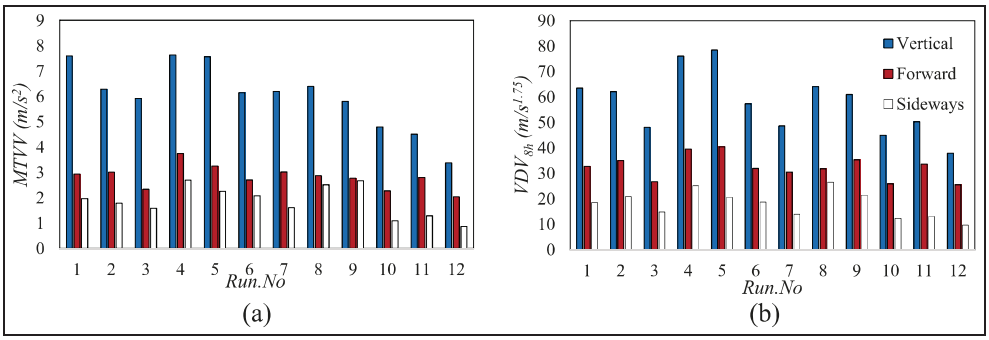


Figure 8. (a) MTVV and (b) VDV_{8h} in different directions on the seat base.

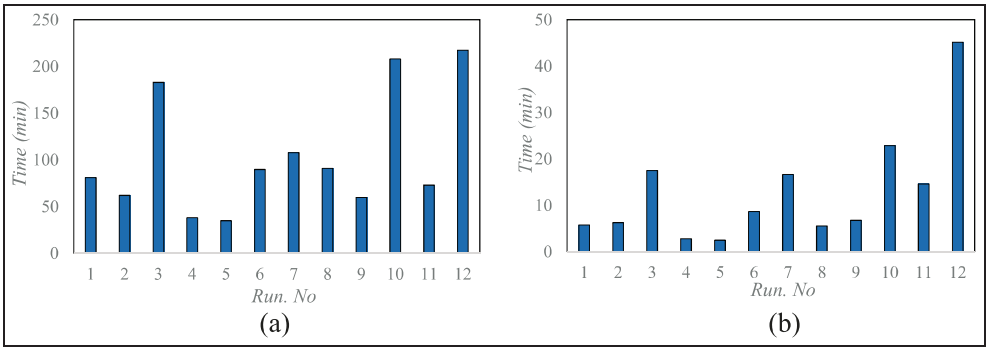


Figure 9. Time for VDV of (a) forward and (b) vertical acceleration to exceed 21 $m/s^{1.75}$.

acceleration over a time span exceeding 34.8 min could heighten the likelihood of health issues (see Figure 9(a)). In contrast, the potential health risk posed by vertical accelerations is anticipated to manifest after just 4.7 min of work, emphasizing the swifter onset of concerns associated with this direction of acceleration exposure.

Multidirectional acceleration. The findings highlighted the exposure to forward, sideways, and vertical accelerations, indicating potential effects on human health. Consequently, exploring the combined effects of acceleration in various directions is essential, as real-world vibrations and shocks often occur multidirectional.

To evaluate the effect of multidirectional acceleration exposure, the mean RMS values of the seat base acceleration across 12 test runs are analyzed for different combinations, as shown in Figure 10. Vertical acceleration is the dominant direction, while including forward and/or sideways accelerations significantly increases the RMS. The forward-vertical (VF) combination raised RMS by up to 35.2%, while including all three directions (VFS) increased it by up to 39.3% over vertical alone. These findings emphasize the critical impact of forward acceleration, a factor often neglected in conventional seat designs and safety assessments onboard the HSC. Detailed data are given in Appendix 1Figures 20–22.

Further, the effects of multidirectional acceleration on VDV_{8h} and time for VDV to exceed the limit value of 21.0 $m/s^{1.75}$ are shown in Figure 11. Mean values of VDV_{8h} across 12 test runs show that combining all directions (VFS) increases VDV_{8h} by 1.8% to 4.9% compared to vertical alone. The influence of sideways acceleration is minor, as vertical and sideways combinations (VS) increase VDV_{8h} by only 0.1% to 0.7%. These findings confirm the dominance of vertical acceleration and the notable role of forward motion, while sideways effects remain limited under the tested conditions.

Figure 11(b) indicates that including forward acceleration significantly reduces the time to reach the limit value for VDV. For instance, in test 12, vertical acceleration alone exceeds the limit value after 45.2 min, whereas adding forward motion reduces this time to 37.4 min. Across all runs, forward and vertical combinations reduce exposure time by 5.7% to 17.2%, and VFS combinations by 7.0% to 17.5%. These results

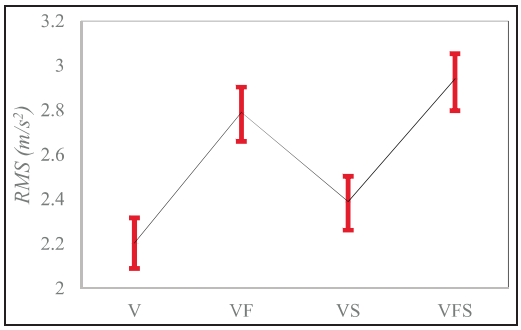


Figure 10. Mean RMS value for multidirectional acceleration on the seat base. (V: vertical, F: forward, and S: sideways). Error bars represent the standard uncertainty across 12 test runs.

highlight the importance of considering forward accelerations when evaluating cumulative acceleration exposure.

ISO 2631-1:1997[8] recommends using the highest value of RMS to estimate human health risks when the vibration in other directions is not comparable in magnitude. Therefore, in most previous studies on the human safety evaluation onboard HSC and vibration and shock reduction devices, researchers focused on vertical acceleration, which has the highest magnitude.[13] However, the current results indicate that in conventional HSC operation, sideways and forward accelerations may be significant, providing an argument for considering multidirectional acceleration in safety evaluation of HSC occupants and when studying shock mitigation seat performance with respect to vibration and shock in different directions.

Investigating the two-directional shock mitigation seat model

As the measured accelerations onboard the HSC demonstrate, forward and vertical accelerations transmitted to the occupant can cause potential health risks and discomfort.[8,24] Therefore, reducing WBV and shocks in these directions is essential to improve human safety. Shock mitigation seats are an effective solution to mitigate accelerations transmitted to the seated human. Published studies by Rebelle,[28] Cho and Yoon,[29] and Maciejewski et al.[30] indicate that mathematical models can efficiently predict shock mitigation seat performance. However, most mathematical models of HSC seats, such as those by Coe et al.[31] and Olausson,[32,33] are limited to the vertical direction.[13]

Here, the shock mitigation seat model with forward and vertical suspension systems presented in section 2.2 is used to evaluate multidirectional shock mitigation. The model's accuracy is validated by comparing calculated and measured vertical accelerations on seat cushion across 12 test runs. The vertical spring stiffness and damping coefficients follow Olausson and Garme,[18] while forward coefficients are based on Stein and Múčka[26] (see Table 1). The shock mitigation efficiency is evaluated by comparing the RMS and VDV of the seat and the seat base.

Validation for seat modeling. Vertical accelerations at the seat base are used as the model input, with outputs compared against seat cushion measurements. RMS_z and $VDV_{8h,z}$ for both experimental and model results are presented in Table 2, across all 12 runs. According to Table 2, the current seat model slightly underestimates RMS (–5.4% to –0.6% error) and VDV (–5.8% to 4.1% error), except in runs 1 and 8. However, overall accuracy is acceptable.

It should be noted that Olausson and Garme[18] previously proposed a 2DOF vertical mathematical model for this seat, with VDV errors ranging from −7.1% to 1.3%. The current model uses a simplified 1DOF vertical configuration to reduce complexity, while maintaining comparable accuracy to the previous model. A time history of recorded and predicted vertical acceleration on seat cushion is presented in Figure 12.

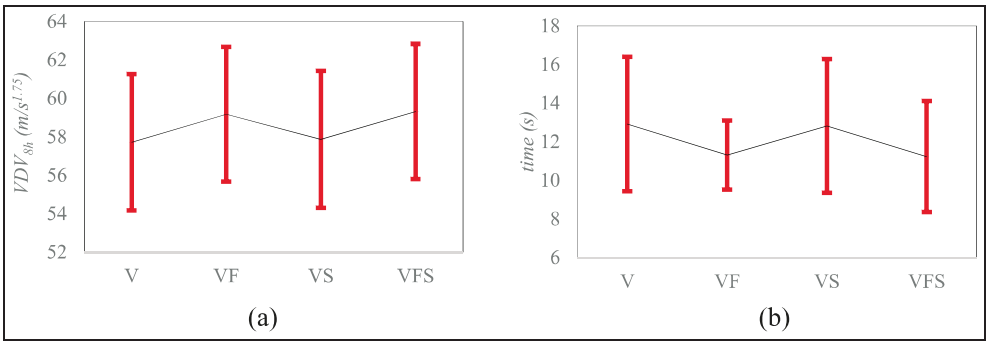


Figure 11. (a) Mean VDV_{8h} and (b) time to VDV $>$ 21 $m/s^{1.75}$ for multidirectional acceleration on seat base (V: vertical, F: forward, S: sideways). Error bars represent the standard uncertainty across 12 test runs.

Table 2. A comparison between modeled and measured RMS_z and $VDV_{8h,z}$.

	RMS_z			$VDV_{8h,z}$			Relative displacement (m)		
Test run	Measured	Modeled	Diff. (%)	Measured	Modeled	Diff. (%)	Max.	Min.	Travel length
1	2.0	1.9	−5.4	49.6	50.3	1.6	0.03	−0.04	0.07
2	2.4	2.3	−3.9	53.4	52.2	−2.3	0.03	−0.04	0.06
3	2.1	1.9	−5.4	41.7	40.1	−3.8	0.02	−0.03	0.04
4	2.8	2.8	−1.1	63.0	62.6	−0.7	0.03	−0.04	0.07
5	3.1	3.0	−0.9	66.7	64.7	−3.0	0.03	−0.04	0.07
6	2.4	2.3	−1.7	49.4	48.5	−1.9	0.02	−0.03	0.05
7	1.9	1.8	−2.7	41.5	41.5	−0.1	0.02	−0.03	0.05
8	2.1	2.1	−1.1	46.0	47.9	4.1	0.02	−0.03	0.05
9	2.6	2.5	−0.6	51.6	51.4	−0.4	0.05	−0.03	0.08
10	2.2	2.1	−5.0	41.1	39.3	−4.4	0.01	−0.02	0.04
11	2.0	1.9	−4.0	43.9	43.1	−1.8	0.02	−0.03	0.04
12	1.8	1.8	−4.8	35.0	33.0	−5.8	0.01	−0.02	0.03

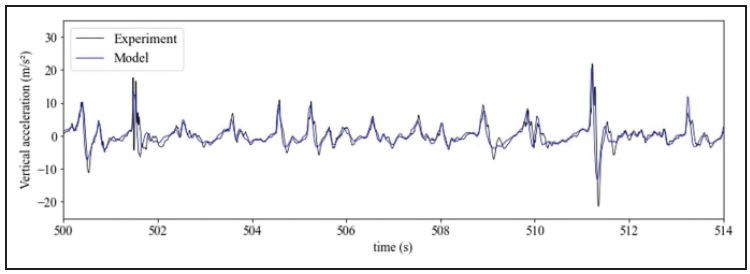


Figure 12. Time history of predicted and recorded vertical acceleration on seat cushion at test run 1.

According to Figure 12, the model underestimates negative peak accelerations. This might be related to ignoring the effects of the seat cushion and assuming linear damper coefficients. In addition, effects of footrest and friction are not considered in the model.

The maximum and minimum relative vertical displacement in the seat model, ranging from −40.4 to 28.3 mm (see Table 3). This range is well below the defined vertical travel length of 160 mm,[18] and no bottoming-out event occurs.

Statistical differences between measured accelerations on experimental seat and model are summarized in Table 3. The mean difference during the measured time, $\overline{u}$, and standard deviation σ is calculated using,

$$\overline{u} = \frac{1}{N}\sum_{t=0}^{T} u(t) \tag{17}$$

$$\sigma = \sqrt{\frac{\sum_{t=0}^{T} (u-\overline{u})^2}{N-1}} \tag{18}$$

where N is the number of samples, T is the measurement time, and $u(t) = \ddot{z}_1(t) - \ddot{z}_{1,exp}(t)$ for $\ddot{z}_1$ and $\ddot{z}_{1,exp}$ referring to calculated and measured vertical acceleration, respectively. And the 95% tolerance interval, assuming that $u(t)$ is normally distributed, is given by,

$$\overline{u} - 1.96\sigma < u < \overline{u} + 1.96\sigma \tag{19}$$

According to Table 3, the standard deviation ranges between 0.84 and 1.64 m/s^2 across the 12 sea trials, with

Table 3. Statistical properties for the difference between vertical accelerations of seat model and experimented seat.

			95% tolerance interval	
Test run	$\overline{u}$ (mm/s^2)	σ (m/s^2)	Lower limit (m/s^2)	Upper limit (m/s^2)
1	−0.47	1.13	−2.22	2.21
2	0.08	1.10	−2.16	2.16
3	0.08	1.02	−1.99	1.99
4	−0.06	1.43	−2.79	2.79
5	−0.45	1.64	−3.22	3.22
6	0.02	1.12	−2.19	2.19
7	−0.05	0.87	−1.70	1.70
8	0.04	1.11	−2.17	2.17
9	0.01	1.28	−2.51	2.51
10	0.05	0.99	−1.93	1.93
11	0.07	0.93	−1.82	1.82
12	0.02	0.85	−1.66	1.66

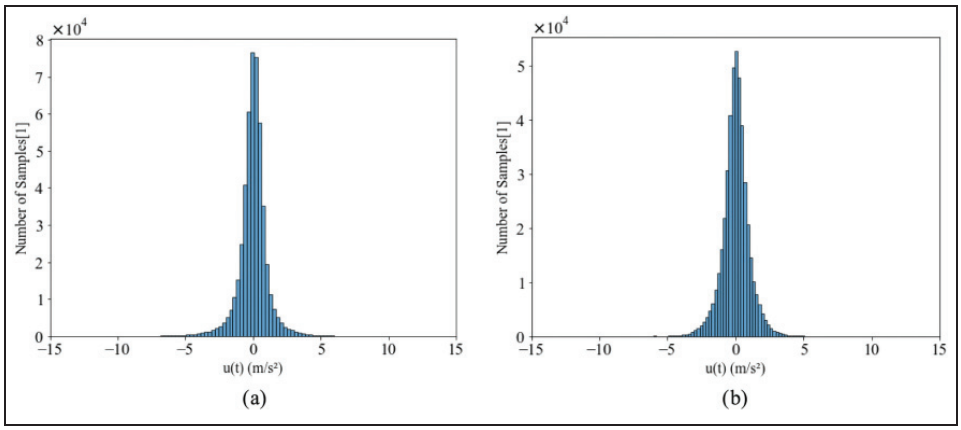


Figure 13. Distribution of difference *u(t)* for (a) test run 2 and (b) test run 3.

an average 1.12 m/s^2. Although these standard deviations may appear large compared to the RMS values in Table 2, they are small relative to the measured accelerations. For instance, the measured acceleration on the seat cushion ranged between −19.38 and 26.35 m/s^2 in test run 2, with RMS of 2.4 m/s^2 and a standard deviation of 1.1 m/s^2. The mean differences remain within the range of –0.47 and 0.08 mm/s^2, indicating that deviations are cantered very close to zero. The distribution of differences in test runs 2 and 3, shown in Figure 13, is predominantly cantered around zero, supporting alignment between computation and measurement. Furthermore, the 95% tolerance interval indicates that most differences fall within a statistically acceptable range. These observations suggest a good agreement between the mathematical model and the experimental results.

To compare the result in frequency domain, Figure 14 shows the frequency response functions (FRFs) between the seat base and the seat cushion for both the experimental measurements and the proposed seat model during test run 2 and 3. The FRFs are presented in terms of transmissibility magnitude, and phase. The results indicate that the model accurately reproduces the experimental transmissibility and phase trends. Although experimental coherence decreases and the measured FRF becomes less consistent at higher frequencies, the model maintains a smooth and physically realistic transmissibility curve. This low coherence, particularly at higher frequencies, can be attributed to noise and nonlinearities in the measurement signal. Generally, this indicates that the simplified one-degree-of-freedom model can capture not only the essential low-frequency seat dynamics but also provide stable predictions across a broader frequency range.

Efficiency of the two-directional shock mitigations seat model. To assess the effect of the proposed seat model in reducing forward and vertical accelerations, the time histories of the modeled and measured seat accelerations are compared with the seat base in Figure 15. In this figure, vertical acceleration at the seat base is calculated by equation (1), with data recorded by accelerometers 1 and 2. Moreover, forward acceleration on the seat base is assumed to be equal to the forward acceleration measured on the seat cushion by accelerometer 3. According to Figure 15, the presented seat model reduces the forward and vertical accelerations; however, investigating RMS and VDV in these directions is required to assess potential for safety improvements by a shock mitigation seat with the present characteristics.

A comparison between the RMS_z and $VDV_{8h,z}$ on the seat cushion and the seat base is presented in Figure 16. The measured and predicted RMS_z on the seat cushion are higher than those at the seat base in most runs, which has also been reported previously by Garme et al.[23] However, $VDV_{8h,z}$ on the seat is between 14.3% and 33.8% lower than at the seat base, indicating a reduction in vertical acceleration peaks. Comparable reduction in VDV_z by implementing suspension seat have been reported in the literature. For instance, Coe et al.[31] reported 47% reduction in VDV_z, while Dobbin et al.[15] indicates 19% reduction when using suspension seat. These comparisons indicate that the present model provides a vertical response consistent with previously reported seat behaviors.

Nevertheless, despite this reduction, the seat $VDV_{8h,z}$ values remain higher than the limit value defined by EU Directive 2002/44/EC[24] for avoiding human health risks. This suggests that although the suspension seat provides significant reduction in severe vertical acceleration, it does not fully eliminate the risk of adverse health effects under the tested operating conditions.

In the previous sections, the acceleration evaluation for an HSC highlighted potential safety risks due to forward and vertical accelerations. Consequently, mitigating forward acceleration, in addition to vertical, could enhance occupant comfort and safety. Although

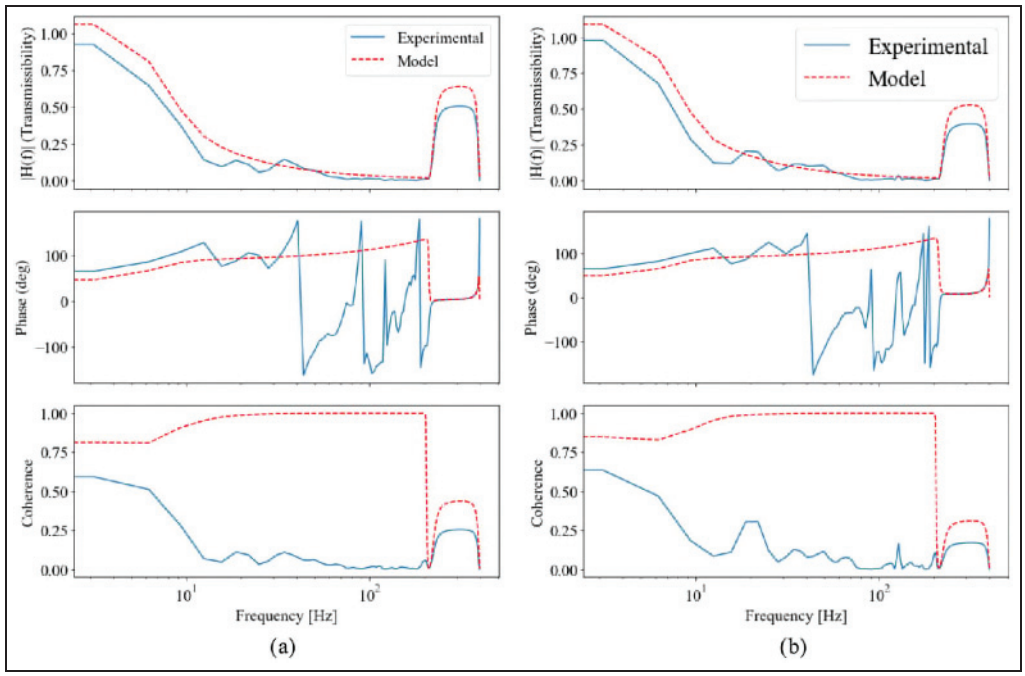


Figure 14. Frequency response functions (magnitude, phase, and coherence) between the seat base and seat cushion for experimental and model during (a) test run 2 and (b) test run 3.

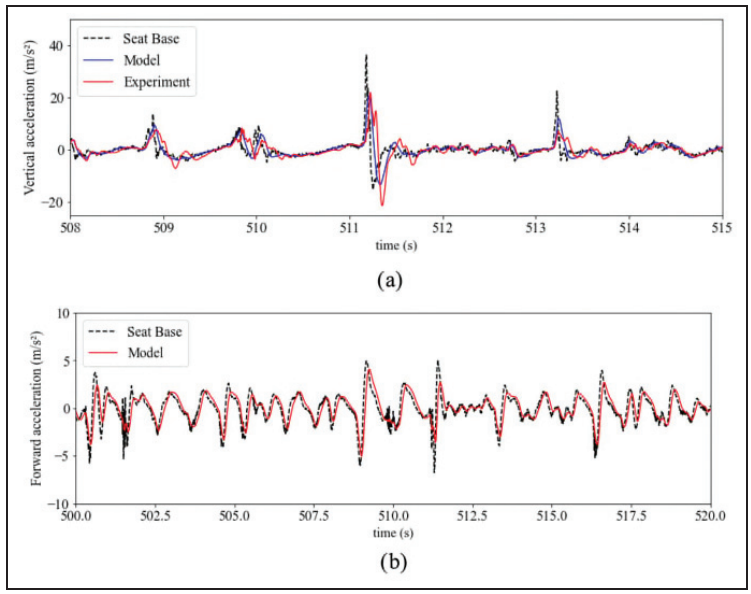


Figure 15. Computed and measured time history of (a) vertical and (b) forward accelerations in test run 1.

current information on forward suspension system for HSCs is limited, there are some published studies for trucks and off-road vehicles seats. Such seat models could potentially be adapted to investigate the seat potential to mitigate high forward acceleration on HSCs.

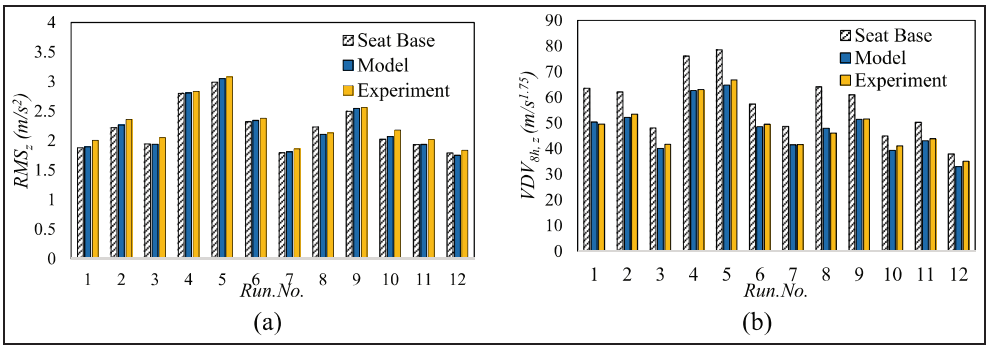


Figure 16. (a) RMS_z and (b) $VDV_{8h,z}$ at the seat base and the seat cushion in the vertical direction.

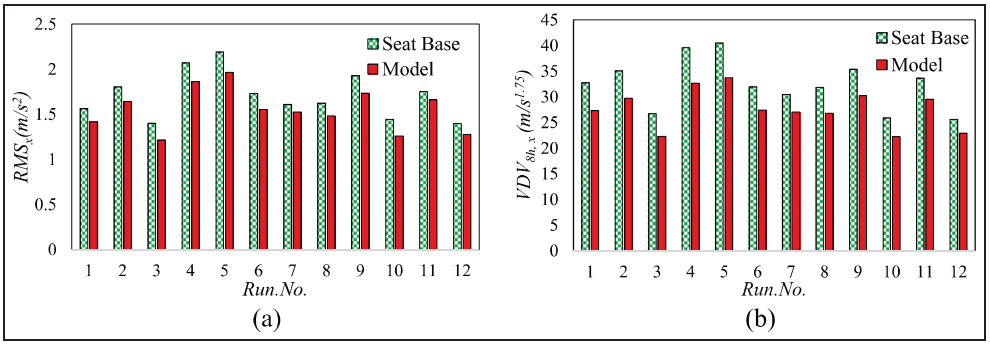


Figure 17. (a) RMS_x and (b) $VDV_{8h,x}$ at the seat base and the seat cushion in the forward direction.

The efficiency of a seat with a forward suspension system has been studied previously by Stein and Múčka[26] for a loader that operates in off-road terrain with harsh forward shocks. As HSCs also experience high forward accelerations, this section examines the potential benefits of similar suspension systems for improving human safety onboard the HSC. A schematic of the seat model configuration is presented in Figure 3.

The RMS_x and $VDV_{8h,x}$ values of the seat model, when fed with measured seat cushion forward acceleration (assumed to represent the seat base forward acceleration), are compared with the measured data from 12 sea trials, as presented in Figure 17. The seat model reduces RMS_x by 5.4% to 15.3%. This reduction improves human comfort. For instance, in test run 5, RMS_x reduces from 2.19 to 1.97 m/s^2.

Similarly, $VDV_{8h,x}$ is reduced by 11.8%–21.2%. Although values remain above the EU Directive 2002/44/EC[24] limit ($VDV_{8h} > 21\ m/s^{1.75}$), multidirectional suspension systems still mitigate acceleration exposure.

A dangerous condition for a seated human on a shock mitigation seat is bottoming out, which amplifies the impact shocks. Bottoming out occurs when the seat relative displacement exceeds its free travel, causing motion to stop abruptly. Therefore, predicting seat displacement in both forward and vertical directions is essential.

The results indicate that the seat oscillates in the forward direction between 5.4 and 11.8 mm forward from its initial position (Figure 18(a)). Similarly, the seat oscillation point in the vertical direction is between −4.9 and −8.4 mm (Figure 18(b)). These results demonstrate a potential risk of bottoming out in case the vertical travel length designed is lower than 68.6 mm (28.3 mm upward, 40.3 mm downward) and 102.8 mm forward (59.8 mm forward, 43.0 mm backward).

The RMS_{xz} and $VDV_{8h,xz}$ values for the seat base, experimental seat, and modeled seat are shown in Figure 19, assuming that the seat base forward acceleration is equal to that measure on the seat cushion. The RMS_{xz} on the seat model is 1.9%–20.5% lower than the seat base, however it remains an "extremely uncomfortable" condition referring to ISO 2631-1:1997.[8] Adding the forward suspension system to the vertical suspension system causes a 3.7 to 7.8% reduction in RMS_{xz} compared to the measurement.

Additionally, $VDV_{8h,xz}$ at the modeled seat cushion is 14.3% to 33.8% lower than the seat base (Figure 19(a)).

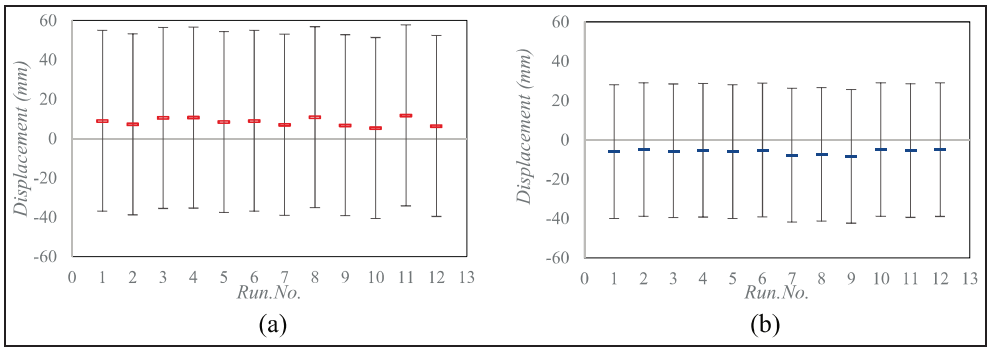


Figure 18. (a) Forward and (b) Vertical relative displacement of the seat.

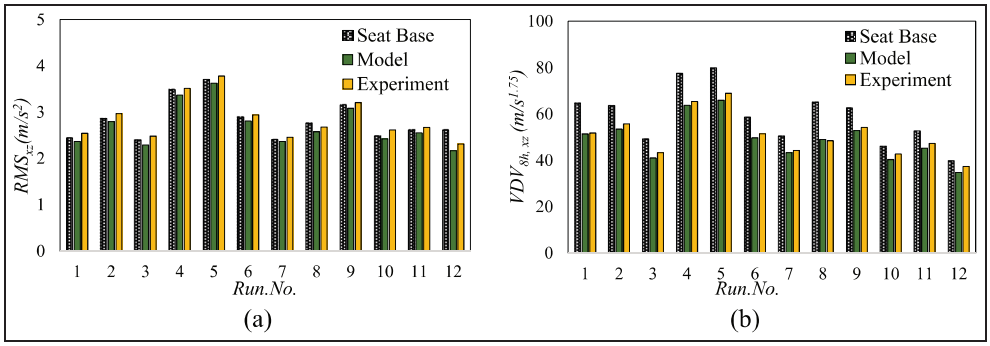


Figure 19. (a) RMS_{xz} and (b) $VDV_{8h,xz}$ at the seat base and at the seat cushion in combining forward and vertical directions.

Furthermore, VDV_{xz} for the suggested seat model is 0.7% to 6.8% lower than measurements, except for test run 8, where 1.2% increase occurs.

These results demonstrate that a shock mitigation seat with both forward and vertical suspension enhances human safety onboard the HSC. Considering that sideways accelerations can also affect comfort, future seat designs should address lateral acceleration mitigation.

Conclusions

This study makes two main contributions: (1) highlighting the impact of forward and sideways accelerations on human safety and comfort onboard High-speed crafts (HSCs), which have been largely overlooked, and (2) developing a shock mitigation seat model combining forward and vertical suspension systems. These contributions address critical gaps in previous research and design practices, which have primarily focused on vertical acceleration.

Analyzing multidirectional acceleration data from HSC sea trials indicates that while vertical acceleration has the highest intensity, forward acceleration also contributes significantly to adverse effects on human health. Additionally, vertical, forward, and sideways accelerations can each have serious impacts on human comfort, indicates that none of these directions should be overlooked.

A mathematical model was developed to assess the performance of the proposed seat, and the results demonstrate that integrating forward suspension alongside vertical systems can effectively reduce harmful acceleration exposure in these directions and improve occupant safety and comfort.

In summary, this study provides a novel and practical framework for improving HSC crew safety by both expanding the scope of acceleration analysis and introducing a more comprehensive seat suspension design.

This study has certain limitations. The forward suspension parameters were adopted from published literature due to unavailable data for the referenced seat, and horizontal seat base accelerations were not directly measured during the original sea trials. While these assumptions enabled a vertical and horizontal analysis, further experimental characterization and multidirectional measurements are recommended to refine model validation.

ORCID iDs

Fatemeh Roshan https://orcid.org/0000-0002-4713-7368
Karl Garme https://orcid.org/0000-0002-9110-9401

Author contributions

Fatemeh Roshan: Conceptualization, Methodology, Formal analysis, Visualization, Validation, Investigation, Writing—original draft. Karl Garme: Data curation, Resources, Supervision, Writing—Review & Editing. Abbas Dashtimanesh: Conceptualization, Supervision, Writing—Review & Editing.

Funding

The authors received no financial support for the research, authorship, and/or publication of this article.

Declaration of conflicting interests

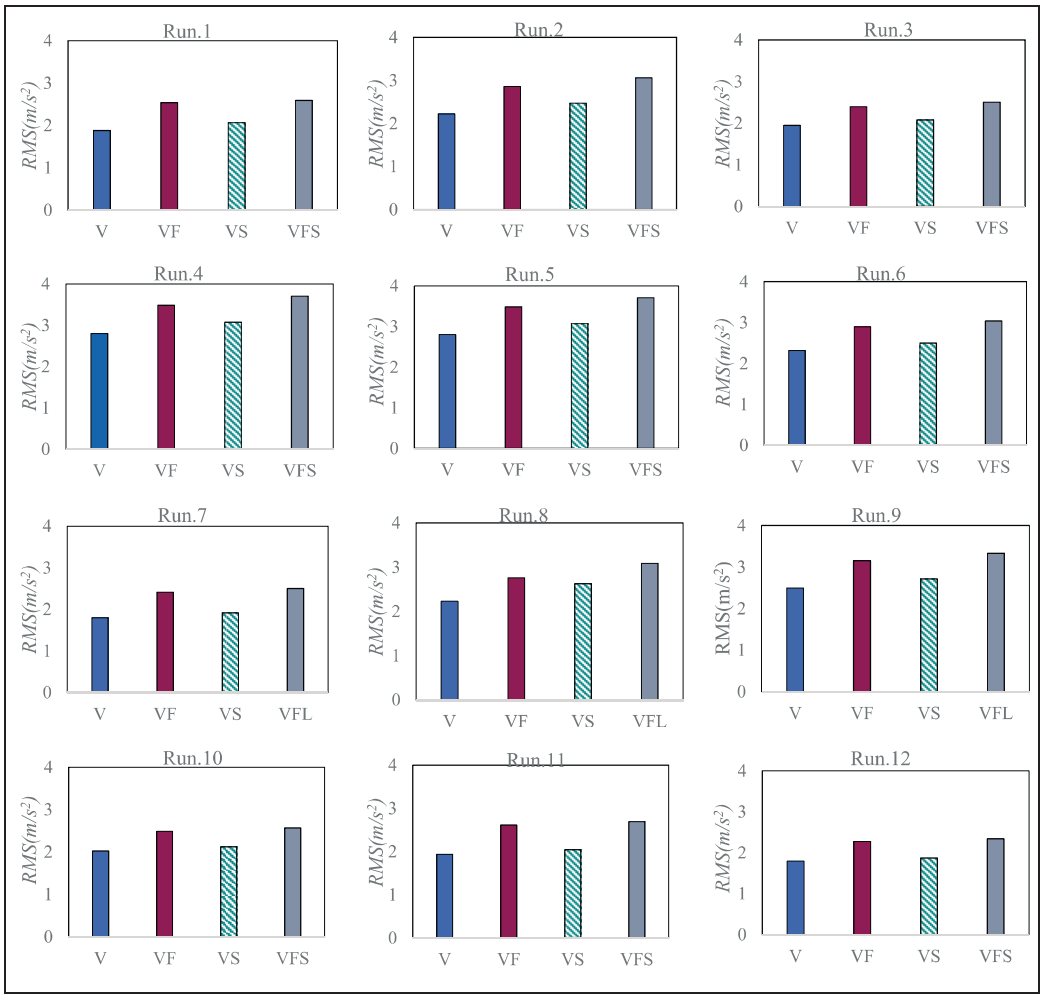
The authors declared no potential conflicts of interest with respect to the research, authorship, and/or publication of this article.

References

1. Wikström BO, Kjellberg A and Landström U. Health effects of long-term occupational exposure to whole-body vibration: a review. *Int J Ind Ergon* 1994; 14(4): 273–292. https://doi.org/10.1016/0169-8141(94)90017-5
2. Myers SD, Dobbins TD, King S, et al. Effectiveness of suspension seats in maintaining performance following military high-speed boat transits. *Hum Factors* 2012; 54(2): 264–276. https://doi.org/10.1177/0018720811436201
3. Lo Martire R, de Alwis MP, Äng BO, et al. Construction of a web-based questionnaire for longitudinal investigation of work exposure, musculoskeletal pain and performance impairments in high-performance marine craft populations. *BMJ Open* 2017; 7(7): e016006. https://doi.org/10.1136/bmjopen-2017-016006
4. de Alwis MP, LoMartire R, Äng BO, et al. Exposure aboard high-performance marine craft increases musculoskeletal pain and lowers contemporary work capacity of the occupants. *Proc Inst Mech Eng M J Eng Marit Environ* 2021; 235(3): 750–762. https://doi.org/10.1177/1475090220981466
5. Corbridge C and Griffin MJ. Vibration and comfort: vertical and lateral motion in the range 0·5 to 5·0 Hz. *Ergonomics* 1986; 29(2): 249–272. https://doi.org/10.1080/00140138608968263
6. Howarth HVC and Griffin MJ. The frequency dependence of subjective reaction to vertical and horizontal whole-body vibration at low magnitudes. *J Acoust Soc Am* 1988; 83(4): 1406–1413. https://doi.org/10.1121/1.395947
7. Griffin MJ. Measurement and evaluation of whole-body vibration at work. *Int J Ind Ergon* 1990; 6(1): 45–54. https://doi.org/10.1016/0169-8141(90)90049-8
8. International Standard Organization (ISO). *Shock—evaluation of human exposure to whole-body vibration—part 1: General requirements*. International Organization for Standardization, 1997.
9. ABCD Group. *High-speed craft human factors engineering and design guide*. ABCD TR-08-01 V1.0 edition, ABCD Group, 2008.
10. Ullman J, Hengst D, Carpenter R, et al. Does military high-speed boat slamming cause severe injuries and disability? *Clin Orthop Relat Res* 2022; 480(11): 2163–2173. https://doi.org/10.1097/CORR.0000000000002420
11. Ensign W, Hodgdon JA, Prusaczyk WK, et al. *A survey of self-reported injuries among special boat operators*. Naval Health Research Center, 2000.
12. Carvalhais A. Incidence and severity of injuries to surf boat operators. In: *75th shock and vibration symposium*, Virginia Beach, VA, 20 October 2004, Vol. 37.
13. Roshan F, Dashtimanesh A and Kujala P. Safety improvements for high-speed planing craft occupants: a systematic review. *J Mar Sci Eng* 2024; 12(5): 845. https://doi.org/10.3390/jmse12050845
14. Roshan F, Niazmand Bilandi R, De Luca F, et al. High speed planing craft dynamics in irregular waves: Safety improvement using interceptor systems. *Appl Ocean Res* 2025; 161: 104692. https://doi.org/10.1016/j.apor.2025.104692
15. Dobbins T, Myers S, Dyson M, et al. High speed craft motion analysis: impact count index (ICI). In: *43rd United Kingdom Conference on human responses to vibration*, September 2008.
16. Allen DP, Taunton DJ and Allen R. A study of shock impacts and vibration dose values onboard highspeed marine craft. *Trans R Inst Nav Arch Int J Marit Eng* 2008; 150(A3): 1–0.
17. Riley MR, Murphy HP and Coats TW. *Initial investigation of wave impact load transfer through shock isolation seats in high speed craft*. Naval Surface Warfare Center carderock Division, 31 August 2013.
18. Olausson K and Garme K. Prediction and evaluation of working conditions on high-speed craft using suspension seat modelling. *Proc Inst Mech Eng M J Eng Marit Environ* 2015; 229(3): 281–290. https://doi.org/10.1177/1475090213515641
19. Wice AM. *Spatial dynamic modelling of high speed craft suspension seating*. Doctoral dissertation, Carleton University, 2015.
20. Ereq K. *Active suspension seat for high speed craft*. Degree project in Mechanical Engineering, KTH Royal Institute of Technology, 2018.
21. Marshall JT and Riley MR. *A comparison of the mechanical shock mitigation performance of a shock isolation seat subjected to laboratory drop tests and at-sea seakeeping trials*, 2020.
22. Sorensen FW. *Development of control strategies and testing procedures for suspension seats used in high speed craft*. Doctoral dissertation, Carleton University, 2020.
23. Garme K, Burström L and Kuttenkeuler J. Measures of vibration exposure for a high-speed craft crew. *Proc Inst Mech Eng M J Eng Marit Environ* 2011; 225(4): 338–349. https://doi.org/10.1177/1475090211418747
24. EU-OSHA. Directive 2002/44/EC of the European Parliament and of the Council of 25 June 2002 on the minimum health and safety requirements regarding the exposure of workers to the risk arising from physical agents (vibration) (sixteenth individual Directive within the meaning of Article 16(1) of Directive 89/391/EEC). *Off J Eur Communities* 2002; L177: 13–19.

25. Taunton DJ, Hudson DA and Shenoi RA. Characteristics of a series of high speed hard chine planing hulls-part II: performance in waves. *Int J Small Craft Technol* 2011; 153: B1–22.
26. Stein GJ and Múčka P. Study of simultaneous shock and vibration control by a fore-and-aft suspension system of a driver's seat. *Int J Ind Ergon* 2011; 41(5): 520–529. https://doi.org/10.1016/j.ergon.2011.03.003
27. Burden RL and Faires JD (eds). *Numerical analysis*. 9th ed. Brooks/Cole, Cengage Learning, 2011.
28. Rebelle J. Development of a numerical model of seat suspensions to optimize the end-stop buffers. In: *UK conference on human responses to vibration*, University of Southampton, 13 September 2000.
29. Cho Y and Yoon YS. Biomechanical model of human on seat with backrest for evaluating ride quality. *Int J Ind Ergon* 2001; 27(5): 331–345. https://doi.org/10.1016/S0169-8141(00)00061-5
30. Maciejewski I, Blazejewski A, Pecolt S, et al. A sliding mode control strategy for active horizontal seat suspension under realistic input vibration. *J Vib Control* 2023; 29(11-12): 2539–2551. https://doi.org/10.1177/107754632 21082716
31. Coe T, Shenoi RA and Xing JT. Human body vibration response models in the context of high speed planing craft and seat isolation systems. In: *Proceedings of the Sixth International Conference on High-performance marine vehicles (HIPER'08)*, Naples, Italy, September 2008, pp.18–19.
32. Olausson K. *Vibration mitigation for high speed craft*. MSc Thesis, KTH Royal Institute of Technology, 2012.
33. Olausson K.Evaluation and modelling of human exposure to vibration on HSC. PhD Thesis, KTH Royal Institute of Technology, 2015.

Appendix I


Run.1
Run.2
Run.3
Run.4
Run.5
Run.6
Run.7
Run.8
Run.9
Run.10
Run.11
Run.12
RMS(m/s²)
RMS(m/s²)
RMS(m/s²)

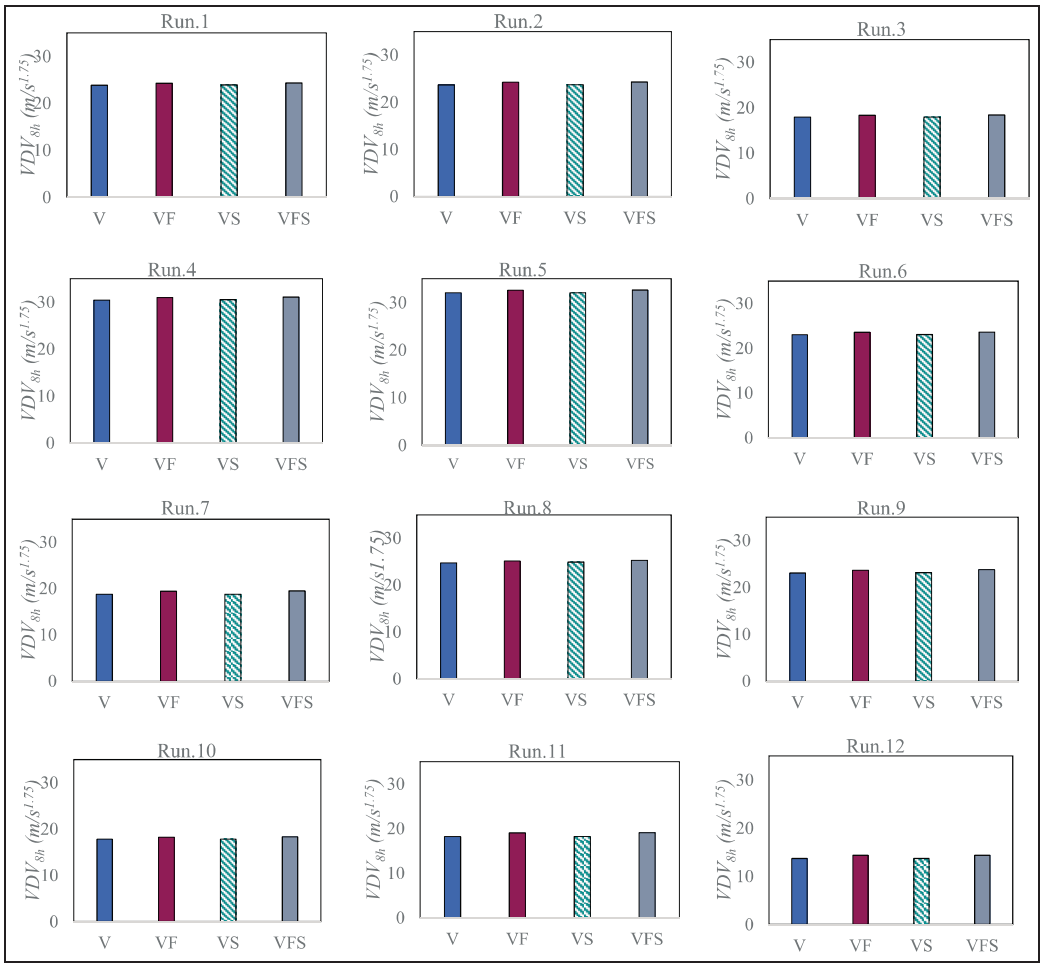


Figure 21. VDV_{8h} based on acceleration in different directions (V: Vertical, VF: Vertical and Forwards, VS: Vertical and Sideways, VFS: Vertical, Forwards, and Sideways) of the seat base.

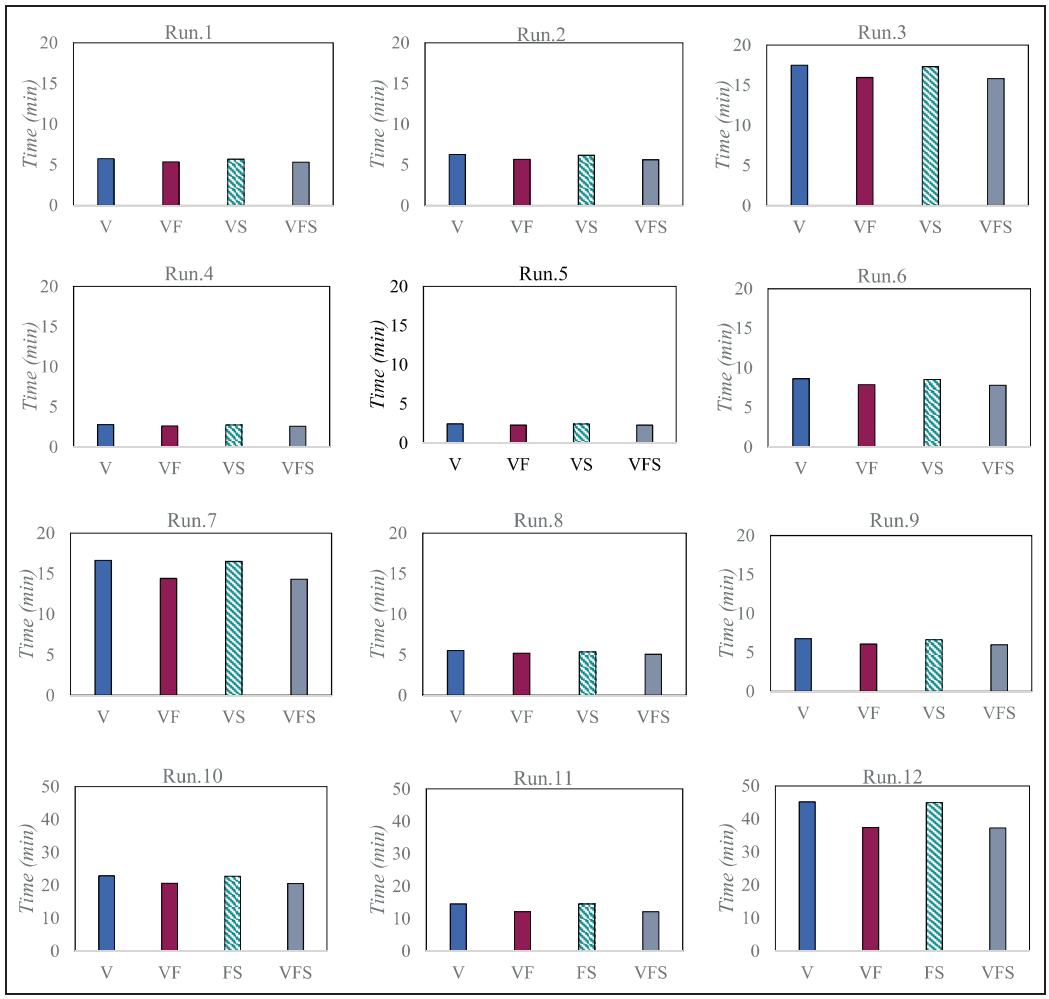


Figure 22. Time to exceed VDV $>$ 21 m/s$^{1.75}$ based on acceleration in different directions (V: Vertical, VF: Vertical and Forwards, VS: Vertical and Sideways, VFS: Vertical, Forwards, and Sideways) of the seat base.

Curriculum vitae

Personal data

Name: Fatemeh Roshan
Date of birth: 02/10/1992
Place of birth: Shiraz, Iran
Citizenship: Iran

Contact data

E-mail: Fatemeh.roshan@taltech.ee

Education

2021–2025	Tallinn University of Technology, Estonian Maritime Academy, Engineering Sciences, PhD.
2015–2018	Persian Gulf University, School of Engineering, Naval Architecture, Hydromechanics, MSC.
2011–2015	Persian Gulf University, School of Engineering, Naval Architecture, Marine Engineering, BSC.

Language competence

English	Fluent
Estonian	A1
Persian	Native

Professional employment

2021−2024	Tallinn University of Technology, Estonian Maritime Academy, Early-stage Researcher.
2018−2021	Lecturer, Engineering Department, Persian Gulf University.

Visiting activities:

27.11.2023−08.12.2023 Visiting researcher at KTH Royal Institute of Technology, Department of Engineering Mechanics, SCI by Erasmus+ scholarship.

01.05.2024−30.09.2024 Visiting researcher at University of Naples "Federico II", Department of Industrial Engineering by Erasmus+ scholarship.

Workshop:

2024 DNV Nordic Maritime Universities Workshop 2024 at Aalto University. The abstract I have presented is titled " Safety improvement of High-speed planing craft: Gaps and challenges".

Summer schools

07.10.2024-11.10.2024 PhD School on “Towards Zero Emission Mobility” organized by the Department of Industrial Engineering of the University of Naples “Federico II”.

24.07.2023-28.07.2023 Summer school of “human factors for naval architecture design for safety” organized by Centre for Marine Technology and Ocean Engineering (IST-CENTEC) of Técnico Lisboa in collaboration with the Western Norway University of Applied Science (HVL) and the Norwegian University of Science and Technology (NTNU).

Publications

Roshan, F., Niazmand Bilandi. R., De Luca, F., Mancini, S., Kõrgesaar, M., (2026). Numerical Investigation of Transom and Double Interceptor Systems on a High-Speed Planing Craft in Regular Waves with Experimental Validation. Ocean Engineering, 367, p. 128197. https://doi.org/10.1016/j.oceaneng.2026.128197.

Roshan, F., Garme, K., & Dashtimanesh, A. (2026). Acceleration effects in the horizontal plane on the safety assessment aboard a high-speed craft. Proceedings of the Institution of Mechanical Engineers, Part M: Journal of Engineering for the Maritime Environment, 14750902261440461.

Link: https://doi.org/10.1177/1475090226144046.

Tavakoli, S., Niazmand Bilandi, R., **Roshan, F.**, Singh, M., Mancini, S. (2026). Planing hull dynamics in water waves: Physical insights from nonlinear strip theory models and fully nonlinear computational fluid dynamics simulations. Physics of Fluids, 38(2).

Link: https://doi.org/10.1063/5.0311446.

Niazmand Bilandi, R., Dashtimanesh, A., Tavakoli, S., Mancini, S., **Roshan, F.** (2026). Performance prediction of swept stepped hulls in calm water. *Ships and Offshore Structures*, 1–11.

Link: https://doi.org/10.1080/17445302.2025.2608828.

Roshan, F., Niazmand Bilandi, R., De Luca, F., Mancini, S., Kujala, P., & Dashtimanesh, A. (2025). High speed planing craft dynamics in irregular waves: Safety improvement using interceptor systems. Applied Ocean Research, 161, 104692.

Link: https://doi.org/10.1016/j.apor.2025.104692.

Roshan, F., Dashtimanesh, A., De Luca, F., Mancini, S. (2025). High-Speed Craft with Double Interceptor System in Calm Water: URANS Solution. Progress in Marine Science and Technology.

Link: https://doi.org/10.3233/pmst250047.

Roshan, F., Dashtimanesh, A., Kujala, P. (2024). Safety Improvements for High-Speed Planing Craft Occupants: A Systematic Review. Journal of Marine Science and Engineering, 12(5), 845.

Link: https://doi.org/10.3390/jmse12050845.

Roshan, F., Tavakoli, S., Mancini, S., Dashtimanesh, A. (2022). Dynamic of Tunneled Planing Hulls in Waves. Journal of Marine Science and Engineering, 10(8), 1038.

Link: https://doi.org/10.3390/jmse10081038.

Roshan, F., Dashtimanesh, A., Tavakoli, S., Niazmand Bilandi, R., Abyn, H. (2021). Hull–propeller interaction for planing boats: A numerical study. Ships and Offshore Structures, 16(9), 955-967.

Link: https://doi.org/10.1080/17445302.2020.1790295.

Niazmand Bilandi, R., Vitiello, L., Mancini, S., Nappo, V., **Roshan, F.,** Tavakoli, S., Dashtimanesh, A. (2020). Calm-water performance of a boat with two swept steps at high-speeds: Laboratory measurements and mathematical modeling. Procedia Manufacturing, 42, 467-474.

Link: https://doi.org/10.1016/j.promfg.2020.02.046.

Dashtimanesh, A., **Roshan, F.**, Tavakoli, S., Kohansal, A., Barmala, B. (2020). Effects of step configuration on hydrodynamic performance of one-and doubled-stepped planing flat plates: A numerical simulation. Proceedings of the Institution of Mechanical Engineers, Part M: Journal of Engineering for the Maritime Environment, 234(1), 181-195.
Link: https://doi.org/10.1177/1475090219851917.

Roshan, F., Dashtimanesh, A., Niazmand Bilandi, R. (2020). Hydrodynamic characteristics of tunneled planing hulls in calm water. Brodogradnja: An International Journal of Naval Architecture and Ocean Engineering for Research and Development, 71(1), 19-38.
Link: https://doi.org/10.21278/brod71102.

Niazmand Bilandi, R., Jamei, S., **Roshan, F**., & Azizi, M. (2018). Numerical simulation of vertical water impact of asymmetric wedges by using a finite volume method combined with a volume-of-fluid technique. Ocean engineering, 160, 119-131.
Link: https://doi.org/10.1016/j.oceaneng.2018.04.043

Elulookirjeldus

Isikuandmed

Nimi: Fatemeh Roshan
Sünniaeg: 02.10.1992
Sünnikoht: Shiraz, Iraan
Kodakondsus: Iraan

Kontaktandmed

E-post: Fatemeh.roshan@taltech.ee

Hariduskäik

2021–2025	Tallinna Tehnikaülikool, Eesti Mereakadeemia, inseneriteadused, doktorantuur (PhD)
2015–2018	Pärsia Lahe Ülikool, Inseneriteaduskond, laevaehitus, hüdromehaanika, magistrikraad (MSc)
2011–2015	Pärsia Lahe Ülikool, Inseneriteaduskond, laevaehitus, laevandustehnika, bakalaureusekraad (BSc)

Keelteoskus

Inglise keel	Sorav
Eesti keel	A1
Pärsia keel	Emakeel

Teenistuskäik

2021–2024	Tallinna Tehnikaülikool, Eesti Mereakadeemia, varajase etapi teadur
2018-2021	Inseneriteaduskond, Pärsia Lahe Ülikool

Külastustegevused

27.11.2023 – 08.12.2023	Külalisteadur Kuninglikus Tehnoloogiainstituudis (KTH), Insenerimehaanika osakond, SCI – Erasmus+ stipendiumiga
01.05.2024 – 30.09.2024	Külalisteadur Napoli Ülikoolis "Federico II", Tööstustehnika osakond – Erasmus+ stipendiumiga

Töötuba

2024 DNV Põhjamaade Merendusülikoolide töötuba 2024 Aalto Ülikoolis. Esitatud abstrakti pealkiri: "Kiirete planeerivate alustega seotud ohutuse parandamine: lüngad ja väljakutsed"

Suvekoolid

07.10.2024–11.10.2024	Doktoriõppe kool “Zero Emission Mobility suunas”, korraldaja: Napoli Ülikooli “Federico II” tööstustehnika osakond
24.07.2023 – 28.07.2023	Suvekool “Inimfaktorid laevaehituse ohutuse projekteerimisel”, korraldajad: IST-CENTEC (Técnico Lisboa), Lääne-Norra Rakendusteaduste Ülikool (HVL) ja Norra Teadus- ja Tehnoloogiaülikool (NTNU)

ISSN 2585-6901
ISBN 978-9916-80-608-1